Stellingen behorende bij het proefschrift

Photophysical Properties of Opto-Electric Molecules studied by Time-Resolved Microwave Conductivity

1. De grote polariseerbaarheid in de aangeslagen toestand van 9,9'-bianthryl is niet het gevolg van flip-flop uitwisseling van de lading tussen de twee anthraceen eenheden, zoals geconcludeerd door Fessenden et al., maar wordt veroorzaakt door de formatie van het radikaal anion op één van de anthraceen eenheden.

D.B. Toublanc, R.W. Fessenden and A. Hitachi, *J. Phys. Chem.* **1989**, *93*, 2893.

Dit proefschrift Chapter 8.

2. De bewering van Wasielewski et al., dat multichromophore systemen beter geschikt zijn dan bichromophore systemen, om langlevende ladingsgescheiden toestanden te genereren, is tot op heden niet experimenteel bewezen.

M.R. Wasielewski, M.P. Niemczyk, W.A. Svec and E.B. Pewitt, *J. Am. Chem. Soc.* **1985**, *107*, 5562.

3. De veronderstelling dat de geleiding hoger zal zijn in horizontaal gestapelde aggregaten van discotische macromoleculen dan in de onder een tilthoek gestapelde aggregaten is niet juist.

H. Schultz, H. Lehmann, M. Rein and M. Hanack, *Struct. Bonding* **1991**, *74*, 41.

P.G. Schouten et al., *J. Am. Chem. Soc.*, **1994**, *116*, 6880.

4. De interpretatie door Baum van de resultaten in het artikel van Barton et al., dat DNA kan fungeren als een "molecular wire", is te speculatief.

R. Baum, *Chemical & Engineering News*, **1993**, *71*, 52.

C.J. Murphy, M.R. Arkin, Y. Jenkins, N.D. Ghatlia, S.H. Bossmann, N.J. Turro and J.K. Barton, *Science* **1993**, *262*, 1025.

5. De "dc conductivity" techniek van Braun is geen alternatief voor, maar een nuttige aanvulling op de "time-resolved microwave conductivity" techniek.

S.N. Smirnov and C.L. Braun, *J. Phys. Chem.*, **1992**, *96*, 9587.

6. De vrije vertaling voor het begrip TICT (Twisted Internal Charge Transfer) luidt: Twijfel Inducerende Conflict Theory.

7. Het uitloven van één hoofdprijs van 7 miljoen gulden i.p.v. 7 hoofdprijzen van 1 miljoen gulden in een loterij, om zo de lotenverkoop te stimuleren, speelt in op het feit dat de hebberigheid van de potentiële deelnemers het zal winnen van hun statistisch inzicht.

8. De stormachtige ontwikkeling van de computertechnologie zal leiden tot het verlies van het handschrift in volgende generaties.

9. Autorijdende forensen ervaren de werktijd als de tijd tussen twee files.

10. Alleen geoefende gebruikers kunnen de helpfuncties van computerprogramma's optimaal benutten.

11. Het beleid om de studieduur nog verder te bekorten heeft tot gevolg dat de uitdrukking "studententijd" moet worden bijgesteld tot "studentenpoosje".

12. Het nut van andermans antwoordapparaat kan pas ten volle worden ingezien wanneer men er zelf één heeft aangeschaft.

13. Het zoeken naar een permanente baan in de huidige economische situatie is een volledige dagtaak.

14. Golfers die een hole-in-one hebben geslagen onderschatten de kundigheid van de groundsman die de hole op de bewuste dag op de goede plek in de green heeft geplaatst.

Photophysical Properties of Opto-Electric Molecules studied by Time-Resolved Microwave Conductivity

Wouter Schuddeboom

Interfaculty Reactor Institute
Delft University of Technology
november 1994

Cover: Laser beam incident on the Time-Resolved Microwave Conductivity resonant cavity cell containing a solution of the donor-acceptor molecule 4-dimethylamino-4-nitrostilbene (DMANS). The yellow light emitting from the TRMC cell is fluorescence from laser-excited DMANS molecules.

Photophysical Properties of Opto-Electric Molecules
studied by
Time-Resolved Microwave Conductivity

PROEFSCHRIFT

ter verkrijging van de graad van doctor
aan de Technische Universiteit Delft,
op gezag van de Rector Magnificus, Prof. Ir. K.F. Wakker,
in het openbaar te verdedigen ten overstaan van een commissie,
door het College van Dekanen aangewezen,
op donderdag 17 november 1994 te 13.30 uur
door

Wouter SCHUDDEBOOM

doctorandus in de scheikunde

geboren te Zaandijk

Dit proefschrift is goedgekeurd door de promotor:

Prof. dr. A. Hummel

en de toegevoegd promotor:

Dr. J.M. Warman

VOORWOORD

In mijn hoedanigheid als OPA (Onderzoeksproject Assistent) heb ik in de afgelopen drie jaar met veel plezier in de afdeling stralingschemie van het IRI gewerkt. Het onderzoek betrof het bestuderen van een breed scala van bijzondere moleculen in oplossing, die, nadat ze met laserlicht zijn beschoten, de spanning opvoeren of zelfs onder stroom komen te staan. De meeste van deze "relatief" korte (10^{-9} - 10^{-12} seconden) electronische hoogstandjes zijn met behulp van de Time-Resolved Microwave Conductivity (TRMC) techniek vastgelegd. De TRMC techniek is een unieke en elegante methode om ladingsscheiding (dipoolmoment) en zelfs electronen bewegingen (polariseerbaarheid) van geëxciteerde moleculen in oplossing te bestuderen. Deze methode is in Delft ontwikkeld en wordt uitgebreid in dit proefschrift beschreven. Het was voor mij zeer boeiend om met de TRMC techniek te mogen werken.

Het uitvoeren van wetenschappelijk onderzoek is, in tegenstelling tot wat veel mensen misschien denken, een sociale aangelegenheid. Ik wil daarom dan ook een groot aantal mensen bedanken. Als eerste natuurlijk Dr. J.M. Warman, die als dagelijks begeleider en wetenschappelijk stimulator een onmisbare bijdrage heeft geleverd aan de verkregen resultaten. *Beste John, ik heb het als zeer prettig en een eer ervaren om met jou samen te mogen werken.* Jouw ideeën, voorspellingen en het feit dat je na het zien van de ruwe data (bijna) altijd een correcte voorstelling van zaken had, hebben diepe indruk op mij gemaakt. Verder zal ik je humor, het entropie effect van je koffielepeltjes (meestal in vele stukken), de vrijdagmiddagborrel, het roken (heeft er iemand een "shaggie" bij zich?) en de voetbalavondjes (lekkerbekkies, head-draw etc.) niet snel vergeten. John bedankt.

Als ik John heb genoemd kom ik gelijk bij Dr. M.P. de Haas. Beste Thijs, jou wil ik bedanken voor de grote bijdrage die je hebt geleverd aan het goed laten functioneren van zowel de apparatuur, alsmede de computerprogramma's. Jouw nuchtere en direkte manier van handelen heb ik zeer gewaardeerd.

Mijn promotor Prof. Dr. A. Hummel wil ik bedanken voor de flexibele wijze waarop mij de OPA-plaats ter beschikking is gesteld, waardoor het mogelijk werd om dit promotieonderzoek uit te voeren.

De "tandem" Leo Schouten en Garrelt (Gerrit) van der Laan wil ik bedanken voor het creëren van de prettige onderzoekssfeer, waarbij ik met name het lekker direct met elkaar omgaan enorm heb gewaardeerd. Verder zal ik onze unieke conversaties niet snel vergeten.

De "Tanzania-ganger" Stephan Jonker ben ik dank verschuldigd voor het inwijden in de wondere wereld van de TRMC techniek en de vele perfecte maaltijden, na weer een lange dag van vele experimenten.

Van de overige leden van de afdeling stralingschemie wil ik Martien Vermeulen bedanken voor het optimaal laten functioneren van de lasers en niet in de laatste plaats voor het vele malen onderzoeken en repareren van mijn auto. Paul Rijkers ben ik dank verschuldigd voor het uitbreiden en in stand houden van de software. De overige leden van de afdeling; Lee Luthjens,

CONTENTS

Chapter 1 Photon-Induced Charge Separation in Molecular Systems

Chapter 2 The Time-Resolved Microwave Conductivity (TRMC) Technique: Theory, Apparatus and Data Analysis

Chapter 3   Influence of the Alkyl Chain Length and Effective Solvent Polarity on the Excited-State Dipole moments of 4-(Dialkylamino)benzonitriles

Chapter 4   The Formation of Extended and Folded Charge Separated States of Donor-Spacer-Acceptor Molecules with Flexible and Semi-rigid σ-Bond Spacers

Chapter 5   Charge Separation in Sigma-Bond separated Trichromophoric Donor-Acceptor Compounds

Chapter 6   Second Harmonic Generation by Bridged Donor-Acceptor Compounds: π- versus σ-conjugation

Chapter 7   Sudden Polarization in the Twisted, Phantom State (^{1}P*) of Tetraphenylethylene

Chapter 8   Polarization and Polarizability in the Excited States of Symmetrical Molecules

Chapter 1

Photon-Induced Charge Separation

in Molecular Systems

1.1 INTRODUCTION

The absorption of light by molecules is invariably accompanied by a change in spatial distribution of the bound electrons. For some molecules this can result "immediately" in a large change in dipole moment in the Franck-Condon excited state. For others, rearrangements of the electrons and/or nuclei occur subsequent to vertical excitation, which possibly can induce or accentuate charge separation. The formation of charge separated states is most likely to occur for molecules (DSA), which consist of a donor moiety, D, and an acceptor moiety, A, joined by an intervening spacer, S. The spacer may be a conjugated π-bond system which strongly couples the donor and acceptor or it may be a σ-bonded bridge which acts as an insulator, allowing only very weak "through bond" coupling.[1,2] In some special cases charge separation may even occur in symmetrical molecules without any clearly definable donor and/or acceptor sites.[3]

The properties (and formation) of a charge separated state are very sensitive, amongst other things, to the nature of the donor and acceptor group, the length and nature of the bridging unit, geometrical aspects such as flexibility and rotation, orbital symmetry and the dielectric properties and viscosity of the bulk medium. In this thesis these various aspects will be investigated using the Time-Resolved Microwave Conductivity (TRMC)[4] technique for π-bond and σ-bond separated donor-acceptor molecules as well as for symmetrical molecules. This technique proves to be a unique way of gaining insight into the basic opto-electrical properties of compounds of potential use in solar energy conversion devices, molecular optical switching and nonlinear optics.

The TRMC technique is used in combination with steady-state and time-resolved fluorescence techniques. In contrast to the TRMC technique, which allows direct probing of the changes which occur in the charge distribution of a molecule on photoexcitation, the fluorescence technique can only provide this information indirectly via solvent or electric field effects on the emission bands. The fluorescence methods do however provide complementary information on locally excited states, which have little extra charge separation and are therefore invisible to TRMC.

1.2 DONOR-ACCEPTOR MOLECULES

Schematic representations of the relative energy levels, which can be occupied after photo-excitation of donor-acceptor molecules, are shown in Figure 1.1. After excitation of a DSA molecule into a Franck-Condon state, reorganisation of the molecule and enviroment (solvent)

A: Strong coupling (conjugated spacer)

B: Weak coupling (σ-bond spacer)
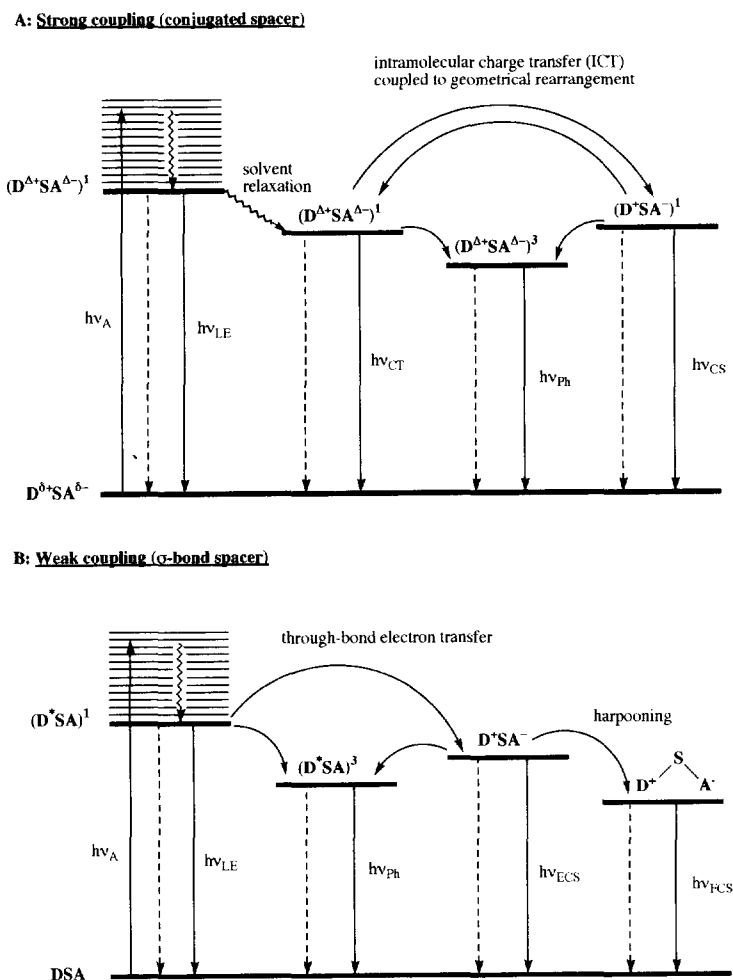
Figure 1.1: Schematic representation of the relative energy levels for: (A) strong coupling between donor and acceptor, as is usually the case for conjugated spacers, and (B) weak coupling between donor and acceptor, as is mostly the case for σ-bonded compounds. hv_A is the absorption, hv_{LE} is the local fluorescence, hv_{Ph} is the phosphorescence, hv_{CT} is the fluorescence from a charge transfer state, hv_{CS} is the fluorescence from a charge separated state, hv_{ECS} is the fluorescence from an extended charge separated state, and hv_{FCS} is the fluorescence from a folded charge separated state. The dashed arrows represent radiationless decay.

results in the formation of a relaxed singlet excited state, $(DSA)^{1*}$. From this state the molecule can, via fluorescence and/or non-radiative decay, return to the ground state. Another possibility is the occurrence of intersystem crossing to a triplet state, $(DSA)^{3*}$. The process of main interest in the present work is electron transfer (ET), with the molecule ending up in a charge separated state, $(D^+SA^-)^1$, which returns to the ground state via fluorescence decay and/or radiationless decay, or via intersystem crossing to a locally excited or charge separated triplet state, $(D^+SA^-)^3$. In the charge separated state or during the ET process very often electronically induced geometrical changes, such as twisting and folding may occur, most commonly accompanied by a change in hybridization of the donor and/or the acceptor moieties. If the coupling between donor and acceptor is strong enough, it is possible that excitation occurs directly to a state with a high degree of charge transfer character. This is particularly important for the occurrence of non-linear optical effects.[5]

1.2.1 π-bond spacers

1.2.1.1 Charge separated singlet states of π-conjugated donor-acceptor molecules

Conjugated D-π-A compounds have been known for many years to undergo large dipole moment changes when photo-excited. This can most easily be demonstrated by TRMC measurements or by the fluorescence of such compounds, which undergoes very large red shifts with increasing polarity of the medium.[6] The high degree of coupling between donor and acceptor by the conjugated π-electrons of the spacer ensures, that on photon absorption, an optical transition can occur directly, i.e. within femtoseconds, to the upper charge transfer state. The strong coupling results in the lifetime of the relaxed S_1 state, being usually never much longer than a few nanoseconds. The net change in dipole moment is also reduced, because of mixing of completely charge separated, CS, and locally excited, LE, states in both S_0 and S_1. Ground state dipole moments are therefore usually already quite high at 5 to 7 debye (D) (1 D = 3.33×10^{-30} Cm) and the S_1 dipole moment tends to saturate with increasing length of the spacer at a maximum value of approximately 30 D.[7] This is illustrated in Figure 1.2 for a series of π-bond separated dimethylamino-nitro compounds. The net difference of 20 to 25 D, however, still represents a high degree of photon-induced charge separation, corresponding as it does to the displacement of a complete electron over a distance of 4 to 5 Å. Such molecules could therefore certainly earn the title of molecular opto-electric switches if it were not for the fact that the S_1-state lifetimes tend to be only nanoseconds or less.[8]
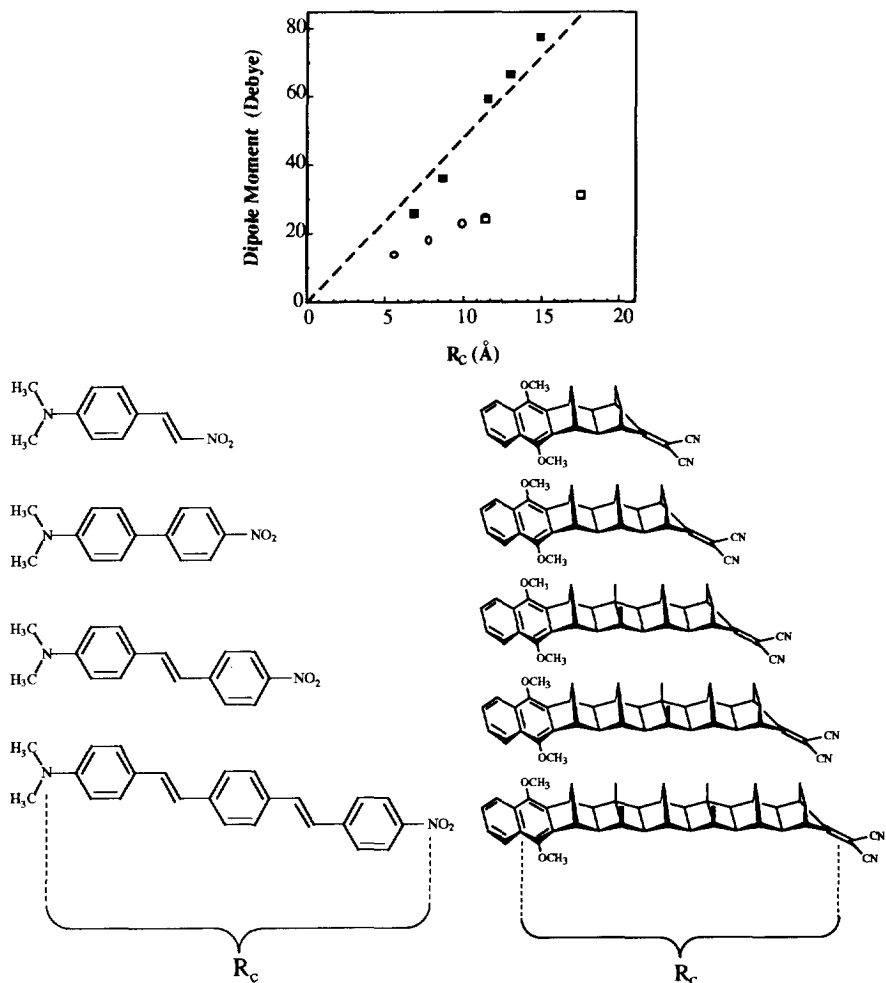
Figure 1.2: Excited state dipole moment as function of the distance for a series of π-conjugated donor-acceptor compounds compared to a series of σ-bond donor-acceptor compounds with their structures shown. Filled squares are the dipole moments of the σ-bond donor-acceptor compounds and the open symbols are the dipole moments of the π-conjugated donor-acceptor compounds with squares determined by TRMC and circles by electrochromic shifts.[7]

1.2.1.2 Dual fluorescent π-conjugated compounds

In the molecules described above, excitation occurs directly to the upper charge transfer (CT) state, due to the high degree of coupling between donor and acceptor. There are however many π-conjugated donor-acceptor molecules, for which excitation occurs initially to a relaxed S_1 state ($D^{\Delta+}SA^{\Delta-}$) with a relatively small net increase in charge separation compared with the

S_0 state ($D^{\delta+}SA^{\delta-}$). The resulting fluorescence displays only a weak dependence on solvent polarity and is sometimes referred to as emission from a locally excited state. A subsequent conformational change within S_1 can result in an increase in charge separation (D^+SA^-) and the emission of a second, highly solvent dependent band, referred to here as CS-fluorescence (see Figure 1.1A).

More than thirty years[9] ago 4-(dimethylamino)benzonitrile (DMABN) was found to show dual fluorescence, resulting from a reversible intramolecular charge transfer (ICT) process. Since then a lot of other related compounds have been found to show the same behaviour. From the initially excited singlet state, a species, (CS), with a considerably larger dipole moment is produced.[9-19] It has been shown[20] that the CS state is not accessible by direct excitation, so it must be formed from the LE state. The mechanism of formation and the properties of the CS state have been extensively studied since the publication of Lippert[9] and have given rise to considerable debate and discussion about the exact mechanism.

The most widely accepted mechanism of this phenomenon is the TICT ("twisted internal charge transfer") model involving rotational isomerization around the amino-phenyl bond. In this model, the CS state of DMABN and related molecules is postulated to be a rotational isomer of a planar LE state, with the amino group in a plane perpendicular to that of the phenyl ring.[13-15] This bond rotation is supposed to lead to localization of unit positive charge on the nitrogen atom of the amino group. The negative charge is thought to be delocalized as in the radical anion of benzonitrile.[21-24] Such a complete decoupling of the amino group from the benzonitrile subunit in the aminobenzonitriles has also been described as "the principle of minimum overlap".[25,26]

Although TICT is the currently favoured model in discussions of dual fluorescence, its acceptance is by no means universal. Other models have been proposed.[19,27-32] For example, Varma et al., suggest a solute/solvent exciplex as the origin of the anomalous emission in DMABN and related molecules.[18,19,30,31]

The mechanistic relationship between the twisting motion in the first excited singlet state and the charge transfer reaction (TICT) has been questioned, based on results from excitation spectra of jet-cooled DMABN and a number of its derivatives.[33] From the spectra of bare and monosolvated DMABN in a supersonic jet, no evidence for the TICT phenomena has been found.[34-37]

1.2.1.3 Charge separated triplet states of π-conjugated donor-acceptor molecules

Many conjugated donor-acceptor compounds are known to undergo a change of spin multiplicity which results in intersystem crossing from S_1 to the lowest lying triplet state, T_1.

17
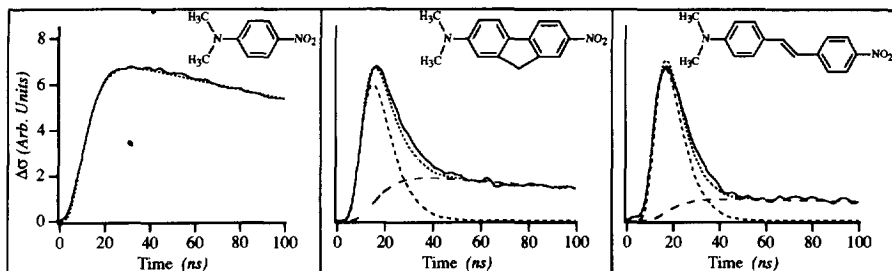
Figure 1.3: *Transient changes in the microwave conductivity (dielectric loss) on flash-photolysis at 308 nm, pulse width 7 ns of ca 10^{-4} M solutions of the compounds with the molecular structure shown. The dotted line is the kinetic fit to the data based on a three state model with the individual S_1 and T_1 components shown as dashed lines. The results illustrate the dependence of the yield of the long-lived triplet state on the length of the conjugated bridge.*

Even at room temperature in liquid solution T_1 states can have lifetimes of many microseconds or more. While the energy level of T_1 lies somewhat lower than S_1, the triplet state can still have a very high degree of charge separation, compared to the ground state, as has been determined in previous TRMC experiments.[4,38,39] The intramolecular spin conversion process would therefore appear to be a very convenient way of providing the necessary long-lived third state for extending the lifetime of optically induced charge separation and providing a practical opto-electric switch (see Section 1.4 for further details).

The efficiency of intersystem crossing from S_1 to T_1 in donor-acceptor compounds is extremely sensitive to the molecular structure and solvent in ways which are as yet not
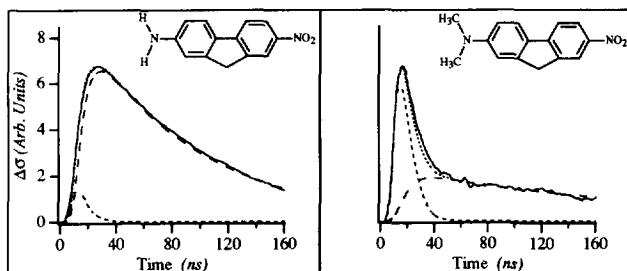
Figure 1.4: *Transient changes in the microwave conductivity (dielectric loss) on flash-photolysis at 308 nm, pulse width 7 ns of ca 10^{-4} M solutions of the compounds with the molecular structure shown. The dotted line is the kinetic fit to the data based on a three state model with the individual S_1 and T_1 components shown as dashed lines. The results illustrate the influence on the yield of the long-lived triplet state on methyl substitution at the amino donor group.*

completely understood. A substantial problem in the research into intersystem crossing has been the necessity of using usually two different techniques for observing S_1 and T_1 states; optical emission and absorption spectrophotometry respectively. With the TRMC technique it is however possible to monitor both states in one experiment, as shown by the transients for molecules containing a dimethylamino-donor and a nitro-acceptor group in Figure 1.3. The transients consist of short-lived, singlet and long-lived, triplet contributions.[8]

Even without a full quantitative analysis of the data, it is immediately apparent from the TRMC transients shown in Figure 1.3, that the yield of triplet state decreases dramatically as the length of the conjugated spacer increases. This is not simply a function of the length itself, but depends also very markedly on the actual nature of the spacer.

In Figure 1.4 are shown the TRMC transients of amino- and dimethylamino-nitro-fluorene, which reveal that the yield of the triplet state is dramatically influenced by what might appear to be a small change, such as methyl substitution in the donor group.[8] For the two fluorene derivatives the T_1 quantum yield is found to decrease from 0.65 to 0.05 on dimethyl substitution. Clearly methyl substitution has in some way considerably reduced the efficiency of the mechanism responsible for intramolecular spin inversion.

1.2.2 σ-bond spacers

1.2.2.1 Long-distance electron transfer in bichromophoric compounds

As mentioned in Section 1.2.1 the coupling between the donor and acceptor moieties in π-conjugated molecules is very strong due to the overlapping π-electrons of the conjugated spacer. It was in fact thought for many years that this was the only way to achieve a high degree of charge separation in the excited state of a donor-acceptor molecule, other than by direct π-π overlap of the donor and acceptor orbitals. In recent years, however, TRMC experiments in particular have shown that high degrees of intramolecular charge separation can result even in molecules for which the donor and acceptor are separated by extensive, rigid, sigma-bonded bridges.[40-42]

Many different types of hydrocarbon bridges[43] have been employed to study the distance dependence and other factors of the electron transfer dynamics in these molecules, which include cyclohexane, decalin, and steroid-based systems,[44-46] bicyclo[2.2.2]octane,[47] triptycene,[48] polyspirocyclobutane,[48,49] cubane[50] and polynorbornyl type bridges.[51-54] Such studies have demonstrated that very rapid ET rates ($>10^9$ s^{-1}) can occur over inter-chromophore separations as great as 13 Å and that this is due to a through bond[1,2,55,56] coupling mechanism, involving mutual interactions of the chromophore orbitals with the bridge orbitals. Recent

19

review articles about the various types of systems are to be found in references 57 and 58.

The dependence of the ET rate constant on the donor-acceptor distance in a specific solvent is expected to be of the form:

$$k(r) = k_0 \exp[-\beta(r-r_0)] \tag{1}$$

where r is the donor-acceptor distance, r_0 is the distance, usually van der Waals contact, at which the largest rate occurs, and β is a constant. The largest possible rate, k_0, is 10^{15}-10^{16} s^{-1}, but is usually close to the frequency of a single molecular vibration, 10^{13} s^{-1}. The value of β, which usually varies between 0.8-1.5 Å^{-1}, is the principal piece of information that can be derived from systematic studies of the distance dependence of ET rates.

In most cases the initial Franck-Condon transition is to a local excited state of either the donor or acceptor chromophore as illustrated in Figure 1.1B. This is then followed by long-distance ET by tunneling through the saturated hydrocarbon barrier. An example of a series of such molecules, DIADs (Donor-Insulator-Acceptor Devices), as synthesized by the group of Paddon-Row, is shown in Figure 1.2. In this series convincing evidence has been presented, that long distance ET occurs subsequent to photoexcitation of the donor moiety. From the magnitudes of the transients the dipole moments of the intermediates could be estimated to increase from 26 D for the shortest to almost 80 D for the longest. These values are slightly larger than those expected for complete ET over the length of the intervening spacer which varies from 4.6 to 13.5 Å. Also the lifetimes of the CS states are found to increase markedly with increasing distance, corresponding to a close to exponential dependence on distance with β = 0.88 Å^{-1}. Furthermore the rate constants for charge recombination show significant solvent variations indicating the rate to be very sensitive to changes of the energy level of the CS state.

Closs and Miller have studied the distance dependence of ET from the biphenyl radical anion to naphthalene across cubane,[50] decalin and cyclohexane spacers,[59-61] with distances from 4 to 11 Å. General structures of these compounds are shown in Figure 1.5. They found that the donor-acceptor orientation modulates the distance dependence of ET reactions to a significant degree. A β value of 0.9 Å^{-1} was found for the cubane-bridged compounds and a value of 1.1 Å^{-1} was found for the cyclohexane and decalin compounds. The same value was found by Johnson et al.[62], who studied the same systems, as depicted in Figure 1.5, by hole transfer from the biphenyl cation radical to the naphthalene unit.

Interestingly the study of intermolecular ET between biphenyl anions and various acceptors in glassy matrices by Miller et al.[63,64] resulted in a β value of 1.2 Å^{-1}. Comparison of these results with those for intramolecular ET in bridged compounds indicates that the introduction of
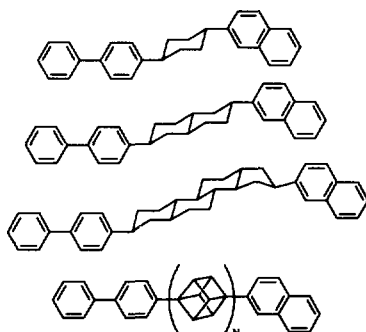
Figure 1.5: *General structures of the compounds as studied by Miller and coworkers.[50,59-61]*

a hydrocarbon spacer decreases the value of β. Therefore the intervening medium must play an important role in the mediation of ET. In fact the electronic coupling is most efficient, as predicted by theory, in a confined rigid zig-zag or "all-trans" configuration.[55,56] Furthermore the orientation of the donor and acceptor orbitals with respect to the spacer orbitals is expected to be important for overlap and efficient coupling.

Comparison of π-conjugated and σ-bond separated molecules

In comparing the σ-bond separated DIADs with the π-bond separated dimethylamino-nitro compounds (see Figure 1.2), it is obvious that the extent of charge separation in the π-conjugated series saturates with lengthening of the bridges, whereas for the σ-bond separated compounds charge separation is linearly dependent on the length and is complete. This is one of the most striking differences between π-conjugated and σ-bond separated donor-acceptor molecules.

As mentioned above, unlike π-conjugated systems, the optical transition in DIADs does not usually occur directly to the CS state but rather to a local excited state of the donor or acceptor moiety. The time for charge development is determined, for DIADs, by the time taken for electron tunneling to occur. The tunneling process occurs in competition with the natural decay of the locally excited donor or acceptor and the quantum yield of charge separation will depend on the relative rates of these two processes. A significant difference, therefore, between conjugated D-π-A compounds and DIADs, is that in the former the quantum yield for formation of the CS state is unity but charge separation is incomplete, whereas for the latter the quantum yield may be less than unity, but if it occurs charge separation is complete.[7] For example, the quantum yield for charge separation for the longest of the σ-bond separated compounds in Figure 1.2 is only approximately 70%.

1.2.2.2 Long-distance electron transfer in trichromophoric compounds

The larger the inter-chromophoric distance the weaker the interaction, so that in bichromophoric systems there is a limiting distance above which the efficiency of charge separation decreases rapidly as local decay processes begin to compete effectively with long distance ET. An approach, necessary to overcome larger distances and create longer living CS states, which is important for the application in solar energy devices, is to introduce more chromophores in one molecule. In such a multi-chromophoric system electron transfer occurs in a sequence of steps. This is the manner in which nature has organized things. Lifetimes into the microsecond region with up to five chromophores (PENTAD) have been reported by Gust, Moore and coworkers[65] and for three chromophores (TRIAD) by Wasielewski et al.[66]

In Figure 1.6 are shown the TRMC transients in benzene[67] of a rigidly bridged D_2-S-D_1-S-A compound (TRIAD) with its bichromophoric counterpart (DIAD) and the D_2-D_1 model compound, recently synthesized by the group of Paddon-Row. These molecules are made to test the efficiency of two-step electron transfer in extending the lifetime of the fully, charge separated, giant dipole states following flash photolysis. The signal for the TRIAD is seen to be considerably larger and longer lived than for the DIAD and the D_2-D_1 compound, despite the increase in size and hence dipole relaxation time, which would result in a lower TRMC transient if the dipole moments were equal. This is clearcut evidence that the second step in the ET process is in fact occuring to yield a giant dipole state with a dipole moment close to 100 D.
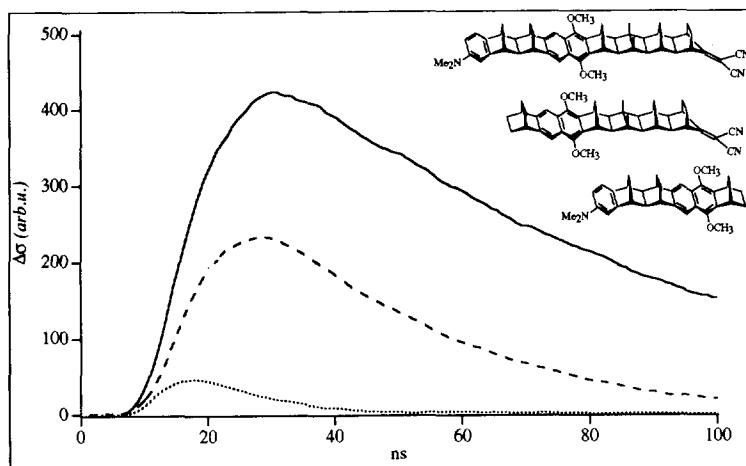
Figure 1.6: TRMC transients of the TRIAD (full line) and DIAD (dashed line) and the D_1-D_2 model compound (dotted line) with the structures as shown in the figure, as synthesized by the group of Paddon-Row.[67]

1.2.2.3 Molecular folding

Flexible σ-bond spacers

As is shown in the previous section, systems containing rigid σ-bond bridged spacers allow photon-induced charge separation to take place very efficiently across extended bridges comprising a large number of saturated bonds. In contrast to this, most of the early research has been carried out on photoexcitation of flexible bichromophoric molecules of the type D-$(CH_2)_n$-A. The results have indicated the formation of states which resemble very closely, those of the sandwich type, π-π exciplexes of the same non-bonded donor and acceptor molecules. This has been attributed to initial local photoexcitation of the donor or acceptor moiety followed by conformational diffusion within the flexible methylene chain, resulting in a statistical close encounter of the D and A moieties. Short range ET can then occur to form the dipolar exciplex in the folded configuration.[68-75] Strong evidence for this mechanism was found for certain D-A systems in the form of a viscosity dependence of the growth of the exciplex-type fluorescence. A classical molecule in this respect is the trimethylene assembly of pyrene and dimethylaniline, $Py(CH_2)_3DMA$, which displays a viscosity dependent growth of exciplex emission over a timescale of nanoseconds in saturated hydrocarbon solvents at room temperature.
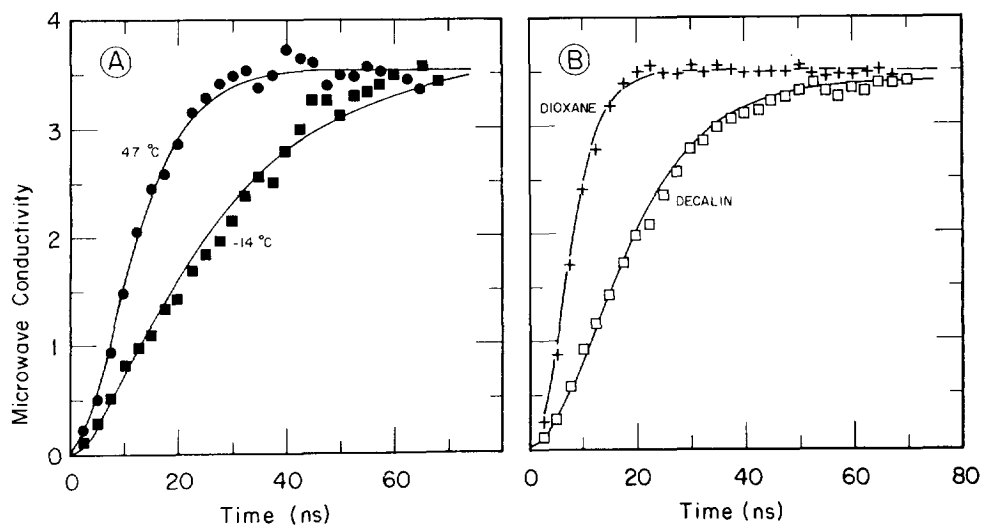
Figure 1.7: Growth of the microwave conductivity on flash-photolysis of $Py(CH_2)_3DMA$: (A) t-decalin solvent at 47 and -14°C; (B) t-decalin and dioxane solvents at room temperature.

If this mechanism is correct then one should observe on photolysis of Py(CH$_2$)$_3$DMA using the TRMC technique, initially, a negligible change in dielectric loss corresponding to local excitation of the pyrene moiety.[76] An increase in loss should subsequently occur as the dipolar exciplex state is formed with molecular folding as the rate controlling step. This delayed growth of the TRMC transient was in fact observed as is shown for a trans-decalin solution of Py(CH$_2$)$_3$DMA in Figure 1.7. Both the rate of growth and decay of the TRMC signal match very closely those found for the fluorescence attributed to the folded exciplex state.

The TRMC results, therefore, provide conclusive evidence that Py(CH$_2$)$_3$DMA after photo-excitation folds up to subsequently give charge separation in hydrocarbon solvents and in particular, that rapid, long-distance ET does not occur in the outstretched configuration, but requires considerable conformational rearrangement. The situation is more complex in polar solvents for which much more rapid development of exciplex and TRMC signal is observed.

Semi-flexible σ-bond spacers

In some cases involving polar solvents and powerful donor/acceptor combinations, it was concluded from time-resolved measurements that ET initially occurs in an extended conformation, followed by folding to yield a more stable folded conformation. This "Coulomb-induced" or "electrostatically-driven" folding subsequent to charge separation has been called harpooning.[77,78]

The first evidence, based on TRMC measurements,[79] that harpooning can occur for semi-rigid DSA compounds was found for the compound with the structure shown in Figure 1.8.
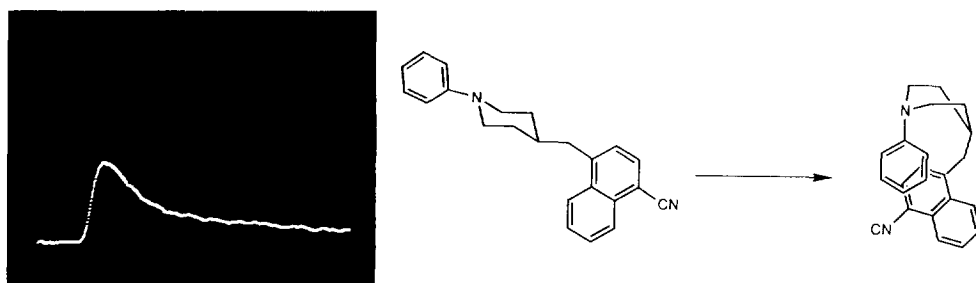
Figure 1.8: Bi-exponential decay of the microwave conductivity of a solution of the compound shown above in trans-decalin at -20 °C (total time 200 ns).

After excitation of the donor or acceptor moiety a charge transfer reaction leads to the subnanosecond formation of a highly dipolar product, which subsequently decays over a timescale of several nanoseconds to yield a longer lived, but less dipolar species. While the final decay was found to be solvent independent with a lifetime of approximately 70 ns, the initial decay displayed a solvent dependent decay time which increased with increasing viscosity and decreasing temperature. A TRMC signal of similar magnitude was observed in dioxane but in this pseudo-polar solvent the decay was found to be monoexponential.

From fluorescence and TRMC measurements it was concluded that in alkane solvents ET between D and A is energetically feasible in the outstretched configuration on a subnanosecond timescale, to be followed, on a timescale of nanoseconds at close to room temperature, by folding up of the molecule under the influence of the Coulomb force as illustrated in Figure 1.8. It is worth noting that this requires inversion of the piperidine ring. In more polar media the extended configuration of the CS state is apparently preferentially stabilized by solvation and by the reduction in the Coulomb force which is necessary to overcome the barrier of ring inversion.

Experiments by Wegewijs et al.[80,81] on the above mentioned compound in a supersonic free jet have shown that the harpooning mechanism also occurs in the gasphase.

1.2.2.4 Charge separated triplet states of σ-bonded donor-acceptor molecules

An example of the solvent dependence of the triplet properties is shown in Figure 1.9 for the compound of Borkent et al.,[82] consisting of a carbazole donor, a tetrachlorophthalimide
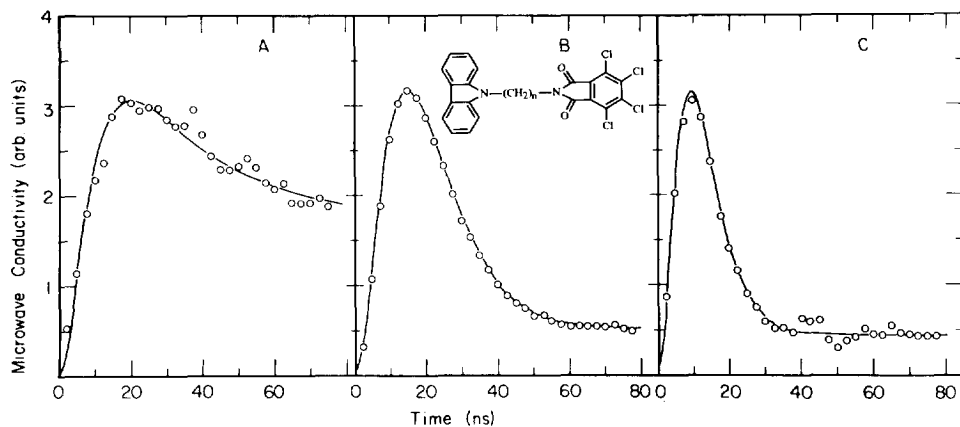
Figure 1.9: The microwave conductivity signals resulting from flash-photolysis of solutions of the tri-methylene compound in (A) cyclohexane, (B) benzene and (C) dioxane. The circles are the experimental data. The full lines are the kinetic fits. The signals have been normalized to give approximately the same height at the signal maximum.

acceptor and a tri-methylene bridging unit. The TRMC traces of the tri-methylene compound in (A) cyclohexane, (B) benzene and (C) dioxane reveal a dramatic decrease in intersystem crossing efficiency.[83] The yield is considerably smaller for benzene (0.06) and dioxane (0.04) than for cyclohexane (0.43). This is a result of the reduced singlet lifetime in going from cyclohexane to benzene to dioxane. The same trend has been found for di- and tetra-methylene bridge compounds. In the case of the hepta-methylene compound, on the other hand, while the singlet lifetime is also found to decrease, the contribution of the triplet remains large and approximately the same in the three solvents, indicating a different mechanism for the formation of the triplet for this compound.

1.2.3 Silicon bond spacers

Though silicon is especially used in polymer chemistry (polysilanes) in the search for photoconducting polymers,[84] the introduction of silicon bond spacers in donor-acceptor compounds has been stimulated by potential applications in the non-linear optics field. Zyss et al.[85] were the first to examine the second harmonic properties of the molecules shown in Figure 1.10.

A detailed description of the binding and delocalization properties of silicon chains is given in reference 84. As for carbon based compounds, also in the silicon compounds there exists σ-conjugation, which is maximized for an all-trans conformation of the bridge. The delocalization and polarizability along the silicon bridges are, however, much larger than for their carbon counterparts. Silicon bridged compounds have therefore the σ-skeleton of σ-bond carbon-carbon bridges but a polarizability approaching that of π-conjugated spacers.[86-91]

A further unique feature of these bridges is that they can act as a donor to photoexcited aromatic moieties. It has been reported that aryldisilanes[92] and arylpolysilanes[93,94] (aryl =

$R = H, (CH_3)_2N, H_3CO$
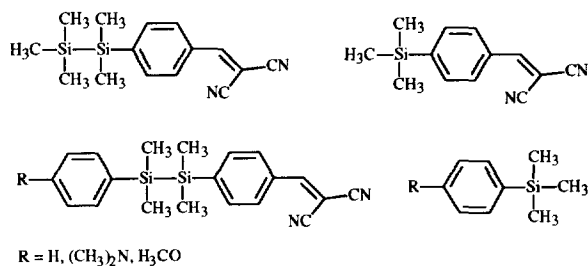
Figure 1.10: A few examples of the silicon compounds studied by Zyss et al.[85,86]

phenyl and naphthyl) exhibit dual fluorescence in polar solvents. One band is assigned to local fluorescence and the other to an intramolecular charge transfer state from the $\sigma(Si$-$Si)$ to the π^* (acceptor) orbitals. The charge transfer is supposed to occur between orthogonal donor and acceptor orbitals and was proposed by Rettig[95] as an example of a TICT state, where the Si-Si bond is suggested to be a donor. Sakurai et al.[92] suggest the term orthogonal internal charge transfer (OICT) states to characterize the existence of the polar low energy (σ-π^*) CS states. Compounds that have only one silicon exhibit no CS fluorescence, owing to the sp^3 hybridization of Si.[86]

1.3 SYMMETRICAL MOLECULES

On photoexcitation of symmetrical molecules with no readily definable donor or acceptor sites ("neutral" molecules) only a "locally excited" singlet state would be expected to be populated. From this state the molecule can convert to the triplet state via intersystem crossing or decay to the ground state, similar to the case of the donor-acceptor molecules. In some special cases, however, charge separation has been found to occur even in symmetrical molecules. Usually a geometrical distortion, such as twisting, is necessary to achieve decoupling of the symmetrical electronic moieties involved in the charge separation process. There has been an increased interest recently in the possibility of symmetrical assemblies of donor and acceptor moieties also having dipolar excited states, because of the potential application in molecular nonlinear optical materials.

The most studied molecule for which this phenomenon occurs is 9,9'-bianthryl, which shows dual fluorescence with one band from a LE state, which is independent of solvent and a second from a CS state which is red-shifted in polar solvents.[96-99] Photophysical and theoretical studies revealed that the CS state has nonequivalent anthracene moieties, A^--A^+, in comparison with the ground state, A-A, which has zero dipole moment.[96-102] The ground state is already *ca* 90° twisted. Pico- and femtosecond measurements have yielded evidence that the ET step leading to A^--A^+, i.e. the symmetry breaking process, is extremely fast at room temperature in fluid solutions, ranging from a few picoseconds in nonhydroxylic solvents to hundreds of pico-seconds in alcohols.[103-110]

Solvatochromic measurements have lead to estimates of a dipole moment of *ca* 20 D for the emissive CS state of bianthryl.[97,101,102,111] Both electrooptical emission measurements[112] and TRMC measurements,[113] which in contrast to the solvatochromic measurements, directly detect the dipole moment, also show a dipole moment of *ca* 20 D. This value indicates the transfer of one electronic charge between the two anthracene moieties.

The symmetry of the system allows the existence of two states (CS and CS') which are

related by reversal of the direction of charge transfer. The time constant for interconversion was determined by Fessenden[114] to be *ca* 10 ps by TRMC measurements, in which the changes in both the real and imaginary components of the conductivity were measured (see Chapter 8).

The induction of (increased) intramolecular charge separation by mutual rotation of parts of a molecule is a topic fraught with controversy whether it comes under the heading of "sudden polarization" involving rotation about an ethylenic double bond or "TICT" involving more subtle rotary motions of the individual chromophoric units.

Theoretical studies predicted that the most stable excited state of even simple, symmetrical ethylene derivatives most probably involves, in addition to partial rotation, complete charge separation across the central carbon carbon bond.[115-124] Sudden polarization in the twisted excited state of symmetrical molecules like tetraphenylethylene (TPE) is only possible, if orbital localization between the two orthogonal π-orbitals can be achieved.[115,117,125] Direct experimental evidence for the "sudden polarization" effect, first proposed by Bonacic-Koutecky et al.,[115] has proven difficult to find. Recently, however, increasing evidence has appeared for the formation of a "zwitterionic" excited state of tetraphenylethylene (TPE).[125,126]

1.4 APPLICATIONS OF PHOTON-INDUCED CHARGE SEPARATION

1.4.1 Solar energy conversion

The importance and complexity of ET reactions in nature have lead many researchers to look for ways to study the fundamental chemistry of these processes in simplified model systems.[58] A significant part of this effort has been devoted to the study of photon-induced charge separation reactions as a means of capturing and storing solar energy. A long-term goal of this research is to develop an understanding of photoinitiated-electron-transfer reactions that is

electromagnetic (solar) energy ⟶ electrical energy ⟶ chemical energy
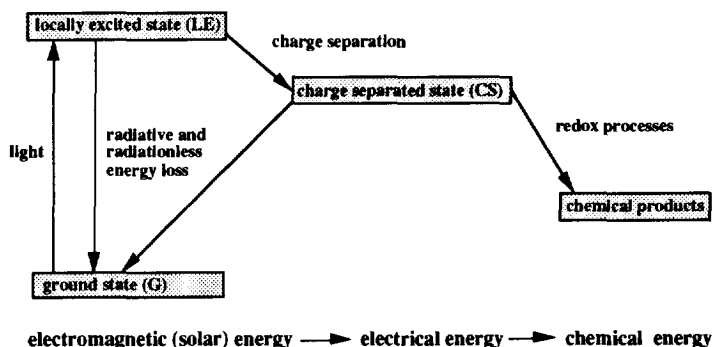
Figure 1.11: Conversion of solar energy into chemical energy.

sufficiently advanced to enable one to design laboratory systems for the conversion of solar energy into electrical and/or chemical potential. In this field the attention is focussed on σ-bond separated donor-acceptor systems, because of their completely charge separated and potentially long-lived excited states. In Figure 1.11 the basic principle of solar energy conversion is depicted.

1.4.2 Nonlinear optics

An indirect application of the ET process is the frequency doubling of laser light using the nonlinear optical properties of donor-acceptor molecules.[5] Photon absorption and the ET reaction itself are not involved in the frequency doubling process, but the interaction between donor and acceptor (asymmetric response of the polarizability) plays a significant role in determining the strength and occurrence of the NLO effect. Until recently attention has been focussed on π-conjugated donor-acceptor molecules. We will however show that σ-bond donor-acceptor systems also may be used to induce frequency doubling. With the same type of materials it is possible to design a wide variety of electro-optical switches, where the change in refractive index as function of an applied external electric field is the basic principle of the switch. An example of such an electro-optical switch (Mach-Zehnder interferometer) is shown in Figure 1.12.
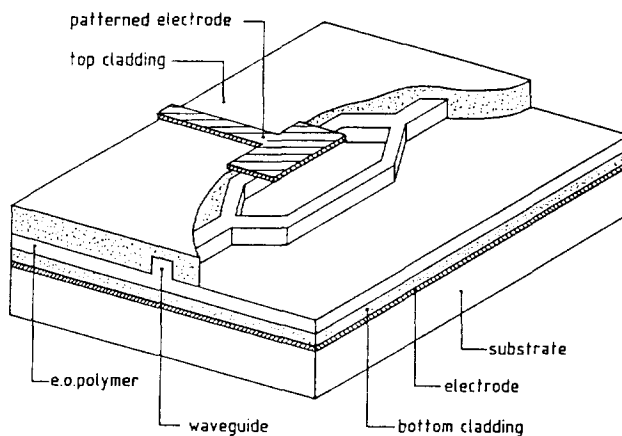
Figure 1.12: Schematic representation of an integrated polymeric Mach-Zehnder interferometer. Without the application of an external electric field light, which propagates in the two channels, will pass through the device. The device is "on". When an external electric field is applied on one of the channels, the refractive index of the NLO material changes, creating a phase difference between the light propagating in the two channels. If the light waves have the opposite phase no light will pass through the device and it is in the "off" position.

1.4.3 Molecular electronics

The scope of molecular electronics ranges from well-defined and well understood phenomena, such as the nonlinear optical response of a single crystal or polymer, to more tantalizing and conceptually difficult areas, that involve designed electrical/electronic response of systems at the individual molecular level. The understanding of the coupling between a system's behaviour on the macroscopic level and the molecular level represent one of the challenges of molecular electronics and is beyond the scope of this thesis. These aspects are to be found in reference 127.

Several theoretical molecular switch models have been presented but the function as a device or molecular switch has not yet been proven in reality.[128-134] A molecular switch is characterized by having two stable states; "on" and "off". Clearly the switching concept can be achieved in donor-acceptor compounds, where the ground state can represent the "off" and the CS state the "on" state.

Using light leads to very fast response times of the switch. The transition between two electronic states of a molecule, resulting from the absorption of a photon, occurs on a timescale on the order of $1/2\pi\nu$, where ν is the frequency in Hz associated with the optical transition.[7] This corresponds to times of only a few tenths of a femtosecond. In such an optically allowed, Franck-Condon transition the spin multiplicity and nuclear coordinates of the molecule remain unchanged. In other words the transition is a "vertical" one within the singlet manifold of states. In the majority of cases the Franck-Condon excited state will relax within a few vibrational periods, corresponding to a few picoseconds or less, to the geometrically equilibrated lowest
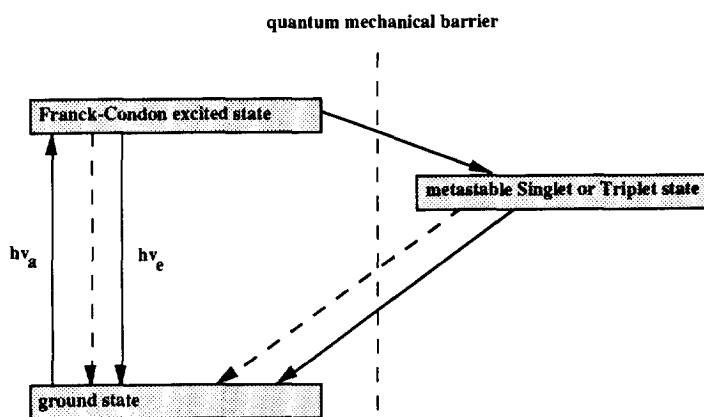
Figure 1.13: General three state model for optical switching.

excited state in the singlet manifold. The eventual return to the ground state then usually occurs either via photon emission or a radiationless transition on a timescale of nanoseconds or less.

In terms of a switch therefore, two-state molecular photoexcitation does have quite good characteristics with an extremely rapid switching time and a large differential, by a factor of a million or more, between the switch-on time and the decay time. For most practical applications, however, the brevity of the latter is a considerable disadvantage. In order to extend the decay time of the "on" state, one is therefore forced to move to three (or more) state systems, as shown in Figure 1.13. Such a third state must be efficiently populated, but extremely weakly coupled to the ground state. This is the case for triplet states of π-conjugated donor-acceptor molecules and the CS states of σ-bond separated donor-acceptor molecules with long spacers.

1.5 EXPERIMENTAL METHODS

1.5.1 Solvatochromic effects

The difference in dipole moment between the ground state and the excited state, $\Delta\mu_*$, of a solute can be derived from the solvent dependence (solvatochromism)[135-138] of the optical absorption and emission frequencies (v_a and v_f) via:

$$v_a - v_f = const + (f-f') [(\Delta\mu_*)^2 / hc\rho^3] \qquad (2)$$

The solvent is considered to be a continous dielectric with a relative dielectric constant $\varepsilon'(0)$ and refractive index n. ρ is the "radius" of the molecules. The difference (f - f') represents a solvent polarity parameter with $f = 2[\varepsilon'(0)-1]/[2\varepsilon'(0)+1]$ and $f' = 2[n^2-1]/[2n^2+1]$. This parameter is only a crude estimate of the solvent/solute interaction, however when the solvents used are carefully selected to eliminate "anomalous", specific interactions, values of dipole moments are determined which are in reasonable agreement with other experimental methods including TRMC. A detailed description of solvatochromic effects is given in reference 135.

1.5.2 Electrochromic effects

Liptay and associates[136] developed the theoretical description of the electric field effect on the absorption and fluorescence of solute molecules. The reader is referred to some review articles on the topic for a fuller survey of the history and literature.[139-141]

Consider a dilute gas of absorbing molecules with ground state dipole moment, μ_0 and excited state dipole moment μ_*. Then if $\mu_0 \neq \mu_*$, a field induced spectral shift Δv of the

31

absorption maximum will result which is dependent on the orientation of the dipole moments relative to the electric field, E:

$$hc\Delta v_a = -\Delta\mu * E \tag{3}$$

Thus, the original absorption spectrum of the molecule without electric field will be red-shifted in an external electric field if the vector $\Delta\mu$ is parallel to E and blue-shifted if anti-parallel. Since in a thermally equilibrated molecular ensemble all molecules are randomly distributed, the electric field causes a symmetric band broadening.

In addition the electric field causes a nonrandom orientation distribution of the molecules in their ground state, in the ensemble. This results in an asymmetric band broadening and therefore in a spectral shift. In solution the same solute/solvent interactions as operating in the solvatochromic shift measurements are important.

The electric field dependence of the fluorescence of a solute is very similar to that for the absorption. The method was developed during the last 15 years by Baumann and coworkers[141-144] and Bischof et al.[145,146]

1.5.3 Time-Resolved Microwave Conductivity (TRMC)

A full description of the TRMC technique is given in Chapter 2. Briefly on laser flash-photolysis small transient changes in the real (dielectric constant) and the imaginary component (dielectric loss) of the permittivity of a medium may occur.[4] These changes in the bulk properties can result from a change in molecular polarizability or in the molecular charge distribution (dipole moment change) respectively. For mainly practical reasons the vast majority of TRMC studies have been applied to the change in dielectric loss of solutions of opto-electric molecules which give a large change in charge distribution on photo-excitation. Recently, however, it has become possible to monitor changes in polarizability which, as will be presented in Chapter 8, can be considerable for symmetrical molecules.

1.5.4 Time-Resolved DC Conductivity

Fast time response, dc photo-current measurements can be used to observe transient changes in intramolecular charge separation.[147] If a molecule that is free to rotate experiences a change in its charge distribution on going from its ground state to an excited state, it will tend to have, on average, different orientations in each of those states with respect to an axis defined by an applied electric field. Since the change in average dipole orientation constitutes a net movement of charge in the field direction, it should be possible to observe such rotational reorientations as

transients currents produced as the molecule is excited and subsequently relaxes. The magnitude and time dependence of the currents can then be used to determine excited state dipole moments if other photophysical properties of the molecule are known.

In this experiment the rotational relaxation time, Θ, is not required, as it is for the TRMC measurements, provided that Θ values are short compared to excited state lifetimes and the time resolution is shorter than Θ. From this experiment it is possible to obtain the value of Θ, by fitting the signal arising from the reorientation of the dipoles in the field after excitation.

A: π-bond conjugated donor-acceptor molecules

$$D^{\delta+} \!\!-\!\! \pi \!-\! A^{\delta-} \quad \xrightarrow[\textit{excitation}]{h\nu} \quad {}^1\!\left(D^{\Delta+} \!\!-\!\! \pi \!-\! A^{\Delta-}\right)^*$$

$${}^1\!\left(D^{\Delta+} \!\!-\!\! \pi \!-\! A^{\Delta-}\right)^* \quad \xrightarrow{\textit{deformation e.g. "twist"}} \quad D^+ \!\!\cdots\!\! \pi \!-\! A^-$$

$${}^1\!\left(D^{\Delta+} \!\!-\!\! \pi \!-\! A^{\Delta-}\right)^* \quad \xrightarrow{\textit{intersystem crossing}} \quad {}^3\!\left(D^{\Delta+} \!\!-\!\! \pi \!-\! A^{\Delta-}\right)^*$$

B: σ-bond separated bichromophoric donor-acceptor molecules

$$D \!-\! \sigma \!-\! A \quad \xrightarrow[\textit{local excitation}]{h\nu} \quad D^* \!\!-\!\! \sigma \!-\! A \text{ or } D \!-\! \sigma \!-\! A^*$$

$$D^* \!\!-\!\! \sigma \!-\! A \quad \xrightarrow[\substack{\textit{electron transfer}}]{\textit{long distance}} \quad D^+ \!\!-\!\! \sigma \!-\! A^-$$

$$D^* \!\!-\!\! \sigma \!-\! A \quad \xrightarrow{\textit{folding}}$$

$$D^+ \!\!-\!\! \sigma \!-\! A^- \quad \xrightarrow[\textit{("harpooning")}]{\textit{folding}}$$

electron transfer

C: σ-bond separated trichromophoric donor-acceptor molecules

$$D_2 \!-\! D_1 \!-\! A^* \quad \xrightarrow{\textit{1}_{st}\textit{ step}} \quad D_2 \!-\! D_1{}^+ \!\!-\!\! A^- \quad \xrightarrow{\textit{2}_{nd}\textit{ step}} \quad D_2{}^+ \!\!-\!\! D_1 \!-\! A^-$$

D: symmetrical donor-acceptor molecules

$$D \!-\! A \!-\! D \quad \xrightarrow{h\nu} \quad D^{\Delta+} \!\!-\!\! A^{\Delta-} \!\!-\!\! D \quad \underset{\textit{switching}}{\overset{\textit{resonant}}{\rightleftharpoons}} \quad D \!-\! A^{\Delta-} \!\!-\!\! D^{\Delta+}$$

E: symmetrical "neutral" molecules

$$N \!-\! N \quad \xrightarrow{h\nu} \quad N^* \!\!-\!\! N \quad \underset{\textit{resonance}}{\overset{\textit{exciton}}{\rightleftharpoons}} \quad N \!-\! N^*$$

$$N^* \!\!-\!\! N \quad \xrightarrow{\textit{charge transfer}} \quad N^+ \!\!-\!\! N^- \quad \underset{\textit{resonance}}{\overset{\textit{charge transfer}}{\rightleftharpoons}} \quad N^- \!\!-\!\! N^+$$

or

$$N \!=\! N \quad \xrightarrow{h\nu} \quad \left(N \!=\! N\right)^*$$

$$\left(N \!=\! N\right)^* \quad \xrightarrow[\textit{twist}]{\textit{double bond}} \quad N^+ \!\!\sim\!\! N^- \quad \underset{\textit{resonance}}{\overset{\textit{charge transfer}}{\rightleftharpoons}} \quad N^- \!\!\sim\!\! N^+$$

Scheme 1.1

1.5 OUTLINE OF THESIS

In Scheme 1.1 the various photophysical processes and the different general types of molecules, which are investigated in this thesis, are presented. Four types of molecules are studied: π-conjugated donor-acceptor molecules (A), σ-bond separated bichromophoric (B) and trichromphoric (C) donor-acceptor molecules, and both symmetrical molecules containing multiple donor and acceptor sites (D) as well as "neutral" symmetrical molecules (E).

In **Chapter 2** the TRMC technique including the background theory, apparatus and data analysis is presented in detail. This is followed, in **Chapter 3**, by a study of the effects of alkyl substitution and solvent on charge separation for a series of dialkylaminobenzonitriles. In **Chapter 4** the influence of the variation of the acceptor strength, the rigidity of the bridge and solvent polarity on the charge separation properties of some rigid and semi-rigid σ-bond bichromophoric donor-acceptor compounds are investigated. In these molecules the aspect of electrostatically-induced folding or "harpooning" is important. **Chapter 5** deals with trichromophoric σ-bond separated donor-donor-acceptor compounds, where two-step charge separation may occur. In **Chapter 6** the non-linear optical properties of some bicromophoric π-conjugated and σ-bond donor-acceptor compounds are compared. **Chapter 7** deals with a special case of charge separation in the symmetrical molecule tetraphenylethylene. For this molecule charge separation induced by twisting around the central double bond is clearly shown to occur. In **Chapter 8**, charge separation in a series of symmetrical molecules is illustrated, whereby switching between resonant dipolar states is important.

1.6 REFERENCES

1   R. Hoffmann, A. Imamura and W.J. Hehre, *J. Am. Chem. Soc.* **1968,** *90,* 1499.
2   R.M. Hoffmann, *Acc. Chem. Res.* **1971,** *4,* 1.
3   F. Schneider and E. Lippert, *Ber. Bunsenges. Phys. Chem.* **1968,** *72,* 1155.
4   M.P. de Haas and J.M. Warman, *Chem. Phys.* **1982,** *73,* 35.
5   D.S. Chemla and J. Zyss in *Nonlinear optical properties of organic molecules and crystals,* Vols. 1,2; Academic Press; New York, **1987.**
6   C. Reichardt in *Solvent Effects in Organic Chemistry;* Verlag Chemie: Weinheim, New York, **1979.**
7   S.A. Jonker, J.M. Warman, M.P. de Haas and M.N. Paddon-Row in *Sensors and Actuators,* Kluwer Technical Books; Enschede, **1990,** 315.
8   J.M. Warman, S.A. Jonker, M.P. de Haas, J.W. Verhoeven and M.P. Paddon-Row, *SPIE Proceedings,* **1991,** *Vol. 1559,* 159.
9   E. Lippert, W. Lüder and H. Boos in *Advances in Molecular Spectroscopy,* Bologna, Italy, **1959;** A. Mangini, Ed.; Pergamon Press; Oxford, U.K., **1962;** 443.
10 E. Lippert, W. Lüder, F. Moll, H. Nagele, H. Boos, H. Prigge and I. Siebold-Blankenstein, *Angew. Chem.* **1969,** *73,* 695.

11 E. Lippert in *Luminescence of Organic and Inorganic Materials*, H.P. Kallmann, G.M. Spruch, Eds.; Wiley: New York, **1962**; 271.

12 E. Lippert in *Organic Molecular Photophysics*, J. Birks, Ed.; Wiley: London, **1975**; Vol. 2, 1.

13 Z.R. Grabowski, K. Rotkiewicz, W. Rubaszewska and E. Kirkor-Kaminska, *Acta. Phys. Pol.* **1978**, *A54*, 767.

14 Z.R. Grabowski, K. Rotkiewicz, A. Siemiarczuk, D.J. Cowley and W. Baumann, *Nouv J. Chim.* **1979**, *3*, 443.

15 W. Rettig, *Angew. Chem., Int. Ed. Engl.* **1986**, *25*, 971.

16 E. Lippert, W. Rettig, V. Bonacic-Koutecky, F. Heisel and J.A. Miehé, *Adv. Chem. Phys.* **1987**, *68*, 1.

17 R.J. Visser, C.A.G.O. Varma, J. Konijnenberg and P. Bergwerf, *J. Chem. Soc., Faraday Trans. 2* **1983**, *79*, 347.

18 R.J. Visser and C.A.G.O. Varma, *J. Chem. Soc., Faraday Trans. 2* **1980**, *76*, 453.

19 M.C.C. de Lange, D.T. Leeson, K.A.B. van Kuijk, A.H. Huizer and C.A.G.O. Varma, *Chem. Phys.* **1993**, *174*, 425-440.

20 U. Leinhos, W. Kühnle and K.A. Zachariasse *J. Phys. Chem.* **1991**, *95*, 2013.

21 A. Carrington and P.F. Todd, *Mol. Phys.* **1963**, *6*, 161.

22 V.F. Starichenko, L.N. Shchegoleva, N.V. Efremova, V.O. Saik and P.V. Schastnev, *Chem. Phys.* **1985**, *100*, 79.

23 G.R. Stevenson, G.C. Wehrmann and R.C. Reiter, *J. Phys. Chem.* **1991**, *95*, 901.

24 C.J. Chen, *J. Chin. Chem. Soc. (Taipei)*, **1989**, *36*, 565.

25 Z.R. Grabowski and J. Dobkowski, *Pure & Appl. Chem.* **1983**, *55*, 245.

26 V. Bonacic-Koutecky and J. Michl, *J. Am. Chem. Soc.* **1985**, *107*, 1765.

27 O.S. Khali, J.L. Meeks and S.P. McGlynn, *Chem. Phys. Lett.* **1976**, *39*, 457.

28 E.M. Kosower and H. Dodiuk, *J. Am. Chem. Soc.* **1976**, *98*, 924.

29 E.A. Chandross and H.T. Thomas, *Chem. Phys. Lett.* **1971**, *9*, 397.

30 R.J. Visser, C.A.G.O. Varma, J. Konijnenberg and P. Bergwerf, *J. Chem. Soc., Faraday Trans. 2* **1983**, *79*, 347.

31 P.C.M. Weisenborn, A.H. Huizer and C.A.G.O. Varma, *Chem. Phys. Lett.* **1989**, *133*, 437.

32 K.A. Zachariasse, Th. von der Haar, A. Hebrecker, U. Leinhos and W. Kühnle *Pure & Appl. Chem.* **1993**, *65*, 1745.

33 V.H. Grassian, J.A. Warren, E.R. Bernstein and H.V. Secor, *J. Phys. Chem.* **1989**, *90*, 3994.

34 T. Kobyashi, M. Futakami and O. Kajimoto, *Chem. Phys. Lett.* **1986**, *130*, 63.

35 E.M. Gibson, A.C. Jones, A.G. Taylor, W.G. Bouwman, D. Philips and J. Sandell, *J. Phys. Chem.* **1988**, *92*, 5441.

36 J. August, T.F. Palmer, J.P. Simons, C. Jouvet and W. Rettig, *Chem. Phys. Lett.* **1988**, *145*, 273.

37 L.W. Peng, M. Dantus, A.H. Zewail, K. Kemnitz, J.M. Hicks and K.B. Eisenthal, *J. Phys. Chem.* **1987**, *91*, 6162.

38 J.M. Warman, M.P. de Haas, A. Hummel, C.A.G.O. Varma and P.H.M. van Zeyl, *Chem. Phys. Lett.* **1982**, *87*, 83.

39 R.W. Fessenden, P.M. Carton, H. Shimamori and J.C. Scaiano, *J. Phys. Chem.* **1982**, *86*, 3803.

40 G.F. Mes, B. de Jong, H.J. van Ramesdonk, J.W. Verhoeven, J.M. Warman, M.P. de Haas and L.E.W. Horsman, *J. Am. Chem. Soc.* **1984**, *106*, 6524.

41 J.M. Warman, M.P. de Haas, M.N. Paddon-Row, E. Cotsaris, N.S. Hush, H. Oevering and J.W. Verhoeven, *Nature* **1986**, *320*, 615.

42 J.M. Warman, K.J. Smit, M.P. de Haas, S.A. Jonker, M.N. Paddon-Row, A.M. Oliver, J. Kroon, H. Oevering and J.W. Verhoeven, *J. Phys. Chem.* **1991**, *128*, 95.

43   M.N. Paddon-Row, M.J. Shephard and K.J. Jordan, *J. Phys. Chem.* **1993**, *97*, 1743.

44   L.T. Calcaterra, G.L. Closs and J.R. Miller, *J. Am. Chem. Soc.* **1983**, *105*, 670.

45   J.R. Miller, L.T. Calcaterra and G.L. Closs, *J. Am. Chem. Soc.* **1984**, *106*, 3047.

46   P. Pasman, G.F. Mes, N.W. Koper and J.W. Verhoeven, *J. Am. Chem. Soc.* **1985**, *107*, 5839.

47   A.D. Joran, B.A. Leland, P.M. Felker, A.H. Zewail, J.J. Hopfield and P.B. Dervan,
     J. Phys. Chem. **1985**, *89*, 557.

48   M.R. Wasielewski, M.P. Niemczyk, D.G. Johnson, W.A. Svec and D.W. Minsek,
     Tetrahedron **1989**, *45*, 4785.

49   C.A. Stein, N.A. Lewis and G. Seitz, *J. Am Chem. Soc.* **1982**, *104*, 2596.

50   B.P. Paulson, K. Pramod, P. Eaton, G. Closs and J.R. Miller, *J. Phys. Chem.* **1993**, *50*, 13042.

51   K.W. Penfield, J.R. Miller, M.N. Paddon-Row, E. Cotsaris, A.M. Oliver and N.S. Hush,
     J. Am. Chem. Soc. **1987**, *109*, 5061.

52   H. Oevering, M.N. Paddon-Row, M. Heppener, A.M. Oliver, E. Cotsaris, J.W. Verhoeven and N.S. Hush,
     J. Am. Chem. Soc. **1987**, *109*, 3528.

53   A.M. Oliver, D.C. Graig, M.N. Paddon-Row, J. Kroon and J.W. Verhoeven,
     Chem. Phys. Lett. **1988**, *150*, 366.

54   J. Kroon, J.W. Verhoeven, M.N. Paddon-Row and A.M. Oliver,
     Angew. Chem., Int. Ed. Engl. **1991**, *30*, 1358.

55   R. Gleiter, *Angew. Chem., Int. Ed. Engl.* **1974**, *13*, 696.

56   M.N. Paddon-Row, *Acc. Chem. Res.* **1982**, *15*, 245.

57   M.R. Wasielewski, *Chem. Rev.* **1992**, *92*, 435.

58   M.R. Wasielewski in *Photoinduced electron transfer*, M.A. Fox and M. Chanon, Eds.; Vol.1, **1988**, 161-206

59   G.L. Closs, L.T. Calcaterra, N.J. Green, K.W. Penfield and J.R. Miller, *J. Phys. Chem.* **1986**, *90*, 3673.

60   J.R. Miller, *New J. Chem.* **1987**, *11*, 83.

61   G.L. Closs and J.R. Miller, *Science* **1988**, *240*, 440.

62   M.D. Johnson, J.R. Miller, N.J. Green and G.L. Closs, *J. Phys. Chem.* **1989**, *93*, 1173.

63   B. Paulson, K. Pramod, P. Eaton, G. Closs and J.R. Miller, *J. Phys. Chem.* **1993**, *97*, 13042.

64   J.R. Miller, J.V. Beitz and R.K. Huddleston, *J. Am. Chem. Soc.* **1984**, *106*, 5057.

65   D. Gust, T.A. Moore, A.L. Moore, S.J. Lee, E. Bittersmann, D.K. Luttrul, A.A. Rehms, J.M. DeGraziano,
     X.C. Ma, F. Gao, R.E. Belford and T.T. Trier, *Science* **1990**, *248*, 199.

66   M.R. Wasielewski, G.L. Gaines, M.P. O'Neil, M.P. Niemczyk and W.A. Svec,
     J. Am. Chem. Soc. **1990**, *112*, 4559.

67   J.M. Lawson, M.N. Paddon-Row, W. Schuddeboom, J.M. Warman, A.H.A. Clayton and K.P. Ghiggino,
     J. Phys. Chem. **1993**, *97*, 13099.

68   M. Migita, T. Okada, N. Mataga, Y. Sakata, S. Misumi, N. Nakashima and K. Yoshihara,
     Bull. Chem. Soc. Japan **1981**, *54*, 3304.

69   T. Okada, T. Saito, N. Mataga, Y. Sakata and S. Misumi, *Bull. Chem. Soc. Japan* **1977**, *50*, 331.

70   F.C. de Schryver, N. Boens and J. Put, *Adv. Photochem.* **1977**, *10*, 359.

71   N. Mataga and M. Ottolenghi in *Molecular Association Vol. 2*, R. Foster Ed.; Academic Press:
     New York, **1978**, 1.

72   N.C. Yang, D.W. Minesk, D.G. Johnson and M.R. Wasielewski in *Photochemical energy conversion*,
     J.R. Norris Jr and D. Meisel, Eds.; Elsevier, Amsterdam, **1989**, 111.

73   K. Nakatani, T. Okada, N. Mataga, F.C. De Schryver and M. van der Auweraer,
     Chem. Phys. Lett. **1988**, *145*, 81.

74   H. Yao, T. Okada and N. Mataga, *J. Phys. Chem.* **1989**, *93*, 7388.

75 H. Staerk, R. Mitzkus, W. Kühnle and A. Weller in *Picoseconds phenomena Vol. 3*, K.B. Eisenthal, R.M. Hochstrasser, W. Kaiser and A. Laubereau, Eds.; Springer, Berlin, **1982**, 205.

76 J.M. Warman, S.A. Jonker, W. Schuddeboom, M.P. de Haas, M.N. Paddon-Row, J.W. Verhoeven and K.A. Zachariasse, *Pure & Appl. Chem.* **1993**, *65*, 1723.

77 M. Polyani in *Atomic reactions*, Williams and Notgate; London, **1932**.

78 J.L. Magee, *J. Chem. Phys.* **1940**, *8*, 687.

79 B. Wegewijs, R.M. Hermant, J.W. Verhoeven, M.P. de Haas and J.M. Warman, *Chem. Phys. Lett.* **1990**, *168*, 185.

80 B. Wegewijs, R.M. Hermant, J.W. Verhoeven, A.M. Kunst and R.P.H. Rettschnick, *Chem. Phys. Lett.* **1987**, *140*, 587.

81 J. Jortner, M. Bixon, B. Wegewijs, J.W. Verhoeven and R. Rettschnick, *Chem. Phys. Lett.* **1993**, *205*, 451.

82 J.H. Borkent, A.W.J. de Jong, J.W. Verhoeven and T.J. de Boer, *Chem. Phys. Lett.* **1978**, *57*, 530.

83 K.J. Smith and J.M. Warman, *J. Lumin.* **1988**, *42*, 149.

84 R.D. Miller and J. Michl, *Chem. Rev.* **1989**, *89*, 1359.

85 G. Mignani, M. Barzoukas, J. Zyss, G. Soula, F. Balegroune, D. Granjean and D. Josse, *Organometallics* **1991**, *10*, 3660.

86 G. Mignani, A. Krämer, G. Pucetti, I. Ledoux, G. Soula, J. Zyss and R. Meyrueix, *Organometallics* **1990**, *9*, 2640.

87 M. Fuzino, *Chem. Phys. Lett.* **1987**, *136*, 451.

88 R. Kepler, *Synth. Met.* **1989**, *28*, C573.

89 H. Sakurai, *J. Organometal. Chem.* **1980**, *200*, 261.

90 A. Bassindale and P. Taylor in *The Chemistry of Organic Silicon Compounds*, S. Patai and Z. Rappoport, Eds.; J. Wiley & Sons, New York, **1989**, Chapter 4, 893.

91 I. Ledoux, *Synth. Met.* **1993**, *54*, 123.

92 H. Sakurai, H. Sugiyama and M. Kira, *J. Phys. Chem.* **1990**, *94*, 1837.

93 M. Ishikawa and M. Kumada, *Adv. Organometal. Chem.* **1981**, *19*, 51.

94 H. Hiratsuka, Y. Mori, M. Ishikawa, K. Okazaki and H. Shizuka, *J. Chem. Soc., Faraday Trans. 2* **1985**, *81*, 1665.

95 W. Rettig, *Angew. Chem., Int. Ed. Engl.* **1986**, *25*, 971.

96 F. Schneider and E. Lippert, *Ber. Bunsenges. Phys. Chem.* **1968**, *72*, 1155.

97 F. Schneider and E. Lippert, *Ber. Bunsenges. Phys. Chem.* **1970**, *74*, 624.

98 E.M. Kosower and K. Tanizawa, *Chem. Phys. Lett.* **1972**, *16*, 419.

99 W. Rettig and W. Baumann in *Progress in Photochemistry and Photophysics*, J.F. Rabek, Ed.; CRC press: Boca Raton, London, **1990**, Chapter 3, 79.

100 H. Beens and A. Weller, *Chem. Phys. Lett.* **1969**, *3*, 666.

101 N. Nakashima, M. Murakawa and N. Mataga, *Bull. Chem. Soc. Jpn.* **1976**, *49*, 854.

102 W. Rettig and M. Zander, *Ber. Bunsenges. Phys. Chem.* **1983**, *87*, 1143.

103 T.J. Kang, M.A. Kahlow, D. Giser, S. Swallen, V. Nagarajan, W. Jarzeba and P.F. Barabara, *J. Phys. Chem.* **1988**, *92*, 6800.

104 M.A. Kahlow, T.J. Kang and P.F. Barabara, *J. Phys. Chem.* **1987**, *91*, 6452.

105 P.F. Barabara and W. Jarzeba, *Adv. Photochem.* **1990**, *15*, 1.

106 T.J. Kang, W. Jarzeba, P.F. Barabara and T. Fonseca, *Chem. Phys.* **1990**, *149*, 81.

107 N. Mataga, H. Yao, T. Okada and W. Rettig, *J. Phys. Chem.* **1989**, *93*, 3383.

108 H. Lueck, M. Windsor and W. Rettig, *J. Phys. Chem.* **1990**, *94*, 4550.

109 M. Marconelli and G.R. Flemming, *J. Chem. Phys.* **1987**, *86*, 6221.

110 M. Marconelli and G.R. Flemming, *J. Chem. Phys.* **1990**, *92*, 3251.

111 M. Zander and W. Rettig, *Chem. Phys. Lett.* **1984**, *110*, 602.

112 W. Baumann, E. Spohr, H. Bischof and W. Liptay, *J. Lumin.* **1987**, *87*, 1143.

113 R.J. Visser, P.C.M. Weisenborn, P.J.M. van Kan, B.H. Huizer, C.A.G.O. Varma, J.M. Warman and M.P. de Haas, *J. Chem. Soc. Faraday Trans. II* **1985**, *81*, 689.

114 T.B. Toublanc, R.W. Fessenden and A. Hitachi, *J. Phys. Chem.* **1989**, *93*, 2893.

115 V. Bonacic-Koutecky, P. Bruckmann, P. Hiberty, J. Koutecky, C. Leforestier and L. Salem, *Angew. Chem., Int. Ed. Engl.* **1975**, *14*, 575-576.

116 L. Salem and P. Bruckmann, *Nature* **1975**, *258*, 526-528.

117 L. Salem, *Science* **1979**, *191*, 822-830.

118 R.J. Beunker, S.D. Peyerimhoff, *Chem. Phys.* **1976**, *9*, 75-89.

119 V. Bonacic-Koutecky, *J. Am. Chem. Soc.* **1978**, *100*, 396-402.

120 V. Bonacic-Koutecky, J. Cizek, D. Dohnert and J. Koutecky, *J. Chem. Phys.* **1978**, *69*, 1168-1176.

121 B.R. Brooks and H.F. Schaefer, *J. Am. Chem. Soc.* **1979**, *101*, 307-311.

122 I. Nebot-Gil and J-P. Malrieu, *Chem. Phys. Letters* **1981**, *84*, 571-574.

123 I. Nebot-Gil and J-P. Malrieu, *J. Am. Chem. Soc.* **1982**, *104*, 3320-3325.

124 V. Bonacic Koutecky, J. Koutecky and J. Michl, *Angew. Chem., Int. Ed. Engl.* **1987**, *26*, 170-189.

125 C.L. Schilling and E.F. Hilinski, *J. Am. Chem. Soc.* **1988**, *110*, 2296-2298.

126 J. Morais, J. Ma and M.B. Zimmt, *J. Phys. Chem.* **1991**, *95*, 3885-3888.

127 C.A. Mirkin and M.A. Ratner, *Ann. Rev. Phys. Chem.* **1992**, *43*, 719.

128 A. Broo, *Chemical Physics*, **1993**, *169*, 135.

129 A. Aviram and M.A. Ratner, *Chem. Phys. Lett.* **1974**, *29*, 277.

130 A. Aviram, *J. Am. Chem. Soc.* **1988**, *110*, 5687.

131 N.S.A.T. Wong, G.B. Bacskay and J.R. Reimers, *J. Am. Chem. Soc.* **1990**, *112*, 4192.

132 C. Joachim and J.P. Launay, *J. Mol. Electron* **1990**, *6*, 37.

133 J.J. Hopfield, J.N. Onuchic and D.N. Beratan, *J. Phys. Chem.* **1989**, *93*, 6350.

134 F.L. Garter in *Molecular electronic devices*, Dekker; New York, **1982**.

135 C. Reichardt in *Solvent Effects in Organic Chemistry;* Verlag Chemie: Weinheim, New York, **1979**.

136 W. Liptay in *Excited States;* E.C. Lim, Ed.; Academic: New York, **1974**; Vol. 1, 129.

137 W. Liptay in *Modern Quantum Chemistry;* O. Sinanoglu, Ed.; Academic: New York, **1965**; Part II, 173.

138 W. Liptay in *Z. Naturforsch.* **1965**, *20a*, 1441.

139 W. Liptay, *Z. Naturforsch.* **1965**, *20a*, 272.

140 W. Baumann and H. Deckers, *Ber. Bunsenges. Phys. Chem.* **1977**, *81*, 786.

141 W. Baumann in *Physical Methods of Chemistry, Vol III, Determination of Chemical Composition and Molecular Structure*, B.W. Rossiter and J.F. Hamilton, Eds.; John Wiley & Sons, New York, **1989**.

142 H. Deckers and W. Baumann, *Ber. Bunsenges. Phys. Chem.* **1977**, *81*, 795.

143 W. Baumann and H. Bischof, *J. Mol. Struct.* **1982**, *84*, 181.

144 W. Baumann and H. Bischof, *J. Mol. Struct.* **1985**, *129*, 125.

145 H. Bischof, W. Baumann, N. Detzer and K. Rotkiewicz, *Chem. Phys. Lett.* **1985**, *116*, 180.

146 H. Bischof and W. Baumann, *Z. Naturforsch.* **1985**, *40a*, 874.

147 S.S. Brown and C.L. Braun, *J. Phys. Chem.* **1991**, *95*, 511.

Chapter 2

The Time-Resolved Microwave Conductivity (TRMC) Technique:

Theory, Apparatus and Data Analysis

2.1 INTRODUCTION

The interaction of the electric field component of microwaves with a weakly conducting, low loss dielectric medium results in absorption of microwave energy and a phase shift of the microwaves (see Figure 2.1).[1,2] These effects have been used to investigate the properties and kinetics of charge carriers from as early as 1949.[3] Initially, the technique was used to study the attachment, recombination and thermalization of high-mobility electrons in pulse irradiated gases[4,5] and electrons and holes in solid-state semi-conductor materials.[6,7] The majority of these studies of high mobility electronic charge carriers made use of the phase-shift because of the relatively large change in the real part of the permittivity, ε. In the early seventies the Time-Resolved Microwave Conductivity (TRMC) technique, in which the dielectric loss component of ε is monitored, was applied to the study of low mobility charge carriers in molecular liquids. By approximately 1975 the sensitivity and time response had increased sufficiently to investigate[8-16] the geminate decay of molecular ions formed on nanosecond pulsed irradiation
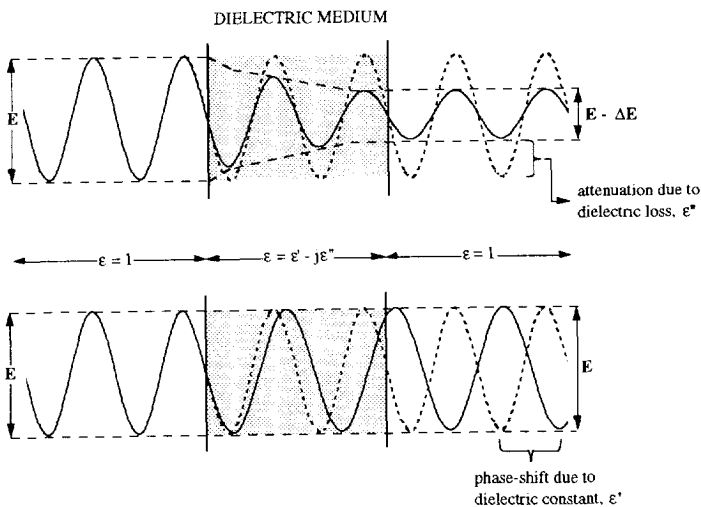
Figure 2.1: Absorption (upper part) and phase-shift (lower part) of microwaves propagating through a weakly conducting medium, due to the dielectric loss ε'' and the dielectric constant ε' respectively.

41

of hydrocarbon liquids. Such incomplete intermolecular geminate charge separation cannot readily be observed using more conventional ac and dc conductivity detection techniques. This aspect of the use of the TRMC method is the more important since very often in condensed media only a small fraction of ionizing events leads to complete charge separation.

In 1979 it was shown by Fessenden et al.[17] that radicals generated by modulated light could also be detected by observing the microwave absorption resulting from changes in the dipole moment of the photo-absorbing species in solution. A few years later this technique was developed by Warman and de Haas[18,19] and by Fessenden et al.[20] into a time-resolved version with the use of pulsed laser light for generation of the transients. Using this flash-photolysis variety of TRMC it was possible to study changes in the intramolecular charge separation in excited singlet and triplet states. The technique has also been used, to a lesser extent, to study photoionization[21-23] and photodissociation.[24,25]

While useful simply as an additional fast detection technique for reactive intermediates formed on flash photolysis, the full potential of TRMC lies in the possibility of gaining quantitative information about the charge distribution of short-lived species. Conversely, if information about the charge distribution of a species is known or can be assumed then quantitative information about the photophysical processes leading to its formation can be derived. In addition to the fact that both dipolar singlet and triplet excited states can be detected in a single experiment, a big advantage is that dipolar charge transfer states can be detected even if they don't fluoresce. On the other hand molecules which fluoresce but undergo no dipole moment change on photoexcitation will be invisible to TRMC detection. The combined application of both TRMC and fluorescence techniques is clearly to be preferred. In the majority of the studies reported, complementary steady-state and time-resolved fluorescence measurements have been carried out either by collaborating groups or using our own system.

In this chapter we will present the important features of the TRMC technique as applied to dipole moment changes of molecules in solution together with a brief theoretical background. We also describe a recently constructed time-resolved fluorescence apparatus used for the determination of excited state lifetimes in particular in cases when these are much shorter than the 5-ns time response of the TRMC equipment. Some useful reviews and extended papers on the applications of TRMC are to be found in references 19, 20 and 26-34.

2.2 BACKGROUND THEORY

The theoretical background to what follows is to be found in numerous basic textbooks on the transmission characteristics of microwaves.[35-39]

2.2.1 General considerations

Three extreme types of charge carrier which can interact with microwaves may be distinguished: (a) quasi-free carriers, which spend most of their time in "free flight" over many molecular diameters between collisions, usually ions or electrons in low-density gases and electronic species in certain "high mobility" condensed media. (b) localized carriers, for which the motion occurs via random displacements over distances on the order of molecular dimensions, as is the case for molecular ions in liquids and glasses or polarons in crystalline solids diffusing by charge hopping. (c) restricted carriers, where the positive and negative centres are in some way limited in their freedom to move in the field, as for example in Coulomb-correlated ion pairs or covalently linked molecular dipoles.

We will from now on focus on the last mentioned type with the correlated charges located on a single molecule. In this special case, the action of an electric field on the rigid dipole is to perturb the otherwise random orientational distribution resulting in a slight preference for those orientations in the field direction which are energetically more favourable. The orienting force of the field is in competition with thermally induced rotational motion which tends to nullify preferential orientations. For a single randomization process this will be characterized by a single dipole relaxation time Θ, which in most cases is equal to the rotational relaxation time, Θ_R, of the molecule perpendicular to the axis of the dipole. Immediately after application of a field, a current will flow due to the work done in perturbing this random orientation of dipoles. This current will be exponentially damped with a time constant Θ, and for times significantly in excess of Θ no net current will be observed.

Since in normal liquids the relaxation times are expected to be much shorter than normal macroscopic observation times even for relatively large molecules, the dc conductivity of dipolar species is usually taken to be effectively zero. In highly viscous media, however, or using fast time resolution techniques, it should be possible to observe conductivity transients due to the formation of dipolar species resulting on pulsed irradiation, even using constant voltage methods. This has, in fact, been demonstrated recently by Braun et al.[40]

When the frequency of the applied field is on the order of or faster than the relaxation frequency $1/\Theta$, a continuous current will be induced which is in phase with the electric field. This corresponds to a dielectric loss of the medium. There will also be a component of the dipolar motion which is out of phase with the field corresponding effectively to an increase in the dielectric constant. These joint effects are discussed in terms of the overall complex permittivity of a solution.

2.2.2 The complex permittivity or conductivity

The propagation of electromagnetic waves in a dielectric material is controlled by the relative permittivity of the medium, $\varepsilon(\omega)$ with ω (= $2\pi f$) the radian frequency of the waves. $\varepsilon(\omega)$ is a complex number with a real component, the relative dielectric constant $\varepsilon'(\omega)$, and an imaginary component, the dielectric loss $\varepsilon''(\omega)$:

$$\varepsilon(\omega) = \varepsilon'(\omega) - j\varepsilon''(\omega) \tag{1}$$

The dielectric constant determines the phase or wavelength of the waves relative to that in vacuum and the dielectric loss determines the attenuation of the amplitude of the wave as it passes through the material. This is illustrated in Figure 2.1.

The theory of dielectrics has been almost exclusively discussed in the past in terms of the polarizability of a medium and the resulting permittivity $\varepsilon(\omega)$. However, when the effects being studied are the result of the movement of charged centres in the electric field of the wave, as is usually the case in TRMC studies, then the complex conductivity, $\sigma(\omega)$, rather than the permittivity is often more appropriate since the real component of the complex conductivity corresponds to charge motion in phase with the electric field and the imaginary component to motion of charge out of phase with the field. The real component of the conductivity is associated with frictional energy loss to the medium and hence attenuation of the wave. The complex conductivity and permittivity are directly related by equation (2) in which ε_0 is the permittivity of vacuum (8.85×10^{-12} F/m):

$$\sigma(\omega) = j\omega\varepsilon_0\varepsilon(\omega) \tag{2a}$$
$$= \omega\varepsilon_0\varepsilon''(\omega) + j\omega\varepsilon_0\varepsilon'(\omega) \tag{2b}$$
$$= \sigma'(\omega) + j\sigma''(\omega) \tag{2c}$$

This often results in confusion because of the fact that the real component of the conductivity corresponds to the imaginary component of the permittivity, i.e.:

$$\sigma'(\omega) = \omega\varepsilon_0\varepsilon''(\omega) \tag{3}$$

In subsequent sections the symbol σ refers to the real component of the conductivity, $\sigma'(\omega)$ as given by equation (3), unless clearly stated otherwise.

2.2.3 A dilute solution of dipoles

In this work we are interested in the change in the permittivity (conductivity) of a nonpolar solvent due to the presence of a low concentration of dipolar solute molecules. Debye[41] derived equation (4) for the condition that the permittivity has contributions from electronic polarization and dipole orientation:

$$\varepsilon(\omega) = \varepsilon(\infty) + [\varepsilon(0) - \varepsilon(\infty)]/[1 + j\omega\Theta] \tag{4}$$

In equation (4), $\varepsilon(\infty)$ is the "infinite" frequency permittivity with infinite usually taken to correspond to the optical region of the electromagnetic spectrum, i.e. $\omega > 10^{15}$ s^{-1} so that $\varepsilon(\infty)$ $\approx n^2$ where n is the refractive index; $\varepsilon(0)$ is the zero frequency permittivity commonly referred to as the "dielectric constant"; and Θ is the dipole relaxation time i.e. the mean time for randomization of any net dipolar orientation in an ensemble of dipoles. Equation (4) was derived on the assumption of a single, exponential dipolar relaxation process. This condition should apply to most of the systems studied in this thesis since they involve dilute solutions of dipolar molecules in low viscosity, nonpolar solvents. See Section 2.5 for a fuller discussion of this topic.

The dipole contribution to $\varepsilon(\omega)$ is seen to be:

$$\Delta\varepsilon(\omega) = [\varepsilon(0) - \varepsilon(\infty)]/[1 + j\omega\Theta] \tag{5}$$

Multiplying top and bottom of equation (5) by $(1 - j\omega\Theta)$, the real and imaginary contributions are found to be:

$$\Delta\varepsilon'(\omega) = [\varepsilon(0) - \varepsilon(\infty)]/[1 + (\omega\Theta)^2] \tag{6}$$

$$\Delta\varepsilon''(\omega) = \omega\Theta[\varepsilon(0) - \varepsilon(\infty)]/[1 + (\omega\Theta)^2] \tag{7}$$

and they are simply related by:

$$\Delta\varepsilon''(\omega)/\Delta\varepsilon'(\omega) = \omega\Theta \tag{8}$$

Various attempts have been made to relate the dipolar permittivity component $[\varepsilon(0) - \varepsilon(\infty)]$ to the microscopic properties of the solute molecules. The difficulty lies in the estimation of the local field experienced by the solute which is an interplay between the external applied field, the

45

molecular dipole and the local dipole-induced polarization of the solvent. Using the Lorentz (L) and Onsager (O) local field formulations the following relationships to the solute concentration, N, and its dipole moment, μ, have been derived:[42-46]

$$[\varepsilon(0) - \varepsilon(\infty)]_L = [\varepsilon(0) + 2][\varepsilon(\infty) + 2]N\mu^2/27\varepsilon_0 k_B T \qquad (9)$$

$$[\varepsilon(0) - \varepsilon(\infty)]_O = [\varepsilon(\infty) + 2]^2\varepsilon(0)N\mu^2/[2\varepsilon(0) + \varepsilon(\infty)]9\varepsilon_0 k_B T \qquad (10)$$

All of the TRMC measurements are carried out in nonpolar solvents for which $\varepsilon(\infty)$ is very close to n^2 and dipolar losses, if any, are extremely small. Also the concentration of dipolar ground- or excited state solute molecules is such that the resulting change in ε due to their presence is always considerably less than 1%. Accordingly, for our purposes we can substitute in equations (9) and (10) for $\varepsilon(0) \approx \varepsilon(\infty)$ which results in both cases in equation (11):

$$[\varepsilon(0) - \varepsilon(\infty)] = [\varepsilon(\infty) + 2]^2 N\mu^2/27\varepsilon_0 k_B T \qquad (11)$$

It is worth stressing that this result is independent of the model used for the local field. For solvents for which $\varepsilon(0) = \varepsilon(\infty)$ is not a good approximation, equations (9) and (10) do of course lead to large differences in the expected dipolar contribution; for example by approximately a factor of 2 for $\varepsilon(0) = 10$.

We can now substitute for $[\varepsilon(0) - \varepsilon(\infty)]$ from equation (11) in equation (7) to obtain an expression for the change in the dielectric loss due to the presence of dipolar molecules with dipole moment μ and dipole relaxation time Θ:

$$\Delta\varepsilon''(\omega) = \omega\Theta[\varepsilon(\infty) + 2]^2 N\mu^2/27\varepsilon_0 k_B T[1 + (\omega\Theta)^2] \qquad (12)$$

or in terms of the conductivity,

$$\Delta\sigma = \omega^2\Theta[\varepsilon(\infty) + 2]^2 N\mu^2/27 k_B T[1 + (\omega\Theta)^2] \qquad (13)$$

$$= [\varepsilon(\infty) + 2]^2 N\mu^2 F(\omega\Theta)/27 k_B T\Theta \qquad (14)$$

with $F(\omega\Theta) = (\omega\Theta)^2/[1 + (\omega\Theta)^2]$ $\qquad (15)$

Equations (14) and (15) have been the most frequently used in discussions of TRMC results.[19]

A term that was introduced at an early stage[19] to facilitate presentation of TRMC data was the rotational charge mobility of a dipolar species, M. This is related to the conductivity in the same way as the mobility of freely diffusing charge carriers:

$$\Delta\sigma = eNM \qquad (16)$$

so that:

$$M = [\varepsilon(\infty) + 2]^2 \mu^2 F(\omega\Theta)/27 e k_B T\Theta \qquad (17)$$

The aim of the TRMC experiments is to measure the change in the conductivity of a solution resulting from photoexcitation of solute molecules. For the simplest case of the formation of a concentration N_* of a single excited state with dipole moment μ_* the change in conductivity should be given by equations (18) and (19):

$$\Delta\sigma_* = eN_*[M_* - M_0] \qquad (18)$$

$$= [\varepsilon(\infty) + 2]^2 N_*\{[\mu_*{}^2 F(\omega\Theta_*)/\Theta_*] - [\mu_0{}^2 F(\omega\Theta_0)/\Theta_0]\}/27 k_B T \qquad (19)$$

In equation (19) account is taken of the fact that the ground- and excited states could have different dipole relaxation times. This can occur if the dipolar axis or molecular geometry change significantly on excitation, or if processes other than rotational diffusion are responsible for relaxation. In many cases studied however it is reasonable to assume $\Theta_* \approx \Theta_0 = \Theta$ which results in a simplified version of equation (19):

$$\Delta\sigma_* = [\varepsilon(\infty) + 2]^2 N_*[\mu_*{}^2 - \mu_0{}^2]F(\omega\Theta)/27 k_B T\Theta \qquad (20)$$

Another case for which a simplified version of equation (19) applies is when the ground state has zero dipole moment resulting in equation (21):

$$\Delta\sigma_* = [\varepsilon(\infty) + 2]^2 N_*\mu_*{}^2 F(\omega\Theta_*)/27 k_B T\Theta_* \qquad (21)$$

Equation (21) can be used to obtain an order-of-magnitude estimate of the values of $\Delta\sigma_*$ that might be expected in a flash-photolysis experiment. Taking N_* to be 10 micromolar (6×10^{21} molecules/m^3), μ_* to be 20 debye (67×10^{-30} Cm) and $\Theta = 200$ ps at X-band (10^{10} Hz)

frequencies, $\Delta\sigma_* = 2 \times 10^{-5}$ S/m. This corresponds to $\Delta\varepsilon" = 3.6 \times 10^{-5}$, which indicates the high sensitivity required of any time-resolved permittivity detection technique.

In later sections the method used to detect such small changes in $\varepsilon"$ will be presented.

2.2.4 Changes in polarizability and ε'

As pointed out in the previous section, a change in the dipole moment of a solute molecule can also result in a change in the real component of the permittivity. This dipolar contribution to $\Delta\varepsilon'$ can be derived from the equations in the previous section to be:

$$\Delta\varepsilon_D' = [\varepsilon(\infty) + 2]^2 N_* \{ [\mu_*^2 F(\omega\Theta_*)/\Theta_*^2] - [[\mu_0^2 F(\omega\Theta_0)/\Theta_0^2] \} 27\omega^2 \varepsilon_0 k_B T \qquad (22)$$

This change in ε' will however only be appreciable if the dipole relaxation time is of the same order of magnitude or shorter than the reciprocal radian frequency of the electric field.

A second contribution to a change in ε' can arise if a pronounced change in the electronic polarizability of a molecule, $\Delta\alpha_e$, occurs on photoexcitation. This will be given by the expression:

$$\Delta\varepsilon_e' = [\varepsilon(\infty) + 2]^2 N_* \Delta\alpha_e/9\varepsilon_0 \qquad (23)$$

The total change will be given by the sum of these two terms

$$\Delta\varepsilon' = \Delta\varepsilon_e' + \Delta\varepsilon_D' \qquad (24)$$

which for the case of a molecule with zero ground state dipole moment results in:

$$\Delta\varepsilon' = [\varepsilon(\infty) + 2]^2 N_* \{ \Delta\alpha_e + \mu_*^2/[1 + (\omega\Theta_*)^2] 3k_B T \}/9\varepsilon_0 \qquad (25)$$

The molecular polarization, p, is related to the polarizability by

$$p = \Delta\alpha_e/3\varepsilon_0 \qquad (26)$$

p has the units of volume with the absolute value expected to be close to the volume of the electronic clouds of a molecule[43] e.g. approximately 45 $Å^3$ for benzene. The change in the total molecular polarization due to excitation of one electron would be expected to be relatively small and less than 10 $Å^3$. Substituting this limit in equation (23) together with a concentration of 10

micromolar of excited states results in an estimated change in ε' of less than 1×10^{-6}.

2.3 EXPERIMENTAL

2.3.1 General

While basically a conductivity technique, the experimental set-up used for TRMC resembles more closely that used for optical absorption studies. The fundamentals are illustrated in Figure 2.2. Microwaves are produced by the source and propagate in a waveguide to a circulator which directs the microwaves to the cell containing the solution of interest. The waves are reflected back through the medium by a metal plate at the back of the cell. The reflected wave is directed by the circulator to a detector where the wave is rectified using a microwave diode and the output of the detector is monitored using a transient digitizer.

The change in the output of the diode, ΔV_R, resulting from flash-photolysis of a solution contained within the cell is displayed and recorded. An example of such an experimental TRMC trace is shown in Figure 2.9.
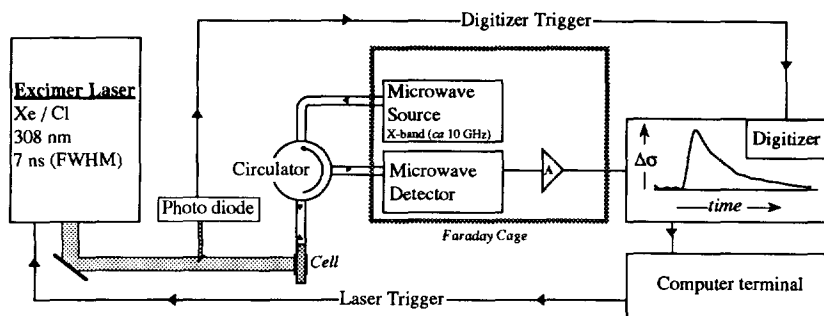
Figure 2.2: Schematic representation of the experimental set-up for the TRMC experiment.

The solutions were usually arranged to have an absorbance of close to 1 cm^{-1} at the wavelength of the excimer laser (308 nm) although other optical densities were sometimes used. The solvents n-hexane (Merck), cyclohexane (Merck) and benzene (Fluka) were UV spectroscopic grade and were used without further purification. The trans-decalin (Fluka, purum) was passed over a column of freshly activated silica gel as was the para-dioxane (Fluka, UV spectroscopic grade) immediately prior to use in order to minimize trace amounts of water. All solutions were purged with CO_2 to remove oxygen and to scavenge any high mobility electrons which might be formed by low yield, multi-photon ionization events.

The solutions were flash-photolysed using single, 7 ns FWHM pulses of 308 nm light from a Lumonics HyperEX 400 excimer laser. The integrated beam intensity incident on the solution is usually *ca* 7 mJ/cm^2. This corresponds to *ca* 0.2 photons per solute molecule in the irradiated region of the cell for an absorbance of 1 cm^{-1} and an extinction coefficient of 10^4 M^{-1}cm^{-1} of the solute at 308 nm. The power per pulse in mJ was routinely measured using a Scientech 365 power meter. The calibration factor for converting the power meter output into the incident photon flux within the cell was determined using a benzene solution of 4-dimethylamino-4-nitrostilbene (DMANS) as an internal TRMC actinometer. Details of the actinometry procedure are presented in a later section.

In what follows a detailed description of the microwave equipment and the method of data analysis is presented.

2.3.2 Microwave circuit components

A more detailed illustration of the experimental set up of the TRMC equipment used is shown in Figure 2.3. The basic microwave circuit is of the source-circulator-cell-circulator-detector type and has been described fully elsewhere.[14,16] The microwave source used is a Gunn Oscillator (Midcentury type) MC 16/34B which can be swept over the range 8.2-12.4 GHz (X-band).
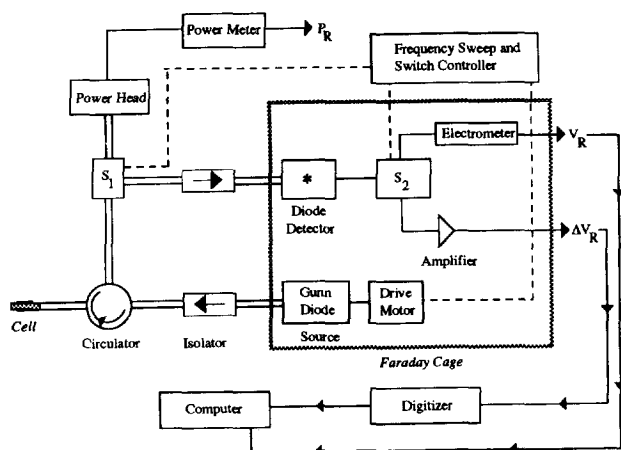
Figure 2.3: Detailed schematic illustration of the experimental set-up for the TRMC experiment.

Transient changes in the output of the detector are amplified 100 times using a Hewlett-Packard 8447A (risetime 1 ns) or 462A (risetime: 4 ns) amplifier. The amplifier output is fed to a Tektronix 7912 transient digitizer and displayed on a 604 monitor. After amplification and averaging of up to 64 traces, the noise level is ± 1 mV which is equivalent to one part in 10^5 on the dc output of the detector.

IN23 type point contact or schottky barrier detector diodes are used for fast time response detection. The voltage output of these devices does not vary linearly with either the power or field amplitude of the incident radiation at the power levels used (*ca* 100 mW). Because of this, either an accurately calibrated variable attenuator or a power meter are necessary in order to calibrate the change in detector output for a small change in microwave power at a given incident power level. For small fractional changes in the power at the detector, $\Delta P_R/P_R$, the relation to the change in detector output, $\Delta V_R/V_R$, will be:

$$\Delta P_R/P_R = n\Delta V_R/V_R \tag{27}$$

The "n-factor", n, can be obtained from the slope of the calibration curve with $n \approx 2$ being usually applicable in the present experiments. The value of n increases from about one to two with increasing microwave power.

The microwave source, its power supply, the detector and the amplifier are enclosed in a Faraday cage to reduce Hertzian pick-up from the high voltage discharge pulse of the laser.

2.3.3 The resonant cavity cell

There are two somewhat different approaches to carrying out TRMC measurements on condensed media: the "normal-reflection" and "cavity-reflection" methods. A full description of these methods together with the background theory has been published.[14,16,47] Only the "cavity-reflection" mode used in this research will be presented here.

Details of the construction of the microwave cavity cell are shown in Figure 2.4. The basic body was constructed of copper and brass which was gold-plated by immersion in "Atomex" gold-plating solution #3609. The internal dimensions are those of X-band waveguide (10 x 23 mm) with a length, from the iris coupling plate to the back, of 47 mm. The coupling plate is a 0.5 mm thick copper plate with a circular hole, 8 mm in diameter, which is made vacuum tight with a piece of 0.15 mm thick mica sheet attached with two-component cement. The front portion of the cell is attached to a length of normal flanged waveguide which can in turn be attached to the microwave circuitry using a "quick release" clamp. In the front part of the cell is an inlet for the solution which is attached to a glass bulb, fitted with stopcocks, which can be

used for deaerating the solution.

The broadwall sides of the back part of the cell are reduced in thickness to 0.8 mm over a rectangular area of 10 x 24 mm. This area contains several 1.5 x 5 mm holes giving a total area which is optically transmitting of 1.16 cm^2. The transmitting regions are covered with Supracil glass plates attached with two-component cement. An O-ring forms a vacuum seal between the front and the back portions of the cell when they are bolted together.
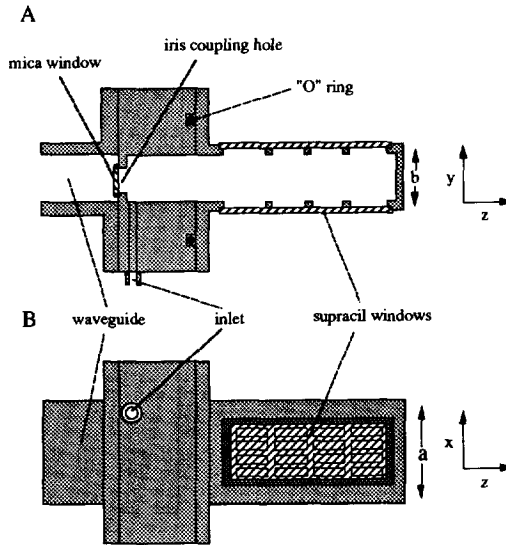
Figure 2.4: (A) Side view and (B) top view of the microwave cell design used in the present experiments. See text for further description.

2.4 DATA ANALYSIS

2.4.1 The cavity resonance

The coupling of energy to the cavity occurs only within a narrow frequency band for which there is a node in the standing wave very close to the position of the iris plate. The frequency at which this "resonance" occurs, f_0, for the normal TE_{10m} mode and with the cavity filled with a uniform dielectric medium is given to a good approximation by:

$$f_0 = c[(m/d)^2 + (1/a)^2]^{0.5}/2\sqrt{\varepsilon'} \tag{28}$$

where c is the velocity of light in vacuum, m is an integer and is equal to the number of half wavelengths in the cavity, d is the cavity length and a is the broad (inner) dimension of the cavity. It is of importance to choose the cell dimensions such that a resonance occurs within the frequency range of the source available. As an example, for the present cell with d = 47 mm and a = 23 mm and taking $\varepsilon' = 2.0$, $f_0 = 1.06 \times 10^{11}[(m/47)^2 + (1/23)^2]^{0.5}$, which results in $f_0 = 8.19$, 10.4 and 12.19 GHz for m = 3, 4 and 5 respectively. Of these frequencies the one corresponding to m = 4 lies within the range of the present microwave source for all solvents used and this is the resonance at which measurements are made.

Cavity resonance curves, such as that shown schematically in Figure 2.5, were obtained by scanning the microwave power reflected by the cavity over a small frequency range close to the resonance frequency and dividing this by the power reflected by a totally reflecting short circuit. The general form of such a curve is given by equation (29) for the fraction of incident power that is reflected by the cavity at a given frequency;[48,49]

$$R(f) = [R_0 + \alpha^2]/[1 + \alpha^2] \tag{29}$$

with $\alpha = 2(f - f_0)/\Delta W$

As shown in Figure 2.5, the curve is characterized by the 3 parameters: f_0 (the resonance frequency discussed above) which is the frequency at which the minimum in R(f) occurs; R_0,
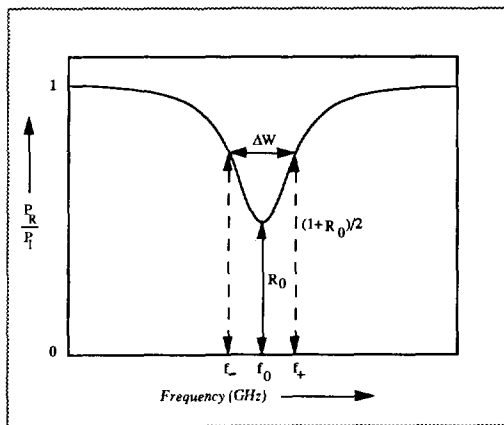
Figure 2.5: *Dependence of the power reflected by a resonant cavity on frequency at close to resonance. The curve is characterized by the 3 parameters: f_0 (the resonance frequency) which is the frequency at which the minimum in R(f) occurs; R_0, the fraction of power reflected at resonance; and ΔW, the full width of the resonance curve at the half-resonance frequencies for which R(f) = $[R_0 + 1]/2$.*

the fraction of power reflected at resonance; and ΔW, the full width of the resonance curve at the half-resonance frequencies for which $R(f) = [R_0 + 1]/2$.

Automatic scans of the cavity resonance-curve are carried out routinely for each solution immediately prior to a flash-photolysis TRMC measurement. The curves are automatically fitted using equation (29) and an iterative fit programme which then calculates the best-fit values of f_0, R_0 and ΔW. The last parameter is actually retained as the "loaded" quality factor of the cavity, Q_L, which is related to ΔW by:

$$Q_L = f_0/\Delta W \tag{30}$$

These parameters are then used to automatically calculate: the sensitivity factors for small transient changes in the permittivity of the solution within the cell as given in a subsequent section, the half-power frequencies f_+ and f_-, and the response time, τ_C. The last parameter is the exponential, "RC", response time of the electric field within the cavity to changes in the input power or cavity characteristics:[50]

$$\tau_C = Q_L/\pi f_0 \tag{31}$$

Typical resonance parameters for the solvents studied are listed in Table 2.1.

Table 2.1: *Characteristics of the microwave cavity containing different solvents with four half wavelengths in the cell at resonance. Included are the cavity resonance frequency, f_0; the fraction of power reflected at resonance, R_0; the loaded quality factor, Q_L; the sensitivity factor, A, the cavity response time, τ_C and one over the unloaded quality factor, $1/Q_U$.*

Solvent	f_0 (GHz)	R_0	Q_L	A (Ω m)	τ_C (ns)	$1/Q_U$
benzene	9.46	0.425	221	921	7.4	7.9
dioxane	9.60	0.082	180	1350	6.0	19.8
t-decalin	9.74	0.539	160	643	5.2	8.3
cyclohexane	10.04	0.540	207	879	6.6	6.4
n-hexane	10.40	0.510	144	634	4.4	9.9

2.4.2 The quality factor(s), Q.

As mentioned in the previous section, the loaded quality factor determines the width of the cavity resonance and the response time. Q_L is related to the the energy stored in the cavity, U, and the power dissipated, P, by:

$$Q_L = 2\pi f_0 \, U/P \tag{32}$$

Several loss processes contribute to the overal power dissipation including losses in the wall of the cavity, P_W, losses in the dielectric material filling the cavity, P_M, and losses to the external circuit via the coupling, P_C. The loaded Q corresponds to the sum of all losses and is therefore given by:

$$Q_L = \omega_0 U/[P_C + P_M + P_W] \tag{33}$$

Other quality factors may be defined in terms of the individual loss processes e.g.:

$$1/Q_L = 1/Q_C + 1/Q_M + 1/Q_W \tag{34a}$$

$$= P_C/\omega_0 U + P_M/\omega_0 U + P_W/\omega_0 U \tag{34b}$$

The wall and medium losses within the cavity are frequently grouped together as the "unloaded" Q, Q_U, given by:

$$1/Q_U = 1/Q_M + 1/Q_W \tag{35}$$

with $1/Q_M$ being equal to the ratio of the dielectric loss of the medium to its dielectric constant[51] resulting in:

$$1/Q_U = \varepsilon''/\varepsilon' + 1/Q_W \tag{36a}$$

$$= \sigma/\omega\varepsilon_0\varepsilon' + 1/Q_W \tag{36b}$$

In the present case of an overcoupled cavity (evidenced by a decrease in R_0 with increase in loss within the cavity) the value of R_0 is related to the quality factors via:[1]

$$R_0 = [1 - 2Q_L/Q_U]^2 \tag{37}$$

The ratio of the power loss to the external circuit to the power lost within the cavity can be determined from equations (34), (35) and (37) to be:

$$P_C/(P_M + P_W) = Q_U(1/Q_L - 1/Q_U)$$

$$= (1 + \sqrt{R_0})/(1 - \sqrt{R_0}) \tag{38}$$

For saturated hydrocarbon solvents and benzene R_0 is approximately 0.5 so that the power lost via the coupling is almost 6 times that lost within the cavity. For dioxane R_0 is never larger than 0.2 and is often lower probably due to trace amounts of water.

2.4.3 Background dielectric loss: M_0 determination

On addition of a concentration N of a dipolar ground state molecule to a solvent the conductivity will become $\sigma = \sigma_0 + eM_0N$ with M_0 the rotational charge mobility as defined in a previous section. From equation (36b) the unloaded Q will then be given by:

$$1/Q_U = (\sigma_0 + eM_0N) / \omega\varepsilon_0\varepsilon' + 1/Q_W \tag{39}$$
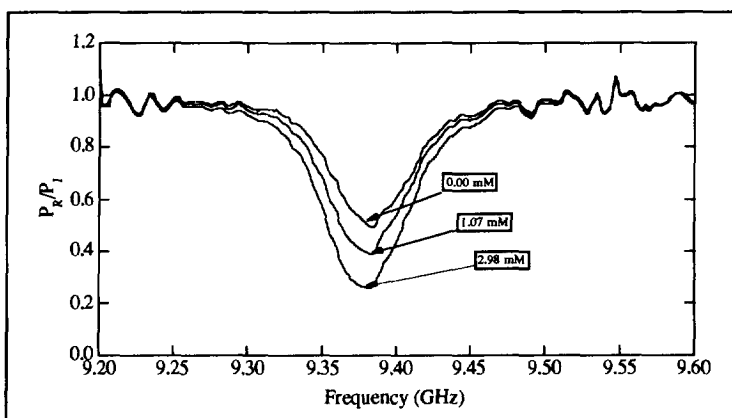
Figure 2.6: *The effect of solute concentration on the cavity resonance curve for DMANS in benzene for the concentrations shown.*

From equation (37) one can obtain $1/Q_U$ in terms of the measured parameters R_0 and Q_L:

$$1/Q_U = (1 - \sqrt{R_0})/2Q_L \tag{40}$$

By making background scans of the cavity resonance for different solute concentrations, as performed for DMANS (see Figure 2.6 and Table 2.2), a plot of $1/Q_U$ against N can be made which from equation (40) should be linear with a slope given by:

$$d(1/Q_U)/dN = eM_0/\omega_0\varepsilon_0\varepsilon' \tag{41}$$

from which M_0 can readily be determined:

$$M_0 = \omega_0\varepsilon_0\varepsilon'\{d(1/Q_U)/dN\}/e \tag{42}$$

Such a plot is shown in Figure 2.7 for DMANS in benzene from which $M_0 = 3.15 \times 10^{-9}$ m^2/Vs is obtained.

The value of M_0 can be used in the interpretation of transient TRMC measurements to determine excited state dipole moments as described in a subsequent section.

Table 2.2: Data of the M_0 measurements of solutions of DMANS in benzene. Included are the DMANS concentration in mM; the loaded quality factor, Q_L; the fraction of power reflected at resonance, R_0; the cavity resonance frequency, f_0; the sensitivity factor times the dielectric constant, $A\varepsilon$, the unloaded quality factor, Q_U, the reciprocal of the unloaded quality factor $1/Q_U$ and the concentration of the DMANS molecules in molecules/m^3.

[Solute] (mM)	Q_L	R_0	f_0	$A\varepsilon$	Q_U	$1/Q_U$	[Solute] (molec./m^3)
0.00	161.50	0.560	9.38	1447	1283.43	7.79E-04	0.00E+00
0.52	158.00	0.520	9.39	1447	1133.06	8.83E-04	3.13E+23
0.52	159.00	0.510	9.38	1464	1112.44	8.99E-04	3.13E+23
1.10	155.60	0.460	9.39	1472	967.16	1.03E-03	6.62E+23
1.10	155.40	0.460	9.38	1478	965.92	1.04E-03	6.62E+23
1.60	153.20	0.410	9.39	1505	851.85	1.17E-03	9.64E+23
1.60	153.20	0.410	9.38	1505	851.85	1.17E-03	9.64E+23
1.90	152.60	0.380	9.39	1537	795.71	1.26E-03	1.14E+24
1.90	151.30	0.380	9.38	1523	788.93	1.27E-03	1.14E+24
2.30	149.90	0.350	9.38	1544	734.10	1.36E-03	1.39E+24
2.30	148.70	0.350	9.39	1534	728.22	1.37E-03	1.39E+24
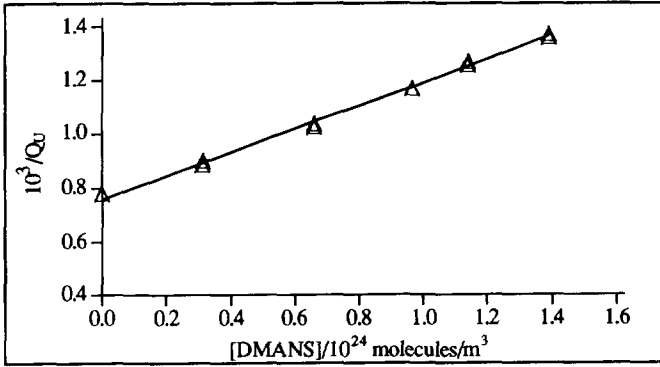
Figure 2.7: Linear plot of $1/Q_U$ against N for DMANS in benzene from which $M_0 = 3.15 \times 10^{-9}$ m^2/Vs is determined.

2.4.4 The TRMC sensitivity factor

In a TRMC experiment a small change in reflected power resulting from a change in the conductivity (dielectric loss) of the medium on flash-photolysis is measured. If the conductivity change is homogeneous throughout the cell then the sensitivity factor A in equation (43) can be readily determined at resonance:

$$\Delta P_R/P_R = \Delta R_0/R_0 = -A\Delta\sigma \tag{43}$$

Starting with equation (37) in Section 2.4.2 and substituting for $1/Q_L = 1/Q_U + 1/Q_C$ relationship (44) can be derived:

$$\sqrt{R_0} = 1 - 2Q_C/(Q_U + Q_C) \tag{44}$$

Since the coupling power loss and hence Q_C is independent of changes in the conductivity of the medium, differentiation of both sides of equation (44) with respect to the conductivity gives:

$$[dR_0/d\sigma]/2\sqrt{R_0} = [d(1/Q_U)/d\sigma]2Q_CQ_U\{Q_C/(Q_U + Q_C) - 1\}/(Q_U + Q_C) \tag{45}$$

Substituting in equation (45) for $Q_CQ_U/(Q_C + Q_U) = Q_L$ and $Q_C/(Q_U + Q_C) = (1 + \sqrt{R_0})/2$ and rearranging leads to:

$$dR_0/R_0 = -2Q_L(1 + 1/\sqrt{R_0})[d(1/Q_U)/d\sigma]d\sigma \tag{46}$$

which on substituting for $[d(1/Q_U)/d\sigma] = 1/\omega\varepsilon_0\varepsilon'$ from equation (36b) in Section 2.4.2 leads to the eventual result:

$$dR_0/R_0 = -2Q_L(1 + 1/\sqrt{R_0})d\sigma/\omega_0\varepsilon_0\varepsilon' \tag{47a}$$

or in terms of the dielectric loss:

$$dR_0/R_0 = -2Q_L(1 + 1/\sqrt{R_0})d\varepsilon''/\varepsilon' \tag{47b}$$

The sensitivity factor A at resonance from equation (43) and (47a), as has been published,[14,19] is given by:

$$A = 2Q_L(1 + 1/\sqrt{R_0})/\omega_0\varepsilon_0\varepsilon' \tag{48}$$

As can be seen in Table 2.1 the A values for the cell used in the present experiments are on the order of 1000. When this is combined with the noise level of approximately 1 part in 10^5, the detection limit for changes in conductivity is found to be 10^{-8} S/m. This limit is for a uniform change in conductivity throughout the whole volume of the cavity. As discussed more fully in the next section, only a limited fraction, *ca* 10%, of the total volume is in fact irradiated so that the conductivity change required in the irradiated region will be an order of magnitude greater than the limit calculated above or *ca* 10^{-7} S/m.

Recently[52] the changes in reflected power at the half-power frequencies, f_+ and f_- in Figure 2.5, have also been routinely monitored. This provides information on changes in both the dielectric loss and the dielectric constant with sensitivity constants B and C (see Chapter 8):

$$(\Delta P_R/P_R)_+ = -B\Delta\varepsilon'' + C\Delta\varepsilon' \tag{49}$$

$$(\Delta P_R/P_R)_- = -B\Delta\varepsilon'' - C\Delta\varepsilon' \tag{50}$$

with

$$B = (1 + \sqrt{R_0})^2 Q_L / (1 + R_0)\varepsilon' \tag{51}$$

$$C = (1 - R_0)Q_L / (1 + R_0)\varepsilon' \tag{52}$$

The derivation of B and C is more involved than that for the sensitivity factor at resonance.

2.4.5 Non-uniform energy deposition

For all practical cell designs, a non-uniform deposition of energy in the sample volume on photolysis is unavoidable. In equation (53), $<\Delta\sigma>_{xyz}$ is therefore the mean field strength weighted conductivity:

$$\Delta P_R / P_R = -A <\Delta\sigma>_{xyz} \qquad (53)$$

If absolute measurements of the conductivity are required this must be taken into account. In addition to the non-uniformity of energy deposition from the irradiation pulse, account must also be taken of the fact that the electric field strength varies from place to place in the cell. For the TE_{10} modes in the present case, the standing wave has a node at the back of the cell (short circuit) and varies sinusoidally in the propagation or z-direction (for axes see Figure 2.4) with wavelength λ_z. In the plane perpendicular to the z direction, the electric field vector lies in the y direction parallel to the narrow wall sides and varies in magnitude sinusoidally in the x direction having nodes at the sides and a maximum in the centre at $x = a/2$. If the conductivity change at a position x,y,z in the cell is $\Delta\sigma$ (xyz) then the mean field strength weighted conductivity change to be used in equation (53) is given by:[39]

$$<\Delta\sigma>_{xyz} = [\int\int\int \Delta\sigma \text{ (xyz)}|E \text{ (xyz)}|^2 \text{ dx dy dz}] / [\int\int\int |E \text{ (xyz)}|^2 \text{ dx dy dz}] \qquad (54)$$

As can be seen in equation (54), the conductivity change is weighted with the square of the field strength. This is an important factor in the choice of the irradiation geometry. Thus, for example, photolysis of a solution of absorbance 1 or more either via the back wall or a side wall of the cell would result in a large fraction of products being formed in unfavourable regions of very low E^2. Because of this, a choice was made for irradiation via a broadwall side of the cell in the present case (see Figure 2.4). We therefore consider the effect of irradiating the sample via a rectangular "window" of dimensions Δx by Δz and defined in position by the coordinates x_1, x_2 and z_1, z_2 with respect to a side and the back of the cell respectively.

The radiation flux is taken to be uniform over the irradiated area. Products will be formed in the sample in the column behind the window with a concentration gradient in the y direction due amongst other things to attenuation of the radiation. The average concentration of a particular product in the sensitive region of the cell, i.e. between the inner broadwall sides at y_1 and y_2, is:

$$N = b^{-1} \int_{y_1}^{y_2} N(y) \text{ dy} \qquad (55)$$

where b is the small internal dimension of the waveguide. Since the electric field strength is uniform in the y direction, there exists an average conductivity change in the irradiated zone, $<\Delta\sigma>_y$, equal to $e\Delta M_*<N>$ for a dipolar species.

In order to arrive at the overall mean weighted conductivity to be used in equation (53), $<\Delta\sigma>_{xyz}$, a weighting factor for the position of the irradiated column in the x,z plane, W(x,z). must be calculated using:

$$W(x,z) = (4ad)^{-1}\iint \sin^2(\pi x/a) \sin^2(2\pi z/\lambda_z) \, dx \, dz \qquad (56)$$

If the field strength were constant in the x and z directions, W(x,z) would in fact be simply the ratio of the light-transmitting area to the total area of the broadwall side. For the cell shown in Figure 2.4, this would have led to W(x,z) = 0.107 rather than the actual value of W(x,z) = 0.185 for four half wavelengths in the cell.

Since W(x,z) can be readily calculated, for a particular window design, the primary parameter of interest which can be derived from the microwave data is the change in the average concentration in the irradiated zone, $<\Delta\sigma>_y$ from:

$$<\Delta\sigma>_y = <\Delta\sigma>_{xyz}/W(x,z) \qquad (57)$$

2.4.6 Product distribution in depth and time

In order to determine an absolute value of the rotational charge mobility of a particular product of photolysis from the measured value of $<\Delta\sigma>_y$, it is necessary to calculate the concentration of that species at a particular time and at a given depth in the cell. This requires knowledge of the incident photon intensity, the optical properties of the solution at the wavelength of irradiation (absorbance and solute extinction coefficient) and usually certain photophysical parameters such as quantum yields, lifetimes and intersystem-crossing efficiencies. The problem can be especially complex for the high photon fluxes involved in laser flash-photolysis. Even in the absence of complications due to multiple photon absorption and stimulated emission, one has to consider the effect of solute depletion on the geometrical distribution of the various products. These considerations increase in significance when the detection method fails to probe the whole irradiated zone uniformly, as is the case for the majority of techniques. In what follows the methods will be described which have been used in an attempt to solve these problems.

The particular case of the formation of singlet and triplet excited states S_1 and T_1, from the ground state solute molecules, S_0, can be represented by:

$$S_0 \quad + h\nu \quad \longrightarrow \quad S_1 \qquad\qquad (58a)$$

$$S_1 \quad \xrightarrow{\quad k_2 \quad} \quad S_0 \qquad\qquad (58b)$$

$$S_1 \quad \xrightarrow{\quad k_3 \quad} \quad T_1 \qquad\qquad (58c)$$

$$T_1 \quad \xrightarrow{\quad k_4 \quad} \quad S_0 \qquad\qquad (58d)$$
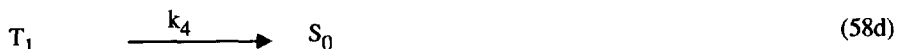
This results in:

$$dN_0/dt = -I(t)\sigma_\lambda N_0 + k_2 N_S + k_4 N_T \qquad\qquad (59)$$

$$dN_S/dt = I(t)\sigma_\lambda N_0 - (k_2 + k_3)N_S \qquad\qquad (60)$$

$$dN_T/dt = k_3 N_S - k_4 N_T \qquad\qquad (61)$$

In equations (59) and (60), σ_λ is the absorption cross section in m^2 of the solute and is related to the extinction coefficient at the irradiating wavelength (in $M^{-1}cm^{-1}$) by $\sigma_\lambda = 3.83 \times 10^{-25}\varepsilon_\lambda$. The units of concentration to be used in equations (59-61) are molecules/m^3.

Solution of the rate equations is complicated not only by the variation of $I(t)$ with depth in the irradiated medium but also by the fact that the pulse profile for most laser sources is anything but square. In addition, because of the high intensities involved, the concentration of ground state molecules cannot be taken to be constant either in time or depth during the course of the pulse.

In order to surmount these problems we consider the irradiated medium to consist of layers perpendicular to the direction of irradiation of thickness Δy chosen such that $a\Delta y < 0.1$, where a is the absorbance of the solution. The light intensity incident on the j_{th} layer is then taken to have a dependence on time in the form of a histogram i.e.

$$I_j(t) = I_{i,j}; \quad i = \text{integer } (1 + t/\Delta t) \qquad\qquad (62)$$

with the suffix i indicating the light intensity in the i_{th} time interval with the width of the intervals being taken as Δt (1 ns in the present case). The intensity profile of the pulse for each

layer is derived from that of the preceding layer beginning with the known profile for the first layer (j=1):

$$I_1(t) = I_{i,1} = (h_i/\Sigma h_i)\varphi/\Delta t; \quad i = \text{integer} \; (1+t/\Delta t) \tag{63}$$

where h_i is the height of the incident pulse in the i_{th} time interval and φ is the total photon flux determined by actinometry. The intensity is assumed to be uniform in the x,z plane. The general calculation procedure is as follows.

For each layer we have the initial (t=0) conditions $N_S = N_T = 0$ and $N_0 = N_0{}^0$ and the development of the concentration in time is calculated by solving the rate equations (59-61), using a Runge-Kutta programme, with the time dependence of the incident light intensity given by equation (63). At the end of the i_{th} time interval the concentrations, $N_{i,j}$, of the various species are summed into separate array elements corresponding to the i_{th} time interval after multiplication by a weighting factor W_j which is proportional to the sensitivity of detection at the j_{th} layer in the medium. At the end of the calculations (n layers), the arrays then contain the weighted average concentrations for a given time interval, i.e.:

$$< N_i^* >_y \; = \Sigma_{j=1}^{n} W_j N_{i,j}^* \Delta y_i \, / \, \Sigma_{j=1}^{n} W_j \Delta y_i \tag{64}$$

Also at the end of the i_{th} time interval, the intensity incident on the $(j + 1)_{th}$ layer in the i_{th} time interval is derived from the concentration of ground state molecules present, according to:

$$I_{i,j+1} = I_{i,j} \exp[-\sigma_\lambda \Delta y_i (N^0{}_{i-1,j} + N^0{}_{i,j})/2] \tag{65}$$

It should be mentioned that for greater accuracy the actual intensity used in the kinetic calculations was not the intensity incident on the layer, but rather the average intensity in the layer which was calculated based on the concentration of ground state molecules present at the beginning of a particular time interval, i.e.:

$$<I>_{i,j} = I_{i,j}[1 - \exp(-\sigma_\lambda N^0{}_{i,j} \Delta y_i)] \, / \, \sigma_\lambda N^0{}_{i,j} \Delta y_i \tag{66}$$

This procedure, beginning with the first time interval in the first layer, leads to the average weighted concentrations as given by equation (64), taking into account depletion of the ground state.

As mentioned above, for irradiation in the y direction, via the broadwall sides, the field strength is uniform between the inner walls. However, there exists a region equal to the thickness of the metallic walls of the cell at the window position which is not probed by the field. In order to take this into account the weighting factor W_j is taken to be zero within this region and unity for y values lying between the inner walls. If necessary a more complex form of weighting could readily be applied. The average value of the conductivity is given by:

$$<\Delta\sigma>_y = e\Sigma M_* <N_*>_y \tag{67}$$

In order to illustrate the effects of various non-kinetic parameters the maximum value of $<N_*>_y/\phi$ as a function of the absorbance of the solution for the case of the formation of only a single excited state are plotted in Figure 2.8. The curves shown are for different initial light intensities and, for the lowest intensity, with no correction for the wall thickness. This last curve is in fact what would be expected if no depletion of the solute occurred and the dead volume was zero. The reduction in the amount of singlet formed in the sensitive region of the cell when the wall thickness is taken into account is apparent for high absorbances. Bleaching effects, which increase with increasing intensity, are apparent as a decrease in the intensity normalized concentration for low absorbance, as expected, and an increase on the high absorbance side due to the light penetrating increasingly further into the sensitive region. The points shown in Figure 2.8 are experimental and were obtained from the maximum value of $\Delta\sigma$ found on flash-
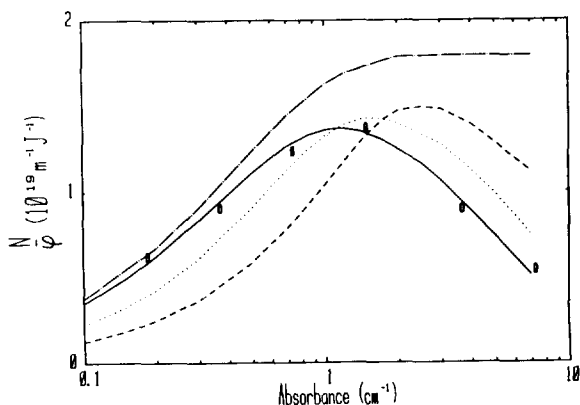
Figure 2.8: *The dependence of the maximum concentration of the excited singlet state of a solute in the sensitive part of the irradiated volume of the cell on absorbance of the solution for different light intensities, with $\Phi_{isc} = 0$, a singlet state lifetime of 2.7 ns, an extinction coefficient of 1.28×10^4 $M^{-1} cm^{-1}$ and a cavity response time of 7 ns. Total energy flux: _._ 0.7 mJ/cm^2 (wall thickness zero), —— 7 mJ/cm^2, ... 70 mJ/cm^2, and ------ 70 mJ/cm^2 (wall thickness 0.8 mm). The circles are experimental measurements obtained from the maximum conductivity in aerated solutions of DMANS in benzene with a total energy flux of 7 mJ/cm^2 using $\Delta M_S = 7.46 \times 10^{-9}$ $m^2 V^{-1} s^{-1}$.*

photolysis of air-saturated benzene solutions of DMANS with a value of φ, the same as that used to construct the full line in Figure 2.8, i.e. 7 mJ/cm^2. The agreement of the absorbance dependence between the experimental and calculated data is seen to be good.

2.4.7 Determination of ΔM*

A change in the microwave conductivity within the cell is monitored in the first instance as the amplified change in the output voltage of the detector diode, ΔV_R. To fit a raw TRMC trace such as that shown in Figure 2.9 the time dependence of the average concentration of a particular intermediate in the irradiated region is calculated as described in the previous section using as input the light intensity, the absorbance and extinction coefficient of the solute, and the
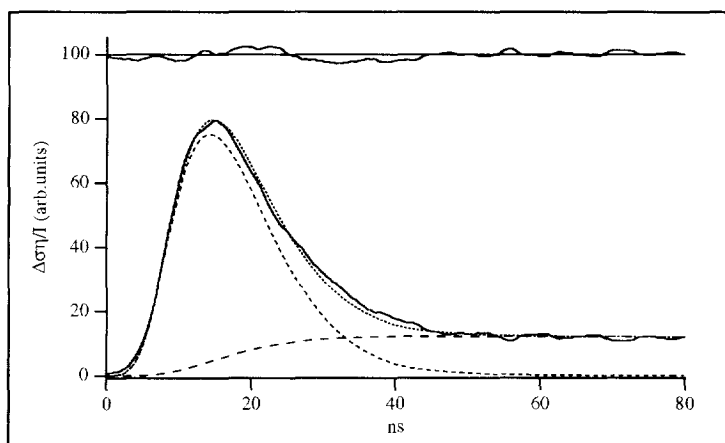
Figure 2.9: Transient change in the microwave conductivity (dielectric loss) of a ca 10^{-4} M solution of DMANS in benzene on flash-photolysis at 308 nm, pulsewidth 7 ns. The dashed lines show the individual contributions from the excited singlet and triplet states. The dotted line is the sum of these contributions.

rate coefficients. The latter are based on either iterative guesses or on values measured using other techniques; for example singlet lifetimes from time-resolved fluorescence measurements. Sensitivity factors, $\Delta V_*/<N_*>y$ in volts per unit concentration, which give a best fit to the absolute magnitude of the ΔV_R versus time trace, are then chosen iteratively for each intermediate. When fitting reaction schemes such as that represented by (58a-d), it is easiest to take initially $\Delta V_T/<N_T>_y = \Delta V_S/<N_S>_y$ and find a best fit to the data using the intersystem crossing efficiency, $\Phi_{isc} = k_3/(k_3 + k_2)$, as a variable. Since the triplet component is proportional to a good approximation to the product of the intersystem crossing efficiency and

65

the sensitivity factor the parameter obtained from the data fit is $\Phi_{isc}\Delta V_T/<N_T>_y$ given by:

$$\Phi_{isc}\Delta V_T/<N_T>_y = \Phi_{isc}(fit)\{\Delta V_S/<N_S>_y\} \tag{68}$$

The fit parameter $\Delta V_S/<N_S>_y$ can be converted to the change in the relative power reflected per unit change in the concentration in the irradiated region using the known signal amplification factor, X, the measured voltage output of the detector, V_R, and the n-factor, discussed in Section 2.3.2:

$$\Delta P_R/P_R<N_S>_y = \{\Delta V_S/<N_S>_y\}n/V_R X \tag{69}$$

The relationships derived in the previous sections between $\Delta P_R/P_R$ and the conductivity change can now be used to derive the value of the rotational charge mobility change on singlet state formation, ΔM_S, i.e.:

$$\Delta P_R/P_R = -AW(x,z)<\Delta\sigma>_y \tag{70}$$

$$= -AW(x,z)e<N_S>_y\Delta M_S \tag{71}$$

from which

$$\Delta M_S = \{\Delta V_S/<N_S>_y\}n / \{eAW(x,z)V_R X\} \tag{72}$$

similarly

$$\Phi_{isc}\Delta M_T = \{\Phi_{isc}(fit)\Delta V_S/<N_S>_y\}n / \{eAW(x,z)V_R X\} \tag{73}$$

The fitting procedure is illustrated in the next section in which results for a benzene solution of DMANS, routinely used for internal actinometry, are presented. In Section 2.5 the derivation of dipole moments from ΔM_* values, which depends on a knowledge of the dipole relaxation time, is described.

2.4.8 Actinometry

The intensity factor gives the relationship between the laser power per pulse monitored routinely during the course of the measurements by a Scientech 365 power meter and the photon flux, φ (photons/cm^2), in the TRMC cell. Over the years N,N-dimethylamino-nitrostilbene (DMANS) dissolved in benzene has been used as the internal actinometer, because the photophysical properties of this compound are well known. The TRMC transient obtained from a flash-photolysized solution of DMANS in benzene is shown in Figure 2.9. As can be seen the transient consists of two components: a large contribution due to a short-lived dipolar species (the singlet) and a small contribution due to a long-lived dipolar species (the triplet).

If we use literature values for $\mu_S = 24.5$ D[53,54] (81.6×10^{-30} Cm) and $\mu_0 = 7.3$ D[53,54] (24.5×10^{-30} Cm) and use the measured value for $M_0 = 3.15\times10^{-9}$ m^2/Vs (see Section 2.4.3), ΔM_S can be calculated, as will be derived in Section 2.5.1, via:

$$\Delta M_S = M_0(\mu_S^2 - \mu_0^2)/\mu_0^2 \tag{74}$$

to be $\Delta M_S = 3.2\times10^{-8}$ m^2/Vs.

The value of the fitting parameter $\{\Delta V_S/<N_S>_y\}$ for DMANS in benzene can then be determined by inverting equation (72) in the previous section and substituting the known experimental parameters n, A, W(x,z), V_R and X:

$$\{\Delta V_S/<N_S>_y\} = eAW(x,z)V_R X \Delta M_S /n \tag{75}$$

The standard kinetic parameters used in the fitting procedure are the singlet lifetime of 3.1 ns determined by time-resolved fluorescence measurements (see Section 2.6), the triplet lifetime of 1.4 μs (determined previously from the long-time decay of the TRMC transient), and a value of Φ_{isc}(fit) of 0.03 which is the average value found after many fitting procedures for this particular solution.

The only remaining variable in the fitting procedure is then the incident intensity of the light within the cell in photons per cm^2. The value of this parameter required to obtain a best fit is then compared with a concurrent measurement of the mJ/pulse using the power meter to obtain the conversion factor. An example of the fit to a typical TRMC actinometry trace is shown in Figure 2.9.

Over the four years of using this approach to actinometry the conversion factor has been found to vary by less than 20%. The most decisive parameter in this actinometry procedure is the dipole moment taken for the S_1 state of DMANS of 24.5 D. All other dipole moments

determined are therefore in effect based on this value for DMANS and will involve any systematic error in it.

2.5 THE DIPOLE MOMENT μ_*, AND DIPOLE RELAXATION TIME, Θ

In Section 2.4.7 we have determined ΔM_S from equation (72). From this value the dipole moment of the singlet excited state, μ_S, can be calculated with knowledge of the values for μ_0 and Θ, by rearrangement of equation (20):

$$\mu_S = \{\Delta M_S \, 27ek_BT\Theta \, / \, [\varepsilon(\infty) + 2]^2 F(\omega\Theta)]\}^{0.5} + \mu_0 \tag{76}$$

Likewise the dipole moment of the triplet excited state, μ_T, can be calculated if Φ_{isc} is known according to:

$$\mu_T = \{(\Phi_{isc}\Delta M_T) \, 27ek_BT \, / \, [\Phi_{isc}[\varepsilon(\infty) + 2]^2 F(\omega\Theta)]]\}^{0.5} + \mu_0 \tag{77}$$

An essential parameter needed to make quantitative estimates of the dipole moments of transient species from the results of TRMC experiments is the dipole relaxation time, Θ. This is the mean time required for spatial randomization of the vectorial component of the dipole. The most common mechanism of dipole relaxation in low viscosity solvents, such as those used in the present experiments, is rotational tumbling of the whole molecule about the dipolar axis resulting in the rotational relaxation time, Θ_R. Internal motions of individual parts of a molecule or interchange between structures with different dipole vectors can sometimes present additional relaxation pathways with a corresponding intramolecular relaxation time, Θ_I.

If rotational and intramolecular relaxation are both single exponential processes the overal relaxation time will be given by:[55,56]

$$1/\Theta = 1/\Theta_R + 1/\Theta_I \tag{78}$$

If Θ_R and/or Θ_I have multiple components the value in equation (78) will be a weighted average. This problem is dealt with in references 55 and 57 and is considered to be outside the scope of this thesis.

As pointed out in Section 2.2.3, it should be possible in principle to determine Θ directly for a given transient species if $\Delta\varepsilon'$ and $\Delta\varepsilon''$ are determined at the same time from $\Delta\varepsilon''/\Delta\varepsilon' = \omega\Theta$. In practice however this is only possible using the present TRMC technique for species for which Θ is approximately $2/\omega$ or less, i.e. ≤ 30 ps. For all except the smallest molecules studied, such

as 4-dimethylaminobenzonitrile (DMABN), the rotational relaxation time is expected to be much longer than 30 ps. Other methods of estimating Θ are therefore necessary.

For emissive singlet states the fluorescence depolarization time could be used if the excited state dipole and the transition dipole are known to have the same axis and the mechanisms of relaxation of the polarization and the dipole vector are the same. Unfortunately we do not have a facility for carrying out such measurements ourselves on the molecules of interest to us.

An experimental approach that can be carried out using the same microwave apparatus as used for the time-resolved measurements is to measure the dielectric loss of the ground state molecule if it has a dipole moment. If the dipole moment is known then the relaxation time can be determined. This value of Θ can then be used in the analysis of the TRMC data on the assumption that the relaxation time of the excited state of the molecules is closely similar to that of the ground state. This method is discussed more fully in the next section.

For molecules for which experimental data can not be obtained, Θ_R is estimated by calculation using theoretical equations for the diffusional motion of molecules with appropriate geometries. This is the most frequently applied approach and is discussed in detail in the next section but one.

The timescales of intramolecular dipole relaxation processes in excited states can only be measured directly by monitoring changes in both the real and imaginary components of the permittivity under identical photolysis conditions. Rapid internal relaxation processes are then indicated by Θ values much shorter than those expected for rotational relaxation. Fessenden et al.[58] were first to introduce the capability of directly measuring Θ for excited states of molecules. We have shown recently that this is also possible using the TRMC method. As mentioned above this is limited to relaxation times of a few tens of picoseconds or less. This will be more fully discussed in Chapter 8.

2.5.1 Determination of Θ from M_0

If the dipole relaxation of the ground state molecule is Debye type then the relaxation time, Θ_0 can be determined from the value of the rotational charge mobility by solving the quadratic equation:

$$M_0 = B\mu_0^2\omega^2\Theta_0 / (1 + (\omega\Theta_0)^2) \tag{79}$$

with $B = (\varepsilon' + 2)^2/27ek_BT$

resulting in:

$$\Theta_0 = B\mu_0^2 \{1 \pm [1 - (2M_0 / \omega B\mu_0^2)^2]^{0.5}\}/2M_0 \tag{80}$$

Equation (80) gives 2 solutions for Θ_0, one of which is shorter and the other longer than the reciprocal radian frequency of the microwaves, $1/\omega \approx 15$ ps in the present work. The longer solution is invariably the correct one for the molecules studied in the present work if relaxation is controlled by rotational diffusion.

As an example, taking the value of $M_0 = 3.15 \times 10^{-9}$ m^2/Vs given previously for DMANS in benzene at room temperature and a value of $\mu_0 = 7.3$ D,[53,54] Θ_0 is determined to be 196 ps.

For relaxation times longer than $3/\omega$, i.e. *ca* 50 ps, Θ_0 is given to within 10% accuracy by the approximate expression:

$$\Theta_0 \approx B\mu_0^2 / M_0 \tag{81}$$

If the assumption is made that the species of interest has the same dipole relaxation time as the ground state then it is not necessary to actually derive Θ from the value of M_0 determined in this way. Since the change in rotational mobility on photoexcitation, ΔM_*, is determined in the flash-photolysis TRMC experiment under exactly the same cavity conditions used to measure M_0, relationship (82) will apply:

$$\Phi\Delta M_* / M_0 = (\mu_*^2 - \mu_0^2)/\mu_0^2 \tag{82}$$

In equation (82) Φ is the quantum yield of the product of photolysis and ΔM_* is the actual parameter experimentally measured. On rearrangement equation (82) leads to:

$$\mu_* = \mu_0(1 + \Phi\Delta M_*/M_0)^{0.5} \tag{83}$$

This equation can usually be applied directly to estimate the dipole moment of excited singlet states since the quantum yield of the singlet state can often (but not always!) be taken to be unity so that $\Phi\Delta M_* = \Delta M_S$ and thus:

$$\mu_S = \mu_0(1 + \Delta M_S/M_0)^{0.5} \tag{84}$$

Cases in which more than one (fluorescing) excited singlet state are formed either in parallel or in succession are not uncommon and are to be found in subsequent chapters. In many cases a triplet state is formed from the initially excited singlet state by intersystem crossing with a

quantum efficiency of Φ_{isc}. The parameter derived from TRMC fits is then $\Phi_{isc}\Delta M_T$ and the dipole moment can only be determined if Φ_{isc} is known.

$$\mu_T = \mu_0(1 + [\Phi_{isc}\Delta M_T] / \Phi_{isc}M_0)^{0.5} \tag{85}$$

In order to be able to determine μ_* using the above approach it is clearly necessary to know the dipole moment of the molecule in its ground state. Values of μ_0 are sometimes available in the literature and the compilations by McLellan[53,54] are particular useful. μ_0 can be determined by accurate, concurrent measurement of the effect of the solute on the permittivity and refractive index of a solution at frequencies much lower than $1/\Theta$. This was done in a collaborative study on the aminobenzonitrile derivatives in Chapter 3.

An interesting aspect of the relationship between the rotational charge mobility and the relaxation time, of the form as shown for the ground state in equation (79), is that a maximum value of the parameter $\omega^2\Theta^2/(1 + (\omega\Theta)^2)$ of 1/2 exists for $\Theta = 1/\omega$. Therefore if the rotational charge mobility is known for a particular species but there is no knowledge of the relaxation time, it is always possible to estimate a minimum value of the dipole moment using equation (86):

$$\mu \geq (2M / \omega B)^{0.5} \tag{86}$$

This can sometimes prove to be useful for discussion purposes.

2.5.2 Calculated values of Θ_R

2.5.2.1 Sphere

The rotational relaxation time of a molecular dipole is related to the coefficient(s) of rotational diffusion, D, about axes mutually perpendicular to that of the dipole. For a sphere the relationship is simply:

$$\Theta_{sph} = 1/6D_{sph} \tag{87}$$

with D_{sph} derived using the Einstein equation:[59,60]

$$D_{sph} = k_B T/6\eta V_M \tag{88}$$

so that:

$$\Theta_{sph} = \eta V_M / k_B T \tag{89}$$

In equation (89), η is the microscopic coefficient of friction towards molecular rotation and has the units of viscosity; V_M is the molecular volume in m^3 which may be derived from the molecular weight of the molecule, M (g/mol) and its density ρ_M (g/cm^3) from:

$$V_M = M / 6.02 \times 10^{29} \rho_M \tag{90}$$

For η in centipoise (1cP = 10^{-3} Pa s) equation (89) becomes:

$$\Theta_{sph} = 1.2 \times 10^{-10} \eta M / \rho_M T \tag{91}$$

Three main problems arise in the use of equation (91). The first is that the molecules of interest are never perfectly spherical. This will be dealt with below where equations for prolate and oblate spheroids ("cylinders" and "disks" respectively) will be presented. Even if the molecules could be approximated very well by a spherical geometry, difficulties exist in deciding what values should be taken for the microscopic coefficient of friction and for the molecular density.

In the absence of additional information, it is usually assumed that η will to a first approximation be equal to the bulk viscosity of the solvent. Any specific microscopic interactions between the solute molecule and the neighbouring molecules of the solvent would be expected if anything to increase the local viscosity to be used in equation (91) over and above that of the bulk viscosity. On the other hand where the bulk viscosity is determined by the intertwining of elongated molecules, as in gels or polymers, the microscopic friction term may be significantly smaller than the bulk viscosity. For the relatively small and nonpolar solvent molecules used in TRMC studies, e.g. cyclohexane, benzene and dioxane, the use of the bulk viscosity in equation (91) should be a reasonably good first approximation. Evidence is found however for somewhat longer viscosity normalised relaxation times in the pseudo-polar solvents than in saturated hydrocarbons.

The average density of a solute molecule can be estimated by summing the weights and the volume increments associated with different contributing elements of the molecule, dividing these and correcting for the associated free volume. In Table 2.3 we have listed the molecular volume increments, ΔV_M in cm^3/mol, for a variety of individual groups taken from Bondi[61] and

Gavezzotti.[62] A much larger collection is to be found in these references. Listed next to ΔV_M is the value of the effective density of the group, ρ_M in g/cm^3, for which a factor of 0.7 has been applied to account for the free volume associated with molecular packing.

Table 2.3: A selection of volume increments, ΔV_M, and effective densities, ρ_M, (based on a packing coefficient of 0.7) of different groups from references 61 and 62.

Group	ΔV_M (cm^3/mol)	ρ_M (g/cm^3)
-CH$_3$	13.7	0.77
-CH$_2$-	10.2	0.96
=CH- (aliphatic)	8.5	1.07
=CH- (aromatic)	8.1	1.13
-OH	8.0	1.48
-NH$_2$	10.5	1.06
-CN	14.7	1.24
-NO$_2$	16.8	1.92

The majority of solutes studied consist of a hydrocarbon skeleton with here and there nitrogen and/or oxygen atoms functioning as components of donor or acceptor groups. The density will therefore be determined in the first instance by the hydrocarbon part. The most commonly occurring -CH$_2$- and conjugated and aromatic =CH- groups are seen to have values of ρ_M associated with them of 1.0 and 1.1 g/cm^3. Since the less frequently occurring oxygen and nitrogen containing groups tend to have somewhat higher densities we believe that a value of 1.2 g/cm^3 should provide a reasonable estimate of ρ_M for the majority of solute molecules studied. As an example, using the values of ΔV_M from Bondi we calculate effective densities for DMABN, DMANS and tetraphenylethylene of 1.15, 1.25 and 1.22 g/cm^3 respectively.

When $\rho_M = 1.2$ g/cm^3 is substituted in equation (91), the rotation time for a spherical molecule of molecular weight 100 in a solvent of viscosity 1.0 cP at 25 °C is determined to be 34 ps. The molecule with the geometry closest to that of a sphere for which the rotational relaxation time has been measured in this work is p-amino-benzonitrile. This has a molecular weight of 118 and on the basis of equation (91) a relaxation time of 40 ps would be predicted in cyclohexane. The value actually found is 47 ps which is somewhat longer as might be expected

73

on the basis of its more elongated geometry (see below).

It is important to point out that the value of the dipole moment determined is proportional approximately to the square root of the relaxation time used. Any error in Θ is therefore roughly halved in the eventual value of μ.

2.5.2.2 Ellipsoids

The use of equation (91) to estimate rotation times will always be an approximate approach since, as pointed out above, the molecules of interest are invariably non-spherical. They do however quite often have molecular structures which come close to being represented by cylindrical or disk-shaped forms. Solutions have been derived for the rotational diffusion of prolate and oblate ellipsoidal shaped molecules[57] which should provide a better description of dipolar relaxation in such cases.

Ellipsoids have two rotational diffusion coefficients; one corresponding to rotation about the axis of symmetry, D_Z, and one corresponding to rotation about the axes perpendicular to the symmetry axis, D_{XY}, as illustrated in Figure 2.10. The value of these diffusion coefficients are given by equations (92) and (93) respectively[63,64] relative to the diffusion coefficient for a sphere of the same volume, D_{sph} (see equation (88)):

$$D_Z/D_{sph} = 3\gamma(\gamma - S) / 2(\gamma^2 - 1) \tag{92}$$

$$D_{XY}/D_{sph} = 3\gamma[(2\gamma^2 - 1)S - \gamma] / 2(\gamma^4 - 1) \tag{93}$$

The parameter γ is the ratio of the longitudinal axis to the equatorial axis; equivalent to L/B in Figure 2.10. The parameter S is given by equations (94) and (95) for a prolate (cylindrical) and oblate (discoid) ellipsoid respectively:

$$\gamma > 1 \qquad S_{cyl} = (\gamma^2 - 1)^{-0.5} \ln[\gamma + (\gamma^2 - 1)^{0.5}] \tag{94}$$

$$\gamma < 1 \qquad S_{disk} = (1 - \gamma^2)^{-0.5} \tan^{-1}[(1 - \gamma^2)^{0.5} / \gamma] \tag{95}$$

If a cylinder or disk with $\gamma = L/B$ is taken to be an approximate representation of an ellipsoid then the molecular volume is given by:

$$V_M = \pi B^2 L / 4 \tag{96}$$

and

$$V_M = M/6.02 \times 10^{29} \rho_M \tag{97}$$

and γ can then be derived in terms of V_M and either B or L:

$$\gamma = 4V_M / \pi B^3 \tag{98}$$

$$\gamma = (\pi L^3 / 4V_M)^{0.5} \tag{99}$$

For cylinder-shaped molecules equation (98) is used with B fixed at 5.5 Å whereas for disk-shaped molecules equation (99) is used with a fixed value of the disk thickness L of 3.4 Å.
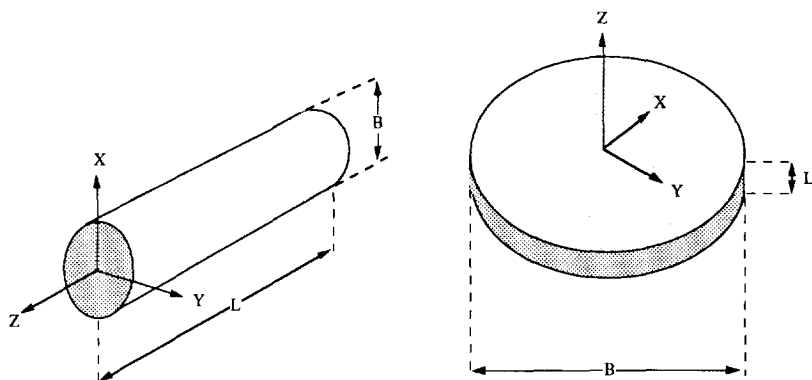
Figure 2.10: Direction of the X-, Y- and Z-axis together with the dimensions L and B for a cylinder and a disk.

2.5.2.3 Cylinder

The fixed value of B = 5.5 Å was determined from best fits to data on relaxation times for a large number of cylinder-shaped molecules determined by both dielectric and fluorescence depolarization measurements.[65] From the fits using this value of B and the bulk viscosity of the solvent, the best average value of the molecular density parameter, ρ_M, was found to be 1.2 g/cm^3 for saturated hydrocarbons and 1.06 g/cm^3 for benzene and dioxane. The value of 1.2 g/cm^3 is in good agreement with the average molecular density estimated in a previous section and supports the non-interactive nature of the alkane solvents. The lower density in the pseudo-polar solvents reflects the in general slower rotation times as might be expected due to solvent solute interaction as discussed above. These values of ρ_M have been generally applied in the

calculations of Θ for a particular solvent for all molecular geometries assumed. The relaxation times listed in Table 2.4, to illustrate the effects of different geometries and sizes were all calculated using a single value of $\rho_M = 1.2$ g/cm^3.

Table 2.4: *Calculated rotational relaxation times about the symmetry (Z) axis and orthogonal (X and Y) axes of prolate (cylindrical) and oblate (discoid) molecules in a solvent of viscosity 1 centipoise using a molecular density of 1.2 g/cm^3, a disk thickness of 3.4 Å or a cylinder diameter of 5.5 Å. Also presented are the rotational relaxation times for an equivalent sphere, Θ_{sph}, and the major relaxation time for a dipole perpendicular to the Z-axis, $\Theta_{XYZ} = 1.5\Theta_Z/(1 + \Theta_Z/\Theta_{XY})$.*

| Molecular Weight | Rotational relaxation time (ps) | | | | | | |
| | sphere | disk | | | cylinder | | |
	Θ_{sph}	Θ_{XY}	Θ_Z	Θ_{XYZ}	Θ_{XY}	Θ_Z	Θ_{XYZ}
50	17	17	20	19	-	-	-
100	34	40	50	46	34	33	34
150	51	67	85	78	63	44	49
200	68	99	124	115	108	54	65
250	85	135	168	155	171	65	82
300	102	175	215	200	255	76	99
400	136	263	319	298	497	98	133
500	170	362	434	407	851	119	168
600	204	471	560	527	1338	141	202
800	272	717	839	794	2774	186	270
1000	340	994	1150	1093	4940	231	339
1200	408	1300	1490	1421	7962	276	407
1500	510	1808	2049	1962	14368	344	509
1750	595	2271	2556	2453	21676	400	594
2000	680	2769	3069	2979	31014	456	679

For most elongated donor-acceptor molecules the dipole is directed along or at least closely parallel to the long axis. Rotation around the Z-axis is therefore ineffective in dipole relaxation. Both the X- and Y-axis tumbling rotations will be effective, however, and since they have identical diffusion coefficients the overal dipole relaxation time will be singular and given by:

$$\Theta_{cyl} = 1/6D_{XY} \tag{100}$$

or

$$\Theta_{cyl} = \Theta_{sph}[D_{XY}/D_{sph}]^{-1} \tag{101}$$

where Θ_{sph} is given by equation (91) and D_{XY}/D_{sph} by equation (93).

To summarise; the rotational relaxation time for a dipole directed along the long axis of a cylindrically shaped molecule is denoted by Θ_{cyl} and is calculated using equation (101). D_{XY}/D_{sph} is calculated using equations (93) and (94). γ is determined using equations (90) and (98) with B = 5.5 Å, η = the bulk solvent viscosity, and ρ_M = 1.2 g/cm^3 for saturated hydrocarbons and 1.06 g/cm^3 for benzene and dioxane.

An approximate formula for D_{XY}/D_{sph}, which is valid for $\gamma^2 \gg 1$, can be useful for rapid calculation, this is:

$$S \approx \gamma^{-1} \ln(2\gamma) \tag{102a}$$

$$D_{XY}/D_{sph} \approx 3\gamma^{-2}[\ln(2\gamma) - 0.5] \tag{102b}$$

which leads to the expression for Θ_{cyl} previously reported:[65]

$$\Theta_{cyl} \approx \Theta_{sph} \gamma^2 / 3[\ln(2\gamma) - 0.5] \tag{103}$$

Cases of molecules with a dipole orientation perpendicular to the Z-axis of the cylinder are less common in donor-acceptor compounds. The dipole relaxation for such molecules will be complex since both Z-axis spinning and XY-axis tumbling are effective. Spinning will be more rapid than tumbling and a complex relaxation process with two decay constants, $1/6D_{XY}$ and $1/(2D_{XY} + 4D_Z)$, is expected.[64] The overal relaxation would in general, however, be expected to be considerably faster and to be much closer to Θ_Z than to Θ_{XY}, as given by equation (104):

$$\Theta \approx \Theta_{sph}D_{sph}/D_Z \tag{104}$$

The values of Θ_{XY} and Θ_Z are listed in Table 2.4 for comparison. In subsequent chapters Θ_{cyl} is used to represent only Θ_{XY}, i.e. the tumbling motion as given by equation (101).

2.5.2.4 Disk

In the present context examples of approximately disk-shaped molecules may be considered to be large aromatic systems such as porphyrins with relatively small donor or acceptor groups attached. Hence the use of a disk thickness, L, of 3.4 Å which is the characteristic contact distance for aromatic π-systems. In these cases the dipole vector will usually be in the plane of the disk. Dipole relaxation can then occur by both spinning about the Z-axis and tumbling about X or Y. The diffusional relaxation under these circumstances has two time constants[64] given by:

$$\Theta_{disk}(1) = 1/6D_{XY} \tag{105}$$

and

$$\Theta_{disk}(2) = 1/(2D_{XY} + 4D_Z) \tag{106}$$

The rotational diffusion times associated with tumbling, Θ_{XY}, and spinning, Θ_Z, are in fact not substantially different for a disk as is shown by the values in Table 2.4. In view of this and the fact that the weighting factor for the second relaxation process is 3 times that of the former,[64] we take equation (106) to be a good approximation for the relaxation time of a dipole lying in the plane of a disk. The use of Θ_{disk} in the text will refer therefore to equation (107).

$$\Theta_{disk} = \Theta_{sph}D_{sph}/(2D_{XY} + 4D_Z) \tag{107}$$

For a disk-shaped molecule with a dipole lying along the axis of symmetry the relaxation time is of course given simply by $\Theta_{sph}D_{sph}/D_{XY}$ with D_{XY}/D_{sph} derived using equations (93) and (95).

2.6 TIME-RESOLVED FLUORESCENCE MEASUREMENTS

Time-resolved fluorescence measurements are carried out using a nitrogen laser (Laser Photonics, LN 1000) with an excitation wavelength of 337 nm, a pulse width of 0.8 ns (FWHM) and an energy per pulse of approximately 1.4 mJ. The experimental set-up as used is depicted in Figure 2.11. The beam cross-section at the position of the cell containing the solution is 3 mm x 7 mm. The light emitted from a 1 cm quartz cuvette containing CO_2 deaerated OD ≈ 0.2 solutions is monitored at 90° to the laser beam and is detected using a ITL TF1850 photodiode with a response time of 100 ps after passing through a monochromator (Jobin Ivon). The
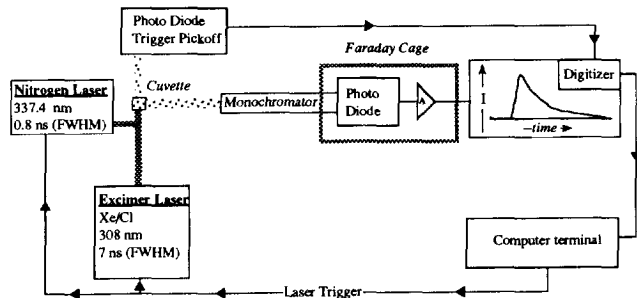
Figure 2.11: Schematic representation of the experimental set-up for the time-resolved fluorescence experiments.

wavelength region covered is 300 to 800 nm with a 400 nm cut-off filter inserted for wavelengths above 600 nm to attenuate the second order reflection of the laser line. The transient output voltage of the photodiode is amplified by a factor of 27, using Picosecond Pulse Labs 5800 series amplifiers (risetime < 150 ps) prior to monitoring with a Tektronix 7912 AD (0.5 GHz) transient digitizer. A single-shot pulse mode was used with a maximum number of 64 traces being averaged. Lifetimes were determined using a convolution procedure with which it is possible to determine accurate values of the lifetimes down to *ca* 200 ps.
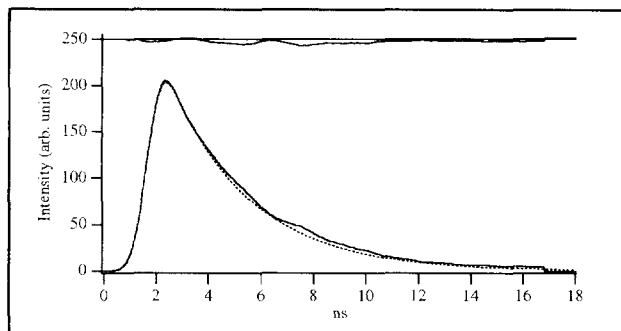
Figure 2.12: *Kinetic trace of the fluorescence decay at 550 nm for a solution of DMANS in benzene excited at 337 nm.*

In Figure 2.12 a kinetic trace taken at 550 nm from a flash-photolysed CO_2 deaerated solution of DMANS in benzene is shown. A convolution fit to the trace using the nitrogen laser pulse shape, resulted in a lifetime of 3.1 ns for the singlet excited state of DMANS.

2.7 SOLVENT PROPERTIES

The properties[66] of the solvents used in studies of the formation of highly dipolar excited states of solute molecules are very important in both TRMC and fluorescence experiments. From the practical point of view it is imperative that the solvents used in TRMC experiments consist of molecules with close to zero dipole moment otherwise the sensitivity to the micromolar or so of dipolar excited molecules produced on photoexcitation becomes negligibly small. The situation is somewhat similar to trying to monitor very small optical absorption changes in a solution with a high background optical density. The upper limit in terms of allowed dipole moment is approximately 0.5 D which is slightly larger than the 0.36 D of toluene. Even the small net dipole moment of n-hexane is apparent as a larger dielectric loss (apparent as a larger value of $1/Q_U$ in Table 2.1) than for cyclohexane. If a very low dipole moment was always associated with a very low solvent "polarity" then the TRMC technique

Table 2.5: *Dimroth's solvent polarity parameter, $E_T(30)$, fluoroprobe emission maximum, E_F, the relative dielectric constant, ε, the refractive index n_D and the theoretical parameter f-f' together with f and f'.*

Solvent	$E_T(30)$ (eV)	E_F (eV)	ε at 25°C	n_D	f	f'	f-f'
n-hexane	1.34	3.04	1.88	1.3749	0.1849	0.1862	-0.0014
cyclohexane	1.35	3.02	2.02	1.4262	0.2024	0.2040	-0.0016
di-n-butyl ether	1.44	2.66	3.08	1.3992	0.2905	0.1948	0.0957
diisopropyl ether	1.47	2.52	3.88	1.3681	0.3288	0.1838	0.1450
benzene	1.49	2.60	2.28	1.5011	0.2302	0.2276	0.0026
diethyl ether	1.50	2.41	4.34	1.3524	0.3450	0.1780	0.1671
1,4-dioxane	1.56	2.44	2.21	1.4224	0.2232	0.2028	0.0205
ethyl acetate	1.65	2.17	6.02	1.3724	0.3850	0.1853	0.1996
dichloromethane	1.78	2.14	8.93	1.4242	0.4205	0.2034	0.2171
acetonitrile	1.99	1.79	37.50	1.3441	0.4803	0.1748	0.3054

would be extremely limited both in terms of the solutes that would dissolve but more importantly in the study of the extremely important area of the effects of solvent interactions on the photophysics of intramolecular charge separation.

Fortunately for TRMC studies, neither the microscopic dipole moment nor the macroscopic dielectric constant are necessarily direct indicators of the "solvating power" of a solvent towards a dipolar solute molecule. For example in Table 2.5 are shown a variety of solvents listed in order of their solvating power as measured by their $E_T(30)$ value, as introduced by Dimroth,[67] which is the most generally accepted criterion of solvent "polarity". The $E_T(30)$ value is the absorption maximum of pyridinium-N-phenol betaine,[66,67] a compound which in the ground state is highly charge separated and undergoes a decrease in dipole moment on photoexcitation. The shift in absorption maximum is therefore hypsochromic. As can be seen a direct relationship between $E_T(30)$ and the dielectric constant of the solvent is not to be found although a general trend to higher values of both parameters is apparent.

The $E_T(30)$ values for benzene and dioxane are in particular much larger than would be expected on the basis of their low dielectric constants and zero dipole moments. They may therefore be considered to be "pseudo-polar" solvents with properties resembling those of the dipolar ethers such as diethylether and tetrahydrofuran. The reasons for the abnormal solvating power of these solvents most probably lies in their high quadrupole and octupole moments respectively which do not contribute to the bulk dielectric constant or the dipole moment of the molecule but could interact with the non-uniform electric fields in the vicinity of a molecular

charge. Whatever the cause, the result is that TRMC studies can in fact be carried out using these pseudo-polar solvents into a region of "polarity" corresponding effectively to a dielectric constant of approximately 6.

Of particular interest in the work presented here is the additional stability of a completely charge separated state of a molecule which results from a change in solvent from a saturated hydrocarbon to either benzene or dioxane. This can be estimated from the bathochromic shift of the fluorescence maximum of "Fluoroprobe", a sigma-bond separated donor-acceptor molecule which undergoes complete charge separation on photoexcitation but nevertheless fluoresces with high quantum yield in most solvents.[68] The emission maximum of Fluoroprobe is listed as E_F in eV for several solvents in table 2.5. E_F is found to parallel quite well the trend found in the $E_T(30)$ values, as would be expected, with the energy shifts being substantially bigger for the former due to the change from zero dipole moment to close to 25 D.[68] The decrease in the energy of a charge separated (CS) state as measured by the E_F value is seen to be 0.4 eV in benzene and 0.56 eV in dioxane. In TRMC studies therefore the level of a CS state can be varied by more than half a volt which in practice is found to be sufficient to produce large changes in the molecular photophysics of opto-electric molecules.

Also included in Table 2.5 are the values of the refractive index of the solvents and the parameters f and f'. The difference (f - f') is routinely used in the "theoretical" treatment of experimental data on solvatochromic shifts of absorption and emission spectra.[69-72]

$$f = 2[\epsilon'(0) - 1] / [2\epsilon'(0) + 1] \tag{108}$$

$$f' = 2[n^2 - 1] / [2n^2 + 1] \tag{109}$$

Since f is based on the bulk dielectric constant it is clear, from the data in Table 2.5, that the parameter (f - f') will be only a crude measure of the solvating power, or polarity, of the solvent. Neverthless relationship (110) is the most frequently used for the estimation of dipole moments of molecules in which charge separation on excitation occurs. $\Delta\mu_{cs}$ can be derived from the solvent dependence (solvatochromism) of the optical absorption and emission frequencies (v_a and v_f) via:

$$v_a - v_f = \text{const} + (f-f') [(\Delta\mu_{cs})^2 / hc\rho^3] \tag{110}$$

where ρ is the radius of a sphere equal to the solvent excluded volume of the molecules.

Clearly when using these relationships (108-110) one has to be careful about the choice of solvents. Data for benzene and dioxane are usually dismissed as "anomalous". As will be seen in subsequent chapters, the agreement between excited state dipole moments determined using the TRMC method and those derived from solvatochromic shifts is, perhaps surprisingly, usually very good.

2.8 REFERENCES

1   J.M. Warman and M.P. de Haas in *Pulse Radiolysis;* Y. Tabata, Ed.; CRC Press: Boca Raton, USA, **1991**; Chapter 6.

2   H. Shimamori in *Progress in Photochemistry and Photophysics;* CRC Press: Boca Raton, USA, **1992**; Vol VI, Chapter 2.

3   M.A. Biondi and S.C. Brown, *Phys. Rev.* **1949**, *87*, 83.

4   R.W. Fessenden and J.M. Warman, *Adv. Chem. Ser.* **1968**, *82*, 222.

5   J.M. Warman and M.C. Sauer, *J. Chem. Phys.* **1970**, *52*, 6428.

6   A.F. Gibson, *Proc. Phys. Soc.* **1956**, *B69*, 488.

7   J.A. Naber and D.P. Snowden, *Rev. Scient. Instrum.* **1969**, *40*, 1137.

8   J.M. Warman, M.P. de Haas and A. Hummel, *Chem. Phys. Lett.* **1973**, *22*, 480.

9   M.P. de Haas, J.M. Warman, P.P. Infelta and A. Hummel, *Chem. Phys. Lett.* **1975**, *31*, 382.

10   M.P. de Haas, J.M. Warman and A. Hummel, *Proc. 5th Int. Conf. on Conduction and Breakdown in Dielectric Liquids;* Delft University Press: Delft, **1975**.

11   J.M. Warman, P.P. Infelta, M.P. de Haas and A. Hummel, *Chem. Phys. Lett.* **1976**, *43*, 321.

12   J.M. Warman, P.P. Infelta, M.P. de Haas and A. Hummel, *Can. J. Chem.* **1977**, *55*, 2249.

13   M.P. de Haas, A. Hummel, P.P. Infelta and J.M. Warman, *J. Chem. Phys.* **1976**, *65*, 5019.

14   P.P. Infelta, M.P. de Haas and J.M. Warman, *Radiat. Phys. Chem.* **1977**, *10*, 353.

15   C.A.M. van den Ende, L. Nyikos, J.M. Warman and A. Hummel, *Radiat. Phys. Chem.* **1980**, *15*, 273.

16   M.P. de Haas, *PhD. Thesis*, University of Leiden, **1977**.

17   R.W. Fessenden, P.M. Carton, H. Paul and H. Shimamori, *J. Phys. Chem.* **1979**, *83*, 1677.

18   J.M. Warman, M.P. de Haas, A. Hummel, C.A.G.O. Varma and P.H.M. van Zeyl, *Chem. Phys. Lett.* **1982**, *87*, 83.

19   M.P. de Haas and J.M. Warman, *Chem. Phys.* **1982**, *73*, 35.

20   R.W. Fessenden, P.M. Carton, H. Shimamori and J.C. Scaiano, *J. Phys. Chem.* **1982**, *86*, 3803.

21   R.W. Fessenden and P.V. Kamat, *Chem. Phys. Lett.* **1986**, *123*, 233.

22   J.M. Warman, M.P. de Haas, M. Grätzel and P.P. Infelta, *Nature* **1987**, *91*, 396.

23   J.M. Warman and R.J. Visser, *Chem. Phys. Lett.* **1983**, *98*, 49.

24   R.W. Fessenden, A. Hitachi and V. Nagarajan, *J. Phys. Chem.* **1984**, *88*, 107.

25   R.W. Fessenden and J.C. Scaiano, *Chem. Phys. Lett.* **1985**, *117*, 103.

26   K.D. Asmus and E. Janata in *The Study of Fast Processes and Transient Species by Electron Pulse Radiolysis;* J.H. Baxendale and F. Busi, Eds.; Reidel: Dordrecht, **1982**, 91.

27   J.M. Warman in *The Study of Fast Processes and Transient Species by Electron Pulse Radiolysis;* J.H. Baxendale and F. Busi, Eds.; Reidel: Dordrecht, **1982**, 129.

28   K.D. Asmus, *Int. J. Radiat. Phys. Chem.* **1972**, *4*, 417.

29   G.C. Barker, P. Fowles, D.C. Sammon and B. Stringer, *Trans. Farad. Soc.* **1970**, *66*, 1498.

30   A. Hummel and W.F. Schmidt, *Radiat. Res. Rev.* **1974**, *5*, 199.

31   G. Beck, *Rev. Sci. Instrum.* **1979**, *50*, 1147.

32   B. Vojnovic, R.F. Anderson and B.D. Michael, *Radiat. Phys. Chem.* **1986**, *27*, 363.

33   E.C. Gregg and G. Bakale, *Radiat. Res.* **1970**, *42*, 13.

34   R.W. Fessenden and J.M. Warman, in *Radiation Chemistry-II;* Advances in Chemistry Series Nr. 82, ACS: Washington, D.C., **1986**, 222.

35   C.G. Montgomery, R.H. Dickie and E.N. Purcell in *Principles of Microwave Circuits;* Radiation Laboratory Series, Vol. 10, McGraw-Hill: New York, **1948**.

36   N. Marcuvitz in *Waveguide Handbook;* Radiation Laboratory Series, McGraw-Hill: New York, **1951**, Vol. 10.

37   M. Sucher in *Handbook of Microwave Measurements;* M. Sucher and J. Fox, Eds.; John Wiley: New York, **1963**, Vol 2, Chapter VIII.

38   F.E. Gardiol in *Introduction to Microwaves;* Artech House Inc.: Dedham, USA, **1984**.

39   H.M. Altschuler in *Handbook of Microwave Measurements;* M. Sucher and J. Fox, Eds.; John Wiley & Sons, Inc., **1963**, Vol. 2, Chapter IX.

40   S.C. Brown and C.L. Braun, *J. Phys. Chem.* **1991**, *95*, 511.

41   P. Debye in *Polar Molecules;* Dover: New York, **1945**, Chapter 5.

42   R. Coelho in *Physics of Dielectrics;* Elsevier: Amsterdam, **1979**, 38-47.

43   R. Pethig in *Dielectric and Electronic Properties of Biological Materials;* John Wiley, New York, **1979**, 15-23.

44   C.J.F. Böttcher in *Theory of Electric Polarisation;* Elsevier: Amsterdam, **1973**; Vol. 1.

45   C.J.F. Böttcher and P. Bordewijk in *Theory of Electric Polarisation;* Elsevier: Amsterdam, **1978**; Vol. 2.

46   H. Fröhlich in *Theory of Dielectrics;* 2nd Ed.; Oxford University Press: London, **1958**.

47   C.A.M. van de Ende, *PhD. Thesis,* University of Leiden, **1981**.

48   M. Sucher in *Handbook of Microwave Measurements;* M. Sucher and J. Fox, Eds.; John Wiley: New York, **1963**, Vol 2, Chapter VIII, 427.

49   F.E. Gardiol in *Introduction to Microwaves;* Artech House Inc.: Dedham, USA, **1984**, pp 109-145.

50   Reference 48, 420 and 471.

51   H.M. Altschuler in *Handbook of Microwave Measurements;* M. Sucher and J. Fox, Eds.; John Wiley & Sons, Inc., **1963**, Vol. 2, Chapter IX, 523.

52   J.M. Warman, W. Schuddeboom, S.A. Jonker, M.P. de Haas, M.N. Paddon-Row, K.A. Zachariasse and J.P. Launay, *Chem. Phys. Lett.* **1993**, *210*, 397-403.

53   A.L. McLellan in *Tables of Experimental Dipole Moments;* Rahara Enterprises: El Cerrito, CA, **1974**; Vol. 2

54   A.L. McLellan in *Tables of Experimental Dipole Moments;* Rahara Enterprises: El Cerrito, CA, **1974**; Vol. 3.

55   G. Williams, *Trans. Faraday Soc.* **1968**, *64*, 1219-1227.

56   D.B. Toublanc, R.W. Fessenden and A. Hitachi, *J. Phys. Chem.* **1989**, *93*, 2893.

57   C.P. Smyth, *Chem. Soc. Spec. Publ.* **1966**, no. *20*.

58   R.W. Fessenden and A. Hitachi, *J. Phys. Chem.* **1987**, *91*, 3456.

59   A. Einstein, *Ann. Phys. Ser.* **1905**, *4*, *17*, 549.

60   A. Einstein, *Ann. Phys. Ser.* **1906**, *19*, 371.

61   A. Bondi, *J. Phys. Chem.* **1964**, *68*, 441-451.

62   A. Gavezzotti, *J. Am. Chem. Soc.* **1983**, *105*, 5220-5225.

63   F. Perrin, *J. Physique et Le Radium* **1934**, *5*, 497-511.

64   T. Tao, *Biopolymers* **1969**, *8*, 609-632.

65   J.M. Warman and M.P. de Haas, *Interuniversity Reactor Institute Report;* No. 134-86-07, **1986**.

66   C. Reichardt in *Solvent Effects in Organic Chemistry;* Verlag Chemie: Weinheim, New York, **1979**.

67   K. Dimroth, C, Reichardt, T. Siepmann and F. Bohlmann, *Liebigs Ann. Chem.* **1963**, *661*, 1.

68   R. M. Hermant, *PhD Thesis*, University of Amsterdam, Amsterdam, **1990**

69   W. Liptay in *Excited States;* E.C. Lim, Ed.; Academic: New York, **1974**; Vol. 1, 129.

70   W. Liptay in *Modern Quantum Chemistry;* O. Sinanoglu, Ed.; Academic: New York, **1965**; Part II, 173.

71   W. Liptay in *Z. Naturforsch.* **1965**, *20a*, 1441.

Chapter 3

Influence of the Alkyl Chain Length and

Effective Solvent Polarity

on the Excited State Dipole Moments

of 4-(Dialkylamino)benzonitriles[1]

3.1 INTRODUCTION

More than thirty years[2] ago 4-(dimethylamino)benzonitrile (DMABN) was found to show dual fluorescence resulting from a reversible intramolecular charge transfer (ICT) process. Since then a lot of other related compounds have been found to show the same behaviour. From the initially excited singlet state, a species with a considerably larger dipole moment is produced,[2-11] as shown in Scheme 3.1, where k_a and k_d are the rate constants of the forward and backward charge-transfer processes, respectively. These states will be referred to respectively as LE and CS in the following text. The LE state may have charge transfer character as indicated in Figure 1.1A in Chapter 1. $\tau_0(LE)$ and $\tau_0(CS)$ are the overall lifetimes of the two states. The radiative rate constants $k_f(LE)$ and $k_f(CS)$ are also indicated.
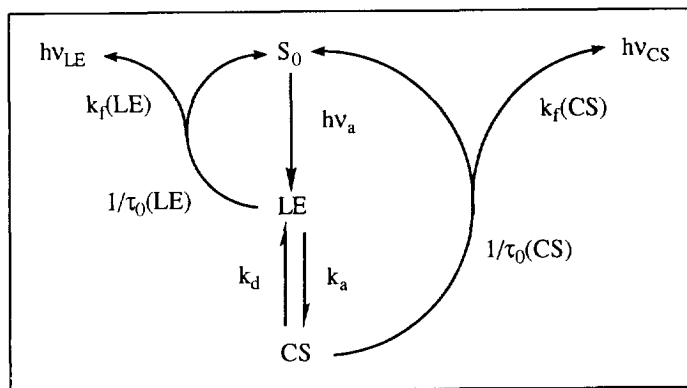
Scheme 1.1

Especially in the case of DMABN, the appearance of dual fluorescence is well documented for polar solvents as well as for the pseudo-polar dioxane.[2-11] In the pseudo-polar solvent benzene, a weak CS emission (shoulder) has been detected at room temperature.[2,12] In the

similar solvent toluene a strong dual fluorescence was found at lower temperatures.[13] For 4-(dialkylamino)benzonitriles in nonpolar solvents, such as cyclohexane, excited state charge transfer and dual fluorescence are generally considered to be absent.[2-12,14] Nevertheless, indications have been found that a CS state is produced in DMABN even in 3-methylpentane and in n-heptane.[15-17]

In the discussions concerning the molecular nature of the LE and CS states in systems such as DMABN, the values for the dipole moments of these two fluorescent species have been a point of considerable interest and debate, with a relatively large variation in the reported data.[2-12,18-22] In the orginal papers on dual fluorescence by Lippert et al.,[2,3] the excited state dipole moments of DMABN and 4-(diethylamino)benzonitrile (DEABN) were determined by solvatochromic shift measurements, based on the difference in energy Δv between the maxima of the LE or CS fluorescence bands and the corresponding absorption maxima as a function of the polarity and polarizability of the solvent.[23-25] From these measurements, a value of 23 D was deduced in the case of DMABN for the dipole moment $\mu_S(CS)$ of the new anomalous emission, based on a ground state dipole moment, μ_0, of 6.0 D.[2-5] In this determination of $\mu_S(CS)$, it was assumed that the CS state can be populated directly by light absorption. This assumption is a direct consequence of the interpretation initially given by Lippert,[2-5] that the new "anomalous" CS band is equivalent to the solvent-stabilized ^1L_a band of DMABN. It has, however, been shown[13] that the CS state is not accessible by direct excitation. Under these conditions, $\mu_S(CS)$ can only be determined by plotting the energy of the CS emission maximum versus the solvent polarity parameter f-0.5f'. Using this procedure,[13,26] an excited state dipole moment of 16.1 D has been obtained from the data of reference 2.[27]

As a possible improvement on the Lippert-Mataga method,[23-25] a "simplified microstructural solvent interaction" model was applied to the solvatochroism of intramolecular charge-transfer systems by Rettig.[28] Using this model, considerably lower values for the excited state dipole moment, $\mu_S(CS)$, were found than with the original method (12.2 D for DMABN and 11.5 D for DEABN).[29-31]

From the solvent dependence of the directly excited LE band of DMABN in reference 2, the difference in dipole moments $\Delta\mu = \mu_S(LE) - \mu_0$ is found to be close to zero. For DEABN even a slightly negative value is obtained for $\Delta\mu$. It would therefore appear that for these molecules the dipole moment of the LE state is close to or even smaller than that of the ground state. This somewhat surprising result could orginate from the following difficulty encountered in these solvatochromic measurements. The lowest-energy absorption of DMABN and DEABN consists of two overlapping bands, as was already recognized by Lippert,[2-5] which makes the determination of the energy difference between the absorption and fluorescence maxima

uncertain.

Estimates of the excited state dipole moment of DMABN have also been made by measuring the temperature dependence of the LE and CS fluorescence maxima (thermochromic shift), a method similar in principle to solvatochroism.[32-34] The variation in polarity and polarizability is brought about by changing the temperature instead of using different solvents. From these measurements, Suppan reported the following values for DMABN: $\mu_S(LE) = 10$ D and $\mu_S(CS) = 19.5$ D in tetrahydrofuran.[32,34]

The first more direct, electrical measurements of the overall[35] singlet excited state dipole moment, μ_S, of DMABN were caried out by Czekalla et al.,[36-38] employing the effect of
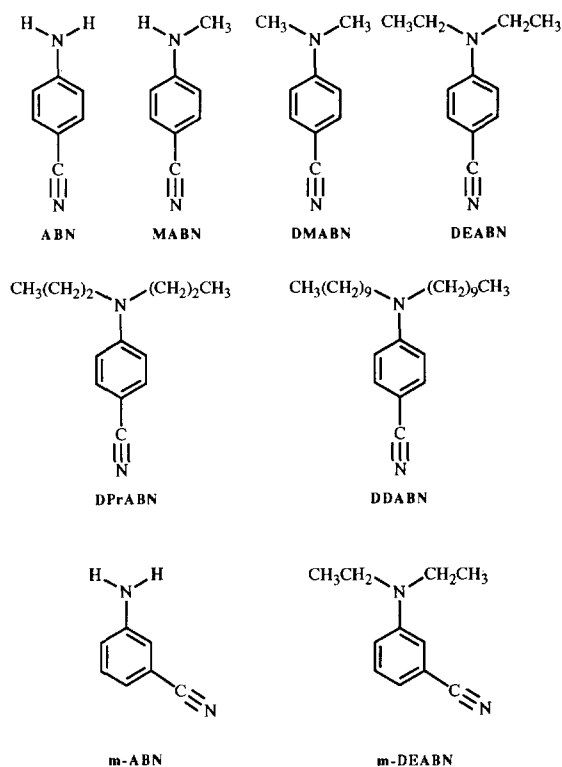
Figure 3.1: Para-substituted donor-acceptor systems studied with a benzonitrile group as acceptor and either a dialkylamino group, an alkylamino group or an amino group as donor: 4-(amino)benzonitrile (ABN), 4-(methylamino)benzonitrile (MABN), 4-(dimethylamino)benzonitrile (DMABN), 4-(diethylamino)benzonitrile (DEABN), 4-(dipropylamino)benzonitrile (DPrABN) and 4-(didecylamino)benzonitrile (DDABN). Meta-substituted donor-acceptor systems: 3-(amino)benzonitrile (m-ABN) and 3-(diethylamino)benzonitriles (m-DEABN).

87

external electric fields on fluorescence band positions and intensities. These electrochromic fluorescence experiments resulted in a dipole moment of 13 D in dioxane. A value of 12.5 D was derived by Labhart[39] and Sinha[40] from electrochromic absorption measurement in dioxane. Using the related integral electrooptical emission measurements, Baumann[18,19] arrived at: $\mu_S(LE) = 5.8$ D and $\mu_S(CS) = 16.5$ D in dioxane, the latter value being an upper limit for the permanent dipole moment, when the specific influence of solvent polarizability is neglected.[20]

In previous publications, using the TRMC technique, dipole moment values for the singlet excited state of DMABN of 9.1 D[21], 13.1 D[22] and 13.0 D[22] have been reported in cyclohexane, benzene and dioxane respectively.

In this chapter the excited state dipole moments measured by the TRMC technique for a series of 4-(dialkylamino)benzonitriles with different alkyl groups (methyl, ethyl, propyl and decyl) are reported in cyclohexane, benzene and dioxane. The compounds were obtained from the group of Zachariasse from the Max-Planck Institute in Göttingen, which also performed the fluorescence measurements from which the relative contributions of the LE and CS states could be determined. The separate dipole moments of the LE and CS states could be estimated, by combining the TRMC data with the results obtained from steady-state and time-resolved fluorescence measurements. In addition, 4-aminobenzonitrile (ABN) and 4-(methyl-amino)benzonitrile (MABN) and also two meta-substituted aminobenzonitriles; 3-amino-benzonitrile (m-ABN) and 3-(diethylamino)benzonitrile (m-DEABN), all of which do not undergo intramolecular charge transfer (see next sections), were investigated for comparative purposes. All structures with their shorthand nomenclature are shown in Figure 3.1. Ground state dipole moments and dipole relaxation times, which are necessary for the data analysis, have also been measured in Göttingen and Delft respectively.

3.2 TRMC MEASUREMENTS

In Figure 3.2 are shown the traces of the change in the microwave conductivity found on flash-photolysis of solutions of MABN, DMABN, DEABN, DPABN and DDABN in cyclohexane, benzene and dioxane. In Figure 3.3 are shown similar traces for ABN, m-ABN and m-DEABN. Most transients display an initial "fast" component that decays within nanoseconds to tens of nanoseconds after the pulse, to be followed by a "slow" component which decays over a much longer timescale of microseconds. The two components are assigned to the excited singlet and triplet states, respectively. Because of the relatively large triplet components the singlet state lifetimes could not be determined accurately from the TRMC traces themselves. The signals were therefore fit using for the singlet state the lifetime derived from fluorescence decay time measurements given in Table 3.1 (see Section 3.3). The lifetimes
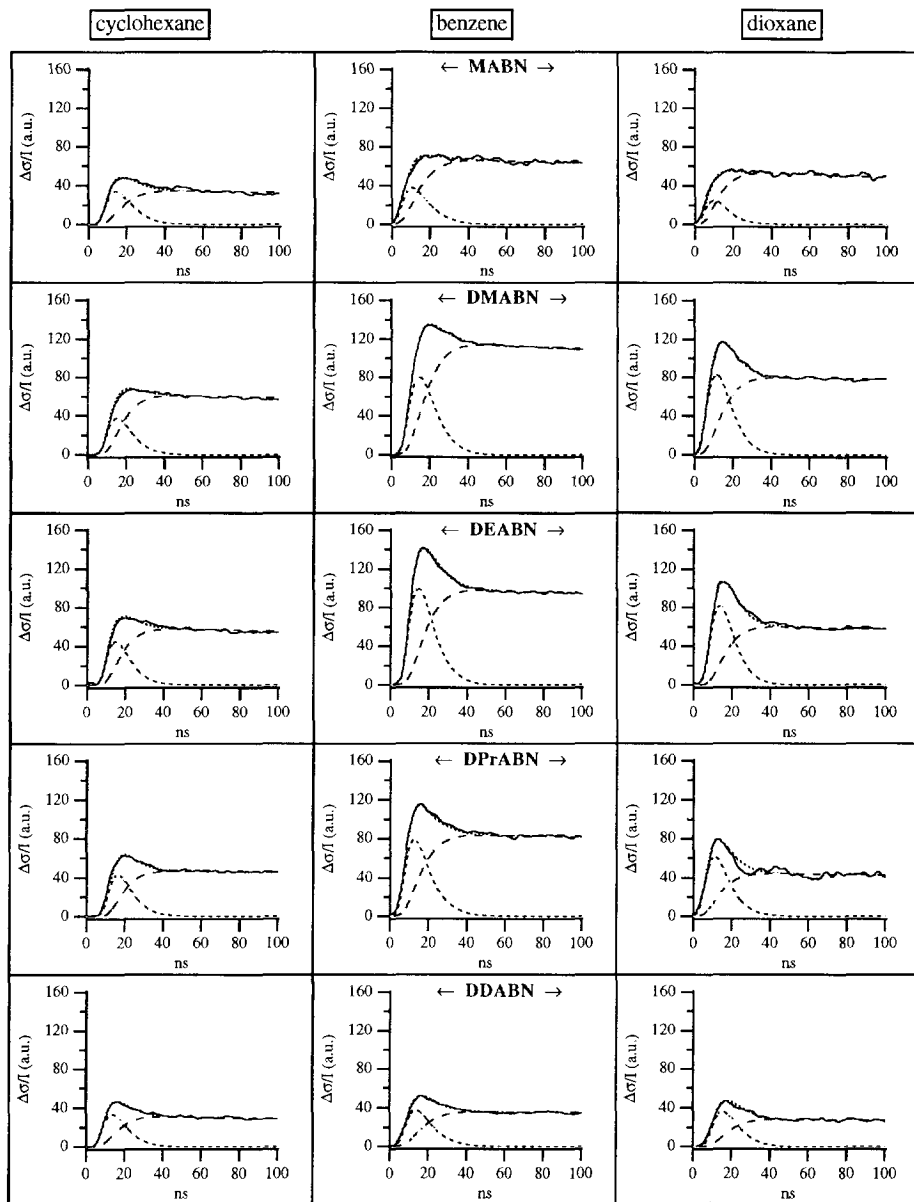
Figure 3.2: *Transient changes in the microwave conductivity (dielectric loss) of ca 10^{-4} M solutions of the 4-(amino)benzonitriles shown in cyclohexane, benzene and dioxane on flash-photolysis at 308 nm, pulse width 7 ns. The dashed lines show the individual contributions from the excited singlet and triplet states to the overall fit curve, shown as a dotted line. The fitting parameters are given in Table 3.1.*

89

of the triplet transients were generally a microsecond or longer and were not always accurately measured. The fits to the heights of the singlet- and triplet state levels, which are carried out on the data within the first 100 ns, are insensitive to the value taken for the triplet lifetime.

From the fits the values of ΔM_S for the singlet state and ΔM_T together with Φ_{isc} for the triplet state are determined. The last two parameters are very close to being inversely related to each other in the fitting procedure, and since Φ_{isc} is usually not known, the actual parameter used to quantitatively fit the triplet component of the data is the product $\Delta M_T \Phi_{isc}$. The fits to the TRMC transients are plotted in Figure 3.2 and Figure 3.3, together with the contributions of the individual singlet and triplet components. The values of ΔM_S and $\Delta M_T \Phi_{isc}$ obtained from the fits of all the solute/solvent combinations studied are listed in Tables 3.1 and 3.2, respectively.
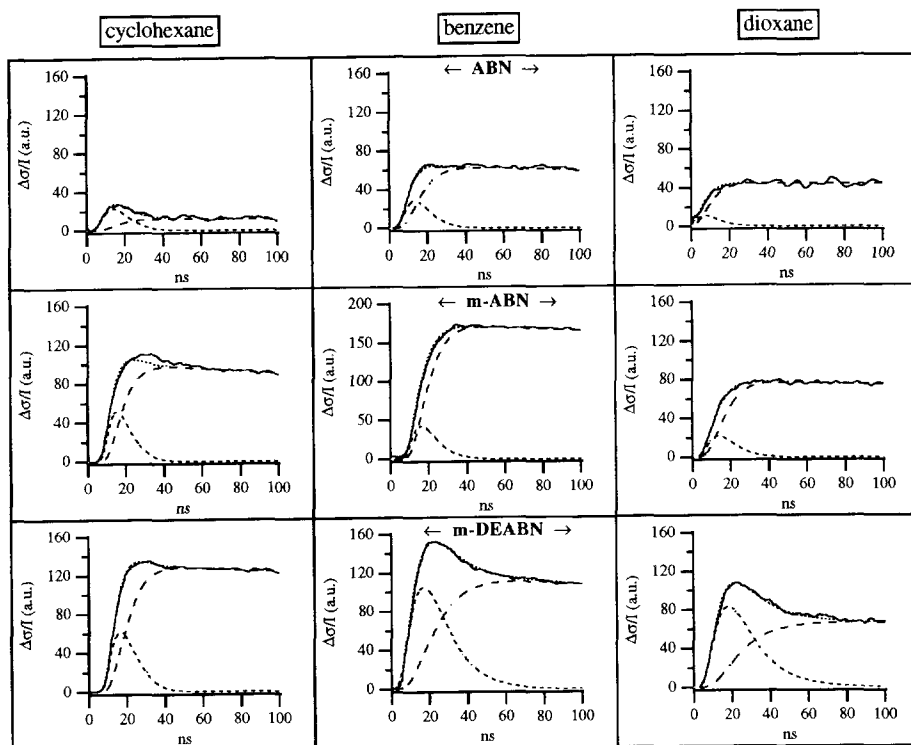
Figure 3.3: *Transient changes in the microwave conductivity (dielectric loss) of ca 10^{-4} M solutions of ABN and the 3-(amino)benzonitriles shown in cyclohexane, benzene and dioxane on flash-photolysis at 308 nm, pulse width 7 ns. The dashed lines show the individual contributions from the excited singlet and triplet states to the overall fit curve, shown as a dotted line. The fitting parameters are given in Table 3.1.*

3.2.1 Qualitative conclusions

A qualitative impression of changes in the dipolar character of the compounds on photo-excitation can often be obtained from the raw TRMC data. For example, as mentioned in the previous section the TRMC transients in Figures 3.2 and 3.3 clearly show the formation of a triplet state with a dipole moment appreciably larger than the ground state as well as a dipolar singlet state. In addition from the traces shown in Figure 3.2, which were all taken under similar conditions of solute optical density and pulse intensity qualitative conclusions can be drawn about changes in the dipole moment of the singlet state with increasing alkyl substitution. In drawing such conclusions from the transients in Figure 3.2 it is important to realize that for all solvents the singlet lifetime either remains constant, as in dioxane, or decreases, as for cyclohexane and benzene, with increasing alkyl substitution. In addition the rotational relaxation time gradually increases with increasing molecular weight in all solvents. These combined effects would result in a decrease in the height of the singlet state component with increasing alkyl substitution if the dipole moment of the singlet state remains constant. The results in Figure 3.2 show clearly that this is not the case. The changes in going from MABN to DMABN are particularly illustrative; for cyclohexane little change occurs indicating only a slightly larger dipole moment of the dimethyl compound; for benzene and particularly dioxane, however, there is a marked increase in signal indicating a very substantial increase in dipole moment on substitution of the second methyl group. For dioxane further lengthening of the alkyl chains leads to a gradual decrease in signal which can be mainly attributed to the increase in rotation time and indicates a close to constant dipole moment. The almost constant signal height up to DPrABN for benzene suggests a gradual further increase in dipole moment. And, of particular interest, the singlet component for cyclohexane increases in going from DMABN to DPrABN indicating a substantial increase in dipole moment even in this completely nonpolar solvent.

For the solutes which display no "anomalous" fluorescence, MABN and the compounds shown in Figure 3.3 the singlet state component is nevertheless always found to be positive, showing that the dipole moment of the LE state must be substantially larger than that of the ground state although considerably less than that of the CS state. The surprisingly long lifetimes of the LE state of m-DEABN in benzene and dioxane are also clearly shown by the traces in Figure 3.3.

3.2.2 Quantitative TRMC results

The effective dipole moment of the singlet excited state, μ_S, can be calculated from ΔM_S and M_0, if μ_0 is known, via equation (1) (see for derivation equation (84) in Chapter 2). The assumption made is that the rotational relaxation times, Θ, are the same for the ground and excited state:

$$\mu_S = \mu_0 (\Delta M_S / M_0 + 1)^{0.5} \tag{1}$$

The dipole relaxation times of the solutes can be evaluated from the rotational charge mobility in the ground state M_0, using the ground state dipole moment μ_0 via equation (2), as derived in Chapter 2:

$$M_0 = (\varepsilon + 2)^2 \mu_0^2 F(\omega\Theta) / 27ek_B T\Theta \tag{2a}$$

$$F(\omega\Theta) = (\omega\Theta)^2 / [1 + (\omega\Theta)^2] \tag{2b}$$

with the term $F(\omega\Theta)$ being taken to be that for a single, Debye relaxation. The ground state dipole moments μ_0 (see Table 3.1) were determined in dioxane at 25 °C from measurements of the dielectric constant, the refractive index, and the density of solutions at five or six solute mole fractions, extrapolated to zero solute concentration. This method is based on that of Hedestrand,[41] restricted to a single temperature. The dioxane used in these measurements was dried over molecular sieves. The value of $\mu_0 = 6.6$ D obtained for DMABN is similar to literature[42-45] values.

For all aminobenzonitriles studied here the value of M_0 was determined in benzene as well as for several compounds in cyclohexane and for DMABN in dioxane as described in Chapter 2. The results are presented in Table 3.1. The corresponding rotational relaxation times Θ were calculated using equation (80) in Chapter 2 and these are also listed in Table 3.1. In cyclohexane and dioxane, values of M_0 for solutes not directly measured were calculated from those determined in benzene, by multiplying Θ for benzene by a constant factor and using this value in equation (2). The multiplication factor used was 2.08 for dioxane, determined from the ratio of the Θ values measured in both solvents for DMABN. This is close to the ratio of the viscosities of dioxane and benzene. For cyclohexane the factor used to calculate the M_0 values for DPrABN and DDABN was 1.17 which is the average ratio found between the Θ values for the two solvents. This is considerable smaller than the value of 1.54 for the ratio of the viscosity of cyclohexane to that for benzene,[46-48] indicating a relatively smaller resistance to rotational

Table 3.1: *Fluorescence lifetimes, τ_{fl}, overall dipole moments of the excited singlet state, μ_S and CS state, $\mu_S(CS)$ determined from the TRMC parameters, as shown in the table.*

Solvent	Solute	$\tau_{fl}{}^a$ (ns)	$M_0{}^b$ (10^{-9} m²Vs)	Θ^c (ps)	$\Delta M_S{}^e$ (10^{-9} m²Vs)	$\mu_S/\mu_0{}^f$	$\mu_0{}^g$ (D)	$\mu_S{}^h$ (D)	$\mu_S(CS)^i$ (D)
c-hexane	ABN	5.3	8.48	47	4.12	1.21		8.0	
	MABN	4.0	7.41	56	7.37	1.41		9.3	
	DMABN	3.2	7.54	55	9.51	1.50		9.9	17.0
	DEABN	2.6	5.75	77	13.20	1.82		12.2	17.5
	DPrABN	2.6	(4.08)		12.50	2.01		13.5	18.1
	DDABN	2.6	(2.23)		9.30	2.27		15.2	19.6
	m-ABN	2.5	5.98	42	d	d		7-10^d	
	m-DEABN	4.3	4.57	64	11.9	1.89		10.4	
benzene	ABN	4.0	9.68	46	6.4	1.29		8.5	
	MABN	3.6	9.49	47	8.8	1.39		9.2	
	DMABN	3.1	9.26	49	22.6	1.85	6.6^{44}	12.2	15.1
	DEABN	2.8	7.52	65	28.5	2.19	6.7^j	14.7	15.4
	DPrABN	2.9	5.35	95	23.6	2.33		15.6	16.1
	DDABN	3.0	2.94	175	12.2	2.27		15.2	15.7
	m-ABN	2.9	7.42	36	d	d		7-10^d	
	m-DEABN	12.1	6.58	47	11.3	1.65		9.1	
dioxane	ABN	3.3	(4.48)		2.8	1.26	6.6	8.3	
	MABN	3.2	(4.73)		5.9	1.50	6.6	9.9	
	DMABN	3.8	4.57	102	19.1	2.29	6.6	15.1	16.1
	DEABN	3.6	(3.59)		19.4	2.55	6.7	17.1	17.3
	DPrABN	3.6	(2.48)		13.7	2.57		17.2	17.4
	DDABN	3.9	(1.34)		7.5	2.57	6.7	17.2	17.4
	m-ABN	4.9	(3.92)		d	d	5.3	7-10^d	
	m-DEABN	14.3	(3.28)		8.1	1.87	5.5	10.3	

(a) Nanosecond fluorescence decay time. For the 4-(dialkylamino)benzonitriles DMABN, DEABN, DPrABN and DDABN, this time represents the longest decay time in a multiexponential fluorescence decay.[13,16] For the other compounds the value is that for the lifetime τ_0.

(b) Measured M_0 in the ground state, bracketted values are calculated as described in the text.

(c) Dipole relaxation time in the ground state, calculated from measured M_0 and μ_0 values (eqn (2)).[30,31]

(d) Due to the large triplet component only lower and upper limits of 7 and 10 D could be estimated (Fig. 3.3).

(e) The change in rotational charge mobility on excited singlet state formation.

(f) Calculated from ΔM_S and M_0 via equations (1) and (2).

(g) μ_0 determined in dioxane at 25 °C. The dioxane data were also used for cyclohexane and benzene.

(h) The absolute values of ΔM_S determined for a given solute/solvent combination have been found to differ by up to 10% over a long period of time. The error limits for the dipole moments μ_S in the table correspond to this magnitude of error in ΔM_S. As a typical example, $\mu_S = 17.2 \pm 0.7$ D for DDABN/dioxane.

(i) Calculated using equation (7) from μ_S and f(CS) (equation (4)) with $\mu_S(LE) = 9.7$ D.

(j) For DEABN in benzene at 25 °C a value of 6.68 D has been reported in reference 43.

motion in the saturated hydrocarbons at the molecular level than suggested by the bulk viscosity. The calculated M_0 values are listed bracketted in Table 3.1. In the subsequent data analysis, experimental values of M_0 were used where available and calculated ones otherwise.

3.2.3 Overall singlet-state dipole moments

The values of the singlet excited state dipole moments of the aminobenzonitriles in the three solvents have been derived from the values of M_0, ΔM_S and μ_0 using equation (1). The data for μ_S are listed in Table 3.1 together with the ratio μ_S/μ_0.[49] The qualitative conclusions reached in Section 3.2.1 can now be seen quantitatively in the μ_S values. A general tendency for μ_S to increase, from a lower limit of approximately 9 D to an upper limit of approximately 17 D, with increasing alkyl substitution and with increasing effective solvent polarity can be clearly seen.

For ABN and MABN the dipole moments for all three solvents are close to the average values of 8.3 and 9.5 D respectively, showing no trend with increasing effective solvent polarity. This confirms the results of fluorescence measurements which show only a single, short wavelength band, indicating that the ICT process does not occur in the singlet excited state of these compounds. The dipole moments observed can therefore be assigned to the LE state alone.

For DMABN the situation is clearly different with μ_S increasing dramatically from cyclohexane, 9.9 D, to benzene, 12.2 D, and further to dioxane, 15.1 D. The value for DMABN in cyclohexane is what might have been expected for the LE state on the basis of the results for ABN and MABN (Table 3.1). The μ_S values for benzene and dioxane however are substantially larger. These results are in agreement with the fluorescence spectra depicted in Figure 3.5 in Section 3.3, which show that for DMABN a second emission band, attributed to the CS state, is hardly discernible for cyclohexane, visible as a shoulder for benzene, and becomes the dominant feature for dioxane.

The further increase in μ_S with increasing length of the N-alkyl substituents found for the 4-(dialkylamino)benzonitriles also parallels the observation of the increasing importance of the CS emission bands in their fluorescence spectra as shown in Figure 3.5. Of particular interest is that this trend is apparent for the compounds with the longer alkyl groups even in the case of the nonpolar solvent cyclohexane. The occurrence of a specific solvent interaction or "exciplex" with the LE state would therefore appear to be an unnecessary prerequisite for the formation of the highly polar charge transfer state.[12]

In the case of m-ABN the large triplet component in the TRMC transients, see Figure 3.3, prevented an accurate evaluation of the contribution due to the singlet state. Only lower and upper limits for μ_S of 7 and 10 D could therefore be estimated for this compound. While the

triplet transients for m-DEABN were also large, as shown in Figure 3.3, the substantially longer singlet lifetimes in benzene and dioxane allowed reasonably accurate estimates of μ_S to be made. The values found are within the range of 9-10 D and show no dependence on solvent polarity, in contrast with the results for the para-substituted isomer. This is in agreement with the conclusion from the fluorescence measurements, presented in the next section, that only one excited singlet state (LE) is formed in the case of the meta-substituted molecules. The increase in dipole moment for the meta derivatives is significantly larger at *ca* 4 D than the *ca* 3 D found for the para compounds, despite the closer proximity of donor and acceptor in the former. A higher degree of charge separation would therefore be appear to characterise the LE state of the meta compounds.

3.2.4 Individual LE- and CS-state dipole moments

The singlet excited state of the 4-(dialkylamino)benzonitriles is composed of contributions from the CS and LE states (Scheme 3.1). The equilibrium between these two species in the excited singlet state is established on a timescale considerably shorter than the several nanoseconds time response of the TRMC detection system, but longer than the 15 ps radian revolution time of the microwaves. Consequently on the timescale of the measurements the equilibrium concentrations of LE and CS may be taken to contribute independently to the overall microwave conductivity. Under these conditions, the change in rotational charge mobility is given by:

$$\Delta M_S = [1 - F(CS)]\Delta M_S(LE) + F(CS)\Delta M_S(CS) \tag{3}$$

where F(CS) is the fractional CS concentration:

$$F(CS) = [CS] / ([CS] + [LE]) \tag{4}$$

On substituting for ΔM_S, using equation (17) in Chapter 2, and assuming equal rotational relaxation times for LE and CS, one obtains:

$$\mu_S^2 = [1 - F(CS)][\mu_S(LE)]^2 + F(CS)[\mu_S(CS)]^2 \tag{5}$$

Equation (5) can be rearranged to give:

$$\mu_S^2 = \mu_S(LE)^2 + F(CS)[(\mu_S(CS))^2 - (\mu_S(LE))^2] \tag{6}$$

95

If μ_S(LE) and μ_S(CS) are constant parameters, then a plot of μ_S^2 against F(CS) should be linear and give as intercepts $(\mu_S(LE))^2$ for F(CS) = 0 and $(\mu_S(CS))^2$ for F(CS) = 1. Such a plot is shown in Figure 3.4, taking the values for μ_S from Table 3.1 and F(CS) determined from fluorescence measurements as described in the next section. While the data show considerable scatter, the general trend expected from equation (6), is seen to be obeyed. The intercept values of the straight line drawn through the data points in Figure 3.4 lead to the individual dipole moments of μ_S(LE) = 10.1±0.5 D and μ_S(CS) = 16.7±0.8 D.
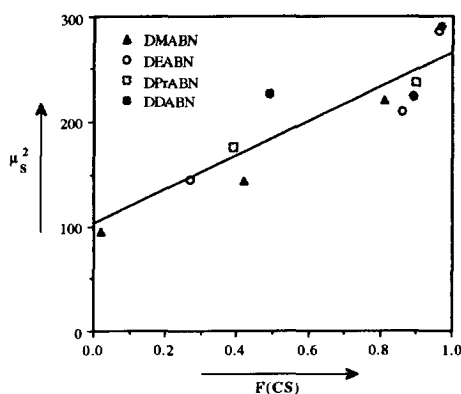
Figure 3.4: *Plot of the square of the excited state dipole moment μ_S^2 (Table 3.1) of the 4-(dialkylamino)-benzonitriles DMABN, DEABN, DPrABN and DDABN, in cyclohexane, benzene and dioxane, against the concentration factor F(CS) (see eqn. (6) and text). From the intercepts F(CS) = 0 and F(CS) = 1 of the least-squares fit to the data points, the dipole moment $\mu_S(LE)$ = 10.1 D and $\mu_S(CS)$ = 16.7 D are determined (eqn. (6)).*

By rearrangement of equation (5) an expression for the dipole moment of the CS state can be obtained from:

$$\mu_S(CS) = \{[\mu_S^2 - (1 - F(CS))(\mu_S(LE))^2]/F(CS)\}^{0.5} \qquad (7)$$

Using equation (7) we can derive separate values of μ_S(CS) for each individual solute/solvent combination making the assumption only that μ_S(LE) is constant rather than that both μ_S(LE) and μ_S(CS) are constant which was the basis of the plot in Figure 3.4. A μ_S value of 9.5 D is found for MABN which shows no evidence for CS formation and a value of 9.9 D for DMABN in cyclohexane which shows evidence of only a few percent contribution of a CS state. Therefore we believe that a reasonable estimate for μ_S(LE) would be 9.7 D.

With this fixed dipole moment for LE and the data for F(CS), determined from photostationary and time-resolved fluorescence measurements (Table 3.2), the dipole moments $\mu_S(CS)$ were determined, using equation (7). The results are listed in Table 3.1. An average value of 17 ± 1 D for $\mu_S(CS)$ is found, when the data for the three solvents (cyclohexane, benzene and dioxane) are combined. While there is admittedly a certain amount of scatter within the individual values we feel that they do support the conclusion that $\mu_S(CS)$ is in fact constant and has an absolute value close to 17 D. This value compares well with literature data discussed in the introduction, in particular with those obtained from solvatochromic measurements using the data treatment of reference 27, as well as from electrooptical emission measurements.[20]

As can been seen from the data in Table 3.1, the values for $\mu_S(CS)$ in benzene are in general somewhat lower than the values in cyclohexane and dioxane. A possible explanation of this is the formation of an exciplex between the solute and a benzene molecule in the CS state as has recently been suggested.[12] As a consequence the rotational relaxation time used in the derivation of μ_S, which is measured in the ground state for the bare molecule, would be too small for the CS state. This would lead then to an underestimate of the dipole moment.

3.2.5 Triplet state dipole moments

From the fitting procedure of the long-lived triplet component in the transient microwave decay, the product $\Delta M_T \Phi_{isc}$ is derived.[29,30] The results are presented in Table 3.2. From these data, the triplet excited state dipole moment μ_T can be evaluated, using equation (9). This expression is analagous to equation (1), written in terms of the fitting parameter $\Delta M_T \Phi_{isc}$:

$$\mu_T = \mu_0[1 + (\Delta M_T \Phi_{isc}) / (\Phi_{isc} M_0)]^{0.5} \tag{9}$$

The values for M_0 and μ_0, appearing in equation (9), can be found in Table 3.1. Values for the intersystem crossing efficiency have only been published for DMABN in cyclohexane ($\Phi_{isc} = 0.18$) and dioxane ($\Phi_{isc} = 0.40$).[11,50] Using these values, triplet excited state dipole moments of 11.9 and 12.0 D are determined for DMABN in cyclohexane and dioxane respectively. The independence of μ_T on the effective solvent polarity contrasts with the change in the singlet excited state dipole moments μ_S from 9.9 to 15.1 D for DMABN in the same solvents. It is therefore concluded that DMABN does not undergo intramolecular charge transfer in the triplet state. This conclusion is in agreement with observations in the literature,[9] where also indications are found that ICT is limited to the singlet excited state only. Interestingly the triplet state has a substantially larger dipolar character than the LE singlet state.

Table 3.2: *Fitting parameter $\Delta M_T \Phi_{isc}$ derived from the long lived component of the TRMC transients and estimates of the intersystem crossing efficiency, Φ_{isc}, assuming $\Delta M_T/M_0 \approx 2.3$ for all solutes.*

Solute	cyclohexane			benzene		dioxane		
	$\Delta M_T\Phi_{isc}$ $(10^{-9}\ m^2/(Vs))$	$\Phi_{isc}{}^a$	$\mu_T{}^b$ (D)	$\Delta M_T\Phi_{isc}$ $(10^{-9}\ m^2/(Vs))$	$\Phi_{isc}{}^a$	$\Delta M_T\Phi_{isc}$ $(10^{-9}\ m^2/(Vs))$	$\Phi_{isc}{}^a$	$\mu_T{}^b$ (D)
ABN	0.62	0.03		3.31	0.15	2.63	0.24	
MABN	1.73	0.10		3.20	0.15	2.69	0.25	
DMABN	3.08	0.18[c]	11.9	5.66	0.27	4.20	0.40[c]	12.0
DEABN	2.90	0.22		4.80	0.28	3.29	0.40	
DPrABN	2.32	0.25		4.28	0.35	2.28	0.40	
DDABN	1.48	0.29		2.08	0.31	1.38	0.45	
m-ABN	4.88	0.35		8.59	0.50	3.77	0.42	
m-DEABN	6.37	0.61		5.74	0.38	3.39	0.45	

(a) Φ_{isc} was calculated from $\Delta M_T\Phi_{isc}$ and M_0 (Table 3.1), using a constant value of 2.3 for the ratio $\Delta M_T/M_0$, as determined for DMABN in dioxane and cyclohexane employing the measured values for Φ_{isc} given in the table.[56,57] This is equivalent to assuming a constant μ_T of 12 D for the 4-aminobenzonitriles and 10 D for the meta-substituted derivatives.

(b) μ_T was calculated with M_0 and μ_0 taken from Table 3.1 and the value of Φ_{isc} reported in the literature.

(c) Experimental value, see references 56 and 57.

3.2.6 Intersystem crossing efficiencies

The values of Φ_{isc} listed in Table 3.2 for the different solute/solvent combinations have been derived from the parameter $\Delta M_T\Phi_{isc}$ assuming the value of μ_T/μ_0 to be the same for all solutes and equal to the value of 1.8 found for DMABN. This amounts to the assumption of a constant value of $\mu_T = 12.0$ D for the para-substituted compounds and $\mu_T = 9.7$ D for the meta derivatives. These data show a definite tendency for the intersystem crossing efficiency to increase substantially with increasing alkyl substitution i.e. with increasing CS contributions in S_1 for the para derivatives. Φ_{isc} also increases with solvent polarity particularly strongly for ABN and MABN which may be related to the higher dipole moment of the triplet state for these compounds i.e. $\mu_T > \mu_S$(LE). Φ_{isc} also tends to be larger for the meta compounds when compared with their para analogues.

3.3 FLUORESCENCE MEASUREMENTS

Three different fluorescence measurements were made on solutions of the present compounds: Steady state fluorescence spectra were measured using a quantum-correlated Perkin-Elmer MPF-44E spectrofluorimeter and quinine sulphate in 1.0 N H_2SO_4 as a quantum yield standard (Φ = 0.546 at 25°C). Picosecond decay and growth kinetics were monitored using a laser system consisting of an argon ion laser (Coherent, Innova 100-10), a dye laser (Coherent 701-1CD; Rhodamine 6G), and a frequency doubler (KDP, 296 nm). The detector was a Hamamatsu R2809 U-07 MCP photomultiplier and the overall instrument response function was 30-40 ps wide at the excitation wavelength. The analysis of the picosecond kinetic traces was carried out using modulating functions, extended by global analysis.[51,52] Nanosecond time-resolved single-photon counting (SPC) measurements were made at the wavelength maximum of the LE emission. Additional photostationary and time-resolved fluorescence measurements of these and related systems will be published separately.[53]
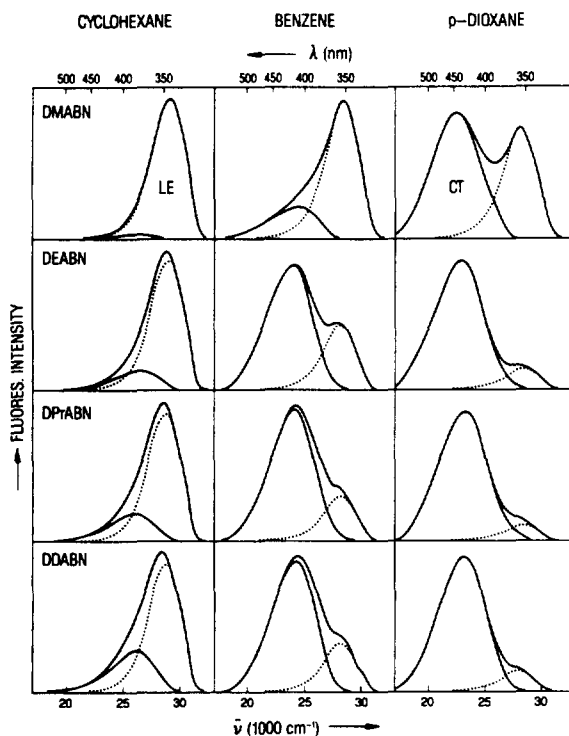
Figure 3.5: *Fluorescence spectra of the 4-(dialkylamino)benzonitriles at 25 °C in cyclohexane, benzene and dioxane. The two emission bands CS and LE (see text (Scheme 3.1)) were separated by taking the fluorescence spectrum of 4-(methylamino)benzonitrile (MABN) to be representative of the LE state alone.*

99

3.3.1 Spectra and quantum yields

The fluorescence spectra of the 4-(dialkylamino)benzonitriles DMABN, DEABN, DPrABN and DDABN in the solvents cyclohexane, benzene and dioxane are presented in Figure 3.5. All spectra exhibit a red-shifted CS emission, typical for a highly dipolar state, in addition to the emission from the LE state. In the case of cyclohexane, the CS band is apparent only as a broadening of the emission spectrum without a distinct maximum being observed as for the other solvents. The dotted spectra in Figure 3.5 are those for MABN, which shows no evidence of CS state formation. The MABN spectrum was taken to represent that of the LE state for all dialkylamino derivatives in order to derive the CS contribution from the overall spectrum. In this way the λ_{max} values and fluorescence quantum yields of the LE and CS states given in Table 3.3 were determined.

It can be seen from the spectra in Figure 3.5, and also from the CS/LE fluorescence quantum yield ratio $\Phi(CS)/\Phi(LE)$ shown in Table 3.3, that the relative intensity of the CS band increases in the order cyclohexane, benzene, dioxane. This effect is due to the increase in the effective solvation and hence stabilization of the CS state exerted by the solvent, as can be expressed by the well known solvent polarity parameters f-0.5f' or $E_T(30)$.[54-56] The increasing solvent polarity in the present solvent series is apparent as a decrease in the energy maximum of the CS band from 3.24 to 3.00 to 2.85 eV in going from cyclohexane to benzene to dioxane.

Furthermore, in agreement with the TRMC results, the CS/LE fluorescence intensity ratio of the compounds also tends to increase eventually to a plateau value in each of the three solvents with increasing length of the N-alkyl substituents, from DMABN to DDABN (Figure 3.5). This is even the case for cyclohexane, for which, as mentioned above, clear evidence for intra-molecular charge transfer in 4-(dialkylamino)benzonitriles has not previously been reported.

No evidence is found for the formation of a CS state for ABN and MABN, nor for m-ABN and m-DEABN, in any of the three solvents.[13,16] The fluorescence spectra of these molecules (see for MABN dotted spectra in Figure 3.5) are similar in shape to those of unsubstituted anilines such as N,N-dimethylaniline.[57] Even in strongly polar solvents such as acetonitrile or methanol a CS emission does not occur for ABN, MABN, m-ABN and m-DEABN, down to close to the freezing point of the solvent. This means that the CS state is not formed upon excitation in the case of ABN and the other three compounds and hence that the excited state dipole moment determined by TRMC is that of the pure LE state.

Table 3.3: *Fluorescence quantum yields $\Phi(LE)$ and $\Phi(CS)$, the ratio $\Phi(CS)/\Phi(LE)$, the fractional CS concentration F(CS) and the emission maximum $h\nu_{CS}$ of the CS state of the aminobenzonitriles.*

Solvent	Solute	$\Phi(LE)$	$\Phi(CS)$[a]	$\Phi(CS)/\Phi(LE)$[b]	F(CS)	$h\nu_{CS}$ $(1000\ cm^{-1})$
cyclohexane	ABN	0.150				
	MABN	0.160				
	DMABN	0.122	0.001	0.01	0.02	26.0
	DEABN	0.076	0.012	0.16	0.26	26.0
	DPrABN	0.073	0.020	0.28	0.38	26.2
	DDABN	0.062	0.026	0.42	0.47	26.2
	m-ABN	0.100	0.000	0.00	0.00	
	m-DEABN	0.120	0.000	0.00	0.00	
benzene	ABN	0.150	0.000	0.00	0.00	
	MABN	0.180	0.000	0.00	0.00	
	DMABN	0.081	0.024	0.30	0.41	24.0
	DEABN	0.013	0.032	2.48	0.85	24.2
	DPrABN	0.011	0.042	3.75	0.90	24.3
	DDABN	0.014	0.049	3.47	0.89	24.3
	m-ABN	0.120	0.000	0.00	0.00	
	m-DEABN	0.310	0.000	0.00	0.00	
dioxane	ABN	0.130	0.000	0.00	0.00	
	MABN	0.150	0.000	0.00	0.00	
	DMABN	0.022	0.033	1.49	0.81	22.7
	DEABN	0.007	0.059	8.52	0.96	22.9
	DPrABN	0.005	0.047	10.40	0.97	23.2
	DDABN	0.005	0.052	9.70	0.97	23.2
	m-ABN	0.180	0.000	0.00	0.00	
	m-DEABN	0.350	0.000	0.00	0.00	

(a) no CS state formation for ABN, MABN, m-ABN and m-DEABN.

(b) Fractional CS concentrations (equation (4)). F(CS) is determined from $\Phi(CS)/\Phi(LE)$, using the following values for the ratio $k_f(CS)/k_f(LE)$ (equation (11)): 0.45 (cyclohexane), 0.43 (benzene), 0.35 (dioxane) (see Table 3.4). For DDABN/cyclohexane, DDABN/benzene and DMABN/dioxane, f(CS) is calculated from the [CS]/[LE] concentration ratios given in Table 3.4.

3.3.2 Kinetics

The fluorescence transients of the compounds p-ABN, p-MABN, m-ABN and m-DEABN could be described in terms of the direct formation and decay of a single emissive LE state. The lifetimes, $\tau_0(LE)$, are listed in Table 3.1. Of particular interest in this group of compounds are the exceptionally long lifetimes for m-DEABN in benzene and dioxane which were also apparent in the TRMC experiments (Figure 3.3).

Picosecond time-resolved experiments on the N,N-dialkyl derivatives, however, clearly show an initial rapidly decaying component at the wavelength maximum of the LE emission found for MABN and a corresponding growth of a component at longer wavelengths. This is illustrated in Figure 3.6. The transients can be described by a mechanism involving the direct formation of an excited state emitting at short wavelengths (the LE state) which converts to a state emitting at longer wavelengths (the CS state) according to reaction Scheme I. From a global analysis fitting procedure of the picosecond timescale transients values of k_a and k_d for different solvent/solute combinations have been determined and a selection are given in Table 3.4.

τ_i (ns)	0.025	3.88	χ^2
$A_{2i}(CT)$	–18.6	18.7	1.0
$A_{1i}(LE)$	38.4	8.8	1.1
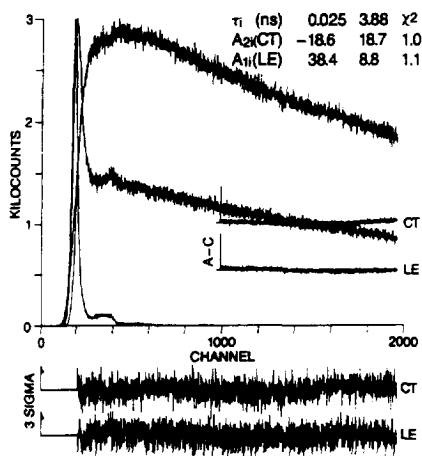
Figure 3.6: Initially excited (LE, at 328 nm) and charge transfer (CT, at 480 nm) fluorescence response functions of DMABN in dioxane at 25 °C. The LE and CT decays are analyzed simultaneously (global analysis). The decays were obtained using picosecond laser excitation (295 nm).

At longer times the LE and CS states exist in rapid equilibrium and have a common overall lifetime towards return to the ground state τ_0. The values of τ_0 determined at the wavelength maximum of the LE state by nanosecond flash-photolysis are listed for the dialkylamino compounds in Table 3.1. These lifetimes were used in the analysis of the TRMC transients to obtain the ΔM_S values from which the net excited singlet state dipole moments μ_S were derived.

Table 3.4: *Ratio of CS to LE radiative rates $k_f(CS)/k_f(LE)$ (Scheme 3.1) and data derived from fluorescence decays of DMABN and DDABN in various solvents at 25 °C.*

Solvent	Solute	k_a $(10^9\,s^{-1})$	k_d $(10^9\,s^{-1})$	$1/\tau_0$ $(10^9\,s^{-1})$	[CS]/[LE]	$\Phi(CS)/\Phi(LE)^a$	$k_f(CS)/k_f(LE)$
cyclohexane	DDABN	13.5	14.7	0.56	0.90	0.40^g	0.45
benzene	DDABN	28.8	3.3	0.34	7.90	3.47	0.43
dioxane	DMABN	32.3	7.4	0.26	4.20	1.49	0.35
toluene	DMABN	16.8	27.8	0.40	0.60	0.25^g	0.42
toluene	DDABN	28.6	3.2	0.35	8.06	3.31	0.41

(a) From Table 3.3. The accuracy of $\Phi(CS)/\Phi(LE)$ is limited by the relatively small spectral separation between the CS and LE fluorescence bands (cyclohexane) and by the low value of $\Phi(CS)/\Phi(LE)$ (toluene). The separation between the CS and LE bands is smaller in cyclohexane than in benzene and dioxane due to the larger effective polarity of the latter solvents.

3.3.3 Concentration ratio of CS and LE states

The equilibrium concentration ratio [CS]/[LE] which was used in a previous section to derive the individual dipole moments of the two contributing singlet states has been derived from the fluorescence data for the different solute/solvent combinations in two ways. For systems for which the rate coefficients k_a and k_d could be determined directly from a global analysis[51,52] of the picosecond timescale fluorescence transients, [CS]/[LE] could be determined directly using:

$$[CS]/[LE] = k_a/(k_d + 1/\tau_0) \tag{10}$$

This was for example the case for the combinations DMABN/dioxane, DDABN/benzene and DDABN/cyclohexane at room temperature for which the values [CS]/[LE] = 4.2, 7.9 and 0.9 respectively could be determined from the data given in Table 3.4.

While the values of k_a and k_d could not be accurately determined for DMABN in benzene at room temperature because of the relatively small CS component, it was possible to measure these parameters accurately at low temperatures in the similar solvent toluene. By extrapolation of the linear Arrhenius plots for the forward and backward rate constants to room temperature a value of [CS]/[LE] = 0.60 could be estimated. A similar procedure for DDABN in toluene yielded a value of [CS]/[LE] = 8.06, in reasonably good agreement with the value determined in

benzene itself at room temperature indicating the room temperature value for DMABN to be also valid for benzene.

The value of [CS]/[LE] can also be determined from the ratios of the fluorescence quantum yields of the two states, $\Phi(CS)/\Phi(LE)$, if the radiative rate constants $k_f(CS)$ and $k_f(LE)$ are known via:

$$[CS]/[LE] = k_f(LE)\Phi(CS)/k_f(CS)\Phi(LE) \qquad (11)$$

In Table 3.4 the values of $k_f(CS)/k_f(LE)$ have been determined from the measured quantum yield ratios and the calculated values of [CS]/[LE]. As can be seen $k_f(CS)/k_f(LE)$ for both DMABN and DDABN determined in benzene and toluene is close to 0.42. We therefore make the assumption that $k_f(CS)/k_f(LE)$ is in fact the same for all of the dialkylamino compounds in a given solvent. Accordingly we have used the values $k_f(CS)/k_f(LE) = 0.45, 0.42$ and 0.35 for cyclohexane, benzene and dioxane to determine the [CS]/[LE] from the quantum yield ratios given in Table 3.2.

3.4 GENERAL DISCUSSION

3.4.1 Conclusions

The dipole moments in the singlet excited states of a series of aminobenzonitriles have been determined at room temperature using the TRMC technique. For the 4-(dialkylamino)-benzonitriles the value of the overall dipole moment μ_S increases with increasing length of the alkyl groups, as well as with increasing effective solvent polarity in the series cyclohexane, benzene and dioxane.

With DMABN, DEABN, DPrABN and DDABN, the presence of an additional red-shifted emission in the fluorescence spectrum indicates that intramolecular charge transfer occurs at room temperature in benzene and dioxane, and unexpectedly, also in the nonpolar solvent cyclohexane. ICT does not take place for the aminobenzonitriles ABN, MABN, m-ABN and m-DEABN, for which no additional fluorescence band was observed. The fluorescence quantum yield ratio $\Phi(CS)/\Phi(LE)$ of the 4-(dialkylamino)benzonitriles becomes larger with increasing effective solvent polarity in the series cyclohexane, benzene and dioxane, as well as with increasing chain length of the alkyl groups on the amino nitrogen (methyl to decyl).

The individual dipole moments of the two excited singlet states of the 4-(dialkylamino) benzonitriles $\mu_S(LE)$ and $\mu_S(CS)$ could be determined separately by combining the TRMC data with the values for the equilibrium concentration ratio [CS]/[LE] evaluated from time-resolved

and steady-state fluorescence measurements. As a general result it is concluded that the dipole moment of the 4-(dialkylamino)benzonitriles increases, upon light absorption, from 6.6 D in the ground state to *ca* 10 D for the LE state. From this LE state intramolecular charge transfer takes place on a timescale of tens of picoseconds with substantial further charge separation leading to a CS state with a dipole moment of approximately 17 D. The triplet excited state dipole moments, μ_T, determined for DMABN in cyclohexane and dioxane are the same, independent of effective solvent polarity, with a value of close to 12 D. This indicates that ICT does not occur in the triplet state of these molecules.

The intersystem crossing efficiency, Φ_{isc}, of the 4-amino-benzonitriles is found to increase with the length of the N-alkyl substituents as well as with solvent polarity.

3.4.2 Dipole moment and amino group conformation

The observation of a dipole moment $\mu_S(CS) = 17$ D for the 4-(dialkylamino)benzonitriles confirms that substantial additional intramolecular charge separation takes place subsequent to excitation to the LE state for which $\mu_S(LE) \approx 10$ D. An increase in the net positive charge on the amino group could result from conformational changes involving (a) the TICT model,[6-9] i.e. rotational isomerization around the amino-phenyl bond or (b) a change from planar (sp^2) to pyramidal (sp^3) hybridization of the amino nitrogen. These two possibilities correspond to changes in the angles ϑ and φ in Figure 3.7.[58] In the TICT ("twisted internal charge transfer") model, the CS state of DMABN and related molecules is postulated to be a rotational isomer of a planar LE state, with the amino group in a plane perpendicular to that of the phenyl ring.[6-9] This bond rotation is supposed to lead to localization of unit positive charge on the nitrogen atom of the amino group. The negative charge is thought to be delocalized as in the radical anion of benzonitrile.[59-62] Such a complete decoupling of the amino group from the benzonitrile subunit in the aminobenzonitriles has also been described as "the principle of minimum overlap".[63,64]

The dipole moment of such a hypothetical, decoupled species (D$^+$-A$^-$) can be calculated by vector summation of the point charge dipole moments using the charge distribution of the benzonitrile anion. This charge distribution can be derived from the spin densities of the anion taken from ESR measurements and by scaling with the coefficients of the lowest anti-bonding molecular orbital of benzonitrile.[59-62,65] It should be noted that only approximately one-seventh of the total negative charge of the benzonitrile anion resides on the cyano group. Taking as bond lengths those obtained from an X-ray analysis of DMABN,[66,67] a dipole moment of 15.9 D results, which is quite close to the value measured.

A charge distribution as expected for a quinonoid resonance structure of DMABN would
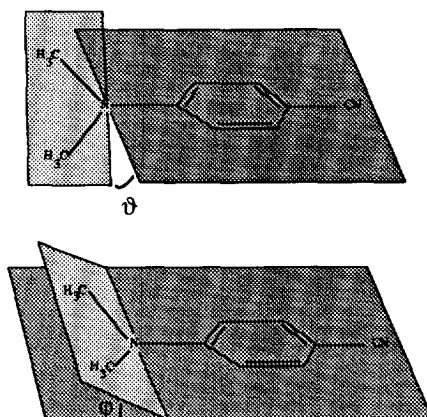
Figure 3.7: Twist angle ϑ and dihedral angle φ for DMABN.

lead to a much larger dipole moment, of between 30 and 33 D.[2,3] Note that a quinonoid structure, with a double bond between the amino nitrogen and the phenyl ring would be planar. Even without rotational isomerization, pyramidalization of the amino nitrogen could in principle also decouple the nitrogen lone pair from the π electrons of the phenyl ring. This would also lead to an increase in the localization of the positive charge on the amino nitrogen group and, hence, result in a larger value of the dipole moment of the CS state. Our results do not allow us to distinguish between these possibilities.

Our observation that the extent of intramolecular charge separation, i.e., [CS]/[LE], increases from DMABN to DDABN indicates that in the singlet excited state the amino nitrogen in the 4-(dialkylamino)benzonitriles becomes more pyramidal with increasing alkyl chain length. This conclusion is supported by photoelectron spectroscopy measurementS,[68] which show that the amino nitrogen is less strongly coupled to the phenyl ring in DEABN than in DMABN. Gleiter and Rettig[68] assumed that the amino group of ground state DEABN is already twisted with respect to the plane of the phenyl ring, whereas DMABN was supposed to be planar. An alternative interpretation is that the differences found between DEABN and DMABN arise from an increase in the sp^3 character of the amino nitrogen.[14]

In addition to conformational changes involving the amino group, molecular deformation similar to the loss of 6-fold symmetry of the phenyl ring which occurs on radical anion formation of benzene, could possibly take place for the present compounds and lead to an increase of charge separation in the CS state of the 4-(dialkylamino)benzonitriles.[63,69-72] This Jahn-Teller distortion[73-76] causes an asymmetry in the local charge densities, which could result in an increase in the solvation energy of the deformed radical anion.

3.5 ACKNOWLEDGEMENT

3.6 REFERENCES AND NOTES

1   W. Schuddeboom, S.A. Jonker, J.M. Warman, U. Leinhos, W. Kühnle and K.A. Zachariasse, *J. Phys. Chem.* **1992**, *96*, 10809.
2   E. Lippert, W. Lüder and H. Boos in *Advances in Molecular Spectroscopy*, Bolonga, Italy, **1959**; A. Mangini Ed.; Pergamon Press; Oxford, U.K., **1962**; 443.
3   E. Lippert, W. Lüder, F. Moll, H. Nagele, H. Boos, H. Prigge and I. Siebold-Blankenstein, *Angew. Chem.* **1969**, *73*, 695.
4   E. Lippert in *Luminescence of Organic and Inorganic Materials*, H.P. Kallmann, G.M. Spruch, Eds.; Wiley: New York, **1962**; 271.
5   E. Lippert in *Organic Molecular Photophysics*, J. Birks, Ed.; Wiley: London, **1975**; Vol. 2, 1.
6   Z.R. Grabowski, K. Rotkiewicz, W. Rubaszewska and E. Kirkor-Kaminska, *Acta. Phys. Pol.* **1978**, *A54*, 767.
7   Z.R. Grabowski, K. Rotkiewicz, A. Siemiarczuk, D.J. Cowley and W. Baumann, *Nouv. J. Chim.* **1979**, *3*, 443.
8   W. Rettig, *Angew. Chem., Int. Ed. Engl.* **1986**, *25*, 971.
9   E. Lippert, W. Rettig, V. Bonacic-Koutecky, F. Heisel and J.A. Miehé, *Adv. Chem. Phys.* **1987**, *68*, 1.
10   R.J. Visser, C.A.G.O. Varma, J. Konijnenberg and P. Bergwerf, *J. Chem. Soc., Faraday Trans. 2* **1983**, *79*, 347.
11   R.J. Visser and C.A.G.O. Varma, *J. Chem. Soc., Faraday Trans. 2* **1980**, *76*, 453.
12   M.C.C. de Lange, D.T. Leeson, K.A.B. van Kuijk, A.H. Huizer and C.A.G.O. Varma, *Chem. Phys.* **1993**, *174*, 425-440.
13   U. Leinhos, W. Kühnle and K.A. Zachariasse *J. Phys. Chem.* **1991**, *95*, 2013.
14   P. Suppan, *Chem. Phys. Lett.* **1986**, *128*, 160.
15   G.Z. Wermuth, *Z. Naturforsch.* **1983**, *38A*, 641.
16   U. Leinhos, *Ph.D Thesis*, University of Göttingen, FRG, **1991**.
17   From the temperature dependence of the fluorescence quantum yield ratio $\Phi(CT)/\Phi(LE)$ (Stevens-Ban plot), ln $[\Phi(CT)/\Phi(LE)]$ versus 1/T for DMABN in 3-methylpentane, a positive stabilization was obtained in ref. 15. The observation of double exponential fluorescence decays for DMABN in n-heptane[16] also leads to the conclusion that a reversible CS reaction takes place in these systems.
18   W.Z. Baumann, *Z. Naturforsch.* **1981**, *36A*, 868.
19   W.Z. Baumann, *Z. Naturforsch.* **1990**, *45A*, 883.
20   W.Z. Baumann, H. Bischof, J-C. Fröhling, C. Brittinger, W. Rettig and K.J. Rotkiewicz, *J. Photochem. Photobiol. A: Chem.* **1992**, *64*, 49.
21   P.C.M. Weisenborn, C.A.G.O. Varma, M.P. de Haas and J.M. Warman, *Chem. Phys. Lett.* **1986**, *129*, 562.
22   S.A. Jonker and J.M. Warman, *Chem. Phys. Lett.* **1991**, *185*, 36.
23   E. Lippert, *Z. Naturforsch.* **1955**, *10A*, 541.
24   N. Mataga, Y. Kaifu and M. Koizumi, *Bull. Chem. Soc. Jpn.* **1956**, *29*, 465.
25   N. Mataga and T. Kubota, *Molecular Interactions and Electronic Spectra;* Dekker: New York, **1970**.

26 A. Weller, *Z. Phys. Chem.* **1982**, *133*, 93.

27 B. Koutek, *Collect. Czech. Chem. Comm.* **1978**, *43*, 2368.

28 W. Rettig, *J. Mol. Struct.* **1982**, *84*, 303.

29 For DMABN a value of μ_S(CT) = 12.2 D was obtained (11.5 D for DEABN) in ref. 23, based on an excited state dipole moment μ_S of 20 D for DMANS, used as a reference compound, measured by TRMC and other methods (see references 30 and 31 and literature cited there), the dipole moments become 14.6 D (DMABN) and 13.8 D (DEABN).

30 M.P. de Haas and J.M. Warman, *Chem. Phys.* **1982**, *73*, 35.

31 M.P. de Haas and J.M. Warman in *Pulse Radiolysis;* Y. Tabata, Ed.; CRC Press: Boca Raton, FL, **1991**; Chapter 6.

32 P. Suppan, *J. Lumin* **1985**, *33*, 29.

33 P. Suppan, *J. Photochem. Photobiol. A: Chem.* **1990**, *50*, 293.

34 These values for the excited state dipole moments were based on a ground state dipole moment μ_0(DMABN) = 5.5 D.[32] With our value of μ_0(DMABN) = 6.6 D, corresponding larger dipole moments μ_S(LE) and μ_S(CT) are obtained. It should be noted for the equivalent spherical radius (ρ) a comparatively small value was used in ref. 32: ρ = 0.38 nm, calculated from the molecular weight and the density of DMABN.[14]

35 With the dual fluorescent molecules studied here, where two excited state species are present in solution (Scheme 1), the overall dipole moment as measured by TRMC and other methods contains contributions from both LE and CT excited state species.

36 J. Czekalla, W. Liptay, and K.-O. Meyer, *Ber. Bunsen-Ges. Phys. Chem.* **1963**, *67*, 465.

37 W. Liptay, *Angewan. Chem.* **1969**, *81*, 195.

38 W. Liptay in *Excited States;* E.C. Lim, Ed.; Academic: New York, **1974**; Vol. 1, 129.

39 H. Labhart, *Adv. Chem. Phys.* **1967**, *13*, 179.

40 H. Sinha and K.J. Yates, *J. Chem. Phys.* **1990**, *93*, 7085.

41 G. Hedestrand, *Z. Phys. Chem. B.* **1929**, *2*, 428.

42 P.P. Shorygin, M.A. Geiderikh and T.I. Ambrush, *Russ. J. Phys. CHem. (Engl. Transl.)* **1960**, *34*, 157.

43 S.F. Beach, J.D. Hepworth, J. Sawyer, G. Hallas, R. Marsden, M.M. Mitchell, D.A. Ibbitson, A.M. Jones and G.T. Neal , *Perkin. Trans. 2* **1984**, 217.

44 A.L. McLellan, *Tables of Experimental Dipole Moments;* Rahara Enterprises: El Cerrito, CA, **1974**; Vol. 2

45 A.L. McLellan, *Tables of Experimental Dipole Moments;* Rahara Enterprises: El Cerrito, CA, **1974**; Vol. 3.

46 To a first approximation, the multiplication factor would be expected to be close to the ratio of the solvent viscosities, η(benzene)[40]=0.603 cP,[47] η(cyclohexane)[40]=0.898 cP[47] and η(dioxane)[40]=1.196 cP.[48] This expectation is fulfilled for dioxane, where the factor of 2.09 required to obtain an adequate fit to the measured TRMC trace for DMABN is close to the ration of 1.98 for the viscosities of dioxane and benzene. For cyclohexane the factore of 1.17 used to obtain the best data fits is considerably smaller than the cyclohexane/benzene viscosity ratio of 1.49, which may indicate that the molecules have a larger rotational freedom in cyclohexane than would be expected on the basis of the bulk viscosity.

47 F.D. Rossini, K.S. Pitzer, R.L. Arnett, R.M. Braun and G.C. Pimentel *Selected Values of Physical and Thermodynamic Properties of Hydrocarbons and Related Compounds;* Carnegie Press: Pittsburgh, PA, **1953**.

48 J. Timmermans *Physico-Chemical Constants of Pure Organic Compounds;* Elsevier: New York, **1950**.

49 The absolute values of ΔM_S determined for a given solute/solvent combination have been found to differ by up to 10% over a long period of time. The error limits for the dipole moments μ_S in Table 3.1 correspond to this magnitude of error in ΔM_S. As a typical example, μ_S = 17.2 ± 0.7 D for DDABN/dioxane.

50 R.J. Visser, C.A.G.O. Varma, J. Konijnenberg and P.C.M. Weisenborn, *J. Mol. Struct.* **1984**, *114*, 105.

51 G. Striker in *Deconvolution and Reconvolution of Analytical Signals;* M. Bouchy, Ed.; University Press: Nancy, France, **1982**; 329.

52 J.R. Knutson, J.M. Beechem and L. Brand, *Chem. Phys. Lett.* **1983**, *102*, 501.

53 U. Leinhos, W. Kühnle and K.A. Zachariasse, unpublished results.

54 The effective solvent polarity as expressed by the $E_T(30)$ value[53] is as follows: cyclohexane, 31.2; benzene 34.5; dioxane 36.0. Also from this parameter it follows that dioxane has the largest polarity of the three solvents used here, between that of diethyl ether (34.6) and tetrahydrofuran (37.4).

55 C. Reichardt and K. Dimroth, *Fortschr. Chem. Forsch.* **1968**, *11*, 1.

56 C. Reichardt *Solvent Effects in Organic Chemistry;* Verlag Chemie: Weinheim, New York, **1979**.

57 I.B. Berlman, *Handbook of Fluorescence Spectra of Aromatic Molecules;* Academic: New York, **1971**.

58 P.P. Salgado, *Ph.D Thesis,* Amsterdam, **1992**.

59 A. Carrington and P.F. Todd, *Mol. Phys.* **1963**, *6*, 161.

60 V.F. Starichenko, L.N. Shchegoleva, N.V. Efremova, V.O. Saik and P.V. Schastnev, *Chem. Phys.* **1985**, *100*, 79.

61 G.R. Stevenson, G.C. Wehrmann and R.C. Reiter, *J. Phys. Chem.* **1991**, *95*, 901.

62 C.J. Chen, *J. Chin. Chem. Soc. (Taipei)*, **1989**, *36*, 565.

63 Z.R. Grabowski and J. Dobkowski, *Pure & Appl. Chem.* **1983**, *55*, 245.

64 V. Bonacic-Koutecky and J. Michl, *J. Am. Chem. Soc.* **1985**, *107*, 1765.

65 T.E. Peacock and P.T. Wilkinson, *Proc. Phys. Soc.* **1962**, *79*, 105.

66 From X-ray analysis of DMABN,[67] the volume V_u of the unit cell containing four molecules is found to be 0.861 nm^3, resulting, with $0.861/4 = (4/3)\pi\rho^3$, in equivalent spherical radius ρ of 0.37 nm.

67 A. Heine, D. Stalke and K.A. Zachariasse, unpublished results.

68 W. Rettig and R. Gleiter, *J. Phys. Chem.* **1985**, *89*, 4676.

69 J.C. Moore, C. Thornton, W.B. Collier and J.P. Devlin, *J. Phys. Chem.* **1981**, *85*, 350.

70 D. Purins and M. Karplus, *J. Chem. Phys.* **1975**, *62*, 320.

71 M. Kimura, H. Kawabe, K. Nishikawa and S. Aono, *Bull. Chem. Soc. Jpn.* **1985**, *58*, 2756.

72 A.L. Hinde, D. Poppinger and L. Radom, *J. Am. Chem. Soc.* **1978**, *100*, 4681.

73 A.D. Liehr, *Z. Naturforsch.* **1961**, *A16*, 641.

74 R.M. Hochstrasser and C.A Marzzacco in *Molecular Luminescence;* E.C. Lim, Ed.; Benjamin: New York, **1969**; 631.

75 E.C. Lim, *J. Phys. Chem.* **1986**, *90*, 6770.

76 K.A. Zachariasse, Th. von der Haar, A. Hebrecker, U. Leinhos and W. Kühnle *Pure & Appl. Chem.* **1993**, *65*, 1745.

Chapter 4

The Formation of Extended and Folded Charge Separated States of Donor-Spacer-Acceptor Molecules with Flexible and Semi-rigid σ-Bond Spacers[1]

4.1 INTRODUCTION

Electron transfer phenomena were first studied in intermolecular donor/acceptor pairs, which on photoexcitation gave rise to highly dipolar "charge transfer" (CT) exciplexes.[2-4] Later, flexibly-linked donor-acceptor compounds with the general structure $D-(CH_2)_n-A$ were investigated.[5-7] In both types of system the donor and acceptor moieties can achieve π-system overlap and it was believed by many that this direct contact was an essential requirement to transfer an electron from donor to acceptor.[8,9] For contact to occur the methylene chain must adopt a folded conformation in the latter case.

For intermolecular exciplexes Mataga provided evidence that the average D^+A^- distance becomes larger with increasing solvent polarity.[4] In the intramolecular $D-(CH_2)_n-A$ systems, the geometry of the exciplexes was suggested to change from "compact" in nonpolar to "loose" in polar media, possibly corresponding to a fully folded and an extended conformation of the polymethylene chain interconnecting D and A. Later measurements on rigidly separated D/A combinations indicated however that the charge separation step could occur in a more or less extended conformation even in nonpolar solvents.[10-17] Apparently electron transfer was possible, in certain cases at least, without donor and acceptor having direct π-system overlap.

Since this discovery many examples of this phenomenon have been found where in rigidly bridged σ-bonded donor-acceptor compounds very efficient photoinduced intramolecular charge separation occurs without the donor and acceptor being in close contact.[18-42] The electron is transferred across the intervening σ-bonds via Through Bond Interaction (TBI).[43,44] Charge recombination can occur either radiationlessly or (perhaps surprisingly) sometimes by an efficient radiative pathway leading to a red-shifted "exciplex-like" emission.[41] This bathochromically shifted emission is absent in the sum spectra of the separate chromophores. In other words, there exists a state below the locally excited donor or acceptor states, which is best described as a charge separated (CS) state, in which an electron has been completely transferred from the donor to the acceptor site.

We use the term "CS" fluorescence for the case of emission from such extended, weakly coupled DSA systems in which charge separation is complete, in order to differentiate it from the terms "CT" or "exciplex" fluorescence which are usually applied to D/A pairs in contact or strongly coupled via conjugated π-systems and with an undefined degree of charge separation. The term ECT, for extended charge transfer state, is used by some authors in place of CS. Because of the complete charge separation and hence very large dipole moments associated with CS states of DSA molecules, they have also been referred to as "giant dipole" states.[45]

A CS state is stabilized more in polar solvents than a locally excited state. It can therefore happen that electron transfer is not possible in solvents of low polarity, because the CS state is above that of the locally excited state, but that it becomes possible in solvents of intermediate or high polarity. If the driving force for charge separation Δ_{CS} (= $-\Delta G_{CS}$) is positive, it is possible to get complete electron transfer over large distances even in a completely nonpolar environment. In general the energy of the CS state is lowered when donor and acceptor are closer together due to the increase in Coulomb energy. A folded exciplex state can therefore be stable with respect to the lowest locally excited state even if formation of the extended CS state is energetically forbidden. For molecules with very flexible spacers, the folded CT exciplex state can be formed by conformational changes occurring in the spacer, which brings the donor
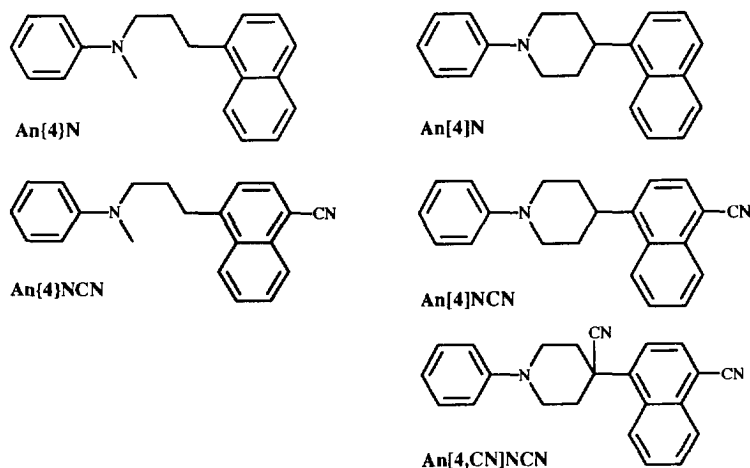
Figure 4.1: Structures of the flexible D{4}A and the semi-rigid D[4]A compounds, containing the weak naphthalene, N acceptor and the 0.6 eV stronger cyanonaphthalene, NCN acceptor with **An**, the anilino donor moiety. The number between brackets is the number of sigma bonds between donor and acceptor p-orbitals.

and acceptor closer together, thus allowing charge transfer to occur.

In flexibly bridged systems the situation can also arise that both the compact exciplex state (folded conformation) and the loose exciplex state (extended conformation) are below that of the locally excited state even in a nonpolar solvent. It is then possible to initially get electron transfer in an extended conformation followed by folding to yield the more stable contact exciplex. This "coulomb-induced" or "electrostatically-driven" folding subsequent to charge separation has been called "harpooning". So in general in a nonpolar environment a DSA molecule with a flexible spacer and with a weak D/A pair will fold prior to electron transfer, whereas for a strong D/A pair electron transfer will occur in an extended conformation followed by folding. The end result of both processes will be a close contact exciplex, but the routes are mechanistically very different.

Harpooning has been found to occur even for semi-rigid spacers by Brouwer et al.,[46] who studied a trichromophoric D_2-D_1-A compound (see also Chapter 5) and by Wegewijs et al.,[47] who studied 1-phenyl-4-((cyano-1-naphthyl)methyl)piperidine using TRMC and fluorescence techniques (see Figure 1.8). In this system the extended CS state is formed first following excitation, after which the molecule folds to bring the opposite charges closer together. The folded conformation of this compound exists only in the gas phase and in nonpolar media.[47-51] In these media the Coulomb attraction between the two opposite charges is large and this provides the large driving force required to overcome the barrier to the piperidine ring inversion which is necessary for folding.

In this chapter some bichromophoric compounds of the type donor-spacer-acceptor (Figure 4.1), synthesized by the group of Verhoeven and Brouwer at the University of Amsterdam,[50,51] are investigated with both TRMC and time-resolved fluorescence techniques. Pronounced effects resulting from changing the driving force for charge separation and the flexibility of the spacer have been observed. A study of the temperature dependence of the steady state fluorescence of the present compounds in nonpolar and polar solvents has been published previously.[50,51]

The data presented here are limited to room temperature and to the solvents cyclohexane and benzene. TRMC measurements were also carried out in t-decalin. These results are not shown, because they were found to be almost identical to those for cyclohexane.

A shorthand nomenclature for the bichromophoric compounds of the type donor-spacer-acceptor is used in the text and is given under each structural representation in Figure 4.1. The symbol An represents an anilino donor group, while N and NCN represent naphthalene and cyanonaphthalene acceptor moieties. The reduction potentials are -2.56 eV and -1.96 eV (versus SCE in acetonitrile) respectively, resulting in an increased stabilization of the CS state by 0.6

eV for the NCN acceptor. [n] and {n} symbolise semi-rigid (piperidine) and flexible (trimethylene) spacers respectively, with n the number of sigma bonds separating the p-orbitals of the donor and acceptor adjacent to the bridge. The compound An[4,CN]NCN is related to An[4]NCN, however, with an additional cyano group attached within the bridge.

4.2 TRMC MEASUREMENTS

In Figure 4.2 are shown the changes in microwave conductivity found on flash-photolysis of solutions of An[4]N, An{4}N, An[4]NCN and An{4}NCN in cyclohexane and benzene. The traces could all be fit reasonably well assuming the formation of a single transient dipolar species with a very small contribution from a long-lived (microseconds) component. The fits are shown in the figure and the lifetimes used are listed in Table 4.1. Also listed in Table 4.1 are the conductivity parameters $\mu_S^2 \Phi / \Theta$ with μ_S^2 the difference between the squares of the dipole moments of the transient excited state and the ground state, Φ the quantum efficiency for formation of the excited state and Θ the dipole relaxation time. Before considering the quantitative aspects of the measurements, qualitative conclusions which can be drawn will be discussed.

Table 4.1: Lifetime of the CS state, τ_S; conductivity parameter $(\mu_S^2 \Phi / \Theta)$; rotational relaxation time Θ_{cyl}, calculated using an extended cylindrical geometry; rotational relaxation time Θ_{sph}, calculated using a spherical geometry; dipole moment μ_{cyl}, calculated using Θ_{cyl} and dipole moment μ_{sph}, calculated using Θ_{sph}. Quantum yield Φ for the formation of the charge separated state is assumed unity.

Compound	τ_S (ns)[a]		$\mu_S^2 \Phi / \Theta$ (D^2/ps)		Θ_{cyl} (ps)		Θ_{sph} (ps)		μ_{cyl} (D)		μ_{sph} (D)	
	CHX	BEN	CHX	BEN	CHX	BEN	CHX	BEN	CHX	BEN	CHX	BEN
An[4]N	9.8[b]	8.5	0.19	2.90	238	200	100	72	6.8	24.1	4.6	14.8
An{4}N	26	37	1.10	1.51	216	182	96	69	15.7	16.6	10.6	10.6
An[4]NCN	16	11	2.89	2.18	287	243	108	78	28.8	25.2	18.0	14.7
An{4}NCN	65	42	1.93	2.01	262	222	104	75	22.4	21.1	14.4	12.7

(a) best fit with single dipolar intermediate.
(b) from fluorescence measurements.

4.2.1 Qualitative considerations

The most prominent feature of the data in Figure 4.2 is the extremely low TRMC signal for An[4]N in cyclohexane. This can not be attributed to a very short lifetime of the S_1 state since a fluorescence decay time of 9.8 ns is found. We conclude that long-distance electron transfer
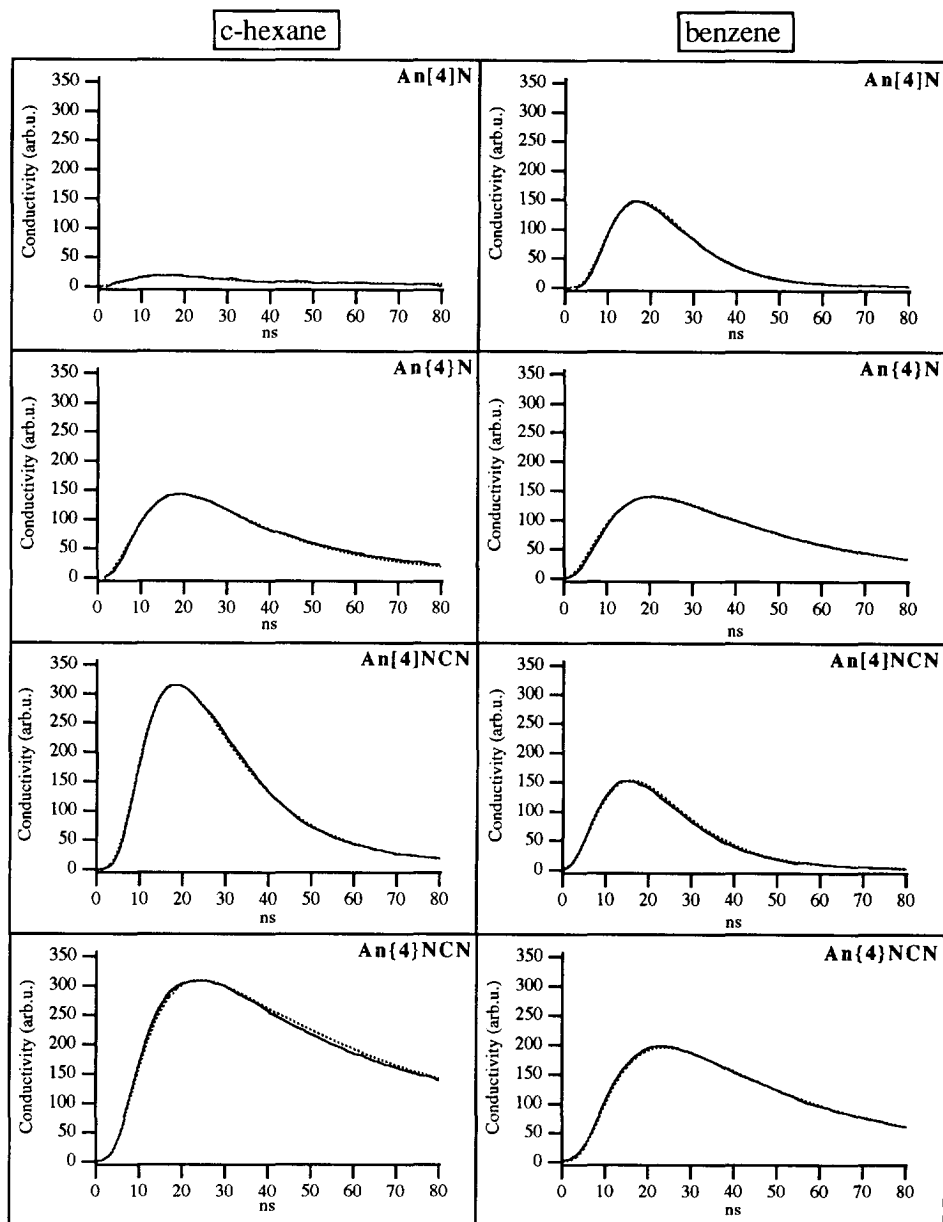
Figure 4.2: *Transient changes in the microwave conductivity (dielectric loss) of ca 10^{-4} M solutions of the compounds shown, in cyclohexane and benzene on flash-photolysis at 308 nm, pulse width 7 ns. The dotted lines are calculated fits, based on the formation of only one transient dipolar species. The fitting parameters are given in Table 4.1.*

115

across the semi-rigid, sigma-bond bridge does not occur for this donor-acceptor pair in a saturated hydrocarbon solvent.

In contrast, a large dipolar transient is found for the flexibly bridged An{4}N compound in cyclohexane showing that efficient electron transfer occurs. Since the result for An[4]N indicates that electron transfer should not be possible in an extended configuration, the large signal for An{4}N must be attributed to trans-gauche conformational diffusion occurring within the trimethylene spacer, which results in closer approach of the donor and acceptor.[53] Because of the increased Coulomb energy associated with the shorter distance, electron transfer becomes energetically feasible and a "folded" charge transfer state is formed.

No evidence for a growth of the TRMC signal for An{4}N in cyclohexane could be found. This indicates that the conformational changes responsible for close approach in the locally excited molecule must occur on a timescale shorter than the time resolution of the measurement which is approximately 3 ns.

It is interesting to compare the lack of an appreciable TRMC signal for An[4]N in cyclohexane with the large dipolar transients found for the same compound in benzene and for the An[4]NCN compound in cyclohexane. The result for An[4]N in benzene can be explained by the pseudo-polar nature of this "anomalous" solvent, which results in the energy level of a fully charge separated state being approximately 0.4 eV lower than in a completely nonpolar saturated hydrocarbon.[30] This decrease in energy is apparently sufficient to make long-distance electron transfer in An[4]N energetically feasible in benzene whereas it was not in cyclohexane. In the case of An[4]NCN in cyclohexane it is presumably the additional 0.6 eV electron affinity of the cyano-naphthalene acceptor[50,51] compared with naphthalene, that is sufficient to result in a positive driving force for long-distance electron transfer and hence its occurrence.

On the basis of the results in the previous paragraph we conclude that a decrease in the energy level of the charge separated state of an outstretched four sigma-bond separated An/N couple in cyclohexane by 0.4 eV, or possibly less, would be sufficient to make electron transfer energetically feasible. Apart from increasing the solvating power of the solvent or increasing the electron donating or accepting power of the chromophores, the energy of the charge separated state can be lowered by bringing the donor and acceptor closer together as proposed for the flexible An{4}N compound above.

The dipole moments derived from solvatochromic shift measurements[50,51] and a quantitative analysis of the present TRMC data, as will be discussed in Section 4.2.2, show that full charge separation in an extended configuration of the present molecules corresponds to a distance of approximately 6 Å between the centres of charge, i.e. a dipole moment close to 30 D. At this distance the Coulomb energy is approximately 1.2 eV in a medium of dielectric

constant 2.0. An increase in the Coulomb energy to 1.6 eV, which would be sufficient to allow electron transfer to occur, would require a decrease in the centre to centre distance to *ca* 4.5 Å. Complete folding to within the 3.4 Å π-π contact distance is therefore probably not necessary for electron transfer to occur.

This may explain why charge separation occurs for An{4}N on a timescale of less than 3 ns. The timescale for complete folding might otherwise be expected to be several nanoseconds as found for intramolecular excimer formation for di(2-pyrenyl)propane.[54] In that case formation of the exciplex would have been apparent as an initial growth in the TRMC signal for An{4}N in cyclohexane. Even in trans-decalin with a viscosity twice that of cyclohexane no delayed development of the TRMC signal could be observed. Such a delayed growth of the dipolar transient has been observed for a trans-decalin solution of a trimethylene-bridged pyrene/dimethylaniline DIAD (see Figure 1.7).[55]

Even though electron transfer may occur at a distance longer than the 3.4 Å π-π contact distance for An{4}N, it is almost certain that a contact pair will still be the final product in low viscosity, low dielectric constant solvents, since the oppositely charged chromophores will be rapidly pulled together under the influence of the field. That this is the case for An{4}N in both cyclohexane and benzene is indicated by the lifetimes of the TRMC transients of 26 and 37 ns respectively. These lifetimes are close to the value of 32±3 ns reported for the decay of the intermolecular exciplex between dimethylaniline and naphthalene in cyclohexane determined by time-resolved optical absorption and emission measurements.[56] Perhaps even more convincing evidence is the similarity of the spectrum of the emission from An{4}N to that found for the intermolecular exciplex.[50,51]

The lifetime of the TRMC transient for the flexible An{4}NCN compound in cyclohexane is 65 ns. This is within the range from 50 to 80 ns found for DMA intermolecular exciplexes with stronger acceptors than naphthalene.[56] We conclude that the transient responsible for the TRMC signal has also in this case a fully folded geometry with a very similar donor-acceptor sandwich configuration to that of the analogous intermolecular exciplex.

In the case of An{4}NCN there is little doubt, based on the observation of efficient electron transfer for An[4]NCN in cyclohexane, that the initial electron transfer step occurs in the outstretched configuration of the flexible compound even in cyclohexane. This must then be followed by rapid electrostatically driven folding. Additional evidence for the occurrence of long-distance electron transfer as the initial step for An{4}NCN has been provided by a study of the temperature dependence of its fluorescence in methylcyclohexane.[50,51] As the temperature is lowered the folded exciplex emission at 450 nm decreases and is gradually replaced by an emission at 370 nm. The latter is still substantially red-shifted compared with the local donor or

acceptor emissions and resembles that found at shorter times for the semi-rigid An[4]NCN in cyclohexane at room temperature.

Somewhat counterintuitively, the lifetimes of the charge separated states of the semi-rigid molecules which are thought to be fully extended, are considerably shorter than those of the close contact, exciplex states formed rapidly by the flexibly bridged compounds. This could possibly be due to the much weaker interaction between the electron spins in the extended configuration which allows a more rapid radiationless transition to occur to a locally excited triplet state via intersystem crossing.[57] It is also possible that symmetry considerations play an important role in the excited state to ground state transition probability. Whatever the reason, it is clear that distance is not the only factor influencing the lifetime towards charge recombination since this would have been expected to produce exactly the opposite tendency to that observed.

4.2.2 Quantitative considerations

In order to estimate absolute values of the dipole moments of the excited states a knowledge of the dipole relaxation time is required. The rotational relaxation times of the present molecules have been calculated based on either a spherical geometry, using the Stokes relation, or a cylindrical geometry, using the semi-empirical equation given previously.[24] The former time would be expected to be a reasonable approximation for the dipole relaxation time of the exciplex state of the flexibly bridged compounds which are tightly folded and the latter for the semi-rigid compounds which, at least initially, must undergo electron transfer in a fully extended cylinder-like configuration.

As can be seen from the calculated dipole moments based on a cylindrical geometry in Table 4.1, the values for the semi-rigid compounds, other than An[4]N in cyclohexane, all lie within the range of 24 to 29 D. These dipole moment values are all very close to the estimate of 29 D made for the extended CS states of the semi-rigid compounds on the basis of solvatochromic shifts of the emission in polar solvents.[50,51] Since the latter estimate can be made independently of a knowledge of the yield of the dipolar species while the TRMC estimate is based on a quantum yield of unity, one may conclude from the good agreement that the quantum yield for giant dipole formation is indeed close to one, in those cases for which it is energetically feasible. A dipole moment of 29 D corresponds to full charge separation over a distance of 6.0 Å which is to be compared with the much smaller 4.2 Å length of the sigma-bond spacer of An[4]N and An[4]NCN.

For the flexibly bridged compounds the dipole moments, based on a spherical geometry, are seen to be somewhat different for the two acceptors. In cyclohexane and benzene an average

value of 10.6 D is found for naphthalene and a substantially larger value of 13.6 D for the cyano-naphthalene acceptor in An{4}N and An{4}NCN respectively. It would appear that the extent of charge separation is greater in the exciplex with the stronger acceptor, as might be expected. Complete charge separation over a π-π contact distance of 3.4 Å would yield a dipole moment of slightly more than 16 D.

While the TRMC signal for the solution of An[4]N in cyclohexane is very much smaller than that for the other solute/solvent combinations, a small change in dipole moment is indicated. The value calculated based on the 9.8 ns lifetime of the fluorescence of the solution is 6.8 D, using a cylindrical geometry. This is slightly larger than the dipole moment of 5.0 D found for the S_1 state of dimethylaniline.[58] A very small equilibrium concentration of CS state, or in other words, a small interaction between donor and acceptor in the excited state is therefore indicated.

4.3 FLUORESCENCE MEASUREMENTS

The conclusions reached in Sections 4.2.1 and 4.2.2 on the basis of the present TRMC results are in general agreement with those reached in a previous publication based on steady-state fluorescence measurements.[50,51] Thus, for An[4]N in cyclohexane only fluorescence at 335 nm (3.70 eV) was found. This is the same wavelength region found[59] for the emission from dimethylaniline and naphthalene which may be considered to be model donor and acceptor compounds respectively. This is in accordance with the lack of occurrence of electron transfer as evidenced by the microwave measurements.

In Figure 4.3 the fluorescence spectra as a function of time are shown for An[4]N, An{4}N, An[4]NCN and An{4}NCN in cyclohexane. The lifetimes and the position of the fluorescence bands are listed in Table 4.2.

Table 4.2: Emission maxima $h\nu_{max}$ and fluorescence lifetimes τ_* of the compounds in cyclohexane and benzene.

Compound	$h\nu_{max}$ (eV)		τ_* (ns)	
	CHX	BEN	CHX	BEN
An[4]N	3.70	-	9.8	-
An{4}N	3.21	-	23.3	-
An[4]NCN	3.24	-	7.0	-
	2.88	2.76	16.0	11
An{4}NCN	2.76	2.62	64.0	42

The decay of the An[4]N fluorescence in cyclohexane displays no wavelength shift with time, as illustrated in Figure 4.3, and is monoexponential with a mean lifetime of 9.8 ns. Interestingly this is much longer than the 2.4 ns of dimethylaniline and much shorter than the 67 ns found for 1-methylnaphthalene. Some interaction between the donor and acceptor moieties in the excited state must therefore occur even in cyclohexane. This is in agreement with the conclusion reached in the previous section based on the small but measurable dipole moment of 6.8 D found.

As shown in Figure 4.3, the flexible analogue An{4}N diplays a fluorescence in cyclohexane at room temperature which is red shifted, compared with An[4]N and the local
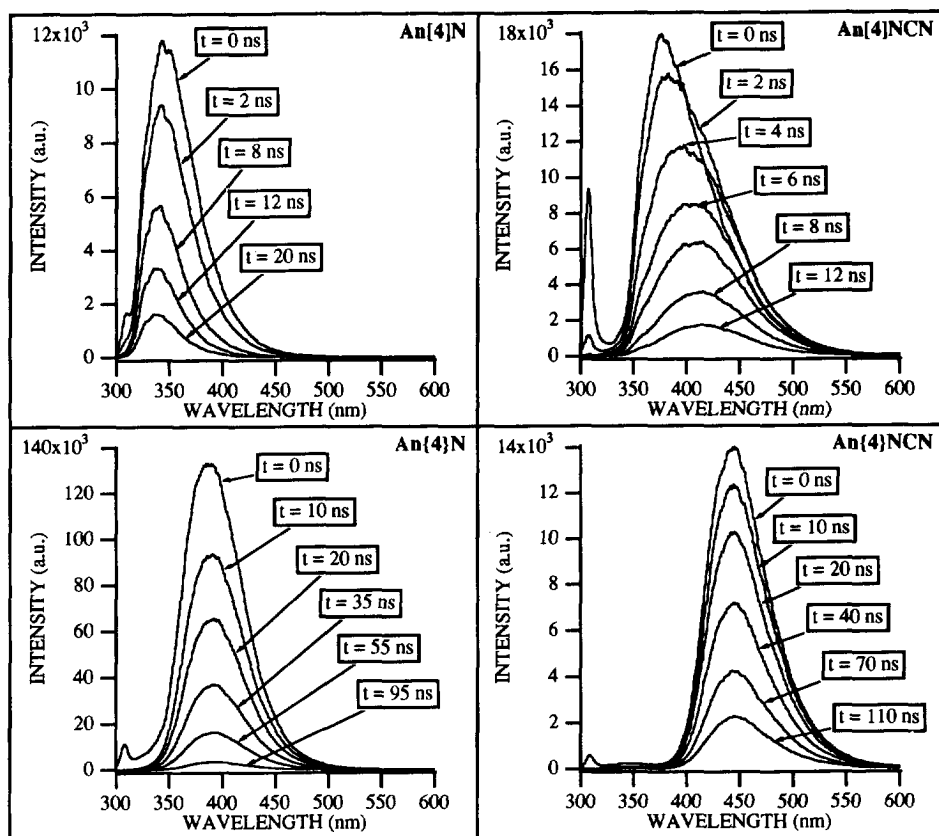
Figure 4.3: *Fluorescence spectra of the compounds shown in cyclohexane solution as a function of time following flash-photolysis at 308 nm, pulse width 7 ns.*

excited state emissions, to 386 nm (3.21 eV). This emission also shows no spectral shift with time and decays monoexponentially with a lifetime of 23.3 ns which is close to the 26 ns found for the TRMC transient. The maximum emission wavelength and lifetime are very similar to those found for the intermolecular exciplex[50,51,56] between dimethylaniline and naphthalene. There is little doubt therefore that the fluorescent state for An{4}N in cyclohexane has a completely folded configuration with donor and acceptor groups in close contact, very similar to the sandwich structure of the intermolecular exciplex.

The conclusion, based on the results for the semi-rigid analogue, that electron transfer in an extended configuration cannot occur for the An/N pair means that a conformational change bringing donor and acceptor groups closer together is necessary for exciplex formation for An{4}N in cyclohexane as discussed in the previous section. This is supported by the gradual disappearance of the exciplex emission of An{4}N with decreasing temperature in methyl-cyclohexane and its replacement by local excited state emission at 330 nm[50,51] similar to that found for An[4]N at room temperature.

The flexibly bridged An{4}NCN compound is found to have an emission spectrum with a maximum at 450 nm (2.76 eV) in cyclohexane (see Figure 4.3). As for An{4}N the spectral shape remains the same during the course of the decay, which is monexponential with a lifetime of 64 ns. The emission spectrum is very similar to that of the intermolecular exciplex between dimethylaniline and cyanonaphthalene[50,51] and, as pointed out in the previous section, the lifetime is close to what would be expected for an exciplex of DMA with a strong acceptor. As for the naphthalene analogue therefore, rapid formation of a folded exciplex is indicated.

In the case of An{4}NCN the initial electron transfer step is expected to take place in the fully extended configuration on the basis of the results for the semi-rigid An[4]NCN molecule in cyclohexane. Only during the pulse however could shorter wavelength emissions be discerned for either An{4}N or An{4}NCN. This indicates that, at room temperature, the folded exciplex states of these flexibly bridged molecules are formed within a few nanoseconds irrespective of whether electron transfer takes place initially in a partially folded configuration as for An{4}N or in a fully extended configuration as for An{4}NCN.

The semi-rigid compound An[4]NCN displays a fluorescence with a maximum initially at 383 nm (3.24 eV) in cyclohexane and 440 nm (2.82 eV) in benzene. The difference between the two solvents of 0.42 eV is similar to that found for other fully charge separated, giant dipole states.[30] This is to be compared with the emission maxima of the flexible counterpart An{4}NCN, which are 2.76 eV and 2.62 eV in cyclohexane and benzene respectively. The difference is only 0.14 eV in this case, indicating that a folded conformation in both solvents is present (see next sections). As evidenced by the fluorescence spectra as a function of time as

shown in Figure 4.4 in benzene, the folding must occur very rapidly in benzene also, because no spectral shift in time is observed.

As shown in Figure 4.4 the spectrum of the emission from An[4]NCN in benzene remains unchanged during the course of the fluorescence decay suggesting that no significant change in conformation of the molecule occurs subsequent to electron transfer. For the cyclohexane solution however a gradual shift from 383 nm (3.24 eV) to 430 nm (2.88 eV) occurs with time, as shown in Figure 4.3. There seems to be little doubt that a substantial change in molecular configuration is occurring subsequent to charge separation in the extended state of An[4]NCN in cyclohexane and that this must involve folding of the spacer unit and a considerable reduction in the donor-acceptor distance. This type of electrostatically driven folding or harpooning on a timescale of several nanoseconds for piperidine type spacers in alkane solvents has been reported previously.[46,47] From the difference in emission maxima the overall driving force for folding can be estimated to be 0.36 eV.

The decay of the emission of An[4]NCN in cyclohexane can be fit quite well[60] on the basis of an initially formed species emitting at 383 nm which interconverts to a second species which

Figure 4.4*: Fluorescence spectra of An[4]NCN and An{4}NCN in benzene solution as a function of time following flash-photolysis at 308 nm, pulse width 7 ns.*

emits at 430 nm. The two species are assigned to the extended giant dipole state formed by rapid long distance electron transfer with a lifetime of 7 ns and a folded exciplex-like state with a lifetime of 16 ns. The emission wavelength and lifetime of the latter state are shorter than those found for the trimethylene bridged An{4}NCN compound (see Table 4.2). We conclude that the overlap between the donor and acceptor moieties in the folded form of the semi-rigid analogue is less because of the more rigid geometrical constraints on folding for An[4]NCN. This difference in conformational possibilities and closest approach of donor and acceptor groups for flexible and semi-rigid donor-spacer-acceptor molecules is discussed at great length in a recent publication.[53]

It is clear from the time-resolved fluorescence measurements on An[4]NCN in cyclohexane that the single dipolar intermediate model used to fit the TRMC data in the previous section, which resulted in a lifetime of 16 ns, was in fact incorrect. A revised analysis of the TRMC data taking into account the conformational changes occurring on a nanosecond timescale as indicated by the fluorescence measurements will be discussed in Section 4.4.

As pointed out above, the fluorescence of An[4]NCN in benzene does not display the delayed bathochromic shift found in cyclohexane (see Figure 4.4). It would appear that the driving force for coulomb-induced folding is less in the pseudo-polar solvent despite the fact that the dielectric constant of benzene is not significantly different to that of cyclohexane; 2.28 versus 2.02. The difference apparently lies in the extra "specific" solvating power of benzene for charged species over and above the polarizability interaction. Thus while the reduction in energy of a fully charge separated, giant dipole state in benzene amounts to approximately 0.4 eV, it appears to be much less for a more compact, contact exciplex state. This can be seen by comparing the emission maxima of the intramolecular exciplex of An{4}NCN in cyclohexane, 450 nm (2.76 eV), and benzene, 473 nm (2.62 eV). Rather than the 0.42 eV difference found for the giant dipole states of the semi-rigid compounds the difference is now seen to be only 0.14 eV for the compact exciplex. The driving force for folding to form a more compact dipolar state will therefore be close to 0.3 eV less in benzene than in a saturated hydrocarbon solvent. Based on the above estimate of 0.36 eV for the driving force in c-hexane, this would mean a driving force of less than 0.1 eV in the aromatic solvent. This would appear to be too small to surmount the barrier to ring-inversion required of the folding process.

We conclude that if the barrier to folding is small, as for polymethylene chains, then it will still occur in benzene. If however there is a substantial barrier to folding, as with the semi-rigid piperidine ring systems, then it may not occur in the psuedo-polar solvent. Having said this we now turn to the fifth molecule shown in Figure 4.1, denoted An[4,CN]NCN, which has an extra cyano group incorporated in the spacer unit. This was a serendipitous byproduct of the synthesis

of compound An[4]NCN.

The time-resolved fluorescence of An[4,CN]NCN in c-hexane shows very clearly the initial formation of a species with an emission maximum at 390 nm (3.18 eV) which decays on a timescale of nanoseconds and gives way to a band centered at 458 nm (2.71 eV) as shown in Figure 4.5. The correlated decay at 390 nm and growth at 460 nm are illustrated by the kinetic traces in Figure 4.6. These data are the clearest proof yet obtained for the successive rather than parallel formation of the different fluorescent species for this type of semi-rigid DSA compound. The lifetimes of the species determined from a kinetic fit are 8 and 35 ns.

From the difference in the emission maxima, the driving force for folding of the giant dipole state of An[4,CN]NCN in cyclohexane is determined to be 0.47 eV; considerably larger than the
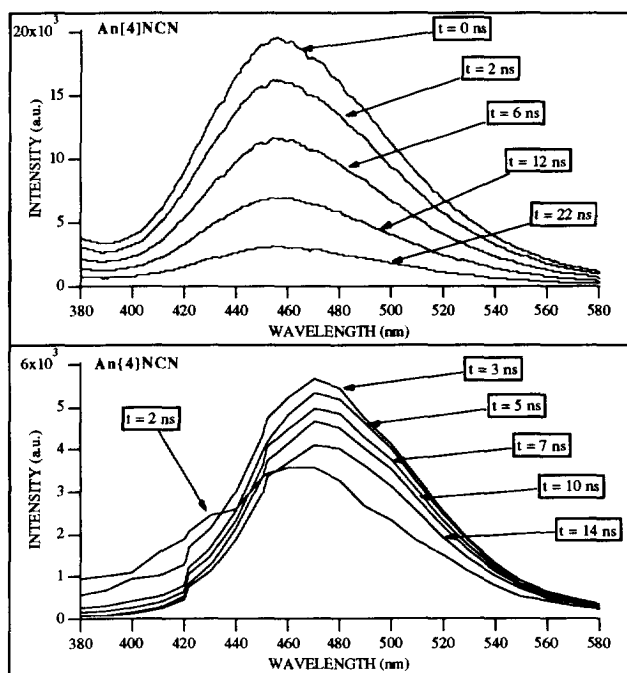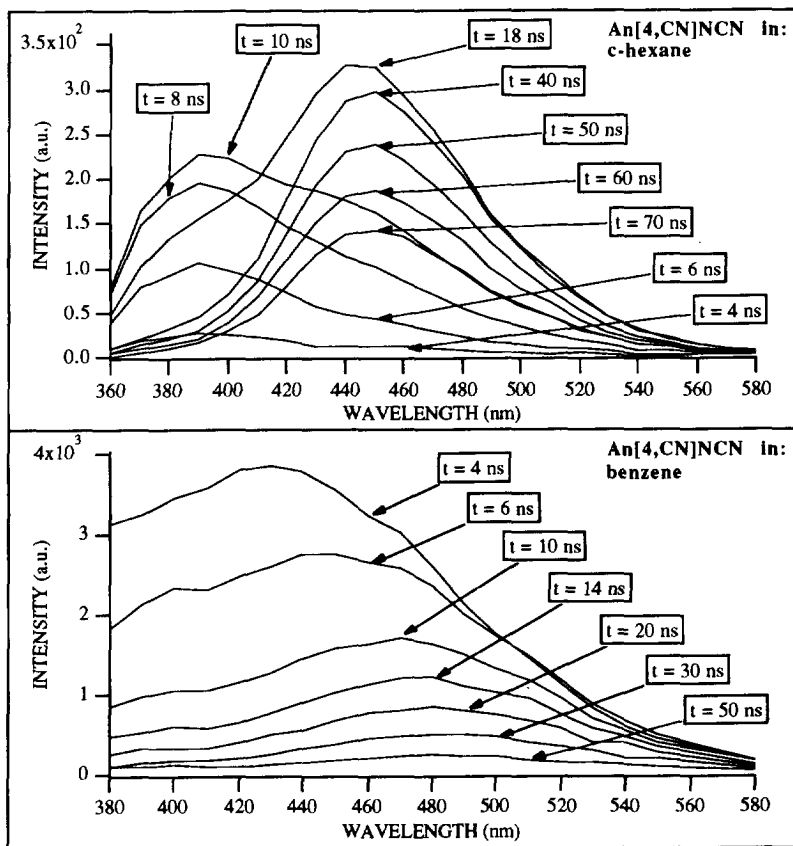

Figure 4.5: *Fluorescence spectra of An[4,CN]NCN shown in cyclohexane and benzene solution as a function of time following flash-photolysis at 308 nm, pulse width 7 ns.*

0.36 eV estimated for An[4]NCN. The reason for the larger driving force for folding of An[4,CN]NCN compared with An[4]NCN is not yet known.

Based on the above discussion, the value for c-hexane would suggest that the driving force for folding of An[4,CN]NCN in benzene should be close to 0.25 eV. It would appear that this is sufficient to make folding possible on a nanosecond timescale in benzene since a readily observable shift in spectrum from 440 nm to 490 nm is found for An[4,CN]NCN in this solvent (see Figure 4.5). Kinetic fits to the data at different wavelengths yield lifetimes of 4 ns and 20 ns for the initial, giant dipole, and final, folded exciplex-like state, respectively. This result for benzene is quite important since it shows that electrostatically-driven folding, even of semi-rigidly bridged donor-acceptor pairs, is not a phenomenon which is limited to completely non-polar media but it can also occur in solvents of intermediate polarity if the energetics are right.
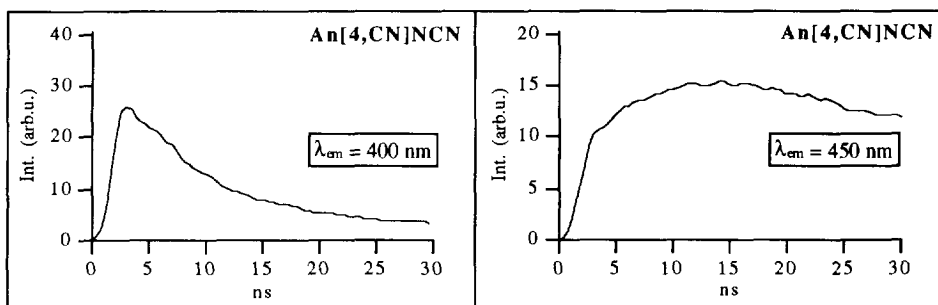
Figure 4.6: The transient fluorescence of a solution of An[4.CN]NCN in cyclohexane monitored at 400 nm and 450 nm resulting from flash-photolysis at 337 nm, pulse width 0.8 ns.

4.4 TRMC MEASUREMENTS REVISITED

The results presented in Table 4.1 were derived from the TRMC data from best-fits based on a kinetic scheme in which only one dipolar intermediate was formed. While this would appear to be a reasonably good assumption for the majority of solute-solvent combinations, it is clear from the fluorescence results for the semi-rigid An[4]NCN compound in cyclohexane that a significant change in conformation of the molecule takes place on a timescale of several nanoseconds. In Figure 4.7, the two proposed conformations of An[4]NCN in cyclohexane are shown. This effect is even more apparent for An[4,CN]NCN in both cyclohexane and benzene. Accordingly, the TRMC results for these systems have been reanalysed using a reaction scheme involving the successive formation of two dipolar intermediates and incorporating the kinetic parameters found for the two emitting states in the time-resolved fluorescence measurements.

125
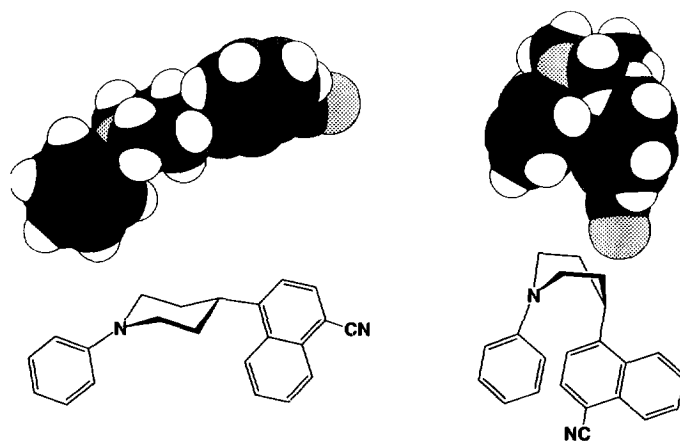
Figure 4.7: The extended and folded conformations of An[4]NCN.

The overall fits obtained and the individual contributions of the two intermediates are shown in Figure 4.8 for An[4]NCN in cyclohexane and An[4,CN]NCN in cyclohexane and benzene. The microwave conductivity parameters derived from the fits are listed in Table 4.3.

The dipole moment values derived for the initially formed species, for which it is reasonable to assume a quantum yield of very close to unity, are all close to 29 D as would be expected for an extended charge separated state. Since the subsequent, presumably folded, dipolar state is formed in competition with other decay modes of the giant dipole state we can only derive a minimum value of its dipole moment based on an assumption of a quantum yield of 1. The dipole moments found in this way, based on an assumed close-to-spherical geometry, are given

Table 4.3: Lifetime of the CS state^a, τ_S; conductivity parameter ($\mu_s^2\Phi / \Theta$); rotational relaxation time Θ_{cyl}, calculated using a cylindrical geometry; rotational relaxation time Θ_{sph}, calculated using a spherical geometry; dipole moment μ_{cyl}, calculated using Θ_{cyl} and dipole moment μ_{sph}, calculated using Θ_{sph}. Quantum yield Φ for the formation of the charge separated state is assumed to be unity.

Compound	τ_S (ns)^a		$\mu_s^2\Phi / \Theta$ (D^2/ps)		Θ_{cyl} (ps)		Θ_{sph} (ps)		μ_{cyl} (D)		μ_{sph} (D)	
	CHX	BEN	CHX	BEN	CHX	BEN	CHX	BEN	CHX	BEN	CHX	BEN
An[4]NCN	7		2.83		287				28.5			
	16		2.14				108				15.2	
An[4,CN]NCN	8	4	2.53	3.22	342	291			29.4	30.6		
	35	20	1.53	1.36			117	84			13.4	10.7

(a) from fluorescence measurements.
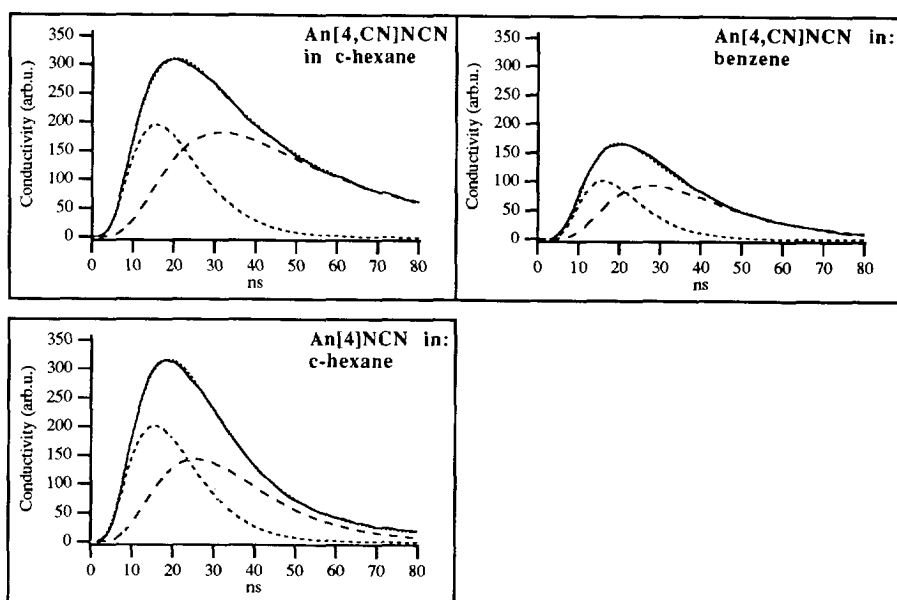
Figure 4.8: *Time-Resolved Microwave Conductivity transients observed observed for the solute/solvent combinations shown. The dotted lines are fits to the experimental data obtained from the Runge-Kutta fitting procedure. The dashed lines show the individual contributions from the extended and folded dipolar S_1 states. The transients are normalized to differences in viscosity and laser power intensity.*

in Table 4.3. The values are seen to be close to those for the folded exciplexes of the trimethylene spacer compounds given in Table 4.1.

To a first approximation the correct value of the dipole moment can be obtained by dividing the value based on $\Phi = 1$ by $\sqrt{\Phi}$. For example for the case of An[4,CN]NCN in benzene, if the efficiency of the folding process were only 50% then the dipole moment calculated would increase from 10.7 D to 15.1 D. Unfortunately it is impossible to estimate the actual value of the folding efficiency from the present TRMC or fluorescence data. Experiments at low temperatures in which the folding process is frozen out could provide an approximate estimate of the lifetime towards other decay modes from which an efficiency could be estimated. Such measurements have not as yet been carried out.

4.5 SUMMARY

In Figure 4.9 and Figure 4.10 schematic energy diagrams are presented for An[4]N, An{4}N, An[4]NCN and An{4}NCN in cyclohexane and benzene respectively. An overview of the situation for all solute/solvent combinations is presented on the next two pages.

127

Situation for cyclohexane

An[4]N   long distance electron transfer energetically unfavourable; only a very small equilibrium concentration of charge separated states present (Figure 4.9a).

An{4}N   charge separation occurs in a folded conformation (Figure 4.9b).

An[4]NCN charge separation in an extended conformation is energetically feasible and is followed by electrostatically driven folding on a timescale of ±7 ns (Figure 4.9c).

An{4}NCN charge separation in an extended conformation is followed by electrostatically driven folding on a timescale of ≤3 ns (Figure 4.9d).

An[4,CN]NCN charge separation in an extended conformation followed by electrostatically driven folding on a timescale of ±8 ns (not included in Figure 4.9).
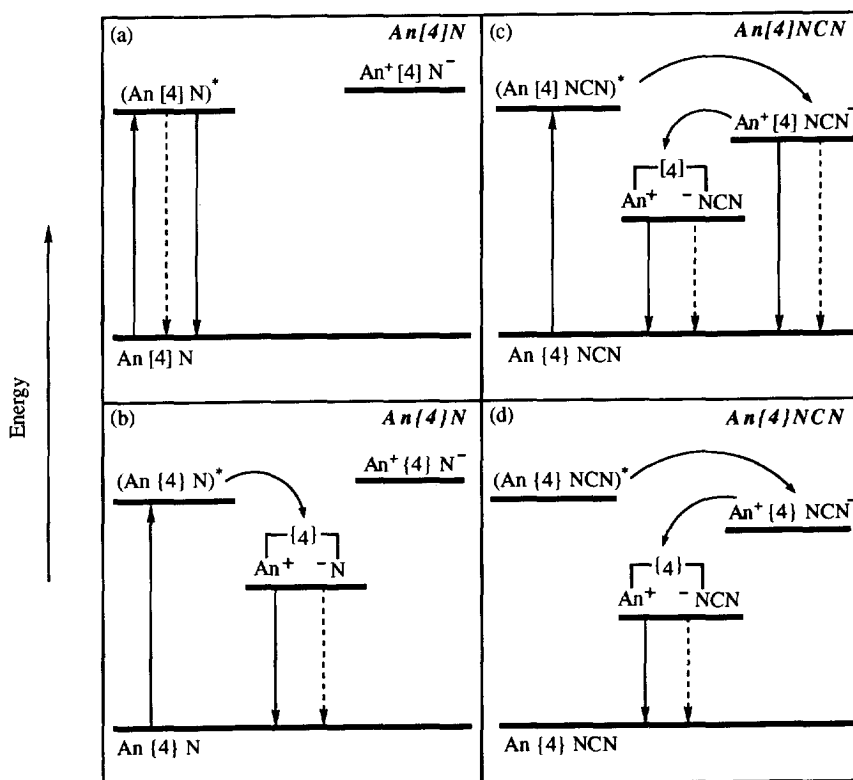
Figure 4.9: *Schematic representation of the relative energy levels of the intermediate states in cyclohexane. The full and dashed downward arrows represent emissive and radiationless transitions respectively.*

128

Situation for benzene

An[4]N	long distance electron transfer can occur (Figure 4.10a), however no electrostatically driven folding occurs.
An{4}N	charge separation in an extended conformation (Figure 4.10b) followed by rapid ≤3 ns electrostatically driven folding.
An[4]NCN	charge separation in an extended conformation (Figure 4.10c), no electrostatically driven folding occurs.
An{4}NCN	charge separation in an extended conformation followed by electrostatically driven folding on a timescale of ≤3 ns (Figure 4.10d).
An[4,CN]NCN	charge separation in an extended conformation followed by electrostatically driven folding on a timescale of 4 ns (not included in Figure 4.10).
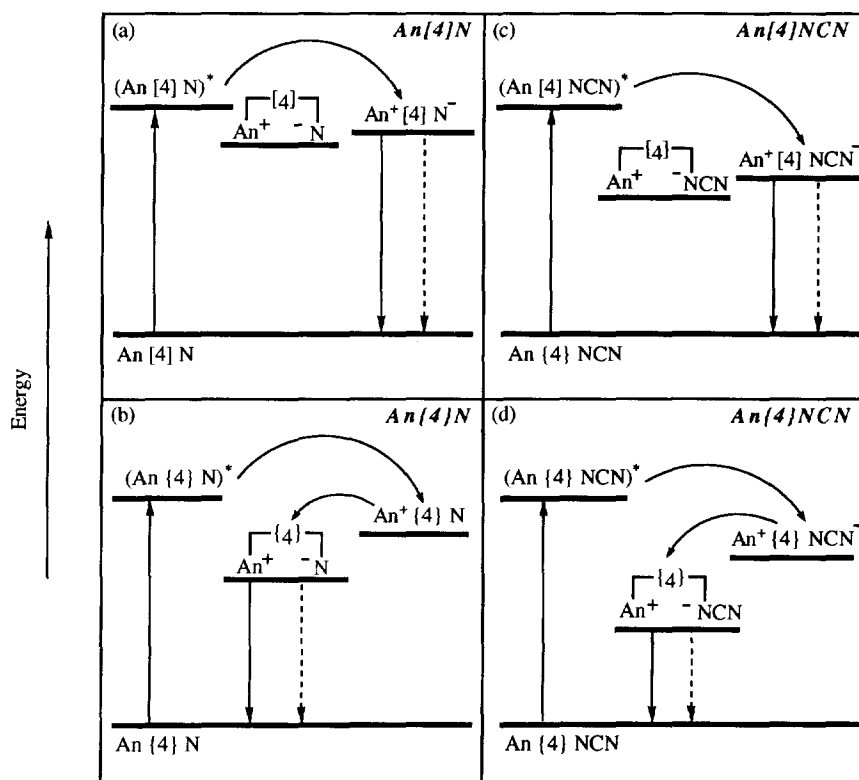
Figure 4.10: Schematic representation of the relative energy levels of the intermediate states in benzene. The full and dashed downward arrows represent emissive and radiationless transitions respectively.

129

4.6 ACKNOWLEDGEMENT

4.7 REFERENCES

1   This chapter was published in part in:
    W. Schuddeboom, T. Scherer, J.M. Warman and J.W. Verhoeven, *J. Phys. Chem.* **1993**, *97*, 13092.
2   *The Exciplex*, Eds.; Gordon and Ware, Academic Press, New York, **1975**.
3   D. Rehm and A. Weller, *Ber. Bunsenges.* **1969**, *73*, 834.
4   N. Mataga and Y. Murata, *J. Am. Chem. Soc.* **1969**, *91*, 3144.
5   S. Masaki, T. Okada, N. Mataga, Y. Sakata and S. Misumi, *Bull. Chem. Soc. Japan* **1976**, *49*, 1277.
6   T. Okada, M. Migita, N. Mataga, Y. Sakata and S. Misumi, *J. Am. Chem. Soc.* **1981**, *103*, 4715.
7   A. Weller, H. Staerk and R. Treichel, *Faraday Disc. Chem. Soc.* **1984**, *78*, 271.
8   F.C. De Schryver, N. Boens and J. Put, *Adv. Photochem.* **1977**, *10*, 359.
9   N. Mataga and M. Ottolenghi in *Molecular Association Vol. 2*, Ed.; R. Foster, Academic Press, New York, **1978**, 1.
10 N.C. Yang, D.W. Minsek, D.G. Johnson and M.R. Wasielewski in *Photochemical energy conversion*, Eds.; J.R. Norris Jr and D. Meisel, Elsevier, Amsterdam, **1989**, 111.
11 K. Nakatani, T. Okada, N. Mataga, F.C. De Schryver and M. van der Auweraer, *Chem. Phys. Lett.* **1988**, *145*, 81.
12 H. Yao, T. Okada and N. Mataga, *J. Phys. Chem.* **1989**, *93*, 7388.
13 H. Staerk, R. Mitzkus, W. Kühnle and A. Weller in *Picosecond phenomena*, Vol. 3, Eds.; K.B. Eisenthal, R.M. Hochstrasser, W. Kaiser and A. Laubereau, Springer, Berlin, **1982**, 205.
14 J.H. Borkent, A.W.J. de Jong, J.W. Verhoeven and Th. J. de Boer, *Chem. Phys. Lett.* **1978**, *57*, 530.
15 M. van der Auweraer, *Comm. Royal Acad. Sci. Belges* **1986**, *48*, No. 6, 27.
16 Y. Hatano, M. Yamamoto and Y. Nishijima, *J. Phys. Chem.* **1978**, *82*, 367.
17 M. Migita, T. Okada, N. Mataga, Y. Sakata, S. Misumi, N. Nakashima and K. Yoshihara, *Bull. Chem. Soc. Japan* **1981**, *54*, 3304.
18 For a complete review see: M.N. Paddon-Row and K.D. Jordan in *Molecular Structure and Energetics*, Eds.; J.F. Liebman and A. Greenberg, VCH publishers, New York **1988**, Vol. 6, Chp. 3.
19 N.S. Hush, M.N. Paddon-Row, E. Cotsaris, H. Oevering, J.W. Verhoeven and M. Heppener, *Chem. Phys. Lett.* **1988**, *117*, 8.
20 J.M. Warman, M.P. de Haas, H. Oevering, J.W. Verhoeven, M.N. Paddon-Row, A.M. Oliver and N.S. Hush, *Chem. Phys. Lett.* **1986**, *128*, 95.
21 J.W. Verhoeven, M.N. Paddon-Row, N.S. Hush, H. Oevering and M. Heppener, *Pure & Appl. Chem.* **1986**, *58*, 1285.
22 H. Oevering, M.N. Paddon-Row, A.M. Olivier, E. Cotsaris, M. Heppener, J.W. Verhoeven and N.S. Hush, *J. Am. Chem. Soc.* **1987**, *109*, 3258.
23 H. Oevering, J.W. Verhoeven and M.N. Paddon-Row, *Tetrahedron* **1989**, *45*, 4751.
24 M.N. Paddon-Row, A.M. Oliver, J.M. Warman, K.J. Smith, M.P. de Haas, H. Oevering and J.W. Verhoeven, *J. Phys. Chem.* **1988**, *92*, 6958.

25 H. Oevering, J.W. Verhoeven, M.N. Paddon-Row, E. Cotsaris and N.S. Hush,
    Chem. Phys. Lett. **1988**, *143*, 488.
26 J. Kroon, A.M. Oliver, M.N. Paddon-Row and J.W. Verhoeven, *Recl. Trav. Chim. Pays-Bas* **1988**, *107*, 509.
27 A.M. Oliver, D.C. Graig, M.N. Paddon-Row, J. Kroon and J.W. Verhoeven,
    Chem. Phys. Lett. **1988**, *150*, 366.
28 J.M. Lawson, D.C. Graig, M.N. Paddon-Row, J. Kroon and J.W. Verhoeven,
    Chem. Phys. Lett. **1989**, *164*, 120.
29 M.N. Paddon-Row, *Chem. Phys. Lett.* **1990**, *167*, 432.
30 J.M. Warman, K.J. Smit, M.P. de Haas, S.A. Jonker, M.N. Paddon-Row, A.M. Oliver, J. Kroon, H. Oevering,
    and J.W. Verhoeven, *J. Phys. Chem.* **1991**, *95*, 1979.
31 J. Kroon, J.W. Verhoeven, M.N. Paddon-Row and A.M. Oliver,
    Angewan. Chem. Int. Ed. Eng. **1991**, *30*, 1358.
32 A.M. Oliver, M.N. Paddon-Row, J. Kroon and J.W. Verhoeven, *Chem. Phys. Lett.* **1992**, *191*, 371.
33 J.S. Connolly, J.R. Bolton in *Photoinduced electron transfer*, Eds.; M.A. Fox and M. Chanon, Elsevier,
    Amsterdam, **1988** .
34 M.R. Wasielewski, in *Photoinduced electron transfer*, Eds.; M.A. Fox and M. Chanon, Elsevier,
    Amsterdam, **1988**.
35 M.R. Wasielewski, D.W. Minsek, M.P. Niemczyk, W.A. Svec and N.C. Yang,
    J. Am. Chem. Soc. **1990**, *112*, 2823.
36 W. Rettig, R. Haag and J. Wirz, *Chem. Phys. Lett.* **1991**, *180*, 216.
37 A.W.J.D. Dekkers, J.W. Verhoeven and W.N. Speckamp, *Tetrahedron* **1973**, *29*, 1691.
38 P. Pasman, F. Rob and J.W. Verhoeven, *J. Am. Chem. Soc.* **1982**, *104*, 5127.
39 P. Pasman, N.W. Koper and J.W. Verhoeven, *Recl. Trav. Chim. Pays-Bas* **1982**, *101*, 363.
40 P. Pasman, G.F. Mes, N.W. Koper and J.W. Verhoeven, *J. Am. Chem. Soc.* **1985**, *107*, 5839.
41 G.F. Mes, B. de Jong, H.J. van Ramesdonk, J.W. Verhoeven, J.M. Warman, M.P. de Haas and
    L.E.W. Horsman-van den Dool, *J. Am. Chem. Soc.* **1984**, *106*, 6524.
42 H. Heitele, P. Finckh and M.E. Michel-Beyerle, *Angewan. Chem. Int., Ed. Engl.* **1989**, *28*, 619.
43 R.M. Hoffmann, A. Imamura and W.J. Hehre, *J. Am. Chem. Soc.* **1968**, 90, 1499.
44 R.M. Hoffmann, *Acc. Chem. Res.* **1971**, *4*, 1.
45 J.M. Warman, M.P. de Haas, M.N. Paddon-Row, E. Cotsaris, N.S. Hush, H. Oevering and J.W. Verhoeven,
    Nature **1986**, *320*, 615.
46 A.M. Brouwer, R.D. Mout, P.H. Maassen van den Brink, H.J. van Ramesdonk, S.A. Jonker and J.M. Warman,
    Chem. Phys. Lett. **1991**, *186*, 481.
47 B. Wegewijs, R.M. Hermant, J.W. Verhoeven, M.P. de Haas and J.M. Warman,
    Chem. Phys. Lett. **1990**, *168*, 1585.
48 J.W. Verhoeven, *Pure & Appl. Chem.* **1990**, *62*, 1585.
49 B. Wegewijs, R.M. Hermant, J.W. Verhoeven, A.G.M. Kunst and R.P.H. Rettschnik,
    Chem. Phys. Lett. **1987**, *140*, 587.
50 J.W. Verhoeven, T. Scherer and R.J. Willemse, *Pure & Appl. Chem.* **1993**, *65*, 1717.
51 T. Scherer, *PhD Thesis*, University of Amsterdam, **1994**.
52 M.P. de Haas and J.M. Warman, *Chem. Phys.* **1982**, *73*, 35.
53 B. Wegewijs, T. Scherer, R.P.H. Rettschnick and J.W. Verhoeven, *Chem. Phys.* **1993**, *176*, 349.
54 K.A. Zachariasse, G. Duveneck, W. Kühnle, P. Reynders and G. Striker, *Chem. Phys. Lett.* **1987**, *133*, 390.
55 J.M. Warman, S.A. Jonker, W. Schuddeboom, M.P. de Haas, M.N. Paddon-Row, J.W. Verhoeven
    and K. Zachariasse, *Pure & Appl. Chem.* **1993**, *65*, 1723-1728.

56 E.J. Land, J.T. Richards and J.K. Thomas, *J. Phys. Chem.* **1972**, *76*, 3805.

57 H. Staerk, W. Kühnle, R. Treichel and A. Weller, *Chem. Phys. Lett.* **1985**, *118*, 19.

58 P.C.M. Weisenborn, C.A.G.O. Varma, M.P. de Haas and J.M. Warman, *Chem. Phys.* **1988**, *122*, 147.

59 I.B. Berlman, *Handbook of fluorescence spectra of aromatic molecules*, Academic Press, New York, **1971**.

60 I.H.M. van Stokkum, A.M. Brouwer, H.J. van Ramesdonk and T. Scherer,
    Proc. Kon. Ned. Akad. Wetensch. **1993**, *96*, 43.

Chapter 5

Charge Separation in Sigma-Bond Separated Trichromophoric Donor-Acceptor Compounds[1-3]

5.1 INTRODUCTION

In recent years a lot of research has been carried out in the field of donor-acceptor compounds which attempt to mimic the electron transfer process in photosynthesis.[4-6] Nature has arranged that charge separation occurs in sequential steps, resulting in the formation of a very long lived charge separated state, with high efficiency. The sequential steps of charge separation within the photosynthetic reaction center have been found to involve electron transfer (ET) over distances between chromophores on the order of 10 Å.[7-10] This discovery has led to renewed interest in long distance electron transfer in general and in particular in the synthesis of compounds which can provide a fundamental insight into the factors controlling this process.

Initially only bichromophoric compounds were investigated. For such systems it is important that the electronic coupling between donor and acceptor is not too strong, in order to get a long living charge separated state. In other words, the charge recombination rate must be slowed down. On the other hand the coupling must be strong enough to ensure that charge separation competes efficiently with other decay pathways of the locally excited state initially formed. In π-conjugated donor-acceptor compounds there exists a strong coupling between the donor and acceptor moieties, which allows very rapid charge separation, but also very rapid charge recombination. Because of this, much of the attention is focussed nowadays on σ-bonded donor-acceptor compounds.[4-7,10-23] In these systems charge separation can still occur rapidly, but the charge recombination is often slowed down because of the much weaker "Through Bond Interaction" (TBI).[24-27] Some examples of charge separation over distances of ca 10 Å with lifetimes up to 1 μs have been reported for bichromophoric compounds.[4-6] Particularly important in this respect are the compounds assembled by Paddon-Row and coworkers which have provided many insights into long distance electron transfer in bichromophoric systems.[27-42] These have been studied previously by both TRMC and fluorescence detection techniques.

Unfortunately the larger the distance the weaker the interaction, so that in bichromophoric systems there is a limiting distance above which the efficiency of charge separation decreases rapidly as local decay processes begin to compete effectively with long distance ET. An approach, necessary to overcome larger distances and create longer living charge separated states, is to introduce more chromophores in one molecule. In such a multichromophoric system electron transfer occurs in a sequence of steps. This is the manner in which nature has organized

things. Lifetimes into the microsecond region with up to five chromophores (PENTAD) have been achieved by Gust, Moore and coworkers[43] and for three chromophores (TRIAD) by Wasielewski et al.[44] It is worth pointing out however that a lifetime in excess of 1 µs has been found for a 13 σ-bond Paddon-Row DIAD compound.[7,12]

In this chapter trichromophoric compounds of the type donor$_2$-bridge-donor$_1$-bridge-acceptor (Figure 5.1), synthesized by the group of Verhoeven and Brouwer at the University of Amsterdam, are investigated with both TRMC and fluorescence techniques.[1-3] The compounds are designed in such a way that the ethenylcyanonaphthyl acceptor (ECN) absorbs the excitation energy (308 nm) initially. This ensures that the subsequent charge separation steps, if they occur, will take place sequentially and unidirectionally. The idealized concept is expressed in Figure 5.2, where after excitation of the acceptor the first electron transfer from donor 1 (D$_1$) to

D$_2$[3]D$_1$[4]A type compounds   **D$_2$[4]D$_1$[3]A type compounds**
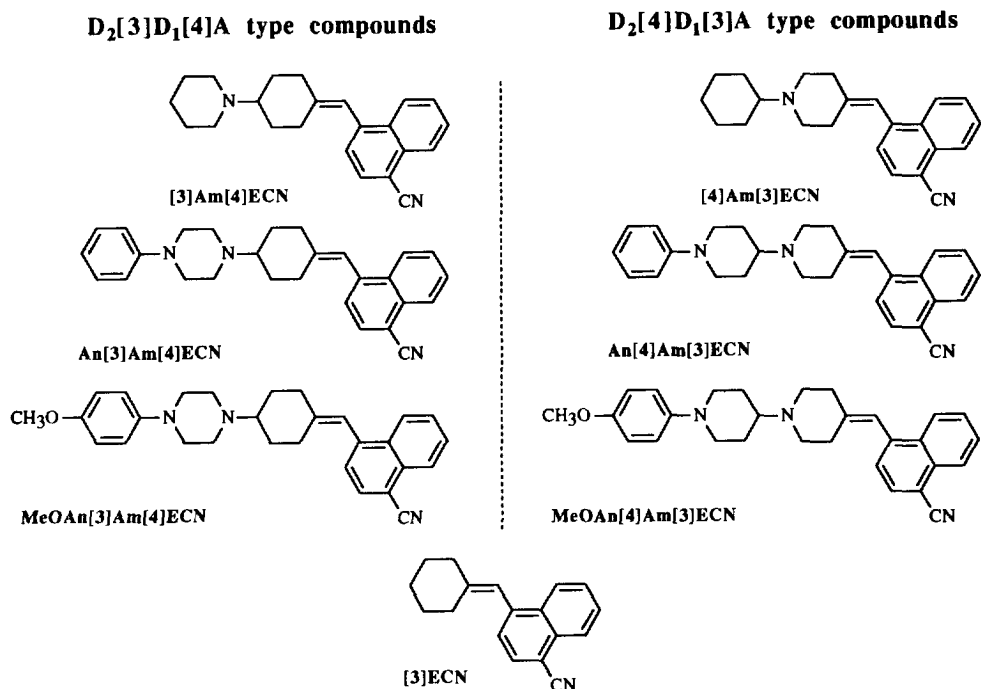
Figure 5.1: The structures of the two types of trichromophores: D$_2$[3]D$_1$[4]A and D$_2$[4]D$_1$[3]A together with the reference bichromophores: [3]D$_1$[4]A and [4]D$_1$[3]A and acceptor [3]A. The abbreviated nomenclature is shown beneath the structural formula, with ECN, the ethenylcyanonaphthalene acceptor; Am, the amino nitrogen donor; and An and MeOAn the anilino and p-methoxyanilino donor moieties respectively.

the acceptor (A) takes place and is followed by the second electron transfer from donor 2 (D_2) to D_1, thus creating the complete charge separated state D_2^+-D_1-A^-.
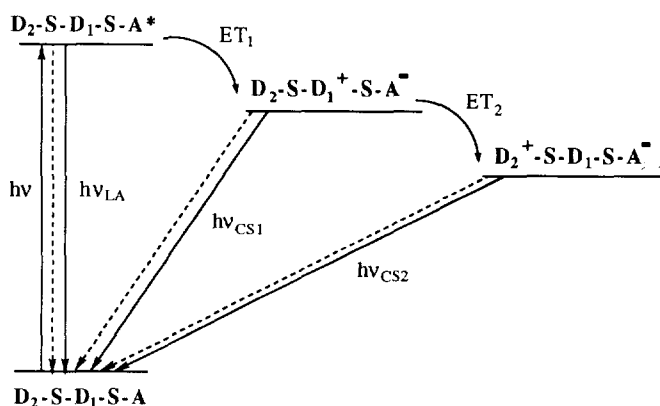
Figure 5.2: *Schematic representation of the ideal relative positions of the energy levels of the states involved in an electron-transfer trichromophore or TRIAD. Where hv_{LA} reprents local fluorescence from the, in the acceptor excited, trichromophore, hv_{CS1} represents fluorescence from the CS1 state and hv_{CS2} represents fluorescence from the CS2 state, where complete, two-step charge separation has occurred. The dashed arrows indicate radiationless decay.*

The compounds investigated can be divided into two types with the only difference being a 1.2 Å shift of the amino nitrogen of D_1. The first series has four sigma bonds between A and D_1 and three between D_2 and D_1, so the general structure is denoted $\mathbf{D_2[3]D_1[4]A}$. The second series has three sigma bonds between A and D_1 and four between D_2 and D_1, so the general structure is denoted $\mathbf{D_2[4]D_1[3]A}$.

The results for the two types of trichromophores are initially presented and discussed separately below. The results are further subdivided into those for the pseudo-polar solvents benzene and dioxane and those for alkane solvents, since they differ considerably. A general discussion in which the results are intercompared is given in Section 5.6.

5.2 $D_2[3]D_1[4]A$ TRICHROMOPHORES IN PSEUDO-POLAR SOLVENTS

5.2.1 TRMC measurements

In Figure 5.3, the TRMC traces are shown for the three compounds [3]Am[4]ECN, An[3]Am[4]ECN and MeOAn[3]Am[4]ECN in benzene and dioxane. In all cases there is evidence of a highly dipolar transient upon flash-photolysis. The data could all be fit with a single dipolar intermediate and a small underlying and slowly decaying signal close to the noise level. The values of the lifetime of the dipolar intermediates determined from the fits to the data

135
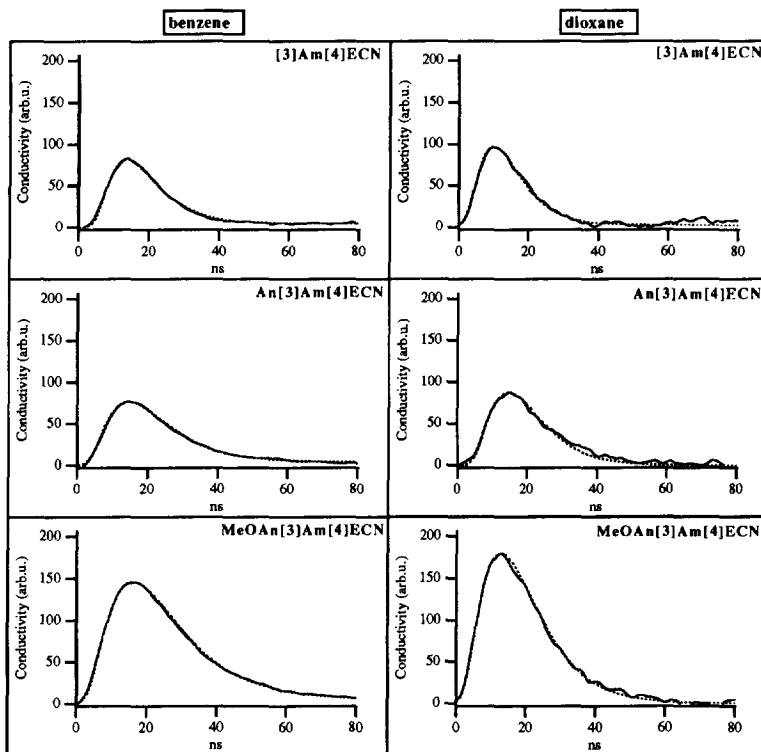
Figure 5.3: *Time-Resolved Microwave Conductivity transients observed on flash-photolysis in benzene and dioxane. The dotted lines are fits to the experimental data obtained from the Runge-Kutta fitting procedure. The transients are normalized to differences in viscosity and laser power intensity.*

are listed in Table 5.1, together with the corresponding values of the conductivity parameter $\mu_S{}^2 \Phi / \Theta$. Using estimates of the dipolar rotational relaxation times and assuming a quantum yield of unity, the dipole moments calculated are given in Table 5.1. The dipole moments are seen to be in reasonable agreement for the two solvents. Of particular interest is the relatively small change in dipole moment of only 2 to 3 D on addition of the anilino donor compared with the *ca* 10 D change for the methoxyanilino moiety. This will be discussed at greater length together with the fluorescence results in Section 5.2.3.

Table 5.1: *Lifetime* τ_S, *conductivity parameter* $\mu_S^2\Phi/\Theta$, *rotational relaxation time* Θ *and the calculated dipole moment* μ_S.

Compound	τ_S (ns)		$\mu_S^2\Phi / \Theta$ (D^2/ps)		Θ^a (ps)		μ_* (D)^b	
	BEN	DOX	BEN	DOX	BEN	DOX	BEN	DOX
[3]Am[4]ECN	4	4	1.91	1.01	277	619	23	25
An[3]Am[4]ECN	8.5	7	1.36	0.77	458	1022	25	28
MeOAn[3]Am[4]ECN	13	9	2.12	1.01	545	1216	34	35

(a) calculated according to equation (103) in Section 2.5.2.3 for a cylindrical geometry.
(b) calculated assuming a quantum yield of unity (Φ=1) for the charge separated state.

5.2.2 Fluorescence measurements

The fluoresence spectra of compounds [3]Am[4]ECN, An[3]Am[4]ECN and MeO-An[3]Am[4]ECN in solvents of medium polarity consist of two bands (see Figure 5.4).[1] The band at *ca* 370 nm, which is present in all spectra in all solvents, is ascribed to radiative decay of the initially formed acceptor excited state. The position of this band is almost the same in all solvents, indicating the nonpolar character of the state.

The second band is a broad emission at longer wavelengths, which shifts to increasingly longer wavelengths and is reduced in intensity as the solvent polarity increases. These features are characteristic for emissions from a highly dipolar excited state.
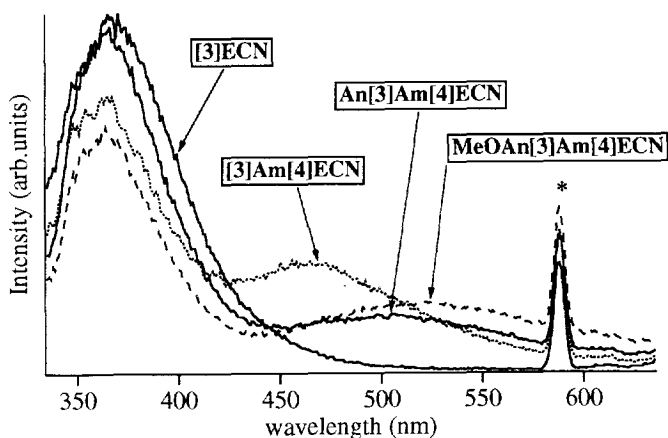
Figure 5.4: *Fluorescence spectra of [3]Am[4]ECN, An[3]Am[4]ECN and MeOAn[3]Am[4]ECN and the reference acceptor [3]ECN in di-n-butylether (from ref. 1).*

In Table 5.2 the maxima and fluorescence decay times of the long wavelength emission in benzene and dioxane are reported. The fluorescence quantum yields are on the order of 1% or lower in all cases.[1,2] Plots of the emission wavenumber of the compounds versus the solvent polarity parameter Δf, for several polar solvents not listed in Table 5.2, give slopes corresponding to $2\mu_S^2/hca^3$. These values are also shown in Table 5.2. Using estimates of the cavity radius a, the dipole moments shown in Table 5.2 were calculated.[1,45]

Table 5.2: Emission maximum of the charge separated state hv_{max}, fluorescence lifetime τ_S, slope of the plot of the emission wavenumber versus solvent polarity parameter Δf; $2\mu_S^2/hca^3$, cavity radius a and the calculated dipole moment μ_S.

Compound	hv_{max} (eV)		τ_S (ns)		$2\mu_S^2/hca^3$ (eV)[a]	a (Å)[b]	μ_* (D)[a]
	BEN	DOX	BEN	DOX			
[3]Am[4]ECN	2.57	2.33	4	4	37.9	5.5	22
An[3]Am[4]ECN	2.38	2.26	10	6	37.0	5.9	24
MeOAn[3]Am[4]ECN	2.31	2.07	14	9	55.4	6.0	31

(a) from solvatochromic shift for several solvents.[1,45]

(b) see reference 1.

5.2.3 Discussion

The TRMC and fluorescence measurements clearly demonstrate the occurrence of fast light-induced intramolecular charge separation in the bi- and trichromophoric compounds investigated. The lifetimes of the dipolar TRMC transients are seen to be very close to those found for the decay of the long wavelength emission. The same species is therefore clearly being monitored by both techniques. Of particular importance is the finding that the dipole moment values of 22, 24 and 31 D, determined from the solvatochromic shifts for [3]Am[4]ECN, An[3]Am[4]ECN and MeOAn[3]Am[4]ECN respectively, are close to the average values of 24, 26.5 and 34.5 determined from the TRMC measurements. The values of μ_S from solvatochromic shifts are independent of the quantum yield of the emissive state, whereas the TRMC values are based on an assumed quantum yield of 1. The good agreement between the two is therefore evidence for the formation of the charge separated states with close to 100% efficiency in benzene and dioxane.

A dipole moment of 24 D for the bichromophoric compound [3]Am[4]ECN corresponds to complete charge separation over a distance of 5Å. This is considerably longer than the 4.0 Å distance between the amino nitrogen and the nearest carbon atom of the ethylenic bond, in

agreement with the formation of the [3]Am$^+$[4]ECN$^-$ state (see Figure 5.5).

Introduction of the anilino moiety results in an increase of dipole moment of 2-3 D for An[3]Am[4]ECN which corresponds to an increase in distance of only *ca* 0.5 Å. This suggests that the positive charge is still localized close to the first donor unit in this compound, thus mainly on the aliphatic amino nitrogen atom, corresponding to D_2-D_1^+-A$^-$. A further electron transfer step to give D_2^+-D_1-A$^-$ is apparently unfavorable. The presence of the second anilino donor does however appear to stabilize the D_2-D_1^+-A$^-$ state as indicated by the two-times longer lifetime and the bathochromic shift of *ca* 0.13 eV in the fluorescence of An[3]Am[4]ECN compared with that of [3]Am[4]ECN. Evidence for this increased stability is also found in the TRMC measurements in alkane solvents presented in the next section.
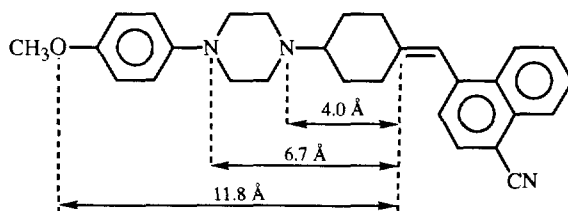
Figure 5.5: Relevant intramolecular distances for full charge separation in MeOAn[3]Am[4]ECN .
(1 Å charge separation ≡ 4.80 D).

Introduction of the methoxy group in D_2 creates a better donor and is apparently sufficient to result in a significantly larger dipole moment of *ca* 35 D. The lifetime of the dipolar excited state is further increased and the bathochromic shift of *ca* 0.26 eV also reveals a further stabilization. The increase of approximately 10 D in the dipole moment compared with those for the single donor compound and An[3]Am[4]ECN indicates that the positive charge center is now situated close to the nitrogen atom of the methoxyanilino group, suggesting that for this compound the second electron transfer step does occur.

The results on the alkane solutions which are presented and discussed below indicate that the coupling between the nitrogen atoms in the piperazine ring of the D_2[3]D_1 compounds may be quite strong. The formation of D_2^+[3]D_1[4]ECN$^-$ may then occur as a single step process rather than via the intermediate formation of the D_2[3]D_1^+[4]ECN$^-$ state. This may also explain why the lifetime of the giant dipole state of the methoxyanilino compound is still only on the order of 10 ns in these pseudo-polar solvents.
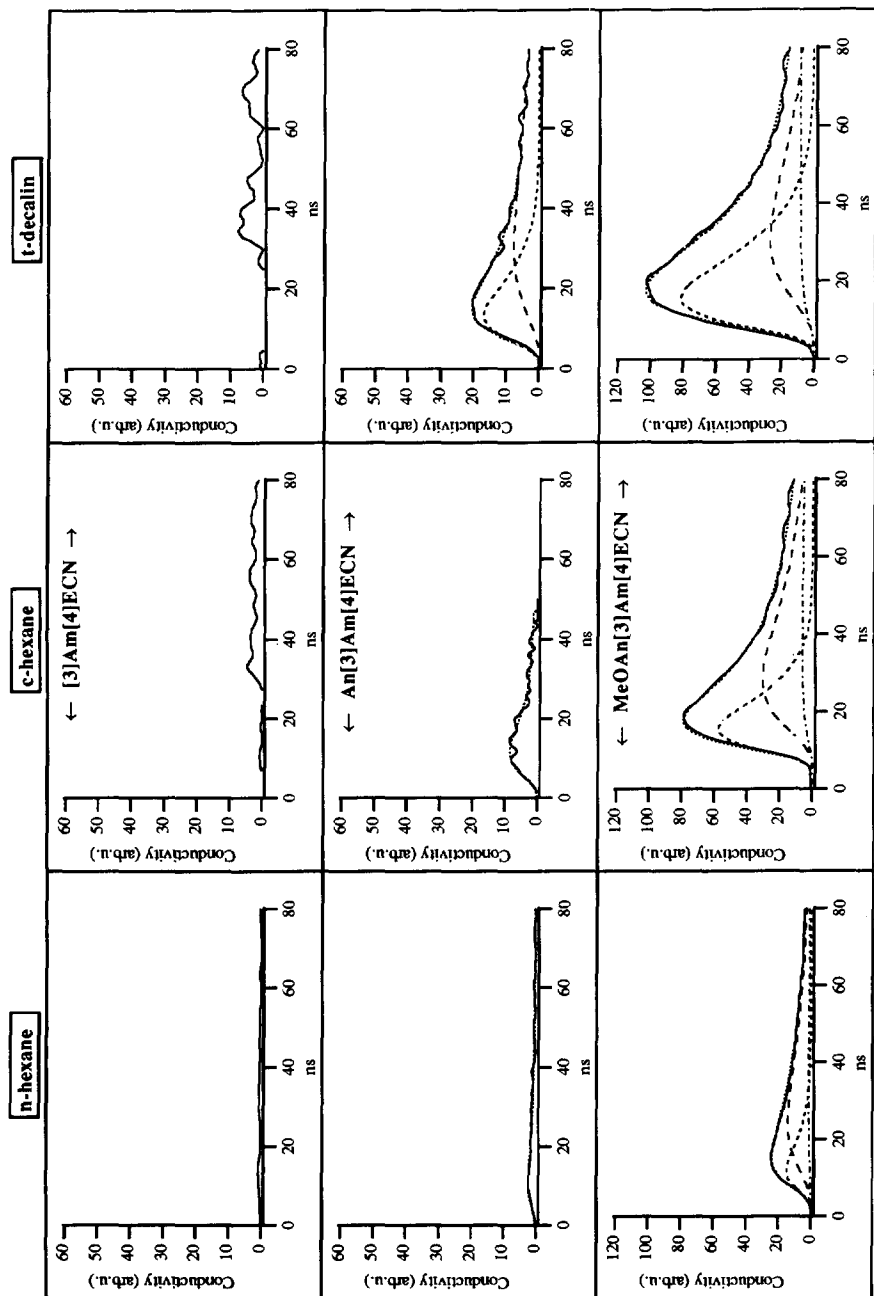
Figure 5.6: *Time-Resolved Microwave Conductivity transients observed on flash-photolysis in n-hexane, cyclohexane and t-decalin. The dotted lines are fits to the experimental data obtained from the Runge-Kutta fitting procedure. The dashed lines show the individual contributions from the different components to the total signal. The transients are normalized to differences in viscosity and laser power intensity.*

5.3 D_2[3]D_1[4]A TRICHROMOPHORES IN ALKANES[2]

5.3.1 TRMC measurements

In Figure 5.6 the TRMC traces for the three compounds in n-hexane, cyclohexane and t-decalin are shown.[2] For [3]Am[4]ECN the transients found are close to the noise level and there is no evidence at all for the formation of a charge separated state, in contrast with the measurements in benzene and dioxane. This implies that the first electron transfer step does not take place in the alkanes.

In the case of An[3]Am[4]ECN, small TRMC signals are observed in the alkane solvents as shown in Figure 5.6. The size of the signals is seen to increase markedly in going from n-hexane to t-decalin. In the latter solvent the decay is clearly multi-exponential and can be fit with a short component with a lifetime of 4 ns and a much longer-lived component with a lifetime of approximately 100 ns. In cyclohexane and n-hexane only a short-lived transient with a lifetime of *ca* 3 ns was clearly definable. The values of $\mu_S^2\Phi / \Theta$, determined for the short-lived component are listed for all three solvents in Table 5.3. With the assumption that the dipole moment of the intermediate responsible for this transient signal is equal to 26.5 D, as found for the pseudo-polar solvents, quantum yields for charge separation can be calculated and are found to be 0.04 in n-hexane, 0.15 in cyclohexane and 0.26 in t-decalin (for results see Table 5.5 in Section 5.3.3).

MeOAn[3]Am[4]ECN gives a comparatively large signal in n-hexane, cyclohexane and t-decalin. The traces could however not be fit assuming a single dipolar intermediate. The experimental decay traces could be analyzed assuming that the initially formed charge separated state CS1 (quantum yield Φ_1) is converted into a second charge separated species CS2 (quantum yield Φ_2), in competition with its decay to the ground state. Quite good fits were obtained using lifetimes of the two dipolar states, τ_1 and τ_2, derived from the fluorescence

Table 5.3: Lifetime of CS1, τ_1, with conductivity parameter $(\mu_S^2\Phi / \Theta)_1$ and lifetime of CS2, τ_2, with conductivity parameter $(\mu_S^2\Phi / \Theta)_2$.

Compound	τ_1 (ns)[a]			$(\mu_S^2\Phi / \Theta)_1$ (D²/ps)			τ_2 (ns)[a]			$(\mu_S^2\Phi / \Theta)_2$ (D²/ps)		
	NHX	CHX	TDC	NHX	CHX	TDC	NHX	CHX	TDC	NHX	CHX	TDC
[3]Am[4]ECN	b	b	b									
An[3]Am[4]ECN	3	3	4	0.17	0.20	0.16						
MeOAn[3]Am[4]ECN	2	6	10	1.98	1.09	0.43	29	29	27	0.37	0.22	0.10

(a) from fluorescence measurements.

(b) no signal measured.

measurements. The individual conductivity parameters for the two states are listed in Table 5.3. The data will be discussed in more detail in Section 5.3.3, after first presenting the fluorescence results.

5.3.2 Fluorescence measurements

In saturated hydrocarbon solvents [3]Am[4]ECN shows only local emission from the acceptor chromophore, which again indicates that electron transfer from D_1 to ECN does not occur in these solvents as expected on the basis of the TRMC results.[2]

An[3]Am[4]ECN also shows only local fluorescence, in agreement with the low quantum yield for the formation of the charge separated state as found with TRMC.

MeOAn[3]Am[4]ECN in contrast shows three fluorescence bands in n-hexane, cyclohexane and t-decalin in the wavelength regions 370, 430 and 530 nm (see Figure 5.7). The relative contributions of the three bands are seen to be solvent dependent.
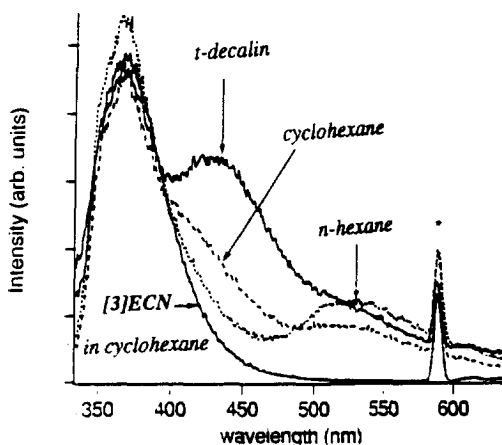
Figure 5.7: Fluorescence spectra of MeOAn[3]Am[4]ECN in n-hexane, cyclohexane and t-decalin and of the reference acceptor [3]ECN in cyclohexane (from ref. 2).

Time-resolved spectral measurements have been performed using a gated optical multi-channel analyzer (OMA) where the time window in which the spectra were observed (width 5 ns) was shifted in time with respect to the pulsed excitation (308 nm, FWHM 7 ns). Some typical results are shown in Figure 5.8. In addition, fluorescence decay curves at single wavelengths were recorded. The kinetics are complex and multiexponential at most wavelengths. However, approximate decay rates could be determined for the three bands based on the contribution of each decay component at different wavelengths in the multi-exponential
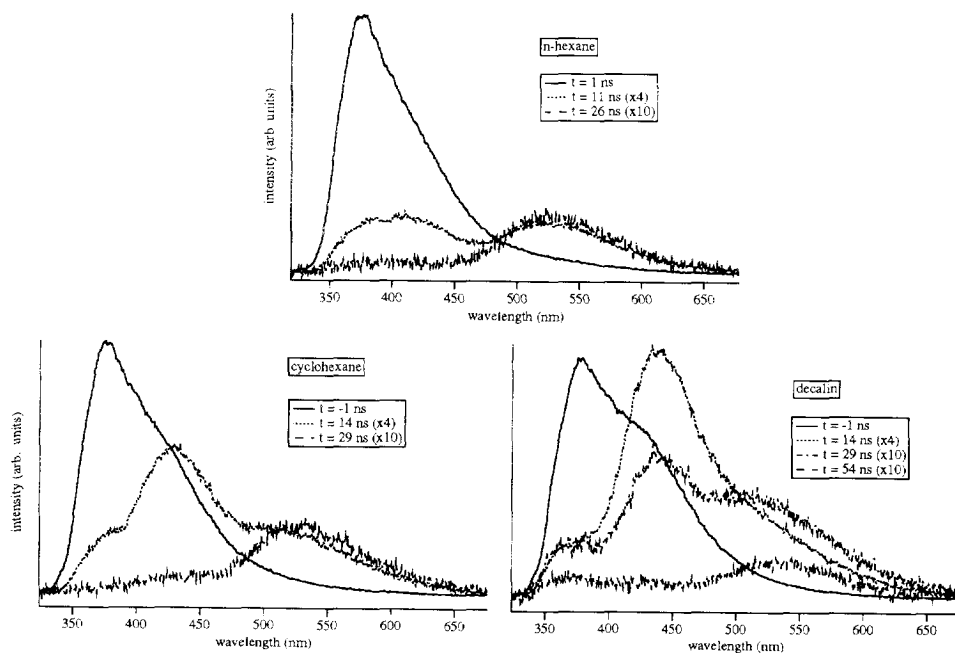
Figure 5.8: *Time-gated fluorescence spectra of MeOAn[3]Am[4]ECN at different time delays relative to the maximum of the exciting laser pulse (t=0) in n-hexane at t=1, 11 and 26 ns; in cyclohexane at t=-1, 14 and 29 ns; in t-decalin at t=-1, 14, 29 and 54 ns (from ref. 2).*

fits. The resulting band positions and decay rates are reported in Table 5.4.

The assingment of the bands is as follows; the short wavelength band results from the partially quenched local acceptor emission, LA, the longer wavelength bands are ascribed to two charge separated species; CS1 and CS2. Of particular interest is the strong solvent dependence of the lifetime of the CS1 band.

Table 5.4: *Emission maxima in nm and approximate decay times in ns (in parentheses) of the three components in the fluorescence spectra of MeOAn[3]Am[4]ECN at room temperature.*

Solvent	LA	CS1	CS2
n-hexane	376 (<1)	418 (2 ± 0.5)	525 (29 ± 3)
cyclohexane	377 (<1)	430 (6 ± 1)	530 (29 ± 3)
t-decalin	377 (<1)	437 (10 ± 2)	535 (27 ± 3)

Experiments at lower temperatures on a solution of MeOAn[3]Am[4]ECN in methyl-cyclohexane reveal that the longest wavelength band belonging to CS2 gradually disappears on cooling, while the intensity and the lifetime of the CS1 emission increases. In the liquid phase at 142 K, the decay time of the CS1 band is found to be 80 ns. In the solid phase at 85 K the lifetime is slightly longer at 90 ns.[2]

5.3.3 Discussion

Both the TRMC and the fluorescence results show that for [3]Am[4]ECN in alkane solvents electron transfer, to create the charge separated D_1^+[4]A⁻ state, does not take place. Presumably this is because the energy level of the charge separated state now lies above that of the locally excited state. Despite this, charge separation is found to occur for both An[3]Am[4]ECN and MeOAn[3]Am[4]ECN.

For An[3]Am[4]ECN the calculated quantum yield is however only 0.04, 0.15 and 0.26 in n-hexane, cyclohexane and t-decalin respectively. Clearly the process of charge separation for this compound must be very close to being energetically neutral and can only weakly compete with the natural decay of the locally excited acceptor. The energetics appear to be so critically balanced that even the differences in dielectric constant between the saturated hydrocarbon solvents are enough to considerably change the quantum yield of charge separation. This sensitivity of the yield of charge separation even to the polarizability of the solvent, when the locally excited and CS states become close to degenerate, has previously been observed for the Paddon-Row D[S]A compounds in saturated hydrocarbon solvents.[46] The second, slowly decaying component, which is clearly visible for An[3]Am[4]ECN in t-decalin, see Figure 5.6, could possibly be due to a conformational change of the molecule in the charge separated state. The possible nature of such changes is discussed at greater length below for the MeOAn[3]Am[4]ECN compound for which the overall TRMC signals are much larger and non-monoexponential decay kinetics are observed in all three alkane solvents.

The TRMC results in Figure 5.6 clearly indicate that for the MeOAn[3]Am[4]ECN compound a very much larger degree of charge separation occurs than for either [3]Am[4]ECN or An[3]Am[4]ECN. Again it is worth emphasizing that charge separation is occurring even though the initial step leading to D_1^+[4]A⁻ is apparently energetically unfavourable. One must conclude therefore that the two donor moieties in the D_2[3]D_1[4]A compounds are in fact not functioning as separate, very weakly coupled electron-transfer entities. Rather they must be more strongly coupled via the proximity of the two nitrogens in the piperazine ring so that D_1 and D_2 function more as a combined donor.

As pointed out in the previous sections, the TRMC and fluorescence results indicate the

formation of two charge separated states CS1 and CS2 for MeOAn[3]Am[4]ECN in saturated hydrocarbon solvents. Indisputable evidence for the sequential formation of CS2 from CS1, as opposed to a mechanism involving the parallel formation of both species from the locally excited acceptor is not easy to obtain. The difficulties in demonstrating the kinetic link between the decay of CS1 and the formation of CS2 are caused by the fact that the fluorescence band of CS2 is obscured by the tails of the much stronger emission bands centered at shorter wavelengths. A definite growth of the fluorescence signal of CS2 could however be detected at wavelengths greater than 600 nm, where the fluorescence intensity due to CS1 is very small.[2]

We conclude therefore that CS2 is in fact formed sequentially from CS1 presumably as result of a conformational change. The data have therefore been analysed using a reaction scheme in which CS1 is formed rapidly after photoexcitation and subsequently converts to CS2 which eventually reverts to the ground state i.e:

$$G \quad \xrightarrow{\text{hv}} \quad G^* \qquad (A)$$

$$G^* \quad \xrightarrow{\tau_{G^*1}} \quad CS1 \qquad (B)$$

$$CS1 \quad \xrightarrow{\tau_{1G}} \quad G \qquad (C)$$

$$CS1 \quad \xrightarrow{\tau_{12}} \quad CS2 \qquad (D)$$

$$CS2 \quad \xrightarrow{\tau_{2G}} \quad G \qquad (E)$$
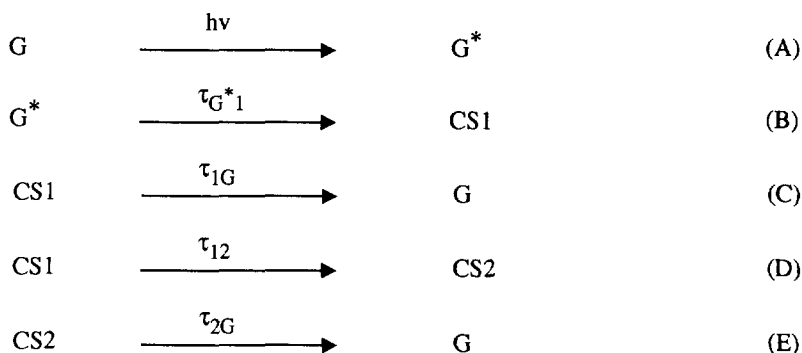
In Table 5.4 the lifetimes of the two states, τ_1 and τ_2, determined at room temperature from a kinetic analysis of the fluorescence data at different wavelengths are given.[2] The wavelength differentiation of the two species makes separation of the lifetime components, using the fluorescence data, more definitive than biexponential fits to the TRMC transients. The good correspondence between the two techniques is however shown by the fits to the TRMC transients in Figure 5.6, which were calculated using the lifetimes from the fluorescence measurements. On the basis of these fits the separate values of $\mu_S^2 \Phi / \Theta$, listed in Table 5.3, were determined for CS1 and CS2 in the three alkanes.

If we make the reasonable assumption that CS1 can be identified with the outstretched CS state formed in the polar solvents with a dipole moment of 34.5 D and values of Θ for a cylindrical rotor, then we can estimate the quantum yield for formation of CS1, Φ_1, from the microwave data. The values found are listed in Table 5.5 and, as can be seen, they lie within the

range of 0.32 to 0.58. The efficiency of charge separation for MeOAn[3]Am[4]ECN is therefore seen to be quite high even in alkane solvents.

As mentioned in the previous section, the lifetime of the CS1 state is markedly dependent on the solvent. The increase in τ_1 with increasing viscosity strongly suggests that the inter-conversion between CS1 and CS2 involves a conformational change with large-scale relative motion of parts of the molecule through the solvent. In view of this it seemed of particular interest to attempt to determine, or at least roughly estimate, the dipole moment of the CS2 state.

In order to obtain an estimate of the dipole moment of the CS2 state of MeO-An[3]Am[4]ECN, we first require a knowledge of its quantum yield, Φ_2. This is related to the quantum yield and the lifetime of the precursor CS1 state according to the above reaction scheme by:

$$\Phi_2 = \Phi_1 \frac{\tau_{1G}}{\tau_{1G} + \tau_{12}} \tag{1}$$

Since the net lifetime of CS1, τ_1, determined in the kinetics fits is given by:

$$\tau_1 = \frac{\tau_{12}\tau_{1G}}{\tau_{1G} + \tau_{12}} \tag{2}$$

substitution in (1) gives:

$$\Phi_2 = \Phi_1 \left(1 - \frac{\tau_1}{\tau_2} \right) \tag{3}$$

Φ_2 can therefore be determined from the measured τ_1 values and the Φ_1 values, derived above, if the lifetime of the CS1 state towards decay to the ground state, τ_{1G}, is known.

A fluorescence study of MeOAn[3]Am[4]ECN in methylcyclohexane has shown the lifetime of the CS1 emission to increase with decreasing temperature eventually to a constant value of 80 ns, which increases further only slightly on going to the solid phase.[2] At the same time the fluorescence from CS2 decreases to zero. We therefore conclude that the 80 ns found at low temperature represents the natural decay time of CS1 to the ground state and that this will be close to the value of τ_{1G} operative at room temperature. Taking this together with the measured τ_1 values one finds, using equation (3), the values of Φ_2 listed in Table 5.5.

It is worth pointing out that the efficiency of the CS1 to CS2 interconversion process is high in all alkane solvents at room temperature. Thus even for t-decalin with the longest value of τ_1, the efficiency, $(1-\tau_1/\tau_{1G})$ is 88%.

Table 5.5: *Dipole moment $\mu_1{}^a$ with rotational relaxation time $\Theta_1{}^b$ and calculated quantum yield Φ_1 for CS1. Calculated quantum yield Φ_2 with calculated upper limit dipole moment $\mu_2(cyl)$ and calculated lower limit dipole moment $\mu_2(sph)$ for CS2.*

Compound	$\mu_1{}^a$	$\Theta_1{}^b$			Φ_1			Φ_2			$\mu_2(cyl)^b$			$\mu_2(sph)^c$		
		NHX	CHX	TDC	NHX	CHX	TDC	NHX	CHX	TDC	NHX	CHX	TDC	NHX	CHX	TDC
[3]Am[4]ECN	24	99	326	681	d	d	d									
An[3]Am[4]ECN	26.5	162	533	1113	0.04	0.15	0.26									
MeOAn[3]Am[4]ECN	34.5	192	632	1320	0.32	0.58	0.48	0.31	0.6	0.42	15	16	18	9	8	9

(a) determined from benzene and dioxane measurements.

(b) cylinder model used to calculate the rotational relaxation time (see Section 2.5.2.3).

(c) spherical model used to calculate the rotational relaxation time (Section 2.5.2.1).

(d) too low to measure.

Knowing Φ_2 we can now estimate the dipole moment of CS2 for different assumed values of the dipole relaxation time, Θ. In Table 5.5 two values of μ_S are given; the first $\mu_2(cyl)$, was calculated using the rotational relaxation time for a cylindrical molecular geometry, as used for CS1; the second, $\mu_2(sph)$, was calculated using the rotational relaxation time for a spherical geometry. The former represents an upper limit for the actual dipole moment and the latter a lower limit.

Even the $\mu_2(cyl)$ values are seen to be considerably smaller than the dipole moment of CS1. This leads to the conclusion that the molecule has in fact folded up, bringing the oppositely charged centers much closer together. Also in this case the "harpooning" mechanism takes place.[47-52] A schematic representation of the folding process is depicted in Figure 5.9.

Possible structures of species CS1 and CS2 have been obtained by molecular-mechanics calculations,[53] using an AM1/UHF optimized structure for the donor radical cation fragment[54] and AM1/UHF calculated charges on both ionic fragments. These are shown in Figure 5.10.

It can be seen that the conformational change involved, consists of an inversion of the trialkylamino nitrogen atom in the piperazine ring, which puts the methylenecyclohexane ring into an axial position, and a rotation about the C-N bond joining the rings.[2] The fact that folding takes place on a timescale of nanoseconds at room temperature indicates that the activation barrier towards ring inversion must be considerably lower for the Coulomb assisted process than the 0.35 eV associated with inversion in N-methylpiperidine.[1]

If the CS species are regarded classically as a pair of ions linked by a bridge, it is meaningful to attribute the driving force for the conversion of CS1 to CS2 to the electrostatic attraction of the opposite charges. The increased Coulomb stabilization in CS2 would then explain its lower emission energy. The donor-acceptor distance in CS1, corresponding to $\mu_* = 34.5$ D, is 7.3 Å.
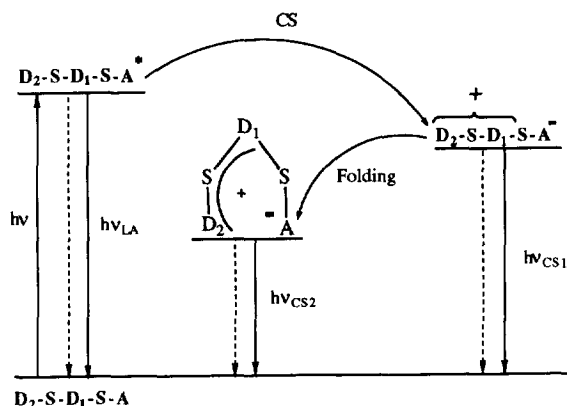
Figure 5.9: *Schematic representation of the relative positions of the energy levels in the folding process of MeOAn[3]Am[4]ECN.*

For CS2, the donor-acceptor distance would appear to be approximately half of this, on the basis of the dipole moment estimates in Table 5.5 and the model calculations. Assuming point charges for the ions, the Coulomb energy gain can be estimated to be approximately 1 eV with $\varepsilon \approx 2$. This is obviously the major driving force for the conformational change. The experimentally oberved difference in the emission energies of CS1 and CS2 is only 0.52 to 0.61 eV, considerably less than the estimated change in the Coulomb energy. This can be explained by taking into account that on bringing the ionic parts closer together, the solvation energy of the CS species may decrease due to overlap of the polarization shells. The observed solvent effect on the electrostatically driven folding could be due to the viscosity alone retarding the conformational change. It could however also be due to the changing dielectric constant, which
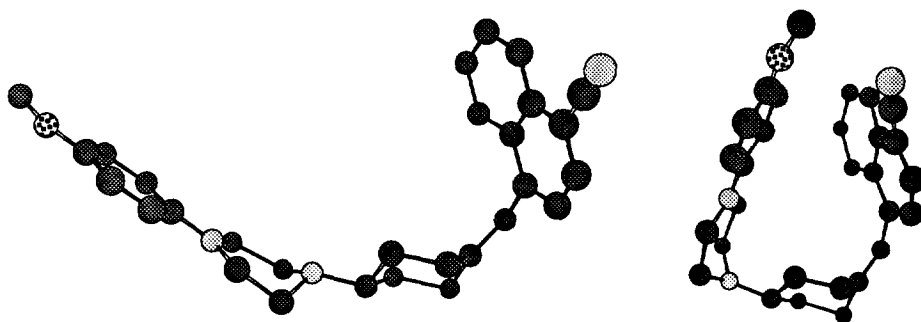
Figure 5.10: *Possible structures of the extended and folded conformations of MeOAn[3]Am[4]ECN obtained by AM1 molecular mechanics modeling (hydrogen atoms omitted for clarity).*

results in a smaller driving force in a higher ε solvent, because of an increased polarization energy and a decreased Coulomb energy gain on folding.

The aim of synthesizing the present compounds was to create a long living charge separated state, formed by two sequential electron-transfer steps. It appears however that the two donor moieties are too strongly coupled and act as a single entity rather than two separate entities. In an attempt to decouple the donors the following series of compounds was synthesised in which the amino nitrogen is moved into the second ring, creating the isomeric counterparts of the structures discussed above with the general formula $D_2[4]D_1[3]A$, as shown in Figure 5.1. In the next sections the consequences of this subtle nitrogen shift of only 1.2 Å will be discussed in the same way as for the $D_2[3]D_1[4]A$ series above.

5.4 $D_2[4]D_1[3]A$ TRICHROMOPHORES IN PDEUDO-POLAR MEDIA[3]

5.4.1 TRMC measurements

In Figure 5.11, the traces are shown for the three compounds [4]Am[3]ECN, An[4]Am[3]ECN and MeOAn[4]Am[3]ECN in benzene and dioxane. In all cases there is evidence for the formation of a highly polar transient on flash-photolysis. The data could be fitted with a single dipolar intermediate and a small underlying slowly decaying signal close to the noise level. For MeOAn[4]Am[3]ECN a small additional short-lifetime component was included in the final fitting procedure (not shown in Figure 5.11) to take into account the presence of the single-step charge separated state $MeOAn[4]Am^+[3]ECN^-$. This is discussed in more detail in Section 5.4.3. The values of the lifetimes of the dipolar intermediates determined from the fits to the data are listed in Table 5.6, together with the corresponding values of the conductivity parameter $\mu_S^2\Phi / \Theta$.

Table 5.6: *Lifetime τ_*, conductivity parameter $\mu_S^2\Phi / \Theta$, rotational relaxation time Θ, quantum yield Φ and the calculated dipole moment μ_S.*

Compound	τ_S (ns)		$\mu_S^2\Phi / \Theta$ (D²/ps)		Θ^a (ps)		Φ		μ_S (D)	
	BEN	DOX	BEN	DOX	BEN	DOX	BEN	DOX	BEN	DOX
[4]Am[3]ECN	7	7	1.91	0.85	277	619	1	1	23	23
An[4]Am[3]ECN	3	6.5	1.59	0.66	458	1022	1	1	27	26
MeOAn[4]Am[3]ECN	16	22	2.23	1.00	545	1216	0.70[b]	0.69[b]	42	42

(a) calculated according to equation (103) in Section 2.5.2.3 for a cylindrical geometry.
(b) derived from fluorescence results according to equation (4).
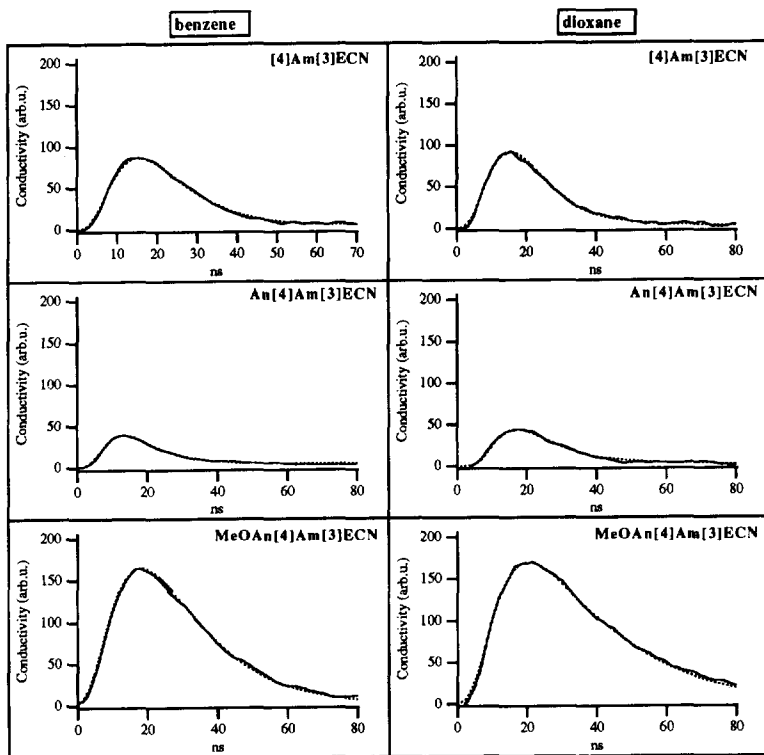
Figure 5.11: *Time-Resolved Microwave Conductivity transients observed on flash-photolysis in benzene and dioxane. The dotted lines are fits to the experimental data obtained from the Runge-Kutta fitting procedure. The transients are normalized to differences in viscosity and laser power intensity.*

For [4]Am[3]ECN and An[4]Am[3]ECN, the dipole moments in Table 5.6 were calculated using estimates of the dipolar rotational relaxation times and assuming a quantum yield of unity. For MeOAn[4]Am[3]ECN, quantum yields of 0.70 and 0.69 in benzene and dioxane respectively were used to calculate the dipole moments in Table 5.6. The quantum yield values were calculated using results from fluorescence measurements as discussed in Section 5.4.3.

At first glance the same behaviour as for the $D_2[3]D_1[4]A$ type molecules is seen. The dipole moments are in good agreement for the two solvents. Again a relatively small change in dipole moment of only 3 to 4 D on addition of the anilino donor is seen. Introduction of the methoxyanilino moiety, however, increases the dipole moment by *ca* 15 D and creates a considerably longer living dipolar state. Even if the quantum yield for the methoxy compound is taken to be unity, the dipole moment determined is 36 D, which is 10 D larger than that of the

other solutes. The reason for taking a lower quantum yield for the methoxy compound will be discussed at greater length together with the fluorescence results in Section 5.4.3.

5.4.2 Fluorescence measurements

The fluorescence spectra of compounds [4]Am[3]ECN, An[4]Am[3]ECN and MeO-An[4]Am[3]ECN all show a single structureless band. The band at *ca* 370 nm, which could still be observed in the $D_2[3]D_1[4]A$ compounds and which is ascribed to radiative decay of the initially formed locally excited acceptor state is now completely quenched. In Table 5.7, the maxima and fluorescence decay times of the long wavelength emission in benzene and dioxane are reported.

The position of the emission band shifts to increasingly longer wavelengths and is reduced in intensity as the solvent polarity increases, which indicates emission from a highly dipolar state. Plots of the emission wavenumber of the compounds versus the solvent polarity parameter Δf, for several polar solvents,[45] give slopes corresponding to $2\mu_S^2/hca^3$. These values are shown in Table 5.7. Using estimates of the cavity radius a, the dipole moments shown in Table 5.7 were calculated.

The observation that the emission maxima and calculated dipole moments are almost the same for [4]Am[3]ECN, An[4]Am[3]ECN and MeOAn[4]Am[3]ECN suggests that the emissive state is similar for all three compounds.

For An[4]Am[3]ECN the fluorescence quantum yield and decay time are similar to those of [4]Am[3]ECN. In the case of MeOAn[4]Am[3]ECN the fluorescence quantum yield and lifetime are however considerably reduced. This indicates a larger decay rate of the emitting dipolar intermediate compared to [4]Am[3]ECN and An[4]Am[3]ECN. No longer wavelength

Table 5.7: Emission maximum of the charge separated state hv_{max}, fluorescence lifetime τ_*, slope of the plot of the emission wavenumber versus solvent polarity parameter Δf; $2\mu_S^2/hca^3$, cavity radius a and the calculated dipole moment μ_S.

Compound	hv_{max} (eV)		τ_S (ns)		$2\mu_S^2/hca^3$ (eV)[a]	a (Å)[b]	μ_* (D)[a]
	BEN	DOX	BEN	DOX			
[4]Am[3]ECN	2.58	2.39	6.9	7.5	3.72	5.5	22
An[4]Am[3]ECN	2.64	2.46	3.7	6.4	3.84	5.9	25
MeOAn[4]Am[3]ECN	2.63	2.46	1.1	2.0	3.84	6.0	26

(a) from solvatochromic shift for several solvents (see ref. 44).
(b) see reference 45.

emission with a lifetime of approximately 20 ns, similar to that found for the TRMC transient, could be detected for the methoxy derivative.

5.4.3 Discussion

Both the TRMC and fluorescence measurements demonstrate the formation of dipolar intermediates in the bi- and trichromophoric compounds investigated. The lifetimes of the TRMC transient and the fluorescence are very similar for both [4]Am[3]ECN and An[4]Am[3]ECN, indicating that the same species is being monitored by both techniques.

For [4]Am[3]ECN a dipole moment of 22 D is determined from the solvatochromic shifts and 23 D from the TRMC measurements. These values are in good agreement, which indicates that the assumption of a quantum yield of unity, used to calculate the TRMC values, is correct. A quantum yield of unity for charge separation was also expected because of the complete quenching of the local acceptor fluorescence. The average dipole moment for [4]Am[3]ECN of 23 D corresponds to complete charge separation over a distance of 4.8 Å. This is considerably longer than the 2.7 Å distance between the amino nitrogen and the nearest carbon atom of the ethylenic bond, in agreement with the formation of the [4]Am$^+$[3]ECN$^-$ state (see Figure 5.12).
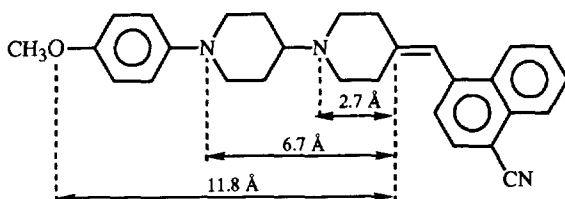
Figure 5.12: Relevant intramolecular distances when considering complete charge separation in MeOAn[4]Am[3]ECN (1 Å charge separation ≡ 4.80 D).

Introduction of the anilino moiety only increases the dipole moment by 3-4 D for An[4]Am[3]ECN, which corresponds to an increase in distance of only 0.9 Å. This indicates that the charge is still mainly localized on the aliphatic amino nitrogen atom, corresponding to An[4]Am$^+$[3]ECN$^-$. Also in this case only the first electron transfer step appears to be taking place. This is confirmed by the fact that the fluorescence quantum yields and decay times even in polar solvents are very similair to those for [4]Am[3]ECN.[3] The insensitivity of the CS emission to the presence of the anilino moiety indicates that the coupling between the amino and anilino nitrogens must be very small, as expected with 4 intervening σ-bonds. This

contrasts with the behaviour found for the $D_2[3]D_1[4]A$ compounds (see Section 5.2.3).

For MeOAn[4]Am[3]ECN the emission maximum is almost the same as for the other two compounds in all solvents, indicating that the emissive state is similar. From the fluorescence measurements therefore it can be concluded that the $D_2\text{-}D_1^+\text{-}A^-$ state indeed is formed as a first step. However, the shorter lifetime and reduced quantum yield indicate that an additional radiationless decay process is operative.

In the TRMC measurements a long living, highly dipolar intermediate is observed for the methoxy compound, with lifetimes of 16 ns and 22 ns in benzene and dioxane, respectively. These lifetimes are considerably longer than those found for the fluorescence, which are 1.1 ns and 2 ns in benzene and dioxane respectively. This indicates that the additional radiationless decay, mentioned above, involves a second electron transfer step to create the $D_2^+\text{-}D_1\text{-}A^-$ state and that charge separation does indeed occur in a stepwise manner for this compound. The TRMC data were therefore analysed using one short living component (quantum yield $\Phi_1 = 1$), to account for the contribution of the $D_2\text{-}D_1^+\text{-}A^-$ state, and one long living component (quantum yield Φ_2), with the intermediate state having a lifetime determined from the fluorescence decay and a dipole moment of 25 D as determined for [4]Am[3]ECN and An[4]Am[3]ECN.

The efficiency of the second step Φ_2 can be calculated from the increased nonradiative decay rate of the $D_2\text{-}D_1^+\text{-}A^-$ state in MeOAn[4]Am[3]ECN compared to An[4]Am[3]ECN as:

$$\Phi_2 = \Phi_1[1 - \tau_S \text{ (MeOAn[4]Am[3]ECN)} / \tau_S \text{ (An[4]Am[3]ECN)}] \qquad (4)$$

In equation (4), τ_S () is the lifetime of the fluorescence state of the compound given in brackets. For benzene and dioxane the yields found are 0.70 and 0.69, respectively. These values result in a dipole moment of 42 D for both solvents. A dipole moment of 42 D corresponds to charge separation over a distance of 8.8 Å, which is considerably longer than the 6.7 Å distance between the anilino nitrogen atom of D_2 and the nearest carbon atom of the ethylenic bond (see Figure 5.12). This is in agreement with the formation of the MeOAn$^+$[4]Am[3]ECN$^-$ state. These results have been confirmed in time-resolved optical absorption measurements, where the radical cation of the methoxyanilino moiety could be detected with an absorption in the 500 nm region, decaying with the same time constants as those of the TRMC signals.

In MeOAn[4]Am[3]ECN the initial goal of sequential charge separation steps, as illustrated in Figure 5.2 in Section 5.2, has been achieved. Comparison of An[4]Am[3]ECN and MeOAn[4]Am[3]ECN shows that the methoxyanilino donor must be considerably stronger than the anilino donor in order to overcome the loss in Coulomb energy on moving the opposite

charges further apart. The effective point charge distances corresponding to the dipole moments of 25 and 42 D measured for the one-step and two-step charge separation processes are 5.2 Å and 8.8 Å respectively. Taking a dielectric constant of 2.2 one finds the corresponding Coulomb energies for these distances to be 1.26 and 0.75 eV, the difference being 0.51 eV. This is substantially larger than the 0.3 eV reduction in the oxidation potential of dimethylaniline found on methoxy substitution.[55] On the basis of this simple calculation therefore it is not possible to explain why the second electron transfer step is energetically allowed for the methoxyanilino compound but not for the unsubstituted anilino donor.

To explain this one should probably take into account the fact that the solvation energy associated with the polarization of the solvents will be reduced for distances less than twice the Bohr radius associated with the charged centers.[56] For molecular ions, Bohr radii of approximately 4.5 Å have been estimated.[57] The total polarization energy associated with two infinitely separated ions in a medium of dielectric constant 2.2 is therefore 1.45 eV. While for a separation distance of 8.8 Å one might expect close to the full complement of polarization energy to be operative, this is unlikely to be the case for a distance of only 5.2 Å. Less than a 15% reduction in the solvation energy due to overlap of the polarization shells would be sufficient to reduce the energy increase associated with the second electron transfer step to less than 0.3 eV. In other words the 0.51 eV loss of Coulomb energy can be at least partially compensated for by the gain of a few tenths of an eV in solvent polarization energy.

It is also possible that the second charge separation step for the anilino donor is in fact energetically favourable but that there is a potential barrier to electron transfer of a few tenths of an eV and it is this barrier that is substantially reduced on methoxy substitution. Even with the methoxyanilino donor the electron transfer time of a few nanoseconds for the second step is rather slow for a distance of only 3.6 Å. For example for the dimethoxynaphthalene-dicyanoethylene Paddon-Row compounds, charge separation over a distance of 4 σ-bonds is found to occur on a subpicosecond timescale.[58] There would appear therefore to be a barrier to the second electron transfer step even for the methoxyanilino donor in the present compounds.

5.5 D₂[4]D₁[3]A TRICHROMOPHORES IN ALKANES

5.5.1 TRMC measurements

In Figure 5.13, traces for [4]Am[3]ECN, An[4]Am[3]ECN and MeOAn[4]Am[3]ECN are shown in cyclohexane and t-decalin. The signals are in general an order of magnitude lower in comparison with those in the pseudo-polar solvents. Because of the low level of the signals we feel that a full quantitative analysis of the data is unwarranted. In what follows therefore we present only a qualitative or, at best, semi-quantitative interpretation of the observations.

Of particular interest is that TRMC transients, while small, can be clearly observed for
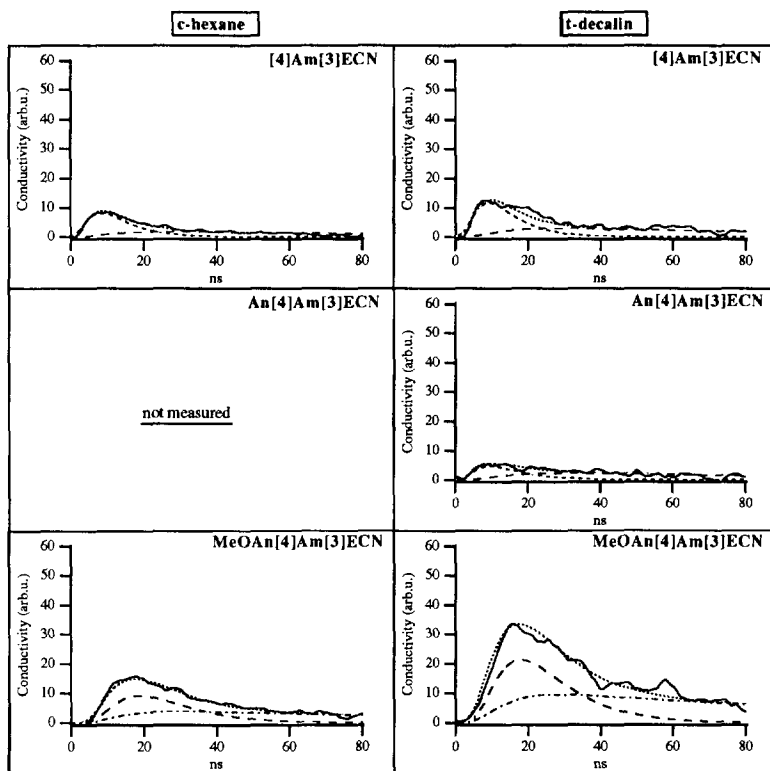
Figure 5.13: *Time-Resolved Microwave Conductivity transients observed on flash-photolysis in cyclohexane and t-decalin. The dotted lines are fits to the experimental data obtained from the Runge-Kutta fitting procedure. The dashed lines show the individual contributions from the different components to the total signal. The transients are normalized to differences in viscosity and laser power intensity.*

155

[4]Am[3]ECN in the alkane solvents whereas for [3]Am[4]ECN no evidence at all could be observed for a dipolar intermediate, see Figure 5.6. We can conclude therefore that moving the amino nitrogen donor 1.2 Å closer to the acceptor has resulted in the first charge separation step now taking place even in the alkanes. When it is taken into account that the lifetime of the [4]Am$^+$[3]ECN$^-$ state, as monitored in the fluorescence measurements, is only a few hundred picoseconds, the small TRMC signals observed correspond in fact to the transient formation of highly dipolar intermediates as discussed in more detail in Section 5.5.3.

The TRMC signal observed for An[4]Am[3]ECN in t-decalin is even smaller, by approximately a factor of 2, than that found for the bichromophore. Because of the much longer rotation time for this molecule, this observation is in qualitative agreement with the occurrence of only one-step charge separation to form An[4]Am$^+$[3]ECN$^-$ as found for benzene and dioxane.

While the signals for MeOAn[4]Am[3]ECN are much smaller in the alkanes than in the pseudo-polar solvents they are still considerable larger than found for either the bichromophore or the anilino trichromophore indicating that for this compound the second charge separation step to form MeOAn$^+$[4]Am[3]ECN$^-$ must be occurring to a certain extent even in the saturated hydrocarbon solvents. What is apparent also from the transients is that, while the kinetics are by no means mono-exponential, the lifetime of charge separation is clearly much longer than for the other two solutes. From a rough analysis of the kinetics two predominant contributions to the signal are found from intermediates with lifetimes of approximately 10 and 100 ns.

5.5.2 Fluorescence measurements

As for benzene and dioxane, the local acceptor fluoresence is completely quenched in alkane solvents and is replaced by a longer wavelength, structureless emission. The wavelength maximum at *ca* 3.0 eV is the same for all three solutes, indicating that a very similar type of dipolar intermediate is responsible for the emission. From picosecond time-resolved studies of the fluorescence, the lifetimes of the emissive states are found to be only a few hundred picoseconds.[59] The lifetimes measured in cyclohexane are listed in Table 5.8.

We conclude from the fluorescence results that the first step of charge separation is still occurring efficiently for the present compounds, even in alkane solvents. The unexpectedly short lifetime of the charge separated state is at present not understood. It could be possibly due to rapid intersystem crossing to the local triplet state of the acceptor since the triplet state of cyanonaphthalene lies 2.5 eV above the ground state,[60] which is lower than the fluorescence emission maximum of the CS1 state at 3.0 eV. However no evidence has been found for triplet state formation in optical transient absorption measurements.

Table 5.8: *Emission maximum of the CS state* hv_{max}, *fluorescence lifetime* τ_S *and quantum yield in cyclohexane.*

Compound	hv_{max} (eV)	τ_* (ns)	Φ
[4]Am[3]ECN	2.95	0.33	0.03
An[4]Am[3]ECN	3.00	0.20	0.02
MeOAn[4]Am[3]ECN	3.00	0.25	0.02

5.5.3 Discussion

As already mentioned in Section 5.5.1 the TRMC signals for [4]Am[3]ECN and An[4]Am[3]ECN are very low in the alkane solvents. However this is clearly a result of the extremely short lifetime of the charge separated state formed rather than the fact that it is not formed at all, as is the case for the $D_2[3]D_1[4]A$ compounds. If in fact we use the fluorescence lifetime given in Table 5.8 to fit the TRMC data in cyclohexane we find a value for the dipole moment for [4]Am[3]ECN of 24 D. This confirms that the first step in charge separation occurs with a quantum yield of close to one.

The much lower TRMC signal for An[4]Am[3]ECN is in agreement with the considerably longer dipolar relaxation time and the even shorter CS state lifetime.

For MeOAn[4]Am[3]ECN the fluorescence energy and lifetime are very similar to those found for the other two compounds indicating the occurrence of the first charge separation step. The TRMC data however indicate the formation of a long-lived dipolar transient for this solute as seen in Figure 5.13. Clearly the second electron transfer step must be taking place for this compound even in a saturated hydrocarbon environment. The fact that the TRMC signal in the alkanes is relatively small compared with benzene and dioxane is due mainly to the much shorter lifetime of the first charge separated state.

The bi-exponential decay of the TRMC transient for MeOAn[4]Am[3]ECN may indicate that the extended, charge separated state formed undergoes electrostatically induced folding on a timescale of *ca* 10 ns to yield a dipolar, exciplex-like species with a lifetime of approximately 100 ns.

5.6 COMPARISON OF $D_2[3]D_1[4]A$ AND $D_2[4]D_1[3]A$ COMPOUNDS

The general features for the two series of bi- and trichromophores in the pseudo-polar solvents and the saturated hydrocarbons (referred to in what follows simply as hydrocarbons) are depicted in Figures 5.14 and 5.15 respectively and will be discussed below.

The most significant differences between the two series are to be found in the hydrocarbon solvents. For example the first electron transfer step does not occur at all for [3]Am[4]ECN in alkanes whereas for [4]Am[3]ECN it occurs with close to 100% efficiency. This is most probably due to the 1.2 Å shorter distance between donor and acceptor in the latter compound and the resulting decrease in energy of the CS state due to the increased Coulomb energy, bringing it below the level of the locally excited acceptor. Unfortunately, while electron transfer does appear to occur for [4]Am[3]ECN, the lifetime of the $[4]Am^+[3]ECN^-$ state is extremely short, making the subsequent electron transfer steps inefficient at least in the hydrocarbon solvents. The reason for the ultrashort lifetime of the $[4]Am^+[3]ECN^-$ state of only a few hundred picoseconds in hydrocarbons, while it has a "normal" lifetime of several nanoseconds in the pseudo-polar solvents, is not yet clear. It would appear that an alternative route to the ground state is available in the former case. One possibility is that the triplet state of the acceptor chromophore lies below the CS state in hydrocarbons and that this functions as a fast recombination route. However, as mentioned above, no evidence has been found for a higher yield of the ECN triplet in hydrocarbons. A solution to this problem awaits further experiments.

Introduction of the anilino moiety as a second donor in An[3]Am[4]ECN makes electron transfer possible in all solvents, even in hydrocarbons, despite the indication that the first electron transfer step does not occur based on the results for An[3]Am[4]ECN. The dipole moment values found however indicate that for both An[3]Am[4]ECN and An[4]Am[3]ECN only the first step of electron transfer takes place, yielding the $D_2D_1^+A^-$ state. The apparent anomaly for An[3]Am[4]ECN suggests that in this case there is electronic coupling between D_2 and D_1 via the piperazine ring, so that the presence of the second donor decreases the energy level of the $An[3]Am^+[4]ECN^-$ state. The two donors, joined via the piperazine ring, in other words appear to function as a combined donor rather than as two decoupled sites.

Introduction of the methoxy group in MeOAn[4]Am[3]ECN allows for the two sequential electron transfer steps leading to $D_2^+[4]D_1[3]A^-$ in pseudo polar solvents, which was in fact the initial goal of the present investigations. For MeOAn[3]Am[4]ECN electron transfer occurs over a larger distance than in the unsubstituted anilino compound, apparently because of the stronger donor, however still over a smaller distance than for the MeOAn[4]Am[3]ECN counterpart. This again confirms that the two donor moieties are coupled in the $D_2[3]D_1[4]A$ series.

In hydrocarbon solvents an additional CS state is formed for both MeOAn[4]Am[3]ECN and MeOAn[3]Am[4]ECN. First the already mentioned electron transfer processes occur in an extended conformation of the molecules. However, because of the strong Coulomb attraction between the opposite charges especially in hydrocarbon solvents, both MeOAn[4]Am[3]ECN and MeOAn[3]Am[4]ECN undergo electrostatically driven folding. The driving force for this

Figure 5.14: Schematic representation of the relative energy levels of both $D_2[4]D_1[3]A$ and $D_2[3]D_1[4]A$ in benzene and dioxane. The full and dashed downward arrows represent emissive and radiationless transitions respectively.

process is a gain in Coulomb energy which is apparently higher than the loss in solvation energy.

Charge separation appears to be less efficient for MeOAn[4]Am[3]ECN in the hydrocarbon solvents in comparison with the situation in the pseudo-polar solvents and compared to MeOAn[3]Am[4]ECN in the hydrocarbon solvents. This is due to the very efficient additional
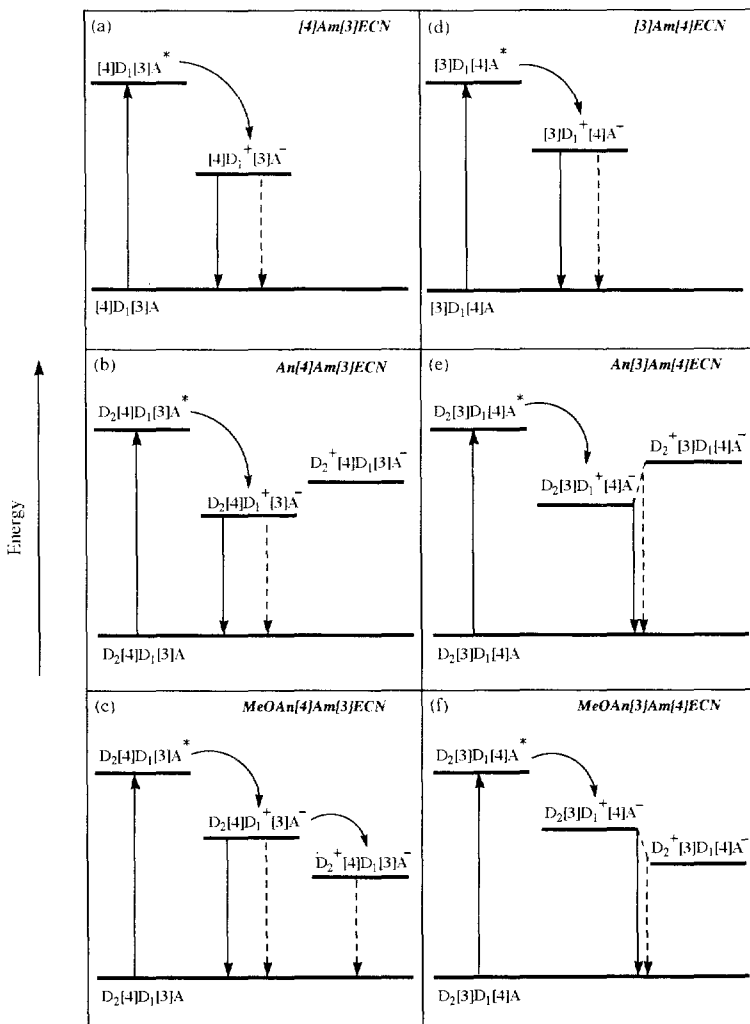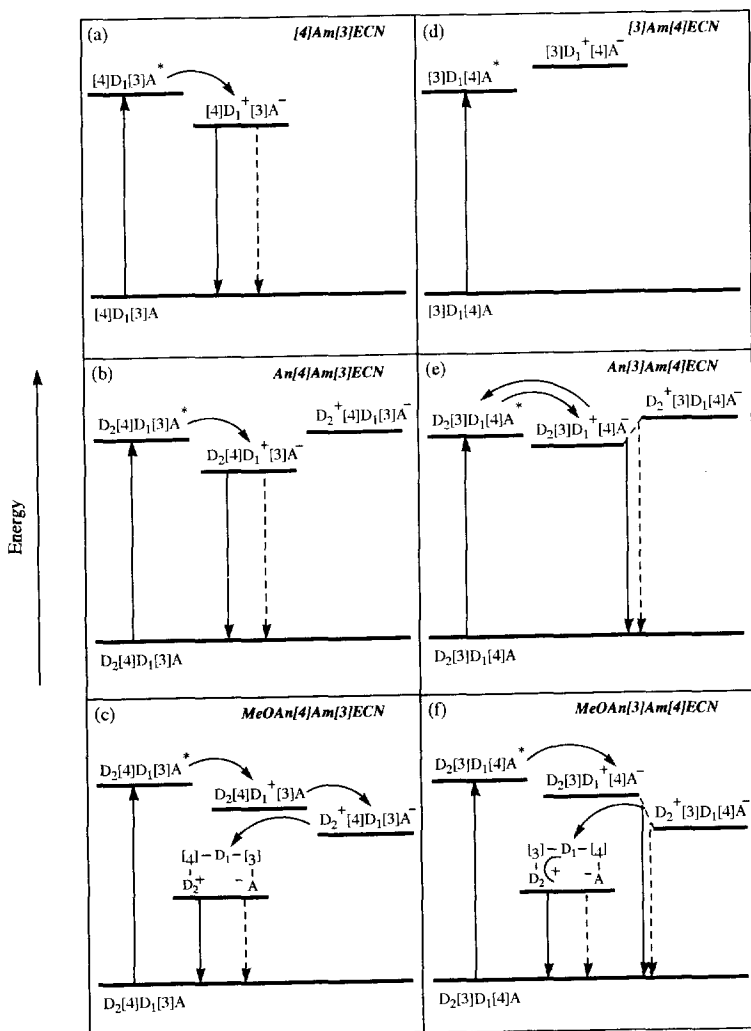

Figure 5.15: *Schematic representation of the relative energy levels of both* $D_2[4]D_1[3]A$ *and* $D_2[3]D_1[4]A$ *in cyclohexane and t-decalin. The full and dashed downward arrows represent emissive and radiationless transitions respectively.*

decay pathway in the first electron transfer step, preventing a high yield of the second electron transfer step. If this pathway was absent, very efficient charge separation would occur, which would probably result in even bigger TRMC signals than found for MeOAn[3]Am[4]ECN in hydrocarbon solvents.

The results reported in this chapter clearly show how the distance, and the polarity of the surroundings play vital roles in the process of electron transfer. Small variations of these features can have a pronounced influence on the coupling between, and the energy levels of the different chromophores and hence dramatically influence the course of electron transfer processes. The reasons are perhaps clear why nobody so far has been able to match, let alone improve on, the speed and efficiency of electron transfer in photosynthesis.

5.7 ACKNOWLEDGEMENT

5.8 REFERENCES

1 A.M. Brouwer, R.D. Mout, P.H. Maassen van den Brink, H.J. van Ramesdonk, J.M. Warman and S.A. Jonker, *Chem. Phys. Lett.* **1991**, *180*, 556.

2 A.M. Brouwer, R.D. Mout, P.H. Maassen van den Brink, H.J. van Ramesdonk, S.A. Jonker and J.M. Warman, *Chem. Phys. Lett.* **1991**, *186*, 481.

3 A.M. Brouwer, C. Eijckelhoff, R.J. Willemse, J.W. Verhoeven, W. Schuddeboom and J.M. Warman, *J. Am. Chem. Soc.* **1993**, *115*, 2988.

4 M.R. Wasielewski, *Chem. Rev.* **1992**, *92*, 435-461.

5 *Photoinduced electron transfer*, M.A. Fox and M.A. Chanon Eds.; Elsevier, New York **1988**.

6 J. Kroon, *Ph.D. Thesis*, University of Amsterdam, **1992**.

7 J. Deisenhofer, O. Epp and K. Miki, *J. Mol. Biol.* **1984**, *180*, 385.

8 J. Deisenhofer, O. Epp and K. Miki, *Nature* **1985**, *318*, 618.

9 C.H. Chang, D. Tiede, J. Tang, U. Smith and M. Schiffer, *FEBS Lett.* **1986**, *205*, 82.

10 J.P. Allen, G. Feher, T.O. Yeates, H. Komiya and D.C. Rees, *Proc. Matl. Acad. Sci. USA* **1987**, *84*, 5730.

11 J.M. Warman, M.P. de Haas, M.N. Paddon-Row, E. Cotsaris, N.S. Hush, H. Oevering and J.W. Verhoeven, *Nature* **1986**, *320*, 615.

12 H. Oevering, *Ph.D. Thesis*, University of Amsterdam, **1988**.

13 J.V. Beitz and J.R. Miller, *J. Chem. Phys.* **1979**, *71*, 4579.

14 G.L. Closs, L.T. Calcaterra, N.J. Green, K.W. Penfield and J.R. Miller, *J. Phys. Chem.* **1986**, *90*, 3673.

15 B. Krijnen, H.B. Beverloo and J.W. Verhoeven, *J. Am. Chem. Soc.* **1989**, *111*, 4433.

16 R.M. Hermant, N.A.C. Bakker, T. Scherer, B. Krijnen and J.W. Verhoeven, *J. Am. Chem. Soc.* **1990**, *112*, 1214.

17 L.T. Calcaterra, G.L. Closs and J.R. Miller, *J. Am. Chem. Soc.* **1983**, *105*, 670.

18 J.R. Miller, L.T. Calcaterra and G.L. Closs, *J. Am. Chem. Soc.* **1984**, *106*, 3047.

19   T.A. Perkins, B.T. Hauser, J.R. Eyler and K.S. Schanze, *J. Phys. Chem.* **1990**, *94*, 8745.

20   A.D. Joran, B.A. Leland, G.G. Geller, J.J. Hopfield and P.B. Dervan, *J. Am. Chem. Soc.* **1984**, *106*, 6090.

21   A.D. Joran, B.A. Leland, P.M. Felker, A.H. Zewail, J.J. Hopfield and P.B. Dervan, *Nature* **1987**, *327*, 508.

22   B.A. Leland, A.D. Joran, P.M. Felker, A.H. Zewail, J.J. Hopfield and P.B. Dervan,
     J. Phys. Chem. **1985**, *89*, 557.

23   M.R. Wasielewski, M.P. Niemczyk, D.G. Johnson, W.A. Svec and D.W. Minsek,
     Tetrahedron **1989**, *45*, 4785.

24   R.M. Hoffmann, A. Imamura and W.J. Hehre, *J. Am. Chem. Soc.* **1968**, *90*, 1499.

25   R.M. Hoffmann, *Acc. Chem. Res.* **1971**, *4*, 1.

26   For a complete review see: M.N. Paddon-Row and K.D. Jordan in *Molecular Structure and Energetics*,
     Eds.; J.F. Liebman and A. Greenberg, VCH publishers: New York, **1988**, Vol. 6, Chp. 3.

27   N.S. Hush, M.N. Paddon-Row, E. Cotsaris, H. Oevering, J.W. Verhoeven and M. Heppener,
     Chem. Phys. Lett. **1988**, *117*, 8.

28   J.M. Warman, M.P. de Haas, H. Oevering, J.W. Verhoeven, M.N. Paddon-Row, A.M. Oliver and N.S. Hush,
     Chem. Phys. Lett. **1986**, *128*, 95.

29   J.W. Verhoeven, M.N. Paddon-Row, N.S. Hush, H. Oevering and M. Heppener,
     Pure & Appl. Chem. **1986**, *58*, 1285.

30   H. Oevering, M.N. Paddon-Row, A.M. Olivier, E. Cotsaris, M. Heppener, J.W. Verhoeven and N.S. Hush,
     J. Am. Chem. Soc. **1987**, *109*, 3258.

31   H. Oevering, J.W. Verhoeven and M.N. Paddon-Row, *Tetrahedron* **1989**, *45*, 4751.

32   M.N. Paddon-Row, A.M. Oliver, J.M. Warman, K.J. Smith, M.P.de Haas, H. Oevering and J.W. Verhoeven,
     J. Phys. Chem. **1988**, *92*, 6958.

33   H. Oevering, J.W. Verhoeven, M.N. Paddon-Row, E. Cotsaris and N.S. Hush,
     Chem. Phys. Lett. **1988**, *143*, 488.

34   J. Kroon, A.M. Oliver, M.N. Paddon-Row and J.W. Verhoeven,
     Recl. Trav. Chim. Pays-Bas **1988**, *107*, 509.

35   A.M. Oliver, D.C. Graig, M.N. Paddon-Row, J. Kroon and J.W. Verhoeven,
     Chem. Phys. Lett. **1988**, *150*, 366.

36   J.M. Lawson, D.C. Graig, M.N. Paddon-Row, J. Kroon and J.W. Verhoeven,
     Chem. Phys. Lett. **1989**, *164*, 120.

37   M.N. Paddon-Row, *Chem. Phys. Lett.* **1990**, *167*, 432.

38   J.M. Warman, K.J. Smith, M.P. de Haas, S.A. Jonker, M.N. Paddon-Row, A.M. Oliver, J. Kroon,
     H. Oevering and J.W. Verhoeven, *J. Phys. Chem.* **1991**, *95*, 1979.

39   J. Kroon, J.W. Verhoeven, M.N. Paddon-Row and A.M. Oliver,
     Angew. Chem. Int. Ed. Eng. **1991**, *30*, 1358.

40   A.M. Oliver, M.N. Paddon-Row, J. Kroon and J.W. Verhoeven, *Chem. Phys. Lett.* **1992**, *191*, 371.

41   J.W. Verhoeven, J. Kroon, M.N. Paddon-Row and J.M. Warman, II NATO Science forum "Supramolecular
     Chemistry", Taormina, Italy, **1991**.

42   D. Gust, T.A. Moore, A.L. Moore, S.J. Lee, E. Bittersmann, D.K. Luttrul, A.A. Rehms, J.M. DeGraziano,

43   X.C. Ma, F. Gao, R.E. Belford and T.T. Trier, *Science* **1990**, *248*, 199.

44   M.R. Wasielewski, G.L. Gaines, M.P. O'Neil, M.P. Niemczyk and W.A. Svec,
     J. Am. Chem. Soc. **1990**, *112*, 4559.

45   H. Beens, H. Knibbe and A. Weller, *J. Chem. Phys.* **1967**, *47*, 1183.

46   J.M. Warman, K.J. Smith, S.A. Jonker, J.W. Verhoeven, H. Oevering, M.N. Paddon-Row, A.M. Oliver,
     Chem. Phys. **1993**, *170*, 359-380.

47 B. Wegewijs, R.M. Hermant, J.W. Verhoeven, M.P. de Haas and J.M. Warman, *Chem. Phys. Lett.* **1990**, *168*, 1585.

48 J.W. Verhoeven, *Pure & Appl. Chem.* **1990**, *62*, 1585.

49 B. Wegewijs, R.M. Hermant, J.W. Verhoeven, A.G.M. Kunst and R.P.H. Rettschnik, *Chem. Phys. Lett.* **1987**, *140*, 587.

50 J.W. Verhoeven, T. Scherer and R.J. Willemse, *Pure & Appl. Chem.* **1993**, *65*, 1717.

51 T. Scherer, *PhD. Thesis*, University of Amsterdam, **1994**.

52 W. Schuddeboom, T. Scherer, J.M. Warman and J.W. Verhoeven, *J. Phys. Chem.* **1993**, *97*, 13092.

53 Sybyl version 5.3, Tripos Associates, St. Louis, Missouri, USA

54 M.J.S. Dewar, E.G. Zoebisch, E.F. Healy and J.J.P. Stewart, *J. Am. Chem. Soc.* **1985**, *107*, 3902.

55 V.D. Parker and M. Tilset, *J. Am. Chem. Soc.* **1991**, *113*, 8778.

56 M. Polanyi, *Atomic Reactions*, Eds.; Wiliams and Norgate, London, **1932**.

57 H. Steark, R. Mitzkus, W. Kühnle and A. Weller, *Picosecond Phenomena Vol. 3*, Springer, Berlin, **1982**, 205.

58 M.N. Paddon-Row, A.M. Oliver, J.M. Warman, K.J. Smit, M.P. de Haas, H. Oevering and J.W. Verhoeven, *J. Phys. Chem.* **1988**, *92*, 6958.

59 A.M. Brouwer, unpublished results.

60 K.A. Zachariasse, *PhD. Thesis*, Free University of Amsterdam, **1972**.

Chapter 6

Second Harmonic Generation by Bridged Donor-Acceptor Compounds:

π- versus σ-conjugation[1-3]

6.1 INTRODUCTION

Interest in nonlinear optics (NLO) has grown tremendously in the last decade, primarily because of applications in the telecommunication- and computer industries. In these industries there is need for optical switches, optical data storage, fiber optics and optical signal processing. All of these processes can, in principal, be achieved by NLO.

Nonlinear optics is concerned with the interactions of electromagnetic fields in a medium to produce new fields altered in phase, frequency, amplitude or other propagation characteristics from the incident fields. There exist many different kinds of NLO effects. Which effect will be operative or dominant depends on the type of molecules or material used, the symmetry and the field characteristics such as strength and frequency. In this chapter only the second order NLO effect known as second harmonic generation (SHG) will be treated. The result of this effect is that upon irradiation of a nonlinear optical material with a laser with frequency ω, the frequency of the laser light will be doubled (2ω). This effect was already observed in 1961 by Franken et al.,[4] who discovered that when light of 694 nm was incident on a quartz crystal, not only light with this wavelength, but also light with a wavelength of 347 nm could be detected.

An example of a practical application of this "frequency doubling" is in the field of the compact disc player. If the frequency of the laser light of a CD-player can be doubled, it is possible to store more information on a CD record. This is because of the existence of the frequency dispersion limit, which states that in order to read information by (laser) light from a CD record, this information must be located at a minimum distance of at least 0.5λ.

Early research was focussed on inorganic materials. Nowadays organic materials[5] and polymers are also considered to be of potential use. These materials are more readily processed and have, from an applications point of view, a potentially shorter response time, because electronic motion, instead of ionic displacements, determine the polarization dynamics.

Molecular engineering and determination of the molecular hyperpolarizability β are essential in order to gain a better understanding of the chemical structure-hyperpolarizability relationship. So far it has been well established that structures which incorporate an electron rich donor group and an electron deficient acceptor group, interconnected by a conjugated π-system, in general

give rise to large molecular second order effects (e.g. p-nitroaniline (PNA) has a prototype molecular structure). An extensively studied molecule is 4-dimethylamino-4'-nitrostilbene (DMANS), having one of the largest β-values.[5-7]

In this chapter the achievement of comparable SHG effects using the π-conjugated compounds **4** and **5** and the σ-bonded donor-acceptor compounds **1**, **2** and **3**, which are of comparable length and incorporate related D/A pairs, as shown in Figure 6.1, are described. Nonlinear effects using the latter compounds have not previously been investigated. We also present results on a side-chain copolymer **7**, which contains the π-conjugated chromophore of **5**. Finally we discuss the question how the "σ-conjugation length" can be expected to influence the molecular hyperpolarizability of D-σ-A systems. In order to understand the nature of the effect involved and the types of molecules required, the theoretical background of NLO will be presented in the next sections.
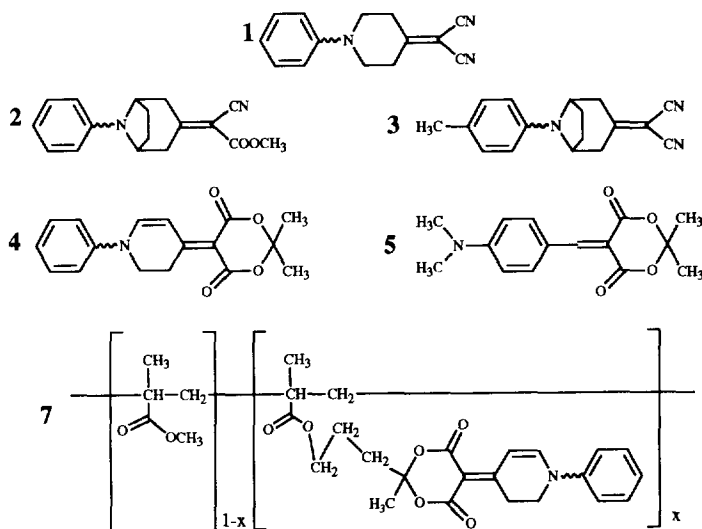
Figure 6.1: Structures of the D-σ-A compounds 1, 2 and 3, the D-π-A compounds 4 and 5 as well as the side-chain functionalized copolymer 7.

6.2 THEORY

An extensive description of NLO theory was given as long ago as 1965 by Bloembergen.[8] Many theoretical and experimental studies and extensions of the NLO theory to organic materials have been collected by Zyss and Chemla.[5] Useful reviews are given by Williams[6] and

Meredith.[7]

In describing NLO theory it is useful to distinguish between the molecular or microscopic features and the material or macroscopic features, as has been done in the next sections.

6.2.1 Second Harmonic Generation at a molecular level

When light passes through a medium the electromagnetic field of the light polarizes the molecules. These, in turn, act as oscillating dipoles broadcasting electromagnetic radiation, which can be detected at some point outside the medium. The velocity of the light is decreased by this process. This linear polarization for a single molecule is given by:

$$P = \mu_0 + \alpha E \tag{1}$$

where E is the electric field component of the incident electromagnetic wave and μ_0 is the permanent dipole moment. α is the familiar linear molecular polarizability and is the source of the refractive index in the case of an ensemble of molecules.

When the electromagnetic field of the incident light is sufficiently strong, as in the case of coherent laser light, the induced polarization becomes a nonlinear function of the applied field, according to:

$$P = \mu_0 + \alpha E + \beta E^2 + \gamma E^3 + \ldots\ldots\ldots \tag{2}$$

In equation (2), β is the quadratic or second order hyperpolarizability and is the source of second order NLO effects. γ is the cubic or third order hyperpolarizability.

The induced dipole is not necessarily in the same direction as the applied field and thus α, β and γ are tensors and will be described within the molecular coordinate system (x,y,z).

An important general statement can be made regarding β: in a centrosymmetric molecule $\beta=0$. This can be readily seen by the following argument. If either a field +E or a field -E is applied to a molecule, equation (2) predicts that the second order polarization will be $+\beta E^2$ in both cases. In a centrosymmetric system, however, the second order polarization should change sign with the field. This contradiction can only be resolved if $\beta=0$ in a centrosymmetric configuration, leading to the conclusion that second order effects will be operative only for non-centrosymmetric molecules. In centrosymmetric molecules only odd order effects can be detected.

In order to get frequency doubling, the induced polarization has to be an asymmetric non-linear response function of the applied electromagnetic field of the laser, which is a cosine
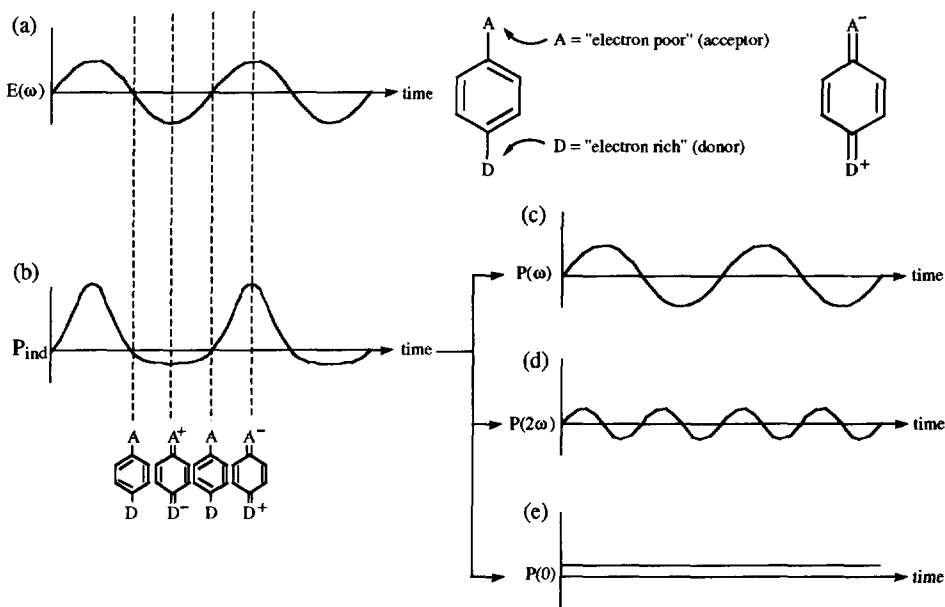
Figure 6.2: *Second Harmonic Generation. (a) The incident electromagnetic optical field $E=\cos(\omega t)$. (b) The induced polarization with the corresponding molecular resonance structures. Enhancement of the signal in the donor-acceptor direction and diminution in the acceptor-donor direction. Fourier transformation of the polarization (b) results in a constant component $1/2\beta E^2$, (e), components oscillating with the same frequency $\alpha E=\cos(\omega t)$, (c) and components oscillating with the doubled frequency $1/2\beta E^2=\cos(2\omega t)$,(d), as the applied field.*

function, $E = E_0\cos(\omega t)$. In the case of a symmetrical molecule, like benzene, this response function P will be completely symmetrical and on Fourier decomposition would consist of responses at ω, 3ω, 5ω etc., with progressively decreasing amplitudes. In a non-symmetrical donor-acceptor compound however the polarization will be enhanced when the field is in the donor-acceptor direction and will be diminished when the field is in the acceptor-donor direction, as illustrated in Figure 6.2. This results in an intrinsic asymmetric response i.e. electrons are pushed more easily from the donor to the acceptor than in the opposite direction. The asymmetric response function P will in this case be an appropriate summation of the Fourier components with frequencies 0, ω and 2ω.

From this the qualitative conclusion can be drawn that in order to get large second order effects, donor-acceptor systems are needed, with donor and acceptor preferentially in conjugation with each other. In that case the polarizability will be enhanced in one specific direction, along the charge transfer axis, and should result in a large asymmetric response. In the

absence of conjugation between donor and acceptor the effect would be expected to be very much reduced.

As a consequence of the above it is clear that when considering a donor-acceptor compound like p-nitroaniline[9,10] (PNA) the component along the donor-acceptor axis will be the dominant contributor to the nonlinear response, under the restriction that the applied field is in the direction of the molecular z-axis, as shown in Figure 6.3. All other 27 tensor components can be neglected and a one-dimensional description is sufficient, so on a microscopic level only the
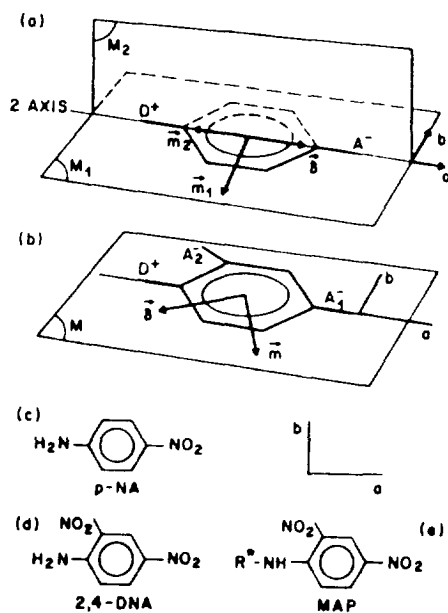
Figure 6.3: (a) Planar CT donor-acceptor molecule with mm2 symmetry. (b) Planar CT molecule with mirror (m) symmetry and two acceptors, interacting with the donor D. Examples of such structures are (c) PNA, (d) DNA and (e) MAP, where R* is an aliphatic chiral group (the a-axis is the x-axis).

β_{zzz} component is important. For 2,4 dinitroaniline (DNA) and methyl-(2,4-dintrophenyl)-aminopropanoate (MAP)[11] a two dimensional description is needed to describe the whole aromatic plane in which the donor and the two acceptors are located, which results in four independent components, namely β_{zzz}, β_{yyy}, β_{zyy} and β_{yzz}.

The hyperpolarizability has been related to the presence of a low-lying charge transfer excited state resulting in a large change in dipole moment upon excitation to the first excited

state as well as in a high oscillator strength for the corresponding electronic transition.[6] Within such a two state model, with the assumption that the transition moment of the CT absorption and $\Delta\mu_{ct}$ have the same direction (one dimensional model) it can be shown that:[12-15]

$$\beta_{ct} = \frac{3e^2\hbar^2}{2m} F_{ct} \Delta\mu_{ct} Q(\omega_{ct}) \qquad (3)$$

$$Q(\omega_{ct}) = \frac{\hbar\omega_{ct}}{(\hbar^2\omega_{ct}^2 - 4\hbar^2\omega^2)(\hbar^2\omega_{ct}^2 - \hbar^2\omega^2)} \qquad (3a)$$

In equation (3) e and m are the electron charge and mass, F_{ct} is the oscillator strength of the lowest CT transition, $\Delta\mu_{ct}$ ($= \mu_S - \mu_0$) is the change in molecular dipole moment resulting from it and $Q(\omega_{ct})$ is the so called dispersion factor, given by equation (3a), where ω_{ct} and ω are the radian frequencies of the CT transition and the incident light. $Q(\omega_{ct})$ accounts for the resonance enhancement when one or both of the frequencies ω or 2ω approach the value of the CT frequency. This is especially important on lengthening of the conjugated system in any particular series of related molecules. The CT absorption shifts in that case to lower frequencies thereby approaching the second harmonic frequency. For comparison of the SHG efficiency of systems with different absorption wavelengths, it is useful to define a $\beta(0)$ factor in which the fundamental frequency is effectively zero:

$$\beta_{ct}(0) = \frac{3e^2}{2m\hbar\omega_{ct}^3} F_{ct} \Delta\mu_{ct} \qquad (4)$$

From the above equations it is clear that materials showing efficient SHG should in general incorporate chromophores characterized by a large difference in dipole moment of the ground state and the first excited state (see however ref. 16 for interesting exceptions) and a large oscillator strength for the transition between the two states. Such a situation is typically realized in structures where electron donor (D) and acceptor (A) groups are linked by a conjugated π-electron system (D-π-A). For such molecules the dipole moment increases considerably upon excitation in their lowest charge-transfer (CT) type absorption (D-π-A + hυ $\rightarrow$ D$^+$-π-A$^-$) and furthermore this transition is characterized by a rather large oscillator strength.

Many studies[15,17-19] have been carried out on the influence of the length as well as the

structure of the interconnecting π-system on the molecular hyperpolarizability β. Thus Barzoukas et al.[17] demonstrated an almost quadratic dependence of β on the number of double bonds separating the donor and acceptor groups in their "push-pull" systems.

Efforts to enhance the SHG efficiency by lengthening the π-bridge[17,20] appear to meet with serious problems, however. Large conjugated systems in general show reduced solubility in polymer matrices, limiting the maximum degree of loading achievable. Furthermore the bathochromic shift of the charge transfer absorption on lengthening the conjugated bridge tends to reduce the transparency in the region of the second harmonic frequency, thereby leading to absorption losses and potentially to photodegradation.

σ–bonded donor-acceptor molecules

Molecules containing donor and acceptor groups connected by an extended saturated hydrocarbon bridge (D-σ-A) may still show discrete CT absorptions: (D-σ-A + hυ → D$^+$- σ-A$^-$).[21-23] The oscillator strengths of such absorptions however are much smaller than those of π-bridged systems since the electronic interaction between D and A is now provided by the much weaker "through-bond interaction"[24] or "sigma conjugation".[25] The changes in dipole moment in such D-σ-A systems can, however, be very large and increase linearly with the bridge length.[26] This is in contrast with π-conjugated compounds where, upon lengthening of the bridge, a levelling off of Δμ occurs,[27] as is shown in Figure 1.2 in Chapter 1. This is an advantage of σ-bonded donor-acceptor systems above that of π-conjugated systems. Furthermore the position of the CT absorption is expected to be rather insensitive to changes in the bridge length and may even shift hypsochromically for longer bridges, thus avoiding loss of transparency. Together with the thermal stability this makes σ-bonded D/A systems of potential interest for applications in NLO materials.

6.2.2 Macroscopic materials

Macroscopic systems can be crystals, polymers, powders, liquids etc. An important restriction in choosing a suitable macroscopic system is the condition that also on the macroscopic level a non-centrosymmetrical configuration is essential in order to get SHG.

On a macroscopic level the induced nonlinear polarization is given by:

$$P = P_0 + \chi^{(1)}E + \chi^{(2)}E^2 + \chi^{(3)}E^3 \ ......$$ (5)

$\chi^{(n)}$ have the same features as the molecular tensors and will be described in the principal or material coordinate system (X,Y,Z). To determine these macroscopic coefficients, especially for

$\chi^{(2)}$, a detailed knowledge of the projection of the molecular hyperpolarizability tensors onto the macroscopic framework containing that molecule, is required.

The general equation for the transformation of $\chi^{(2)}$ from the molecular coordinate system (x,y,z) to the macroscopic coordinate system (X,Y,Z) is given by :[28,29]

$$\chi_{XYZ}^{(2)} = 1/Vf_X(2\omega)f_Y(\omega)f_Z(\omega)\Sigma_{xyz}\cos\theta_{Xx}\cos\theta_{Yy}\cos\theta_{Zz}\beta_{xyz} \qquad (6)$$

In equation (6), V is the volume of the unit cell and $f(2\omega) = [n(2\omega)^2 + 2]/3$ are the Lorentz local field factors,[30] which account for the contributions of the neighboring molecules to the electric field.

According to equation (6) the exact description of the macroscopic coefficient, $\chi_{XYZ}^{(2)}$, which is a tensor with 27 independent parameters, is an almost impossible task. A lot of simplifications can however be made based on the symmetry of the system and the frequency dispersion limit.

The first simplifications can be made when applying the frequency dispersion limit;[31,32] because of the fact that the frequencies and the induced polarizations are coupled, the coefficients are invariant under the interchange of their three indices ($\chi_{XYY} = \chi_{YXY} = \chi_{YYX}$ etc.). For SHG this so called "Kleinman symmetry" is valid[31] when all frequencies and linear combinations of them are far away from the internal frequencies of the system, thus reducing the number of independent coefficients to 10. The same arguments are valid for the microscopic coefficients β_{xyz}.

A lot of research has been carried out in the field of SHG in crystals. This has proven to be difficult, because a non-centrosymmetric crystal structure is needed. The factors that influence the crystallization process, however, are not so well understood, making it very difficult to predict the crystal structure and hence to do systematic research on these systems. Another problem is the transparancy and processability of these materials. For application purposes (devices) it is necessary to make thin films of the materials in which there is very little light scattering.

Many of the problems faced in crystals can be overcome by using poled polymer films, where a non-centrosymmetric configuration is created by aligning the molecules in an external electric field. Much research has been carried out in this area recently.[33-41] The advantages of this technique are an easily obtainable transparent film, high symmetry $C_{\infty V}$ (simplifying the microscopic-macroscopic relationship), easy processable materials and a non-centrosymmetric configuration. A disadvantage is that the films must be poled under very high electric fields, with the risk of electric breakdown of the films.
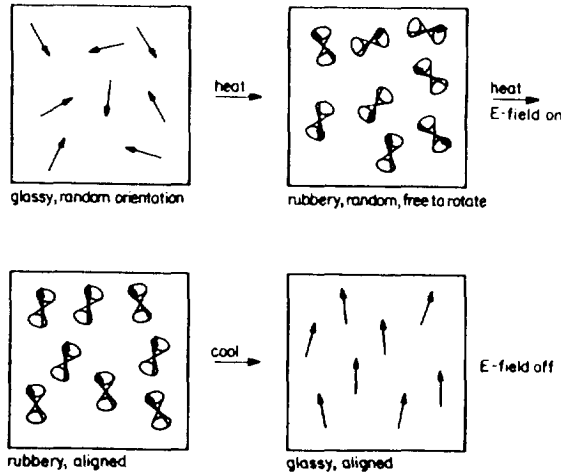
Figure 6.4: Schematic representation of the poling of a guest-host polymer system.

In order to create a non-centrosymmetric system the NLO molecules are dissolved in a polymer and via spincoating a thin transparent film is obtained. In this film the molecules are naturally isotropically distributed, but after heating the film just below or even above T_g of the film and applying an electric field, the molecules will be oriented in the field due to their ground state dipole moments. With the field still on, the film is cooled down to room temperature, thus freezing in the non-centrosymmetric configuration. The general idea is illustrated in Figure 6.4.

There are many different kinds of poled polymer systems. The simplest one is a guest-host system, as described above. Disadvantages of this method are however that only very low concentrations (< 5%) of NLO molecules are achievable, because of the low solubility in the polymer matrix. In addition, at too high concentrations crystallization occurs in the polymer films, resulting in loss of transparancy. Another problem is the high mobility of the molecules, they may be easily aligned in a poling field, but when the field is turned off they also are randomized more easily by thermal motion, resulting in loss of SHG efficiency with time.

A way to overcome these problems is to attach the NLO molecule to the polymer. This can be done by incorporating the chromophore in the back-bone, resulting in the so called "main-chain" polymers or by attaching the chromophore to the side-chain, resulting in the so called "side-chain" polymers. The side-chain polymers have the best perspectives, because the mobility still allows poling to occur, this in contrast to the main-chain polymers where poling is

very difficult and orientation must be achieved during the polymerization process.

The degree of orientation depends on the competition between the Boltzmann thermal energy (kT) and the applied electric poling field E_p, resulting in:[6,42]

$$\left\langle \cos^3 \theta \right\rangle = \frac{\mu_z E_p}{bkT} \tag{7}$$

$$\left\langle (\cos \theta)(\sin^2 \theta)(\cos \phi) \right\rangle = \frac{\mu_z E_p}{ckT} \tag{8}$$

In equation (7), μ_z is the ground state dipole moment in the direction of the molecular z-axis and b and c are factors which depend on the nature of the system.

As a consequence of the high symmetry $(C_{\infty v})$ there are only two important independent components (on a macroscopic level) left,[43] i.e. $\chi_{ZXX}^{(2)} = \chi_{XXZ}^{(2)} = \chi_{ZXZ}^{(2)}$, when the fundamental (incident laser beam) is polarized perpendicular (XX) to the Z-axis and $\chi_{ZZZ}^{(2)}$ when the fundamental is polarized parallel (ZZ) to the Z-axis. The third index shows the direction of the fundamental, the second the direction of the polarization of the fundamental and the first the direction of the polarization of the second harmonic. In the literature and also in this Thesis, $\chi_{ZZZ}^{(2)}$ is often represented as d_{33} which describes SHG in the macroscopic Z-direction or 3-direction only (one dimensional).

The relationship between β and $\chi^{(2)}$ for these poled systems is:[6,39,43]

$$\chi_{ZZZ}^{(2)} = Nf\beta_{ZZZ}\left\langle \cos^3 \theta \right\rangle \tag{9}$$

$$\chi_{ZXX}^{(2)} = Nf\beta_{ZZZ}\left\langle (\cos \theta)(\sin^2 \theta)(\cos \phi) \right\rangle \tag{10}$$

In equations (9) and (10) N is the number density of NLO molecules, f is a local field factor, the parameters between brackets are orientation parameters with θ the angle between the molecular polar z-axis, and ϕ the projection of the molecular z-axis onto the material's X-axis.

An important fundamental problem in macroscopic systems is the phase-matching condition.[44] The frequency doubled signal 2ω has to be in phase with the fundamental ω to get an optimal signal. However a phase difference will occur between the two waves, because of the frequency dependence of the refractive index. This can result in destructive interference between the two waves. The interested reader is referred to review articles on this topic.[5,6,44]

6.3 EXPERIMENTAL

6.3.1 Synthesis

(1) N-phenyl-4-azacyclohexylidenemalonitrile and

(2) N-phenyl-8-azabicyclo[3.2.1]octilydene-3-methylcyanoacetate

The synthesis of these compounds has been described elsewhere.[45]

(3) 3-dicyanomethylene-N-(p-tolyl)-8-azabicyclo[3.2.1]octene-1

After refluxing a mixture of 7.26 g (54.9 mmol) 2,5-dimethoxytetrahydrofuran and 0.15 mL of concentrated sulphuric acid in 60 mL of water for 30 minutes, this mixture was added to a solution prepared from 24.25 g (166.0 mmol) acetonedicarboxylic acid, 22.01 g sodium acetate and 7.85 g (73.3 mmol) p-toluidine in 875 mL of water. The reaction mixture was allowed to stand overnight. The solid which separated was collected by filtration and dissolved in 250 mL of a 5% HCl solution at 60°C. After cooling in an ice bath, it was made basic (pH 9-10) with ammonia. The solid which separated was collected and recrystallized from methanol/water (4:1) to yield an off-white solid 3. Total yield 5.74 g (15.6 mmol, 43% calculated on 2,5 dimethoxytetrahydrofuran): mp.: 94-95°C; ^{1}H-NMR (200 MHz CDCl$_3$): δ 7.12 ppm (d; 2 H), 6.81 ppm (d; 2 H), 4.47 ppm (m; 2 H), 2.71 ppm (dd; 2 H), 2.29 ppm (dd; 2 H), 2.29 ppm (s; 3 H), 2.18 ppm (m; 2 H), 1.78 ppm (dd; 2 H).

(4) 5-(N-phenyl-4-azacyclohexenylidene)-1,3-dioxa-2,2-dimethylcyclohexane-4,6-dione

A mixture of 0.88 g (5 mmol) of 1-phenyl-4-piperidone, 0.80 g (5.5 mmol) of 2,2-dimethyl-1,3-dioxane-4,6-dione (Meldrum's acid) in 3 mL of pyridine was stirred at room temperature for 24 hours. The mixture turned orange and was poured into ice-water. The suspension was extracted with dichloromethane and dried with MgSO$_4$. The product was purified by column chromatography and recrystallization from PE 40-60/dichloromethane, which yielded 650 mg (2.17 mmol, 43 %) of product 4: mp 193°C d.c; ^{1}H-NMR (200 MHz CDCl$_3$): δ 7.45-7.39 ppm (m; 2 H), 7.41 ppm (d; 1 H), 7.30 ppm (d; 1 H), 7.27-7.20 ppm (m; 1 H), 7.15 ppm (m; 2 H), 3.90 ppm (t; 2 H), 3.54 ppm (t; 2 H), 1.70 ppm (s; 6 H).

Scheme 1

175
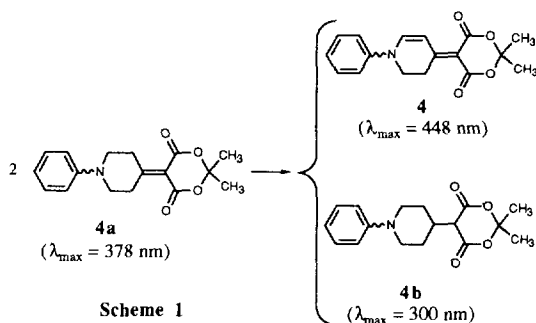
The formation of this product was unexpected since a simple Knoevenagel type reaction leading to **4a** was intended (see Scheme 1). The latter is indeed formed at the onset of the reaction as evidenced by UV-absorption, but cannot be isolated. Instead, after completion, two products are isolated; i.e. **4** and **4b** resulting from disproportionation of **4a**.

(5) 5-(p-N,N-dimethylaminophenyl methylene)-1,3-dioxa-2,2-dimethylcyclohexane-4,6-dione

A mixture of 0.80 g (5.5 mmol) of 2,2-dimethyl-1,3-dioxane-4,6-dione (Meldrum's acid), 0.75 g (5 mmol) of p-N,N-dimethylaminobenzaldehyde and a few drops of piperidine was stirred at room temperature for 30 min. The orange precipitate was filtered and after recrystallization from PE 40-60/dichloromethane, 800 mg (3.18 mmol, 64 %) of product **5** was obtained: mp 164°C-165°C; ^{1}H-NMR (200 MHz CDCl$_3$): δ 8.31 (s; 1 H), 8.28 ppm (d; 2 H), 6.70 ppm (d; 2 H), 3.16 ppm (s; 6 H), 1.77 ppm (s; 6 H).

(6) 5-(p-N,N-dimethylaminophenylmethylene)-1,3-dioxa-2-methyl-2-(3-methacryloyl-propyl)cyclohexane-4,6-dione
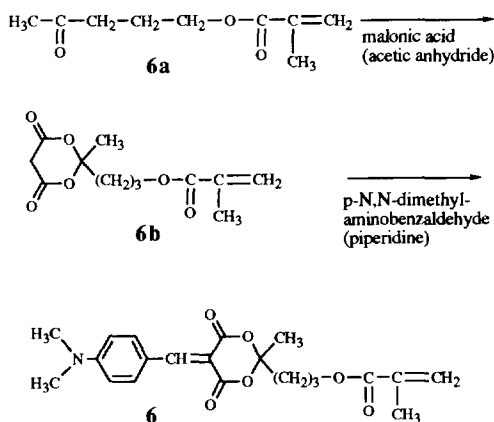
Scheme 2

A mixture of 20 g (195.5 mmol) 5-hydroxy-2-pentanone and 21.46 g (212 mmol) of triethylamine in 25 mL ether was refluxed for a few minutes. Then 20.99 g (200.7 mmol) of methacryloylchloride was added with a rate to keep the mixture boiling without further external heating. After adding all of the methacryloylchloride the mixture was refluxed for another hour. The white precipitate was dissolved in water and the water layer was discarded. The organic layer was washed with 10% sulphuric acid, saturated sodium bicarbonate and dried on MgSO$_4$. After evaporation of the ether a red oil remained, which contained 22.45 g (131.9 mmol, 68%) of almost pure *5-methacryloyl-2-pentanone* (**6a**); ^{1}H-NMR (400 MHz CDCl$_3$): δ 6.05 ppm (m; 1 H), 5.5 ppm (m; 1 H), 4.1 ppm (t; 2 H), 2.1 ppm (s; 3 H), 2.0-1.8 ppm (m; 4 H), 1.9 ppm (s; 3 H).

176

To a solution of 3.7 g (30.44 mmol) malonic acid in 3.65 mL acetic anhydride and 0.09 ml of sulphuric acid was added dropwise 5.7 g (33.5 mmol) **6a**. After stirring for 3 hours a dark oil had formed. The remaining malonic acid was filtered off and the mixture was poured into ice-water. The oil was separated and dissolved in dichloromethane. The organic layer was washed with saturated sodium carbonate solution and dried with $MgSO_4$. The product was purified by column chromatography on silica with ether. This yielded 5.71 g (22.3 mmol, 74%) of *2-methyl-2-(3-methacryloyl propyl)cyclohexane-4,6-dione:*(**6b**); ^{1}H-NMR (400 MHz $CDCl_3$): δ 6.05 ppm (m; 1 H), 5.5 ppm (m; 1 H), 4.15 ppm (t; 2 H), 2.1 ppm (s; 2 H), 2.05 ppm (m; 2 H), 1.95 ppm (m; 2 H), 1.9 ppm (s; 3 H), 1.7 ppm (s; 3 H).

To a mixture of 4 g (15.6 mmol) of **6b** and 2.24 g (15 mmol) of p-N,N-dimethylaminobenzaldehyde were added a few drops of piperidine. After stirring for one hour a thick oil was formed. This was dissolved in 150 mL of dichloromethane, the solution was washed with a 10% sulphuric acid solution and dried on $MgSO_4$, filtered and most of the solvent was removed in vacuo. The product was precipitated in a mixture of cyclohexane/ether 1:1, which yielded 1.62 g (4.18 mmol, 28%) of **6** ; ^{1}H-NMR (400 MHz $CDCl_3$): δ 8.30 ppm (s; 1 H), 8.25 ppm (d; 2 H), 6.69 ppm (d; 2 H), 6.06 ppm (m; 1 H), 5.51 ppm (m; 1 H), 4.18 ppm (t; 2 H), 3.15 ppm (s; 6 H), 2.05 ppm (m; 2 H), 1.95 ppm (m; 2 H), 1.9 ppm (s; 3 H), 1.7 ppm (s; 3 H).

(7) Copolymer of 6 and methylmethacrylate

A solution of monomer **6** (0.4 g = 1.03 mmol) in 5 mL of chlorobenzene was deoxygenated with nitrogen for one hour. A mixture of 103 mg (1.02 mmol) of methylmethacrylate dissolved in 1 mL of chlorobenzene was added followed by 1.7 mg (1 mol%) aza-iso-butyronitrile (AIBN). The mixture was stirred under nitrogen atmosphere for 18 hours at 80°C. The copolymer was precipitated in methanol, filtered off and washed with methanol. The copolymer was dissolved in dichloromethane and reprecipitated in methanol. This procedure was repeated five times, which yielded copolymer **7** containing 75 wt % of **6** (molar ratio 1:1) as determined from integration of the peaks at 3.6 ppm (OCH_3 of the methylmethacrylate moiety) and 3.15 ppm ($(CH_3)_2N$ of **6**) in the ^{1}H-NMR spectrum ($CDCl_3$).

6.3.2 Instrumentation

^{1}H-NMR spectra were obtained on a Bruker AC 200 MHz or a Bruker AC 400 MHz instrument in $CDCl_3$ solution. Melting points were recorded on a Reichert hot stage microscope and are uncorrected. Optical absorption spectra were measured on a Cary 17D spectrophotometer, while emission spectra were determined using a SPEX Fluorolog-2 spectrofluorimeter. The emission spectra of **1, 2** and **3** were found to be independent of the excitation wavelength. In the present measurements excitation was performed at 350 nm. Emission spectra were corrected for the spectral response of the detection system to yield

177

relative fluorescence intensities in quanta per wavelength interval.

6.3.3 SHG measurements

There are several ways to monitor the NLO properties of molecules. For example the Kurtz powder test[46] on powders, electric field induced second harmonic generation (EFISH)[4,47,48] on solutions, Hyper-Raleigh scattering on solutions[49] and the Maker Fringe method[50-52] on crystals and polymer systems. The last two methods are very well suited for overcoming the phase-matching problem.

Electric field induced second harmonic generation was measured under constant corona-poling on spin coated polymethylmethacrylate films containing typically 1% wt of the compounds for **1-5** and on a film of the neat copolymer **7**. A fundamental wavelength of 1064 nm was used.

Thin film samples were prepared by dissolving the solute in DMSO and subsequent spin coating of the solution on an ITO glass plate. The samples were dried in the oven for a few hours.

We used corona poling in order to orient the molecules.[53-57] A schematic representation of the experimental setup is shown in Figure 6.5. A thin tungsten wire, to which a voltage of ±5 kV is applied, is placed 1 cm above the sample. At this voltage the air around the wire above the sample becomes ionized, charge collects on the upper surface of the sample and a field of up to *ca* 1.2 MV/cm is created across the film. This is a convenient way of poling because electrodes do not have to be attached directly to the sample, as is the case for parallel plate poling. This reduces the risk of electrical breakdown of the sample.
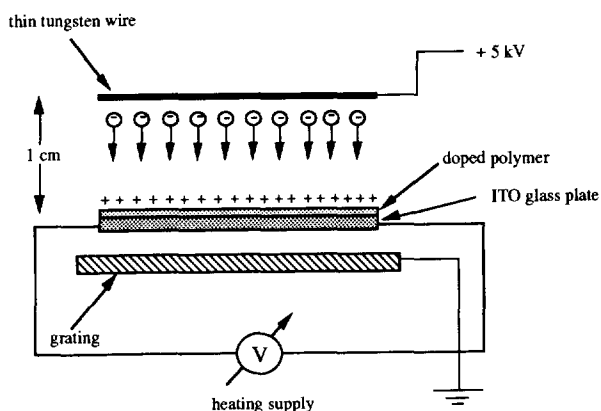
Figure 6.5: Experimental setup as used for the corona-poled SHG measurements

Comparison of the second harmonic intensities measured with a known quartz sample allowed calculation of the inner product of the ground state dipole moment μ_0 and the molecular hyperpolarizability ($\mu_0\beta_{exp}$). The values are listed in Table 6.1.

Table 6.1: Second Harmonic Generation data for the σ-bonded compounds 1, 2 and 3, the π-conjugated compounds 4 and 5 in PMMA and for the copolymer 7, at 95°C under constant corona poling at a fundamental wavelength of 1064 nm.

Compound	N (m^{-3})[a]	d_{33} (pm/V)	$\mu_0\beta_{exp}$ (10^{-30} D esu)	μ_0(D)	β_{exp} (10^{-30} esu)
1	1.1×10^{26}	0.184	26 ± 10	4.1	6.4 ± 2.5
2	8.0×10^{25}	0.265	80 ± 10	$1.7^b/3.9^c$	$46 \pm 7.5 / 20.3 \pm 3.3$
3	8.6×10^{25}	0.294	90 ± 10	3.4	26.7
4	8.2×10^{25}	0.910	423 ± 50	6.2	68
5	9.6×10^{25}	1.860	798 ± 90	5.4	148
7	5.0×10^{27}	102	-	-	-
PMMA	-	0.120	-	-	-

(a) Number of molecules per m^3.
(b) μ_0 value for the s-cis conformation.
(c) μ_0 value for the s-trans conformation.

6.4 COMPARISON OF EXPERIMENTAL AND CALCULATED β VALUES

As stated in Section 6.1, one of the aims of the present work was to compare the SHG efficiency of σ- and π-coupled donor-acceptor compounds. We also want to compare the applicability of the two level model for both kinds of systems.

6.4.1 Ground state dipole moments and β_{exp}

Ground state dipole moments of the molecules **1-5** were calculated employing the SCF-MO semi-empirical AM1 method using MOPAC 5.0.[58] In Figure 6.6, the magnitude (see also Table 6.1) and the direction of the ground state dipole moments are shown.

For **1** and **3** rather similar values (4.1 and 3.4 D resp.) were found although the orientation of the donor phenyl group was taken to be equatorial in **1** and axial in **3**.[59] Evidently it is mainly the local dipole moment of the acceptor group which determines the overall magnitude and direction of μ_0. For **2** the value of μ_0 depends rather strongly on the orientation of the carboxymethyl substituent. From X-ray diffraction data[60] this substituent is known to occupy an s-cis orientation ($\mu_0 = 1.7$ D) with respect to the exocyclic double bond in the solid state. AM1 calculates this orientation to be ~1.5 kcal/mol more stable than the alternative s-trans

1

$\mu_0 = 4.1$ D

$\mu_0 = 1.7$ D

2

$\mu_0 = 3.9$ D

3

$\mu_0 = 3.4$ D

4

$\mu_0 = 6.2$ D

5

$\mu_0 = 5.4$ D
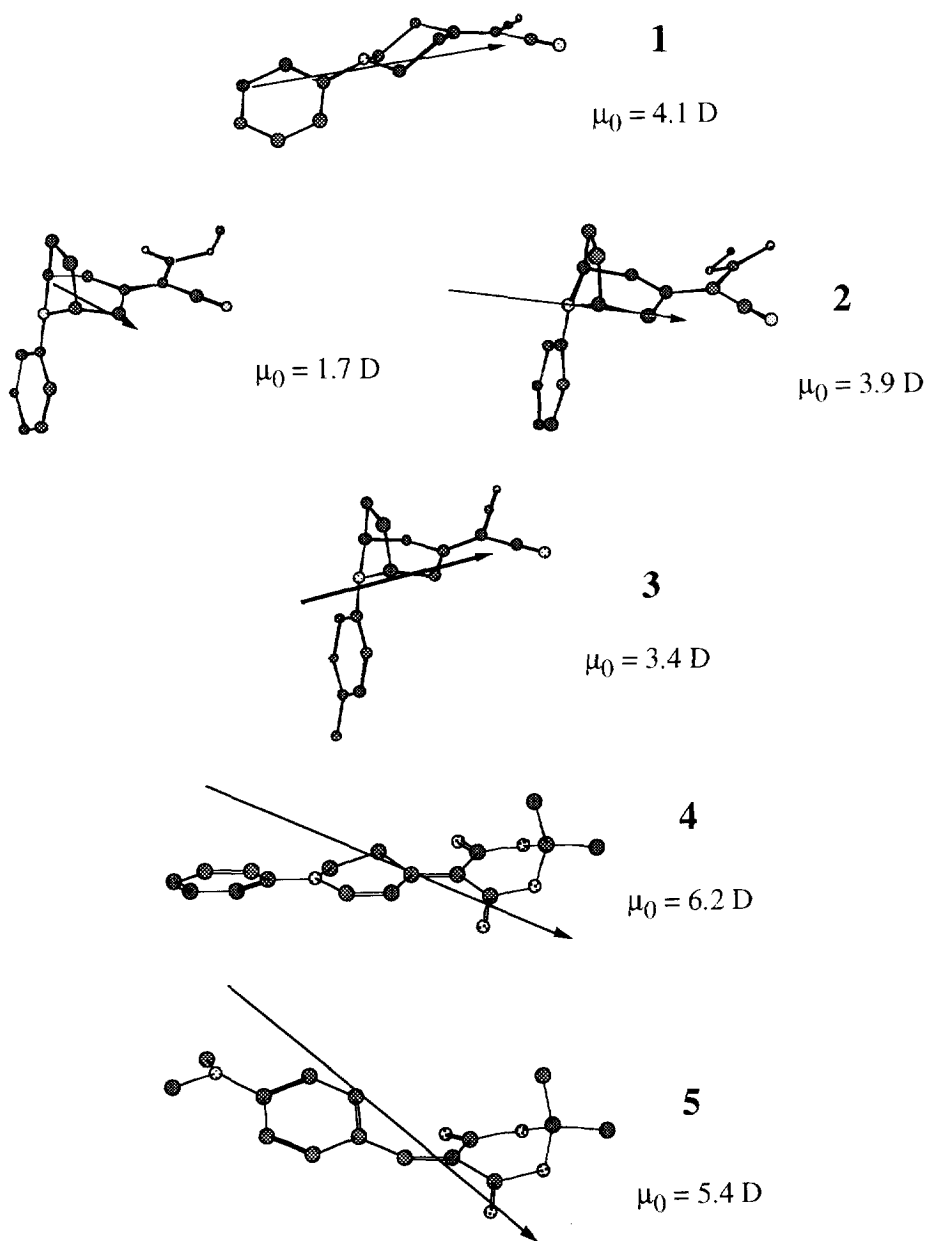
Figure 6.6: *Orientation and magnitude of the ground state dipole moment in 1-5 as derived from AM1 calculations.*

orientation (μ_0 = 3.9 D), implying that under the conditions of the SHG measurements (95 $^{\circ}$C) both orientations may be populated, with the *s-cis*, however, being present predominantly.

For compounds **4** and **5** values of 6.2 D and 5.4 D are calculated respectively. These values are higher than for the σ-bonded compounds, because of increased charge transfer character in the ground state for these molecules due to the stronger donor-acceptor interaction via a π-conjugated bridge in comparison with a σ-bond bridge.

The dipole moments given in Table 6.1 have been used to derive the β_{exp} values from the product $\mu_0\beta_{exp}$, measured experimentally. As can be seen, the β_{exp} values of the σ-bonded compounds **2** and **3**, while smaller than those for the π-bonded compounds, are still of comparable magnitude. This experimental observation on its own is confirmation of the direct, Franck-Condon coupling between S_0 and the charge transfer contribution to S_1.

It was shown by Krijnen et al.,[31,32,60] that through-bond interaction is optimized for an axial orientation of the phenyl group in systems like **1**, **2** and **3**. Evidently such an axial orientation is more highly populated in the tropane derivatives **2** and **3**, where the additional bridging ethylidene unit sterically destabilizes the equatorial orientation of the phenyl group, than in **1**. This difference in conformation has been demonstrated[24,25] to result in stronger charge transfer absorption of the tropane derivatives and now also may be inferred to be related to their higher β values (see Table 6.2).

6.4.2 Calculation of the CT contribution to the molecular hyperpolarizability

For D-π-A systems the molecular hyperpolarizability, β, has been found to be largely determined by a charge-transfer contribution β_{ct} that in general can be estimated[5,12-15] with reasonable accuracy via equation (4), which is based on a simple two level model, without resonance enhancement.

As was stated in earlier publications,[21-23] and also in Chapters 4 and 5, D-σ-A systems, such as **1**, **2** and **3**, display long wavelength absorptions and corresponding emissions (see Figure 6.7, where the spectra are shown for compound **3**) which are absent for the separate chromophores and therefore indicates that, in spite of the lack of direct conjugative interaction between the donor and acceptor, a low lying intramolecular charge-transfer state is accessible. The oscillator strength of this transition must result from significant electronic coupling between the chromophores via the intervening σ-bonds. Equation (4) might therefore also be expected to apply to compounds **1-3**.

For calculation of $\beta_{ct}(0)$, knowledge of the change in dipole moment ($\Delta\mu_{ct}$) of the molecules between that in their electronic ground state (μ_0) and in their electronically excited state (μ_S) is required and also the frequency ω_{ct} and the oscillator strength F_{ct} of the CT transition.

Table 6.2: *Molar extinction (ε), full bandwidth at half height (Δv$_{1/2}$) and oscillator strength (F$_{ct}$) of the intramolecular charge transfer absorption for compounds 1, 2 and 3 in n-hexane and for 4 and 5 in ethanol at 20°C.*

Compound	ε (l.mol^{-1}.cm^{-1})	Δv$_{1/2}$ (cm^{-1})	F$_{ct}$
1	2970	4500	0.057
2	5800	4700	0.117
3	6390	4200	0.115
4	47630	2749	0.563
5	58974	2521	0.639

Calculation of F$_{ct}$

In Table 6.2 we list the oscillator strength of the charge transfer transitions for **1-5** as calculated from the absorption spectra via equation (11). The oscillator strength is related to the bandshape (molar extinction ε, and width at half maximum Δv$_{1/2}$ (in cm^{-1})) via:[61]

$$F = 4.3 \times 10^{-9} \int \varepsilon dv \approx 4.3 \times 10^{-9} \, \varepsilon_{max} \, \Delta v_{1/2} \tag{11}$$

Determination of Δμ$_{ct}$

Δμ$_{ct}$ can be determined either from TRMC measurements or from solvatochromic shift measurements.

The TRMC measurements were performed and the value of Δμ$_{ct}$ was calculated in the same manner as in the previous chapters. The results are shown in Table 6.4. Only values could be obtained in this way for compounds **1, 2** and **3**. For compounds **4** and **5** no measurable TRMC signals were obtained, because of the very short lifetime (< 200 ps) of their excited states.

Δμ$_{ct}$ can be derived from the solvent dependence (solvatochromism)[62,63] of the optical absorption and emission frequencies (v$_a$ and v$_f$) via:

$$v_a - v_f = const + 2 (f-f') [(\Delta\mu_{ct})^2 / hc\rho^3] \tag{12}$$

In equation (12) f and f' are parameters related to the solvent static dielectric constant (ε$_s$) and refractive index (n) as f = (ε$_s$-1)/(2ε$_s$+1) and f' = (n^2-1)/(2n^2+1), while ρ represents the effective radius of the solvent cavity occupied by the molecule.

Typical examples of the solvent dependence of v$_a$ and v$_f$ are shown in Figure 6.7 for compounds **3** and **5** (note the huge solvatochromism of v$_f$ for **3** in comparison with **5**). Relevant numerical data are compiled in Table 6.3.

Table 6.3: *Absorption and fluorescence maxima,* v_a $[v_f]$ *(in* $cm^{-1}x10^{-3}$*), of compounds 1-5 in various solvents.*

Solvent	f	f'	1	2	3	4	5
n-hexane	0.185	0.168	29.50 [22.30]	29.41 [21.60]	28.09 [21.00]	23.36 [21.05]	23.70 [21.93]
cyclohexane	0.020	0.204	29.24 [22.20]	29.24 [21.40]	27.93 [20.80]	23.20 [21.01]	23.53 [21.60]
di-n-butyl ether	0.292	0.195	29.07 [19.50]	29.24 [19.00]	27.62 [19.00]	22.99 [20.70]	23.31 [21.14]
diisopropyl ether	0.329	0.178	29.07 [19.00]	29.24 [18.80]	27.78 [18.30]	22.99 [20.62]	23.26 [21.10]
diethyl ether	0.340	0.178	29.07 [18.50]	29.24 [17.90]	27.78 [17.90]	22.94 [20.49]	23.15 [21.05]
ethylacetate	0.385	0.185	28.99 [16.90]	29.15 [16.80]	27.78 [16.40]	22.68 [20.08]	22.78 [20.58]
tetrahydrofuran	0.407	0.209	-	-	-	22.62 [19.96]	22.68 [20.24]
acetonitrile	0.480	0.305	-	-	-	22.57 [19.68]	22.37 [19.68]
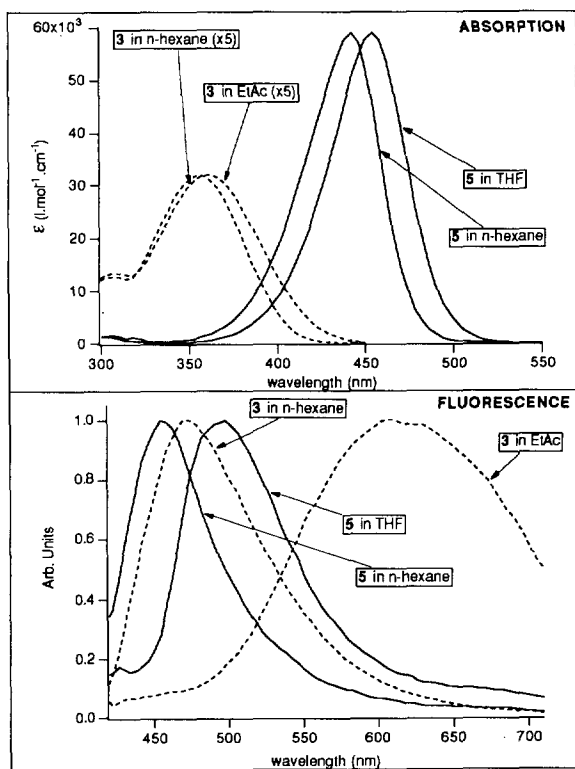
Figure 6.7: *Absorption and emission spectra of 3 (---) and 5 (——) in solvents of different polarity. Note the weaker and hypsochromically shifted absorption as well as the much more pronounced fluorescence solvatochromism of the sigma coupled system 3.*

As demonstrated in Figure 6.8 plots of $(v_a - v_f)$ versus $(f-f')$ are linear as predicted by equation (12). From the slopes of these correlations (see Table 6.4) $\Delta\mu_{ct}$ can be calculated if ρ is known. For ρ we take the radius of a sphere with a volume (V_{mol}) equal to the solvent excluded volume of the molecules:

$$V_{mol} = 4\pi\rho^3/3 \tag{13}$$

The molecular volume can be either determined experimentally, be calculated from addition of appropriate atomic volumes, or be determined via computational calculation. Hermant[64] has compared these methods and found that the latter provides the most consistent results. The widely used method,[62] where ρ is taken as 40% of the long axis of an ellipsoidal cavity, in general overestimates the value of ρ. We therefore have used the computational method in which a contour is constructed around the van der Waals shape of the molecule, thus mimicking the cavity occupied by the molecule in the solvent. The volume included by this contour can then be calculated. Molecular volumes of the systems studied were calculated with the CHEM-X molecular modeling package[65] using the following Van der Waals radii: C: 1.60, N: 1.50, O: 1.40, H: 1.20 Å. Before entering the CHEM-X program, the structures were conformationally optimized with an MM2P force field.

Table 6.4 compiles the results obtained. Note that the results obtained from the TRMC measurements are in good agreement with those obtained from the solvatochromic shift

Table 6.4: Effective radius ρ for compounds 1-5 (determined from molecular modeling), the slope of the correlation (see Figure 6.11) between the difference of their absorption and emission maxima as a function of (f-f'), the change in dipole moment between the ground and the first excited state, $\Delta\mu_{ct}$, determined via TRMC, and calculated via equation (12) from the solvatochromic measurements, the AM1 calculated ground state dipole moment, μ_0, and the resultant excited state dipole moment μ_S.

Compound	ρ (Å)	$2(\Delta\mu_{ct})^2/hc\rho^3$ (cm^{-1})	$\Delta\mu_{ct}$(TRMC) (D)	$\Delta\mu_{ct}$(fluor) (D)	μ_0(AM1) (D)	μ_S (D)
1	4.85	22.958	16.8	16.1	4.1	20.2
2	5.21	20.968	16.4	17.1	1.7[a]/3.9[b]	18.8 / 21
3	5.16	18.650	17.0	16.0	3.40	19.4
4	5.21	2.290		5.7	6.2	11.9
5	5.17	3.510		7.0	5.4	12.4

(a) μ_0 value for the s-cis conformation.
(b) μ_0 value for the s-trans conformation.
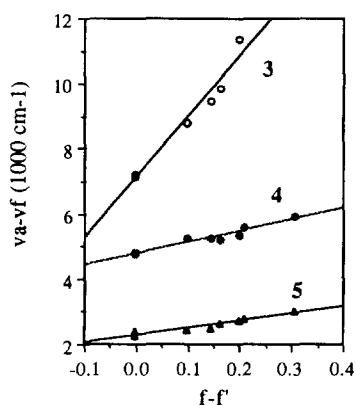
Figure 6.8: *Difference between the absorption and fluorescence frequencies (v_a-v_f) of 3, 4 and 5 as a function of the solvent polarity parameter (f-f'). For clarity the data points of 5 have been offset vertically by 1000 cm^{-1}.*

measurements for compounds **1-3**. Comparison of the results for **1, 2** and **3** with those for **4** and **5** demonstrates the larger $\Delta\mu_{ct}$ typical for σ-coupled systems.[2,26,27] This is partly due to significant ground state mixing between the D-π-A and D$^+$-π-A$^-$ configurations in π-coupled systems leading to enhancement of μ_0 at the expense of μ_S.

With the F_{ct} values thus derived and employing the data for $\Delta\mu_{ct}$ obtained above, equation (3) and equation (4) were used to calculate β_{ct} and $\beta_{ct}(0)$ respectively, as shown in Table 6.5.

Table 6.5: *Experimental molecular hyperpolarizability (β_{exp}) determined from electric field induced second harmonic generation (see Table 6.1), the charge transfer contribution to the molecular hyperpolarizability (β_{ct}) calculated via equation (3), and the molecular hyperpolarizability for zero frequency ($\beta_{ct}(0)$) calculated via equation (4).*

Compound	$\beta_{ct}(0)$ (10^{-30}esu)	$\beta_{ct}(1064{\to}532$ nm$)$[a] (10^{-30}esu)	$\beta_{exp}(1064{\to}532$ nm$)$ (10^{-30}esu)
1	2.4	3.7	23
2	4.8	8.1	21
3	4.7	9.7	27
4	13.8	57.0	68
5	23.5	78.0	148

(a) For ω_{ct} the frequency of the absorption maximum in ethylacetate was used.

6.4.3 Comparison of β for σ-bond and π-conjugated systems

Comparison of the "theoretical" (β_{ct}), as calculated from equation (3), and experimental hyperpolarizabilities (β_{exp}) compiled in Table 6.5 allows some interesting observations to be made. Thus it is evident that, in line with earlier observations[5,12-15] for D-π-A systems, β_{ct} values calculated via equation (3) for **4** and **5**, provide a major contribution to the overall experimental value, β_{exp}. However, for the D-σ-A systems **1**, **2** and **3**, β_{exp} significantly exceeds the calculated β_{ct} value.

From these observations we conclude that the two state model, underlying equation (3) and taking into account only the D-π-A and D$^+$-π-A$^-$ states, may be inadequate for D-σ-A systems such as **1-3** in which the CT transition has been found[21] to derive much of its oscillator strength from interaction between the D$^+$-σ-A$^-$ state and locally excited donor (D*-σ-A) or acceptor (D-σ-A*) states. This implies that also the perturbed local transitions gain significant CT character and since these may have large oscillator strengths they can make an important contribution to the overall hyperpolarizability. This situation is schematized in Figure 6.9 for the contribution from a perturbed local acceptor transition (hv'$_{A \to A}$*) that gains CT character by mixing of the "pure" D-σ-A* and D$^+$-σ-A$^-$ states, which are relatively close in energy (ΔE), thereby allowing significant intensity borrowing by the CT transition from the A→A* transition.

It has been shown[66] that for a general three level situation equation (3) can be expanded to equation (14), where the labels 1 and 2 refer to the electronic transitions from the ground state to the first and to the second excited state respectively.

$$\beta' = \frac{3e^2\hbar^2}{2m}\left[F_1\Delta\mu_1\,Q(\omega_1) + F_2\Delta\mu_2\,Q(\omega_2)\right] \tag{14}$$

Application of equation (14) is thwarted by the fact that for our compounds the parameters related to the second transition (i.e. a perturbed local transition) are not readily available experimentally because of severe spectral overlap and especially because fluorescence is only observed from the lowest excited state, thus making determination via the fluorescence solvatochromism method of the dipole moment changes accompanying higher transitions impracticable. Nevertheless, it is possible to consider the implication of a three level situation, such as that in Figure 6.9, for the deviation of the molecular hyperpolarizability from that estimated via a two level model as well as for the dependence of this hyperpolarizability on the length of the σ-bridge. In doing so we assume a negligible oscillator strength[21] for the "pure" CT transition (hv$_{ct}$). The oscillator strength of the original local A→A* transition is then divided between hv'$_{A \to A}$* and hv'$_{ct}$. If we define the relevant electronic interaction matrix
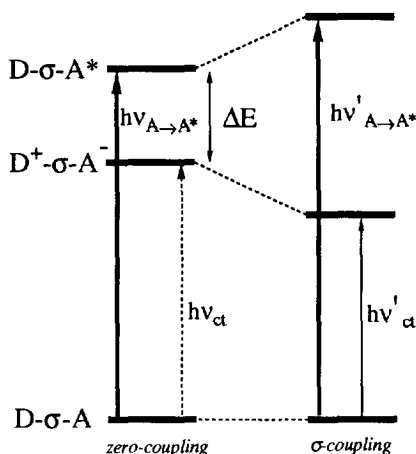
Figure 6.9: *Intensity borrowing by the CT transition from a local acceptor transition as a result of through-bond mediated interaction in a D-σ-A system.*

element describing the through bridge interaction as H_{da}, it follows from first order perturbation theory for weak coupling ($H_{da} \ll \Delta E$) that:

$$F'_{A \to A^*} \approx F_{A \to A^*}/(1+p^2) \tag{15}$$

$$F'_{ct} \approx p^2 \cdot F_{A \to A^*}/(1+p^2) \tag{16}$$

where $p = H_{da}/\Delta E$

Neglecting the dipole moment change connected with the unperturbed $A \to A^*$ transition, the changes in dipole moment connected with $hv'_{A \to A^*}$ and hv'_{ct} are then:

$$\Delta\mu'_{A \to A^*} = p.\Delta\mu_{ct}/(1+p^2)^{0.5} \tag{17}$$

$$\Delta\mu'_{ct} = \Delta\mu_{ct}/(1+p^2)^{0.5} \tag{18}$$

Substitution of equations (15)-(18) in (14) gives equation (19):

$$\beta'_{ct} = \frac{3e^2\hbar^2}{2m}\left[\frac{p^2}{(1+p^2)^{1.5}} Q(\omega_{ct}) + \frac{p}{(1+p^2)^{1.5}} Q(\omega_{A \to A^*})\right] F_{A \to A^*} \Delta\mu_{ct} \tag{19}$$

187

Since $p^2 \ll 1$ and the two dispersion factors in equation (19) will not be very different if ΔE is rather small as compared to the gap between the energy of the fundamental frequency and that of the lowest energy transition (i.e. far from resonance for both transitions), this can be simplified to equation (20):

$$\beta'_{ct} \approx \frac{3e^2\hbar^2}{2m}\, p\; F_{A\to A^*}\, \Delta\mu_{ct}\, Q(\omega_{A\to A^*}) \tag{20}$$

Equation (20) demonstrates that the simple two level model underlying equation (3) is inadequate indeed, since β'_{ct} is in fact linked to the product of the oscillator strength of a local transition and the change in dipole moment accompanying a CT transition whereas in equation (3) these refer to the same (CT) transition. From equations (3), (16) and (20) it is readily derived that the ratio of the molecular hyperpolarizabilities predicted by application of (3) and of (20) is given by equation (21):

$$\frac{\beta'_{ct}}{\beta_{ct}} = \frac{1}{p}\; x\; \frac{Q(\omega_{A\to A^*})}{Q(\omega_{ct})} \tag{21}$$

Clearly the mixing coefficient $p = H_{da}/\Delta E$ is of crucial importance. In fact, Pasman has found previously[21] that across sigma bridges with an effective length of three carbon-carbon bonds, such as that incorporated in **1**, p may be expected to be in the range 0.1-0.3, thus implying that for such molecules the two level approximation of equation (3) may underestimate the molecular hyperpolarizability by up to one order of magnitude.

Importantly, equation (20) also allows us to estimate the influence of the sigma bridge length on the molecular hyperpolarizability. For a given D/A pair ΔE may be assumed to be fairly constant irrespective of the length and nature of the σ-bridge (note that for short DA distances ΔE will increase because of Coulomb stabilization of the D^+-σ-A^- state!), but H_{da} is expected to decrease exponentially upon lengthening of the bridge:

$$H_{da} = H_{da}(0)\exp(-\alpha n_\sigma) \tag{22}$$

In equation (22) the length of the bridge has been expressed in the number of sigma-bonds (n_σ) separating D and A. Since for an extended bridge structure the DA distance increases linearly with n_σ it is evident[26] that $\Delta\mu_{ct}$ is proportional to n_σ and, neglecting the distance dependence of ΔE, it then follows from combination with equations (20) and (22) that β'_{ct} is proportional to $n_\sigma\exp(-\alpha n_\sigma)$. This implies that the highest value of the molecular hyperpolarizability resulting

from through-bond coupling in extended D-σ-A systems is to be expected for an optimal bridge length n_σ(opt) = $1/\alpha$.

From recent studies[67-73] on through-bond electron transfer via saturated hydrocarbon bridges as well as from PES and electron transmission spectroscopy[74] it has been found that the coefficient α is in the range of 0.3-0.6. Thus the optimal bridge length, n_σ(opt), is predicted to be in the range 3.3-1.6. Although slightly larger n_σ(opt) values may be expected, if account is taken of the increase of ΔE upon shortening of the bridge, it appears likely that the n_σ = 3 bridge employed in **1** has a virtually optimal length and that further improvement should be sought rather in changes of the bridge structure and configuration (to enhance H_{da}) and of the chromophores attached (e.g. to enhance $F_{A\rightarrow A^*}$) than in further lengthening of the bridge. This is an important goal especially because of the higher transparancy and eventual higher degree of loading in a polymer matrix that may be achievable with D-σ-A instead of D-π-A systems.

6.4.4 Side-chain functionalized copolymer 7

As an excursionary investigation in the direction of the covalent attachment of D-σ-A chromophores like **1-3**, we prepared (see experimental) the functionalized methacrylate monomer **6** containing a D-π-A chromophore identical to **5**. While it turned out to be impossible to prepare suitable films of a homopolymer of **6** due to "cracking" of the film, the 1:1 copolymer with methylmethacrylate, **7**, gave a clear film upon spin coating from a dimethylformamide solution. In Table 6.1 we report the d_{33} value for this film. The very high value (102 pm/V) testifies to the efficiency achievable, in comparison with a guest host system where compound **5** is dissolved in PMMA (*ca* 1% wt), which only gives a d_{33} of 1.86 pm/V. This is due to a much higher loading and possibly to a more efficient poling in the copolymer system.

6.5 CONCLUSIONS

From the present comparison of σ- and π-bridged donor-acceptor systems it appears that for relatively short bridges comparable β values can be achieved. This is mainly because in the D-σ-A systems a much larger difference in dipole moment of the ground and excited state $\Delta\mu_{ct}$ compensates for the considerably lower oscillator strength of the CT transition.

While a two-level model rather accurately predicts β values for D-π-A systems, expansion to include the effect of mixing between the CT excited state and locally excited D or A states appears necessary for D-σ-A systems. From such an extended model it may be concluded that for bridges consisting of saturated C atoms a length of 2 to 4 C-C bonds is optimal. Further enhancement of β_{ct} for systems with a saturated hydrocarbon bridge should be sought rather in changes of the bridge configuration and of the chromophores attached than in further

lengthening of the bridge. For other types of saturated bridges (e.g. polysilanes[75]) larger optimal lengths may apply if such bridges show a weaker distance dependence of the electronic coupling between D and A.

The very high d_{33} value of the side chain functionalized methacrylate copolymer **5** testifies to the amplification of SHG efficiency achievable with highly D-π-A chromophore loaded systems. Clearly it would be worthwhile to investigate the behaviour of analogous copolymers containing chromophores of the D-σ-A type.

6.6 ACKNOWLEDGEMENT

6.7 REFERENCES AND NOTES

1   W. Schuddeboom, B. Krijnen, J.W. Verhoeven, E.G.J. Staring, G.L.J.A. Rikken and H. Oevering,
     Chem. Phys. Lett. **1991**, *179*, 73.

2   W. Schuddeboom, B. Krijnen, J.W. Verhoeven, E.G.J. Staring, G.L.J.A. Rikken, H. Oevering and
     S.A. Jonker, *Polymer Preprints* **1991**, *32*, 156-157.

3   W. Schuddeboom, B. Krijnen, J.W. Verhoeven, E.G.J. Staring, G.L.J.A. Rikken and H. Oevering,
     Mol. Cryst. Liq. Cryst. Sci. Technol. - Sec. B: Nonlinear Optics **1992**, *2*, 297.

4   P.A. Franken, A.E. Hill, C.W. Peters, G. Weinreich, *Phys. Rev. Lett.* **1961**, *7*, 118.

5   D.S. Chemla and J. Zyss, Eds.; *Nonlinear optical properties of organic molecules and crystals*, Vols. 1,2;
     Academic Press; New York, **1987**.

6   D.J. Williams, *Angew. Chem. Int. Ed. Engl.* **1984**, *23*, 690.

7   G.R. Meredith, *Journal of Materials Education* **1987**, *9*, 719.

8   N. Bloembergen, *Nonlinear Optics*, Benjamin; New York, **1965**.

9   C.C. Teng and A.F. Garito, *Phys. Rev. Lett.* **1983**, *50*, 350-352.

10   J.F. Nicoud and R.J. Twieg, *Nonlinear Optical Properties of Organic Molecules and Crystals Volume 1*,
     D.S. Chemla and J. Zyss, Eds.; Academic Press; New York, **1987**.

11   J.L. Oudar and R. Hierle, *J. Appl. Phys.* **1977**, *48*, 2699.

12   B.F. Levine, *J. Chem. Phys.* **1976**, *37*, 516.

13   J.L. Oudar, *J. Chem. Phys.* **1977**, *67*, 446.

14   J.L. Oudar and D.S. Chemla, *J. Chem. Phys.* **1976**, *66*, 2664.

15   A. Dulcic, C. Sauteret, *J. Chem. Phys.* **1978**, *69*, 3453.

16   J. Zyss, *Nonlinear Optics* **1991**, *1*, 1.

17   M. Barzoukas, M. Blanchard-Desce, D. Josse, J.M. Lehn and J. Zyss, *Chem. Phys.* **1989**, *133*, 323-329.

18   L.T. Cheng, W. Tam, G.R. Meredith, G.L.J.A. Rikken and E.W. Meijer, *SPIE Proc.* **1989**, *1147*, 61.

19   J.O. Morley, V.J. Docherty and D. Pugh, *J. Chem. Soc. Perkin Trans. II* **1987**, 1351.

20   A.E. Stiegman, E. Graham, K.J. Perry, L.R. Khundar, L.T. Cheng and J.W. Perry,
     J. Am. Chem. Soc. **1991**, *113*, 7658.

21   P. Pasman, F. Rob and J. W. Verhoeven, *J. Am. Chem. Soc.* **1982**, *104*, 5127.

22   B. Krijnen, H.B. Beverloo and J.W. Verhoeven, *Recl. Trav. Chim. Pays-Bas* **1987**, *106*, 135.

23   R.M. Hermant, N.A.C. Bakker, B. Krijnen and J.W. Verhoeven, *J. Am. Chem. Soc.* **1990**, *112*, 1214.

24   R. Hoffmann, A. Imamura and W.J. Hehre, *J. Am. Chem. Soc.* **1968**, *90*, 1499.

25   M.J.S. Dewar, *J. Am. Chem. Soc.* **1984**, *106*, 669.

26   M.N. Paddon-Row, A.M. Oliver, J.M. Warman, K.J. Smit, M.P. de Haas, H. Oevering and J.W. Verhoeven,
     J. Phys. Chem. **1988**, *92*, 6958.

27   S.A. Jonker, J.M. Warman, M.P. de Haas and M.N. Paddon-Row, *Sensors and Actuators*
     Kluwer Technical Books; Enschede, **1990**, 315.

28   J.L. Oudar and J. Zyss, *Phys. Rev. A* **1982**, *26*, 2016.

29   J. Zyss and J.L. Oudar, *Phys. Rev. A* **1982**, *26*, 2028.

30   D. Pugh and J.O. Morley, *Nonlinear Optical Properties of Organic Molecules and Crystals Volume 1*,
     D.S. Chemla and J. Zyss, Eds.; Academic Press; New York, **1987**.

31   D.A. Kleinman, *Phys. Rev.* **1962**, *126*, 1977.

32   G.D. Boyd and D.A. Kleinman, *J. Appl. Phys.* **1968**, *39*, 3597-3639.

33   G.R. Möhlmann, *Organic Materials for Non-Linear Optics*, R.A. Hann and D. Bloor, Eds.; Royal Society of
     Chemistry; London, **1988**, 275-287.

34   R.D. Small, K.D. Singer, J.E. Sohn, M.G. Kuzyk and S.J. Lalama, *Spie Proc. 1986*, *682*, 160.

35 J.F. Wolfe, B.H. Loo, R.A. Sanderson and P. Bitler in *Nonlinear Optical Properties of Polymers* Mat. Res. Soc., Vol 109, A.J. Heeger, J. Orenstein and D.R. Ulrich, Eds.; **1988**, 291.

36 S. Nijhuis, G.L.J.A. Rikken, E.E. Havinga, W. ten Hoeve, H. Wijnberg and E.W. Meijer, *J. Chem. Soc., Chem. Comm.* **1990**, *16*, 1093.

37 K.D. Singer, M.G. Kuzyk, W.R. Holland, J.E. Sohn and S.J. Lalama, *Appl. Phys. Lett.* **1988**, *53*, 1800-1802.

38 H.G. Daigo, N. Okamoto and H. Fujimura, *Optics Communications* **1988**, *69 (2)*, 177.

39 S. Esselin, P. Le Barny, D. Broussoux, J.C. Dubois, J. Raffy and J.P. Pocholle, *SPIE Proc.* **1988**, *971*, 120.

40 T.M. Leslie R.N. Demartino, E.W. Choe, G. Khanarian, D. Haas, G. Nelson, J. Stamatoff, D.E. Stuetz, C. Teng and H. Yoon, *Mol. Cryst. Liq. Cryst.* **1987**, *153*, 451-477.

41 K.D. Singer, M.G. Kuzyk, W.R. Holland, J.E. Sohn, S.J. Lalama, R.B. Comizzoli, H.E. Katz and M.L. Schilling, *Appl. Phys. Lett.* **1986**, *49*, 248.

42 G.R Meredith, J.G. Van Dusen and D.J. Williams, *ACS Symp. Ser.* **1983**, *233*, 109-133.

43 D.J. Williams, *Nonlinear Optical Properties of Organic Molecules and Crystals Volume 1*, Academic Press, New York, **1987**, 406-424.

44 S.K. Kurtz, *Quantum Electronics*, H. Rabin and C.L. Tang, Eds.; Academic Press, **1975**, 222-281.

45 B. Krijnen, H.B. Beverloo, J.W. Verhoeven, C.A. Reiss, K. Goubitz and D. Heijdenrijk, *J. Am. Chem. Soc.* **1989**, *111*, 4433.

46 S.K. Kurtz and T.T. Perry, *J. Appl. Phys.* **1968**, *39*, 3798.

47 J.L. Oudar, *J. Chem. Phys.* **1977**, *67(2)*, 446.

48 G. Mayer, *Acad. Sci.* **1968**, *B 267*, 54.

49 K. Clays and A. Persoons, *Phys. Rev. Lett.* **1991**, *66*, 2980.

50 J. Jerphagnon and S.K. Kurtz, *J. Appl. Phys.* **1971**, *41*, 1667-1681.

51 J. Jerphagnon and S.K. Kurtz, *Phys. Rev.* **1970**, *B 1*, 1739-1744.

52 P.D. Maker, R.W. Terhune, M. Nisenoff and C.M. Savage, *Phys. Rev. Lett.* **1962**, *8*, 21.

53 G.R Meredith, J.G. Van Dusen and D.J. Williams, *Macromolecules.* **1982**, *15*, 1385.

54 K.D. Singer, S.J. Lalama and J.E. Sohn, *SPIE Proc.* **1985**, *578*, 130.

55 E.E. Havinga and P. van Pelt. *Ber. Bunsenges. Phys. Chem.* **1979**, *83*, 816-821.

56 M.A. Mortazavi, A. Knoesen, S.T. Kowel, B.G. Higgins and A. Dienes, *J. Opt. Soc. Am. B*, **1989**, *6*, 733.

57 K.D. Singer, S.J. Lalama, J.E. Sohn and R.D. Small, *Nonlinear Optical Properties of Organic Molecules and Crystals Volume 1*, Academic Press, New York, **1987**, 460.

58 J.J.P. Stewart, QCPE program 455, **1989**.

59 X-Ray analysis[60] has shown that for all compounds studied the phenyl group adopts an axial orientation in the solid state. In solution, **2** and **3** retain the axial orientation while both axial and equatorial conformations are populated by **1**.

60 B. Krijnen, *PhD. Thesis* University of Amsterdam, Amsterdam, **1990**.

61 N.J. Turro in *Modern Molecular Photochemistry*, The Benjamins/Cummings Publishing Company; California, **1978**, Chp 5.

62 E. Lippert, *Z. Elektrochem.* **1957**, *61*, 962.

63 P. Suppan, *J. Photochem. Photobiol.* **1990**, *50*, 293.

64 R. M. Hermant, *PhD. Thesis* University of Amsterdam, Amsterdam, **1990**.

65 Chemical Design Ltd., Oxford, UK; the use of the service and facilities of the Dutch National NWO/SURF expertise center CAOS/CAMM is gratefully acknowledged.

66 H. Suzuki and K. Sukegawa, *Appl. Phys. Lett.* **1987**, *51*, 401.

67 H. Oevering, M.N. Paddon-Row, M. Heppener, A.M Oliver, E. Cotsaris, J.W. Verhoeven and N.S. Hush, *J. Am. Chem. Soc.* **1987**, *109*, 3258.

68 H. Oevering, J.W. Verhoeven, M.N. Paddon-Row and J.M. Warman, *Tetrahedron* **1988**, *45*, 4751.

69 K.W. Penfield, J.R. Miller, M.N. Paddon-Row, E. Cotsaris, A.M. Oliver and N.S. Hush, *J. Am. Chem. Soc.* **1987**, *109*, 5061.

70 L.A. Stein, N.A. Lewis and G. Seitz, *J. Am. Chem. Soc.* **1982**, *104*, 2596.

71 S. Knapp, T.G. Murali Dhar, J. Albaneze, S. Gentemann, J.A. Potenza, D. Holten and H.J. Schugar, *J. Am. Chem. Soc.* **1991**, *113*, 4010.

72 M.D. Johnson, J.R. Miller, N.S. Green and G.L. Closs, *J. Phys. Chem.* **1989**, *93*, 1173 .

73 P. Siddarth and R.A. Marcus, *J. Phys. Chem.* **1990**, *94*, 2985.

74 M.N. Paddon-Row and J.W. Verhoeven, *New J. Chem.* **1991**, *15*, 107.

75 G. Mignani, A. Krämer, G. Puccetti, I. Ledoux, G. Soula, J. Zyss and R. Meyrueix, *Organometallics* **1990**, *9*, 2640.

193

Chapter 7

Sudden Polarization

in the Twisted, Phantom State (^{1}P*)

of Tetraphenylethylene[1]

7.1 INTRODUCTION

Photon-induced cis-trans isomerization of ethylenic double bonds is a process of fundamental importance in both biological and technological chemistry. The mechanism of vision is without doubt the most vivid example of this, with rotation around a carbon-carbon bond following photon absorption setting off a chain of events, which leads to data storage of enormous complexity. The twisting process is also the basis underlying the operation of many of the proposed candidates for molecular opto-electric and opto-mechanical switching and storage devices.

Much fundamental theoretical and experimental attention has focussed on the details of the intermediate steps in the isomerization mechanism including the breaking of the π-bond,
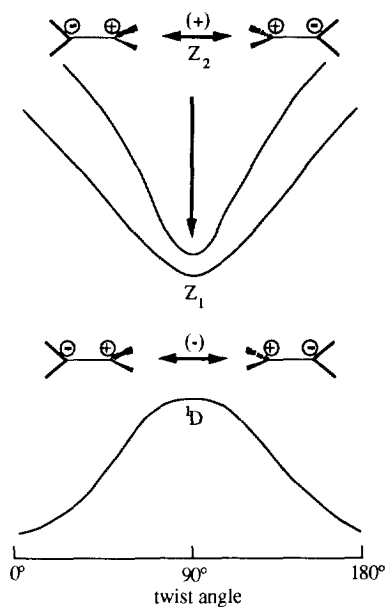
Figure 7.1: Potential surfaces of the singlet manifold for twisting of tetraphenylethylene.

rotation within the biradical state and the reformation of the π-bond either in the original or 180° rotated configuration of the ground state molecule. An intuitively somewhat surprising prediction of theoretical studies has been that the most stable excited state of even simple, symmetrical ethylene derivatives most probably involves, in addition to partial rotation, complete charge separation across the carbon-carbon bond.[2-11] Direct experimental evidence for this "sudden polarization" effect, first proposed by Bonacic-Koutecky et al.,[2] has proven difficult to find. Recently, however, strong evidence was provided for the dipolar, or "zwitterionic", nature of the twisted $^1p^*$ phantom state of tetraphenylethylene (TPE),[12,13] formed from S_1 by rotation around the central carbon-carbon bond.
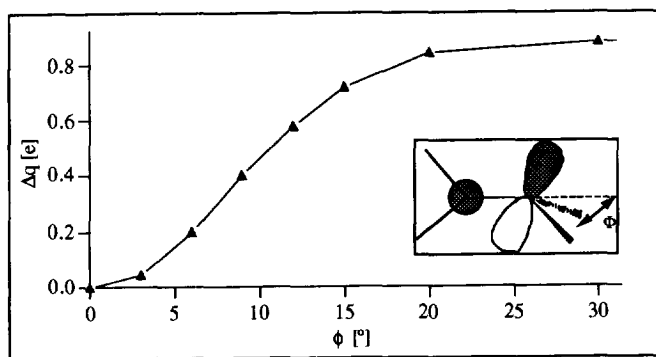
Figure 7.2: *Charge separation, Δq, in the Z_1 excited singlet state of 90° twisted ethylene as a function of the pyramidalization angle Φ. The number Δq has been corrected for intrinsic charge separation in the ground state.[2]*

Sudden polarization in the twisted excited state of symmetrical molecules like TPE is only possible if orbital localization between the two orthogonal π-orbitals can be achieved.[2,4,14] In order to obtain orbital localization a slight energy asymmetry is necessary, which can be brought about by: (a) pyramidalization at one of the carbons, (b) asymmetry of the surroundings (charge in the neighborhood), (c) chemical substitution or non-totally symmetric vibrations destroying the symmetry with respect to the mirror plane between the two carbons. Interestingly, due to the last point even an isolated "symmetrical" molecule like ethylene is virtually never in the perfect symmetric configuration, because it spends most of its time in the classical turning points of vibrations which correspond to symmetry reduced geometry.

In Figure 7.1 are illustrated the covalent, twisted, diradicaloid ^1D ground state and the excited zwitterionic states Z_1 and Z_2 of 90° twisted TPE. The latter states are in fact symmetrized combinations of two ionic resonance structures, with the out-of-phase combination

lying lowest in the two orbital model. The two Z states have been predicted by Wulfman and Kumei[15] in 1971 to have a large polarizability. The two Z states are separated by only a few kilocalories per mole, and each one is a 50 percent mixture of two highly polarized structures (see Figure 7.1). Hence a very small perturbation can mix Z_1 and Z_2. One state, by "borrowing" from the other, can acquire nearly 100 percent of one ionic structure, the other nearly 100 percent of the second ionic structure in which case each state acquires a strong polarization. Hereby the charge is localized on one radical site and a large charge separation is created. Figure 7.2 shows the charge separation, Δq, between the two carbon atoms in the Z_1 excited state of 90° twisted ethylene as a function of the pyramidalization angle ϕ of one of the carbons.[2]

In conclusion: in the zwitterionic states, for perfectly symmetric systems, charge oscillates back and forth between two symmetry-equivalent sites. Slight geometric perturbations can create a sudden polarization of the excited molecule, with localization of almost a full charge at one end of the molecule. A photon is transformed into an electrical signal thanks to an appropriate molecular distortion.

In this chapter we have used the TRMC technique to look directly for the change in dipole moment of tetraphenylethylene and tetra-p-methoxyphenylethylene (MeOTPE) that should accompany photoexcitation, if charge separation does in fact take place and is unidirectional for a timescale large enough to be "seen" as a dipole by the microwaves, i.e. a few picoseconds at least. Indications that this is in fact the case for TPE have been provided recently by flash-photolysis optical absorption spectroscopy[12,16] and picosecond optical calorimetry.[13] The molecules studied are shown in Figure 7.3.

TPE   **MeOTPE**

Figure 7.3: Structures of tetraphenylethylene (TPE) and tetramethoxyphenylethylene (MeOTPE).

7.2 QUALITATIVE TRMC RESULTS

Our initial attempt to look for the sudden polarization effect on photolysis of TPE derivatives using the TRMC technique was carried out on solutions of TPE and MeOTPE in benzene. The results are shown in Figure 7.4, traces A and B. The occurrence of a transient increase in dielectric loss on flash-photolysis of the TPE solution is barely visible even to the "trained eye". That a small transient change does occur can be seen, however, if the TPE data are compared with those for MeOTPE, for which no TRMC signal at all was discernable. Because the TPE signal was so close to the noise level, it was considered that this did not provide convincing evidence for the formation of a dipolar excited state.
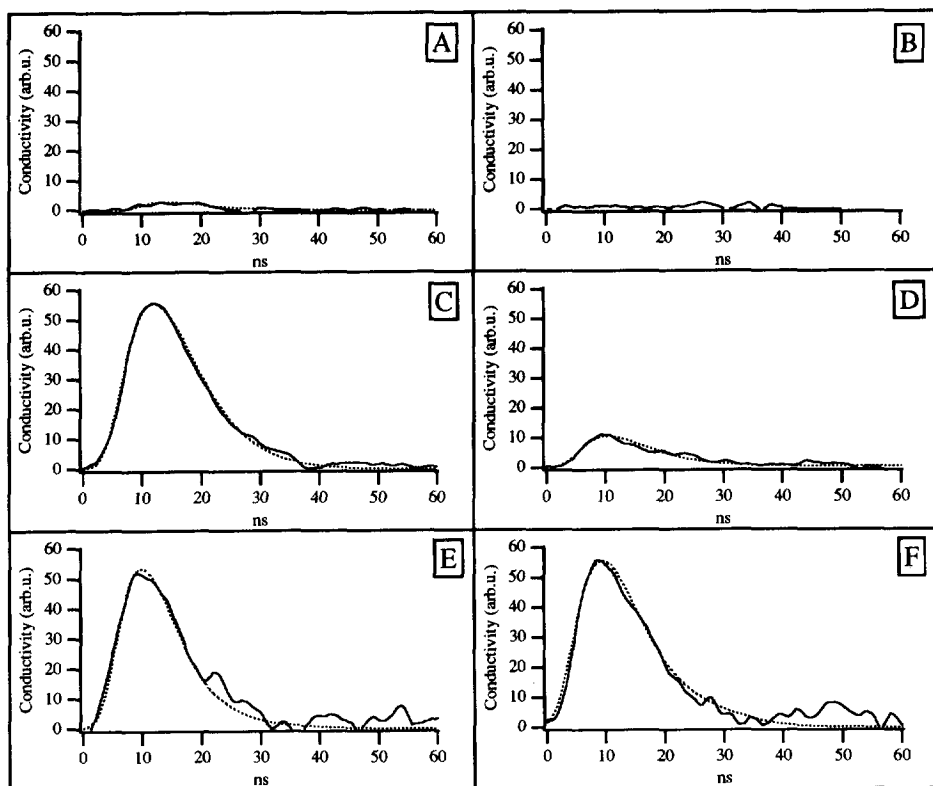
Figure 7.4: *Transient changes in the microwave conductivity (dielectric loss) on flash-photolysis at 308 nm, pulse width 7 ns, of ca 10^{-4} M solutions of: tetraphenylethylene in benzene, trace A; tetraphenylethylene in cyclohexane, trace C; tetraphenylethylene in n-hexane, trace E; tetraphenylethylene in t-decalin, trace F; tetra-p-methoxy-phenylethylene in benzene, trace B; tetra-p-methoxyphenylethylene in cyclohexane, trace D.*

The work of Greene[16] and Schilling and Hilinski[12] using picosecond optical absorption spectroscopy and Morais et al.[13] using picosecond optical calorimetry has provided strong evidence for a zwitterionic nature of the relaxed upper singlet state of TPE in the form of a very pronounced sensitivity of its lifetime to the polarity of the solvent. Of particular relevance was the finding that in all solvents, except saturated hydrocarbons, the lifetimes were only a few hundred picoseconds or less.

Based on the $E_T(30)$[17] parameter for benzene and the correlation found with this parameter by the previous authors,[12,13,16] the expected lifetime in benzene can be estimated to be approximately 200 ps. Such a short lifetime, compared with the 7 ns laser pulse width, would result in a considerably diminished TRMC signal even for a transient with a dipole moment of several debye. For alkane solvents, however, much longer lifetimes of a few nanoseconds have been found. In view of this, it was decided to repeat the TRMC experiments using cyclohexane as a solvent.

As can be seen by trace C in Figure 7.4, the cyclohexane solution of TPE did in fact give a TRMC signal much larger than that found in benzene and well outside of the noise limits of detection. Similar TRMC transients were observed for solutions of TPE in n-hexane and t-decalin, which are also shown in Figure 7.4, traces E and F, respectively. Also, while MeOTPE displayed no detectable dielectric loss at all in benzene, a readily measurable signal was observed in cyclohexane as shown by trace D in Figure 7.4.

We exclude the possibility that the TRMC transients observed are due to multi-photon ionization of the solute on the basis of the relatively low laser pulse intensity. This corresponded to only *ca* 0.3 photons per solute molecule in the irradiated region. Also, if highly mobile electrons did happen to be formed in low yield, multi-photon processes, they would be scavenged within a few tens of picoseconds by the *ca* 10^{-2} molar CO_2 present in the solution.

Therefore we attribute the TRMC transients in the saturated hydrocarbon solutions to the zwitterionic nature of the fully relaxed excited singlet states of TPE and MeOTPE in agreement with the conclusion of previous workers.[12,13,16] The present results thus provide direct, "electrical" confirmation that charge separation can and does occur on photoexcitation of ethylene derivatives even when they have symmetrical ground state configurations.

Interestingly the transients in cyclohexane, n-hexane and t-decalin are equal in intensity, as can be seen in Figure 7.4, traces C, E and F, respectively. This indicates that the dipole relaxation time is viscosity independent.

The TRMC signal follows closely the laser pulse shape convoluted with the instrumental time response of approximately 5 ns. This is in agreement with our expectations if the lifetime of the species responsible is only a few nanoseconds as found for the $^1p^*$ state based on the

work of the previous authors.[12,13,16] Because of the short lifetime, however, quantitative analysis of the TRMC data, which might yield a value for the excited state dipole moment, can only be made if an absolute value of the lifetime is available. The published estimates of the lifetime of the ^{1}p* state of TPE in saturated hydrocarbons show a considerable spread; 1.4 ns,[12] 1.5-1.7 ns,[13] 3.0±0.5 ns.[16] Therefore it was decided to attempt to gain independent information on the lifetime of the ^{1}p* state by single-shot, time-resolved fluorescence measurements, as will be presented in the next section.

7.3 TIME-RESOLVED FLUORESCENCE MEASUREMENTS

7.3.1 Kinetic analysis

In the inset to Figure 7.5A is shown a kinetic trace of the emission from a TPE cyclohexane solution taken at 500 nm. This displays a fast component which follows the pulse shape and a slow component which decays over the first few nanoseconds following the flash. The two components have slightly different spectral characteristics as is shown by the spectra in Figure 7.5A, taken at the peak (in time) of the transient and at a time 1.5 ns later. A shift to longer wavelengths is clearly seen. The bathochromic shift and after-pulse tail are found for all alkane solvents, but are absent for benzene as shown by Figure 7.5B. Solutions in benzene display only a single emission band with a maximum at approximately 490 nm which follows the shape of the laser pulse convoluted with the instrument time response.

Table 7.1: Emission maximum, λ_{max}, lifetime, τ, and quantum yield, Φ, of tetraphenylethylene and the relative dielectric constant and viscosity of the solvents used.

Solvent	ε	η (cP)	λ_{max} (nm)[a]	τ (ps)	$\Phi^c \times 10^4$
n-hexane	1.89	0.31	485	<200	2.3
			530	1800	13.3
cyclohexane	2.02	1.02	495	<200	6.1
			545	1900	10.9
t-decalin	2.17	2.18	500	15[b]	10.0
			545	1900	10.6
benzene	2.28	0.65	485	<200	4.5

(a) Fast and slow decay components separated by kinetic fits to fluorescence transients; both bands had an average fwhm width of 0.65 eV.

(b) Reference 19.

(c) Based on a total (spectrofluorimeter) quantum yield for TPE in cyclohexane of 17.0 x 10^{-4} and the relative areas of time-resolved spectral components.

On kinetic analysis of the data for TPE in the alkane solvents the two spectral components can be resolved into one with a lifetime of less than 200 ps and a maximum at *ca* 490 nm and the other with a lifetime of 1.9 ns and a maximum in the region of 540 nm. The band maxima and quantum efficiencies quoted in the text have been corrected for the spectral response characteristics of the photodiode, the spectral data plotted in Figure 7.5 are raw photodiode outputs. The values of the lifetimes with their emission maxima are listed in Table 7.1. The band

Figure 7.5: *(A) Fluorescence spectra on 337 nm flash-photolysis of a solution of tetraphenylethylene in cyclohexane taken at the maximum (in time) of the transient and 1.5 ns later. Inset: the time-resolved fluorescence emission transient monitored at 500 nm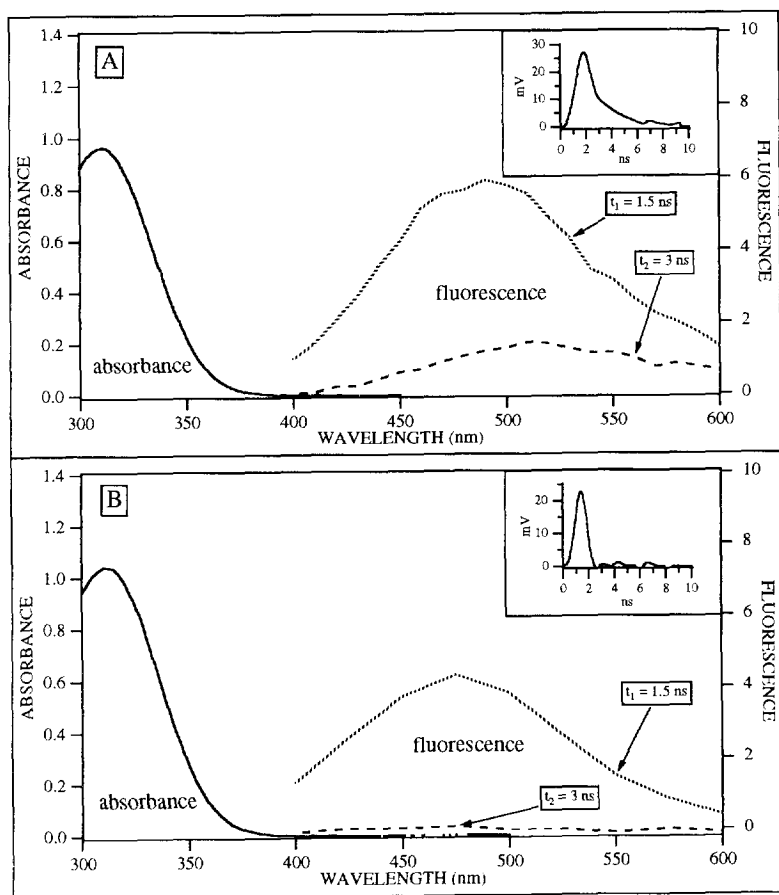. (B) Fluorescence spectra on 337 nm flash-photolysis of a solution of tetraphenylethylene in benzene taken at the maximum (in time) of the transient and 1.5 ns later. Inset: the time-resolved fluorescence emission transient monitored at 480 nm. The spectra shown are experimental data and have not been corrected for the response function of the photodiode detector.*

201

maxima correspond to energies of 2.5 and 2.3 eV. These are to be compared with the first absorption maximum of TPE at 4.0 eV, illustrating the already well-known, large Stokes shift.[18] The quantum yield of the short-lived 490 nm component is found to increase with increasing viscosity of the solvent. This is accompanied by a slight shift in λ_{max} from 485 to 500 nm in going from n-hexane to t-decalin. The 540 nm component is close to viscosity independent both in its quantum yield and lifetime.

The fluorescence band of TPE at *ca* 490 nm is well known from previous work and is attributed to emission from the planar S_1 state. The large Stokes shift is thought to be due to rotation of the phenyl rings from their propeller configuration in the ground state to a close to planar arrangement in the fully relaxed S_1 state. The emission spectrum and decay time are both viscosity dependent.[19-21] It has been suggested, however, that these two effects are most probably due to independent conformational rearrangements.[19] A blue-shift in the spectrum with increasing viscosity has been attributed to increased hindrance to the rotational relaxation of the phenyl groups in the planar configuration. The increase in lifetime and quantum yield with viscosity is attributed to frictional hindrance to the out-of-plane twisting motion around the central C-C bond which leads to formation of the more stable and non fluorescing $^1p*$ state.

The lifetime of the S_1 state of TPE has been determined to be 6 ps and 15 ps for 3-methyl-pentane and t-decalin,[17] respectively, at room temperature. The time resolution of the present measurements was insufficient to be able to determine absolute lifetimes of the "fast", 490 nm component. Its intensity did however increase by a factor of close to 3 on going from n-hexane to cyclohexane and by a further factor of approximately 2 from cyclohexane to t-decalin, in reasonable agreement with the viscosity effect expected, based on the picosecond study. The cyclohexane solution of MeOTPE displayed approximately twice the emission intensity in the 490 nm region than TPE itself, presumably due to the increased lifetime in S_1 resulting from the greater hindrance to twisting caused by the peripheral methoxy groups. The slight red shift with increasing viscosity observed for the rapidly decaying component, could be due to the increased time available for further phenyl group relaxation prior to twisting.

As mentioned above, the intensity and the decay kinetics of the 540 nm emission were found to be almost independent of the alkane used. The lifetimes of 1.8 to 1.9 ns lie within the range of previous estimates for the lifetime of the $^1p*$ state in saturated hydrocarbon solvents given above and are very close to the most recently reported value of 1.7 ns found for methyl-cyclohexane.[22] The fact that no delayed emission is observed for benzene is in agreement with the order of magnitude shorter lifetime expected for the $^1p*$ state in this solvent.

The energy levels of $^1p*$ and the diradicaloid, twisted ground state (^1D) of TPE have been estimated to be 2.90 eV[13] and 1.54 eV[23] with respect to S_0 respectively. Radiative emission

from $^1p*$ would therefore be expected to be situated in the region of 900 nm rather than 500 nm, as found. An explanation for this apparent anomaly, in which the twisted $^1p*$ state of TPE is in equilibrium with the relaxed, planar S_1 state has been proposed recently.[22] The equilibrium lies well to the side of $^1p*$, so that while the emission is characteristic of S_1 it decays with the non-radiative lifetime of the former. This will be discussed further in Section 7.3.2, after considering the fluorescence quantum yields. The situation for TPE, described above is depicted in Figure 7.6.
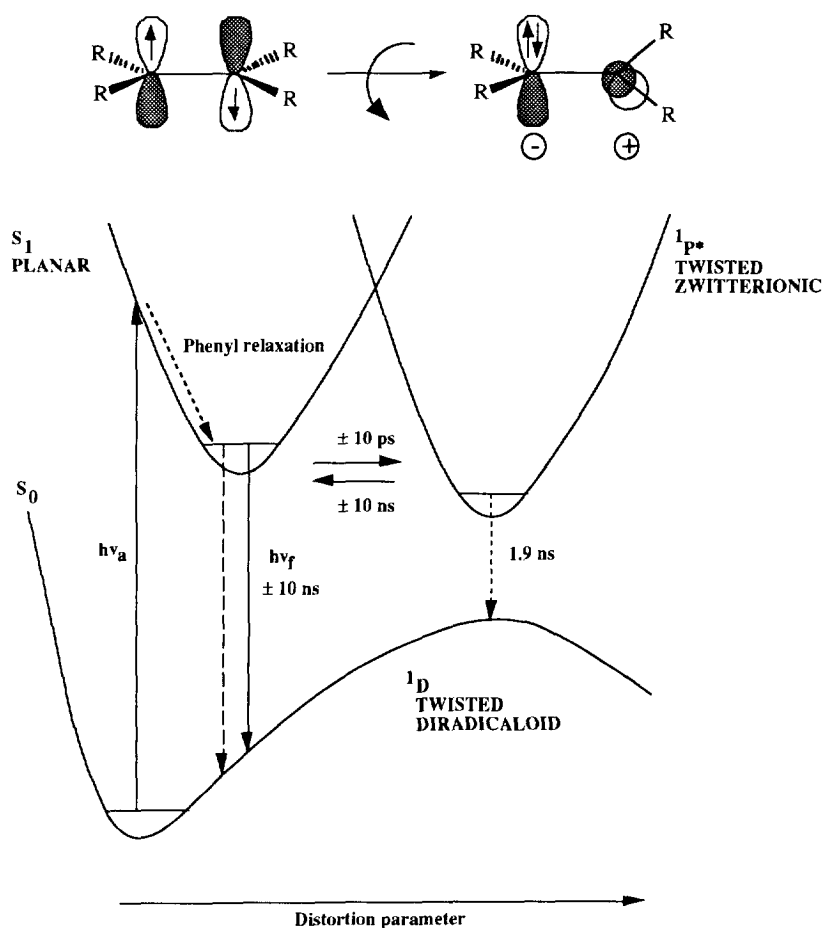

Figure 7.6: Schematic representation of the events taking place after excitation of TPE in cyclohexane.

203

7.3.2 Fluorescence quantum yields

The integrated (390-790 nm) steady-state fluorescence quantum yield of TPE in cyclohexane at room temperature was found to be 17.0×10^{-4}. This is close to the value expected for TPE in a saturated hydrocarbon medium with a viscosity of 1 cP based on previous work.[20] The separate quantum yields of the fast and slowly decaying components were determined, based on the relative values of the products of the intensities and half widths of the individual spectral components derived from a kinetic analysis of the flash-photolysis data. The individual quantum yields are listed in Table 7.1 with their emission maxima.

The quantum yield of the long-lived component is seen to be almost independent of the alkane solvent used and equal to $12 \pm 2 \times 10^{-4}$. The quantum yield of the short-lived, 490 nm emission on the other hand increases substantially with increasing viscosity as mentioned above from 2.3×10^{-4} for n-hexane ($\eta = 0.31$ cP) to 10.0×10^{-4} for t-decalin ($\eta = 2.2$ cP) with benzene ($\eta = 0.65$ cP) lying between n-hexane and cyclohexane ($= 1.02$ cP) as would be expected.

Taking the lifetime of 15 ps for S_1 in t-decalin[19] to be controlled almost exclusively by radiationless internal conversion to $^1p*$, then the natural radiative lifetime of S_1 can be estimated from the fluorescence quantum yield of 10×10^{-4} to be *ca* 15 ns. This is close to the values of several nanoseconds found for the lifetime of S_1 in rigid media,[21] where a quantum efficiency of fluorescence approaching unity is found.

If the same radiative lifetime applies to those planar S_1 states in equilibrium with $^1p*$ during its decay then the fraction of S_1 in the equilibrium can be estimated to be 0.0095. This corresponds to a free energy difference of 0.12 eV between the $^1p*$ and fully relaxed S_1 state; close to the value of 0.11 eV recently obtained by Ma and Zimmt.[22] This difference would be expected to be considerably larger in more polar solvents, or pseudo-polar solvents such as benzene. This, together with the much reduced lifetime of $^1p*$, would explain the lack of observation of delayed S_1 fluorescence in anything but completely nonpolar solvents.

7.4 QUANTITATIVE TRMC RESULTS

7.4.1 The excited state dipole moment

The lifetime of the planar S_1 state with respect to twisting of *ca* 10 ps is sufficiently short to ensure that it could not be responsible for the TRMC transient observed. Furthermore the S_1 lifetime is approximately three orders of magnitude shorter than the mean time for the S_1 to S_0 transition. Therefore the quantum yield for formation of the $^1p*$ state, which is the remaining potential source of the dielectric loss, can be taken to be effectively unity. Taking the $^1p*$ state lifetime to be equal to the lifetime determined from the fluorescence decay we can determine the

parameter $\mu_S^2 F(\omega\Theta)/\Theta$ from the absolute magnitude of the microwave conductivity transients (see Table 7.2). Inclusion in the data analysis of the very small fraction of a non-dipolar S_1 component in equilibrium with $^1p^*$ would result in a correction of less than 1%. In order to derive the excited state dipole moment a knowledge of the dipole relaxation time, Θ, is required.

For the dipolar excited states of donor-acceptor compounds dipole relaxation is controlled usually by molecular rotation. The timescale of relaxation is then expected to be close to linearly dependent on the solvent viscosity. The simplest theoretical expression which allows a quantitative estimate of the rotational relaxation time, Θ_R, is that due to Stokes for a spherical rotor in a medium of viscosity η (see Chapter 2):

$$\Theta_R = V\eta/k_B T \tag{1}$$

Taking a molecular density of 1.2 g/cm^3 together with a molecular weight of 332 for TPE and the known solvent viscosities, the values of Θ_R shown in Table 7.2 are calculated. The dipole moments obtained, assuming $\Theta = \Theta_R$, are also listed in Table 7.2.

Table 7.2: *Lifetime of the $^1p^*$ (phantom) state, τ_S; rotational relaxation time, Θ_R; conductivity parameter, $\mu_S^2 F(\omega\Theta)/\Theta$; calculated dipole moments using the rotational relaxation time, the reciprocal of the microwave frequency and a flip-flop dipole relaxation time of 10 ps.*

Solvent	τ_S	Θ_R a	$\mu_S^2 F(\omega\Theta)/\Theta$	μ_S (D)b		
	(ns)	(ps)	(D^2/ps)	$\Theta = \Theta_R$	$\Theta = 1/\omega$ (15 ps)	$\Theta_I = 10$ ps
n-hexane	1.8	35	35	9.0	7.8	8.6
⁄clohexane	1.9	115	115	13.5	7	7.6
t-decaline	1.9	241	241	22.0	8.1	8.7
benzene	≤ 0.2	83	83	≥ 10.0	≥ 6.0	≥ 7.0

(a) Based on Stokes equation for a sphere of density 1.2 g/cm^3.
(b) the last column is for $1/\Theta = 1/\Theta_R + 1/\Theta_I$.

Dipole moments of 9.0, 13.5 and 22.0 D are calculated on this basis for the $^1p^*$ state dipole moment in n-hexane, cyclohexane and t-decalin respectively. These values are very large with the value in t-decalin corresponding to complete charge separation over a distance of 4.5 Å , i.e. approximately 3 times the length of a C-C bond. Corrections to Θ_R for the non-spherical (more

closely oblate ellipsoidal) shape of TPE would result (see Chapter 2), if anything, in longer relaxation times[24] and correspondingly larger values of the dipole moments calculated. In addition to the unexpectedly large magnitude of μ_S, its marked solvent dependence based on $\Theta = \Theta_R$ is most unusual and highly unlikely.

These results can be explained by taking into account that dipole relaxation can occur in such a basically symmetrical system by rapid charge inversion between the two energetically equivalent zwitterionic states. Since this flip-flop type of process probably involves only small conformational changes it would be expected to be much less sensitive to the viscosity of the medium than molecular rotation.

If both rotation and inversion are operative then the overal dipole relaxation time is given by:[25,26]

$$1/\Theta = 1/\Theta_R + 1/\Theta_I \qquad (5)$$

In Table 7.2, we list the values of the dipole moment calculated taking a charge inversion time of 10 ps, similar to that proposed for dipole inversion for bianthryl,[26] together with the rotational relaxation times listed. While there is some spread in the values, the differences are seen to be much smaller than when $\Theta = \Theta_R$ is used. If Θ_I were to be as short as 3 ps then the dipole moments determined from the present data would be closer to 14 D. It is perhaps worth mentioning that $\Theta_I = 1/2k_I$ where k_I is the rate constant for the forward and backward charge exchange processes.[25]

It is possible to obtain the minimum value of the dipole moment by taking $\Theta = 1/\omega$. These values are also listed in Table 7.2. The data indicate that the dipole moment of the individual zwitterionic states must be at least *ca* 7.5 D. This is somewhat larger than the value of 6 D estimated on the basis of the solvent dependence of the $^1p^*$ state energy.[13] If the dipole relaxation time is either shorter or longer than $1/\omega$ larger dipole moments than obtained for $\Theta = 1/\omega$ will be derived.

The eventual value of the dipole moment determined is relatively insensitive to the lifetime used in fitting the kinetic traces. For transients with lifetimes less than the pulse width the eventual dipole moment derived is inversely proportional to the square root of the lifetime. If we take the extreme limits reported in the literature for the lifetime of the $^1p^*$ state of TPE from 1.4 to 3 ns, mentioned previously, then minimum μ_S values of 9 and 6 D, respectively, would be calculated from the TRMC transients rather than the value of 7.5 D based on our own lifetime determination of 1.9 ns.

7.4.2 The excited state polarizability

Because of the theoretical importance of the sudden polarization phenomenon we have carried out further experiments on flash-photolysed TPE alkane solutions, using the extension of the TRMC technique introduced in Chapter 2, whereby changes in both the real and imaginary components of the microwave permittivity can be monitored.[27] Futher details are presented in Chapter 8.

The sum of the transients taken at f_- and f_+, $\Sigma_\pm$, is a function only of the change in the dielectric loss;

$$\Sigma_\pm = -2B\Delta\varepsilon'' \tag{2}$$

and the difference, $\Delta_\pm$, is sensitive only to changes occurring in the microwave dielectric constant;

$$\Delta_\pm = -2C\Delta\varepsilon' \tag{3}$$

The importance of being able to monitor separately the changes in both components of the permittivity lies in the relationship (4), which applies for the formation of a dipolar transient with a single dipole relaxation time, Θ:

$$\Delta\varepsilon'/\Delta\varepsilon'' = 1/(\omega\Theta) \tag{4}$$

Therefore, if the dipole relaxation time is much longer than the reciprocal radian frequency of the microwaves, $1/\omega$ (*ca* 15 ps), $\Delta\varepsilon'$ will be small relative to $\Delta\varepsilon''$. This should then be reflected in a much lower $\Delta_\pm$ than $\Sigma_\pm$ transient.

In the absence of internal modes of dipole relaxation, Θ will be controlled by rotation of the molecules with a characteristic rotational relaxation time Θ_R. For molecules of molecular weight larger than 300, Θ_R will fulfill the condition $\Theta_R \gg 15$ ps even for a spherical molecular geometry.[27] Therefore, if rotational diffusion is the controlling process in dipole relaxation, one would expect the $\Delta_\pm$ transient to be considerably smaller than $\Sigma_\pm$. This is shown to be the case in Figure 7.7A for the Paddon-Row 6 sigma-bond compound, PR-6σ. For this molecule relaxation of the giant dipole state formed by long-distance electron transfer subsequent to photoexcitation[28,29] can only occur by long-axis tumbling. The small, remaining transient in this case is in fact thought to be due mainly to a slightly unsymmetrical cavity resonance.
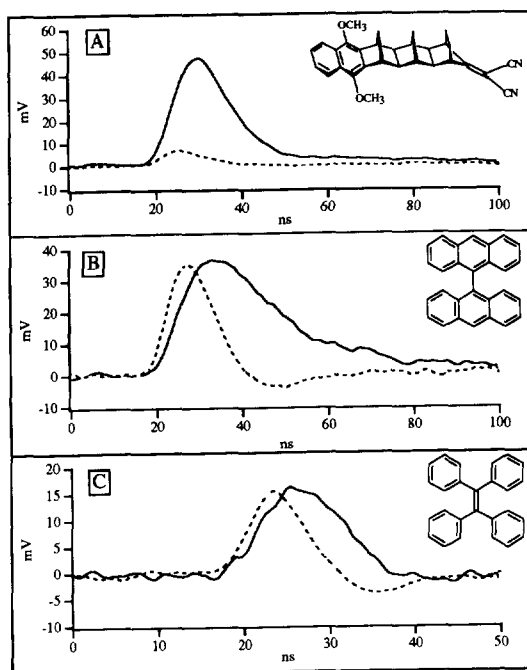
Figure 7.7: *The sum, Σ_+, (full line) and difference, Δ_+, (dashed line) TRMC transients taken at the half-power cavity resonance frequencies for 308 nm flash-photolysed solutions of (A) the Paddon-Row 6 σ-bond compound in benzene; (B) 9,9'-bianthryl in benzene (middle); and (C) tetraphenylethylene in cyclohexane (bottom). Σ_+ is proportional to the change in the dielectric loss, ε'', and Δ_+ is a function of the change in the microwave dielectric constant, ε'.*

In contrast bianthryl, which is a molecule of similar molecular weight to PR-6σ, displays a large Δ_+ transient, of comparable magnitude to Σ_+, as seen in Figure 7.7B. This clearly indicates the occurrence of a large change in polarizability, $\Delta\alpha$, of the molecule in the relaxed S_1 state. These results are in agreement with the work of Fessenden et al.[26] who interpreted the large $\Delta\alpha$ in terms of a flip-flop dipole relaxation time of 9.2 ps.

In Figure 7.7C the results are shown for TPE in cyclohexane. As for bianthryl, a large Δ_+ transient is observed. The relative magnitudes of the Δ_+ and Σ_+ transients are in fact very similar to those for bianthryl, indicating a polarizability change of similar magnitude. If we interpret $\Delta\alpha$ as resulting only from rapid dipole relaxation then, on the basis of equation (4), the off-resonance results would indicate Θ for TPE to be close to the value derived by Fessenden for bianthryl, in agreement with the conclusion reached in the previous section that $\Theta \approx 1/\omega = 15$ ps.

As is discussed in more detail in the next chapter, we consider now that the interpretation of the large change in polarizability for bianthryl in terms of dipole relaxation alone is most probably incorrect. This is based on the fact that the polarizability change found in the microwave experiments of Fessenden is similar in magnitude to that found in the electro-optical fluorescence experiments of Baumann.[30] The latter technique should be insensitive to polarizability changes due to dipole relaxation, $\Delta\alpha_D$, and reflect only changes in the electronic polarizability, $\Delta\alpha_e$. There remains therefore little room for a large contribution to $\Delta\alpha$ from $\Delta\alpha_D$ and a much longer dipole relaxation time for the S_1 state of bianthryl is indicated than the 9.2 ps initially calculated.

No electro-optical experiments, similar to those for bianthryl have been carried out for TPE. Such experiments would in fact be extremely difficult in view of the very low quantum yields of fluorescence. It is therefore not possible to decide whether the large $\Delta\alpha$ for TPE is also a result of an abnormally large electronic polarizability of $^1p^*$ or can be attributed mainly to rapid dipole relaxation as suggested in the previous section.

A fuller discussion of this aspect of the data will have to await a quantitative treatment of the $\Delta_{\pm}$ transients. Unfortunately this is not as yet possible for transients for which the lifetime is of the same order of magnitude as the response time of the cavity. A subsequent quantitative analysis of changes in ε' should in principle not effect the conclusions about flip-flop switching based on changes in the dielectric loss. Also, the minimum dipole moment values calculated on the basis of $\Theta = 1/\omega$ will remain unchanged.

7.5 SUMMARY

Photoexcitation of the symmetrical molecules TPE and MeOTPE dissolved in saturated hydrocarbon solvents results in changes in both the real, ε', and the imaginary, ε'', components of the complex permitivitty of the solutions. The change in ε'' (the dielectric loss) provides evidence for the dipolar, or "zwitterionic", nature of the twisted $^1p^*$ phantom state formed from S_1 by rotation around the central carbon-carbon bond. A minimum dipole moment of *ca* 7.5 D for the individual resonance states is found. Dipole relaxation occurs by intramolecular flip-flop exchange between the zwitterionic structures on a timescale close to $1/\omega$, i.e. *ca* 15 ps.

The fluorescence of TPE in alkane solvents has two decay components, one with a decay time less than 200 ps and a second with a decay time of 1.9 ns. The former ($\lambda_{max} \approx 490$ nm) is assigned to emission from the partially relaxed S_1 state prior to twisting. The latter ($\lambda_{max} \approx 540$ nm) is assigned to emission from a small, *ca* 1%, concentration of the relaxed S_1 state in equilibrium with the $^1p^*$ state in saturated hydrocarbon solvents.

7.6 ACKNOWLEDGEMENT

7.7 REFERENCES

1. W. Schuddeboom, S.A. Jonker, J.M. Warman, M.P. de Haas, M.J.W. Vermeulen, W.F. Jager, B. de Lange, B.L. Feringa and R.W. Fessenden, *J. Am. Chem. Soc.* **1993**, *115*, 3286-3290.
2. V. Bonacic-Koutecky, P. Bruckmann, P. Hiberty, J. Koutecky, C. Leforestier and L. Salem, *Angew. Chem., Int. Ed. Engl.* **1975**, *14*, 575-576.
3. L. Salem and P. Bruckmann, *Nature* **1975**, *258*, 526-528.
4. L. Salem, *Science* **1979**, *191*, 822-830.
5. R.J. Beunker, S.D. Peyerimhoff, *Chem. Phys.* **1976**, *9*, 75-89.
6. V. Bonacic-Koutecky, *J. Am. Chem. Soc.* **1978**, *100*, 396-402.
7. V. Bonacic-Koutecky, J. Cizek, D. Dohnert and J. Koutecky, *J. Chem. Phys.* **1978**, *69*, 1168-1176.
8. B.R. Brooks and H.F. Schaefer, *J. Am. Chem. Soc.* **1979**, *101*, 307-311.
9. I. Nebot-Gil and J-P. Malrieu, *Chem. Phys. Letters* **1981**, *84*, 571-574.
10. I. Nebot-Gil and J-P. Malrieu, *J. Am. Chem. Soc.* **1982**, *104*, 3320-3325.
11. V. Bonacic-Koutecky, J. Koutecky and J. Michl, *Angew. Chem., Int. Ed. Engl.* **1987**, *26*, 170-189.
12. C.L. Schilling and E.F. Hilinski, *J. Am. Chem. Soc.* **1988**, *110*, 2296-2298.
13. J. Morais, J. Ma and M.B. Zimmt, *J. Phys. Chem.* **1991**, *95*, 3885-3888.
14. J.F. Rabek in *Progress in Photochemistry and Photophysics;* CRC Press: Boca Raton, **1992**; Vol. VI, Chapter 3
15. C.E. Wulfman and S. Kumei, *Science* **1971**, *172*, 1061.
16. B.I. Greene, *Chem. Phys. Lett.* **1981**, *79*, 51-53.
17. C. Reichardt, *Solvent Effects in Organic Chemistry;* Verlag Chemie: Weinheim, New York, **1979**.
18. H. Stegemeyer, *Ber. Bunsenges. Phys. Chem.* **1972**, *72*, 335-340.
19. P.F. Barbara, S.D. Rand and P.M. Rentzepis, *J. Am. Chem. Soc.* **1981**, *103*, 2156-2162.
20. S. Sharafy and K.A. Muszkat, *J. Am. Chem. Soc.* **1971**, *93*, 4119-4125.
21. N.H. Klingenberg, E. Lippert and W. Rapp, *Chem. Phys. Lett.* **1973**, *18*, 417-419.
22. J. Ma and M.B. Zimmt, *J. Am. Chem. Soc.* **1992**, *114*, 9723-9725.
23. W.J. Leigh and D.R. Arnold, *Can. J. Chem.* **1981**, *59*, 609-620.
24. T. Tao, *Biopolymers* **1969**, *8*, 609-632.
25. G. Williams, *Trans. Farad. Soc.* **1968**, *64*, 1219-1227.
26. D.B. Toublanc, R.W. Fessenden and A. Hitachi, *J. Phys. Chem.* **1989**, *93*, 2893-2896.
27. J.M. Warman, W. Schuddeboom, S.A. Jonker, M.P. de Haas, M.N. Paddon-Row, K.A. Zachariasse and J.P. Launay, *Chem. Phys. Lett.* **1993**, *210*, 397-403.
28. J.M. Warman, M.P. de Haas, M.N. Paddon-Row, E. Cotsaris, N.S. Hush, H. Oevering and J.W. Verhoeven, *Nature* **1986**, *320*, 615-616.
29. J.M. Warman, K.J. Smit, M.P. de Haas, S.A. Jonker, M.N. Paddon-Row, A.M. Oliver, J. Kroon, H. Oevering and J.W. Verhoeven, *J. Phys. Chem.* **1991**, *95*, 1979.
30. W. Baumann, E. Spohr, H. Bischof and W. Liptay, *J. Luminesc.* **1987**, *37*, 227-233.

Chapter 8

Polarization and Polarizability

in the Excited States

of Symmetrical Molecules[1-3]

8.1 INTRODUCTION

In this chapter we have studied charge separation in 2- and 3-fold symmetrical donor-acceptor compounds as well as in a series of homosymmetric or "neutral" biaryls, with no specific donor and/or acceptor sites. The occurrence of charge separation (CS) in symmetrical molecules is an intriguing and perhaps surprising phenomenon, especially in the homo-symmetric molecules. Intuitively molecules with two- or higher fold D_n symmetry are expected to be non-dipolar. This is invariably found to be the case for molecules in their ground electronic state. There is experimental evidence, however, that this axiom does not always apply to molecules in their excited states. The dipolar nature of the S_1 state of 9,9'-bianthryl, first proposed more than 25 years ago by Schneider and Lippert,[4,5] has been conclusively substantiated in many subsequent investigations.[6-19] Bianthryl was until recently, however, the only well established case of symmetry breaking. Evidence that both S_1 and T_1 states of other symmetrical molecules are dipolar has however gradually accumulated.[1,20-23] Of particular interest was the finding by Ledoux et al.[23] of a large, second-order non-linear-optical (NLO) effect for 1,3,5-trinitro-2,4,6-triamino-benzene, indicating the S_1 state of this 3-fold symmetrical molecule to be dipolar in character. As pointed out,[23,24] this could have important consequences for the design of molecular NLO materials and has led to a surge of interest in the nature of the excited states of centro-symmetric molecules.[24-27]

8.1.1 Symmetry breaking and excitonic interactions

To allow charge separation to occur in symmetrical molecules, a lowering of the symmetry is required, to obtain a certain degree of orbital localization. A geometrical distortion, such as twisting is often sufficient to achieve decoupling of the symmetrical electronic moieties involved in the charge separation process. For example orbital localization of the two orthogonal π-orbitals in tetraphenylethylene is necessary for the occurrence of the "sudden-polarization" effect (see Chapter 7), in which a zwitterionic state is formed.[28-30] This orbital localization is achieved by pyramidalization at one of the carbons.[20] Symmetry breaking can be brought about also by the solvent, by charge in the neighborhood, by chemical substitution or,

211

importantly, by nontotally symmetric vibrations. Interestingly due to the last point even an isolated "symmetrical" molecule such as ethylene rarely has a perfect symmetric configuration, because it spends most of its time close to the classical turning points of vibrations which correspond to symmetry reduced geometries.

In a system of N noninteracting chromophores, with one chromophore raised to an excited state, the energy of the system would be unchanged by transferring the excitation to any other chromophore in the system.[31] In a real system, however, the small but finite interchromophore interactions remove this N-fold degeneracy since it is impossible to construct a stationary state for the system wherein only one selected chromophore is excited. The correct zero-order states for the system with one quantum of electronic excitation correspond to a delocalization of the energy over all chromophores.[32,33] Förster[34] refers to this as the "non-additivity of excited state properties". The phenomenon is known as a molecular exciton interaction.

As proposed by Förster[34,35] and Simpson and Peterson[36] it is convenient to categorize the interaction into three cases. In case A, the strong coupling regime, the rate of excitation transfer between the chromophores is much larger than the frequency of molecular vibrations. This results in a delocalization of the excitation over the entire system. Major differences, such as shifts or splittings, between the absorption spectra of the interacting system and an isolated chromophore are observed. Case B, the weak coupling case, exhibits less profound spectral perturbations, and the rate of energy transfer is comparable to the frequency of molecular vibrations. In case C, the very weak coupling limit, little or no difference exists between the electronic absorption spectra of the isolated and interacting systems. To a reasonable approximation the electronic excitation may be regarded as being temporarily localized on one chromophore. Observed effects may then be interpreted in terms of intramolecular excitation transfer.

8.1.2 Changes in $\Delta\varepsilon$" and $\Delta\varepsilon$'

Until recently,[1] the TRMC technique has involved measurement of only the change in the imaginary (conductivity or dielectric loss) component, ε", of the complex permittivity, ε^*. The derivation of μ_* from measurements of $\Delta\varepsilon$" alone requires, amongst other things, a knowledge of Θ, see Chapter 2. Usually Θ has been identified with the rotational relaxation time perpendicular to the dipolar axis, Θ_R, which has been taken to be equal to either the known value of Θ_R for the ground state molecule or values calculated using theoretical or semi-empirical expressions for the rotational relaxation time.

A change in the dipole moment of solute molecules on photoexcitation will always result in a change in the real (dielectric constant) component, ε', of the permittivity as well as in ε". If no

change in the electronic polarizability of the molecules, $\Delta\alpha_e$, occurs the ratio $\Delta\varepsilon''/\Delta\varepsilon'$ is directly related to the dipole relaxation time, Θ, by:

$$\Delta\varepsilon''/\Delta\varepsilon' = \omega\Theta \tag{1}$$

Since the reciprocal radian frequency, ω, of X-band microwaves is *ca* 15 ps, a measurement of $\Delta\varepsilon''/\Delta\varepsilon'$ can yield information on molecular relaxation processes occurring on a picosecond timescale.

An important development introduced by Fessenden[15,37] was the capability of monitoring the phase shift in the reflected wave on flash-photolysis. In this way information could be gained on changes in the real component of the permittivity and the ratio $\Delta\varepsilon''/\Delta\varepsilon'$ could be determined. Findings of far reaching importance in the measurements of Fessenden were that the values of Θ for the triplet state of 4,4'-bis(dimethylamino)benzophenone (Michler's ketone)[37] and the S_1 state of bianthryl[15] (molecular structures shown in Figures 8.4 and 8.12, respectively) were much shorter, than the estimated rotational relaxation times of the molecules. This was interpreted as being due to an additional, intramolecular dipole relaxation process involving interchange between two, mirror image dipolar resonance structures of these molecules, both of which have an axis of symmetry. This so called flip-flop mechanism is illustrated schematically for a molecule of the donor-acceptor-donor type in Figure 8.1.
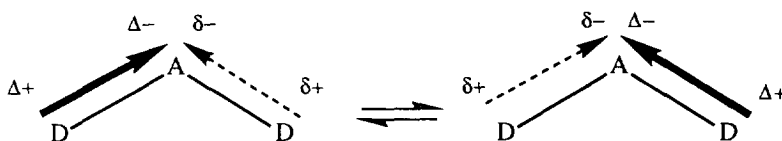
Figure 8.1: Schematic representation of the flip-flop mechanism for a DAD molecule.

If this "flip-flop" dipole inversion is operative with a mean time of Θ_I, then the overall time for dipole relaxation (assuming exponential relaxation processes) will be given by:[38]

$$1/\Theta = 1/\Theta_R + 1/\Theta_I \tag{2}$$

The mean times for the flip-flop inversion processes, Θ_I, were determined to be 7.7 ps[37] and 9.2 ps[15] for Michler's ketone and bianthryl, respectively, in benzene at room temperature.

In the next section we show how the TRMC technique can also be applied to the concurrent measurements of $\Delta\varepsilon'$, by monitoring the reflected power at frequencies other than the resonance frequency of the microwave cavity used. In this way it is possible to monitor effects resulting from picosecond timescale dipole switching and electronic polarizability changes in the excited states of molecules using a single measurement technique.

8.1.3 Off-resonance TRMC measurements

Basically, changes in the microwave power reflected by a microwave resonant cavity containing the solution of interest are monitored with nanosecond time resolution during and after laser flash-photolysis of the solution. The present work differs from previous TRMC experiments in that transient changes in reflected power are made not just at the resonance frequency of the cavity (*ca* 9.4 GHz in the present work), but also at the upper and lower "half-power" frequencies. These are shown as f_+ and f_- in Figure 8.2, which is an ideal cavity resonance curve at close to the resonance frequency, f_0. These measurements contain information on changes occurring in both the real and the imaginary components of the permittivity of the solution. For an overcoupled cavity, a small increase in the dielectric loss of the medium, $\Delta\varepsilon''$, results in a general deepening of the resonance. An increase in the dielectric constant, $\Delta\varepsilon'$, results in an overall shift to lower frequencies.

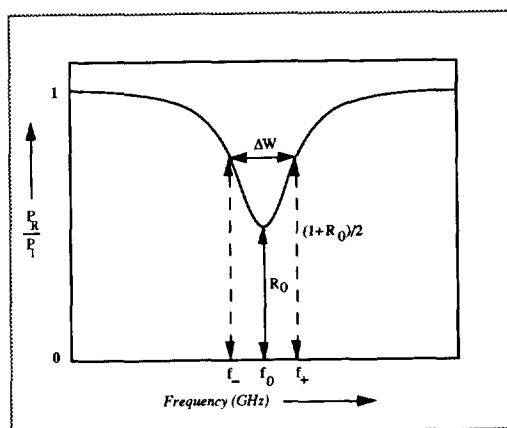*Figure 8.2: Dependence of the power reflected by a resonant cavity on frequencies at close to resonance. The curve is characterized by the 3 parameters: f_0 (the resonance frequency) which is the frequency at which the minimum in R(f) occurs; R_0, the fraction of power reflected at resonance; and ΔW, the full width of the resonance curve at the half-resonance frequencies for which R(f) = [R_0 + 1]/2.*

At resonance the reflected power is sensitive only to changes in ε'', according to the relationship derived in Section 2.4.4 of Chapter 2:

$$(\Delta P_R/P_R)_0 = -2Q_L(1 + 1/\sqrt{R_0})\Delta\varepsilon''/\varepsilon' \tag{3}$$

In equation (3), R_0 is the fraction of the incident power reflected at the resonance frequency and Q_L is the loaded quality factor of the cavity, which is related to the full width at half minimum of the resonance, $\Delta W = f_+ - f_-$, by $Q_L = f_0/\Delta W$. The following relationships between the change in power reflected at the upper and lower half-power frequencies, $f_\pm = f_0 \pm \Delta W/2$, and small changes in the real and imaginary components of the permittivity have been derived:

$$(\Delta P_R/P_R)_+ = +Q_L(1 - R_0)\Delta\varepsilon' / (1 + R_0)\varepsilon' - Q_L(1 + \sqrt{R_0})^2\Delta\varepsilon'' / (1 + R_0)\varepsilon' \tag{4}$$

$$(\Delta P_R/P_R)_- = -Q_L(1 - R_0)\Delta\varepsilon' / (1 + R_0)\varepsilon' - Q_L(1 + \sqrt{R_0})^2\Delta\varepsilon'' / (1 + R_0)\varepsilon' \tag{5}$$

As can be seen in equations (4) and (5), the contribution of $\Delta\varepsilon''$ has the same sign at both frequencies, while that for $\Delta\varepsilon'$ is of opposite sign. Separate effects due to each component can be obtained therefore by taking the sum and the difference of the half-power signals, i.e.:

$$\begin{aligned}\Sigma_\pm(\Delta P_R/P_R) &= (\Delta P_R/P_R)_- + (\Delta P_R/P_R)_+ \\ &= -2Q_L(1 + \sqrt{R_0})^2\Delta\varepsilon'' / (1 + R_0)\varepsilon' \end{aligned} \tag{6}$$

and $$\begin{aligned}\Delta_\pm(\Delta P_R/P_R) &= (\Delta P_R/P_R)_- - (\Delta P_R/P_R)_+ \\ &= -2Q_L(1 - R_0)\Delta\varepsilon' / (1 + R_0)\varepsilon' \end{aligned} \tag{7}$$

For the particular cavity used in the present work filled with benzene, R_0 is close to 0.5. The sensitivity of the technique towards changes in ε' is therefore seen to be a factor of approximately 6 lower than for changes in ε''.

From equations (6) and (7), the ratio of the change in the dielectric loss to the change in the "dielectric constant" can be determined from the half-resonance signals according to:

$$\Delta\varepsilon''/\Delta\varepsilon' = (1 - \sqrt{R_0})\Sigma_\pm / (1 + \sqrt{R_0})\Delta_\pm \tag{8}$$

In equation (8), $\Sigma_\pm$ and $\Delta_\pm$ are used as shorthand symbols for the left-hand side quantities of equations (6) and (7). According to equations (1) and (8), therefore, the dipole relaxation time,

Θ, will be given by:

$$\Theta = (1 - \sqrt{R_0})\Sigma_\pm / (1 + \sqrt{R_0})\omega\Delta_\pm \qquad (9)$$

If more than one relaxation process contributes to Θ, then it is the rates rather than the lifetimes, that are additive, i.e. $\Theta^{-1} = \Sigma_j\Theta_j^{-1}$. Therefore the experimental parameter $\Delta_\pm/\Sigma_\pm$ is proportional to the total rate of dipole relaxation.

As can be seen from equation (1), if Θ is much larger than $1/\omega$, then terms in $\Delta\epsilon'$ in equations (4) and (5) will become relatively very small and the transients observed at the upper and lower half-power frequencies should be similar in magnitude and form. This behaviour is illustrated for the formation of the long-lived giant dipole state of the Paddon-Row 12-sigma bond donor-acceptor compound in Figure 8.3. The transient species responsible for the signal in this case is the completely charge separated state formed by long-distance electron transfer subsequent to local excitation of the donor moiety.[39-42] Dipole relaxation for this molecule can only occur by end-to-end tumbling which is estimated to occur on a timescale of 1600 ps for this high molecular weight, rod-shaped molecule. Even if the rotation time is calculated for a spherical geometry, a value an order of magnitude larger than $1/\omega$ is found. The change in ϵ' in this case should therefore be very small and $\Delta_\pm/\Sigma_\pm$ should be close to zero.

In fact, as can be seen in Figure 8.3, the signal obtained at f_- is slightly larger than at f_+ and corresponds to $\Delta_\pm/\Sigma_\pm \approx 0.07$. In general we have found a limiting value of $\Delta_\pm/\Sigma_\pm$ in the range

Transients at f_0, f_- and f_+   **Calculated sum $\Sigma_\pm$ and difference $\Delta_\pm$**
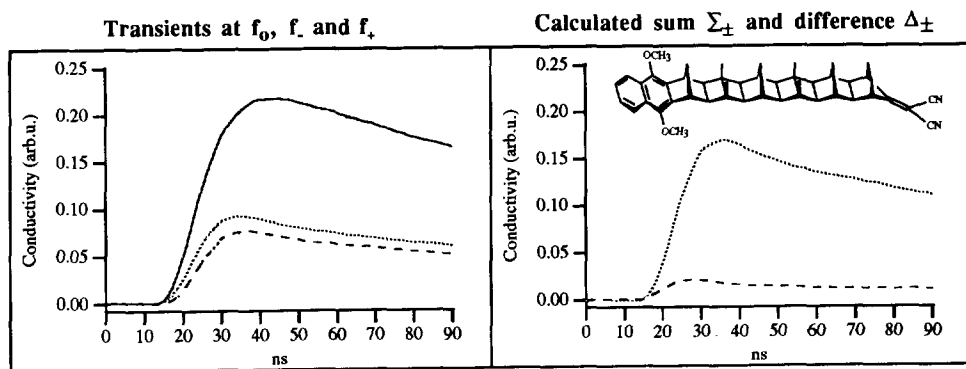
Figure 8.3: On the left hand side is shown the TRMC transient observed on flash-photolysis of the reference Paddon-Row 12 σ-bond compound in benzene, monitored at the cavity resonance frequency, f_0, (full line), and at the upper, f_+ (dashed), and lower, f_- (dotted), half-power frequencies. On the right hand side is shown the sum, $\Sigma_\pm$ (dotted), and difference, $\Delta_\pm$ (dashed), combinations of the transients monitored at the half-power frequencies for the traces on the left. $\Sigma_\pm$ is proportional to ϵ'' and $\Delta_\pm$ is a function of ϵ'.

0.07±0.02 for all donor-acceptor compounds for which $\Delta_{\pm}/\Sigma_{\pm}$ would in fact have been expected to be close to zero. This residual effect could be due to the cavity used not having an ideal symmetrical resonance. It is also possible that changes in the electronic polarizability of the molecules results in a change in ε' in addition to that due to dipole relaxation. This will be discussed more fully in a later section.

Equations (4) and (5) are "steady-state" expressions, valid for times much longer than the reponse time of the microwave cavity, τ_C. At resonance the response time is $Q_L/\pi f_0$ which for the present cavity is approximately 5 ns when the cell is filled with benzene. When changes in both ε' and ε'' occur on a timescale comparable with or shorter than τ_C, complex effects are observed due to the phase and amplitude changes being out of synchronisation. Such effects are apparent, for example, in Figures 8.4 and 8.12 for Michler's ketone and bianthryl, respectively, at short times. One can clearly see that initially the f_- transient rises even more rapidly than the trace taken at resonance while the f_+ transient has an initial period in which it is actually negative going. These effects remain at present simply a semi-quantitative indication of the relative magnitude of changes occurring in ε' and hence the relevant value of Θ. For example an initially negative going TRMC signal at f_+ is almost certainly an indication of a dipole relaxation time close to or shorter than the reciprocal radian frequency of 15 ps. We are at present attempting to develope a fitting procedure that will take this into account quantitatively.

8.2 DONOR-ACCEPTOR COMPOUNDS WITH TWO-FOLD SYMMETRY

In the next sections we have investigated two-fold symmetrical donor-acceptor compounds of the type donor-acceptor-donor (DAD) and acceptor-donor-donor-acceptor (ADDA). The ADDA molecules differ from the DAD molecules, in that the flip-flop interchange is between two decoupled pairs of chrompohores, while the chrompohores are at least partially coupled in the latter molecules.

8.2.1 Donor-acceptor-donor molecules (DAD)

In Figure 8.4 are shown the TRMC transients taken at f_0, f_+ and f_-, together with the calculated sum, Σ_+ and difference, Δ_+, for Michler's ketone, and two asymmetrical DA model compounds N,N-dimethylaminobenzonitrile (DMABN) and N,N-dimethylaminonitrobenzene (DMANB). Also depicted are the transients for 9-oxofluorenone (fluorenone). Michler's ketone, DMABN and DMANB, as well as fluorenone form long-lived triplet states on photoexcitation. Readily apparent from the TRMC signals at long times is the much larger difference between the high and low frequency signals for Michler's ketone. Even without a quantitative interpretation of the results this shows immediately that the relative change in ε' is much larger

Transients at f₀, f₋ and f₊   Calculated sum Σ± and difference Δ±

Figure 8.4: *On the left hand side are shown the TRMC transient observed on flash-photolysis of the compounds shown in benzene, monitored at the cavity resonance frequency, f_0, (full line), and at the upper, f_+ (dashed), and lower, f_- (dotted), half-power frequencies. On the right hand side are shown the sum, Σ_+ (dotted), and difference, $\Delta_\pm$ (dashed), combinations of the transients monitored at the half-power frequencies for the traces on the left. Σ_+ is proportional to ε'' and $\Delta_\pm$ is a function of ε'.*

for Michler's ketone despite its larger size and hence longer rotational relaxation time.

Values of $\Delta_\pm/\Sigma_\pm$ derived from the average height of the triplet transients are listed in Table 8.1. Also listed are the values of the uncorrected dipole relaxation time, Θ_{uncorr}, calculated using equation (9). However, from the results of the Paddon-Row 12 σ-bond compound it is possibly more appropriate in the calculation of Θ, to substract the limiting value of 0.07 from $\Delta_\pm/\Sigma_\pm$. The values so obtained are referred to as Θ_{corr}. The error limits given for Θ correspond to an error of ±0.02 in $\Delta_\pm/\Sigma_\pm$.

Table 8.1: *The fraction of power reflected at resonance, R_0; quotient of the difference and sum, $\Delta_\pm/\Sigma_\pm$ (uncorr) and quotient of the difference and sum, $\Delta_\pm/\Sigma_\pm$ (corr), after substraction of a limiting value of 0.07, together with the calculated dipole relaxation times Θ_{uncorr} and Θ_{corr}; calculated dipole relaxation time by Fessenden,[37] Θ, and rotational relaxation time Θ_{sphere}, calculated using a spherical geometry.*

Solute	R_0	$\Delta_\pm/\Sigma_\pm$(uncorr)[a]	$\Delta_\pm/\Sigma_\pm$ (corr)[a]	Θ_{uncorr} (ps)	Θ_{corr} (ps)	Θ[b] (ps)	Θ_{sphere} (ps)
Michler's ketone	0.517	0.436	0.367	6.4	7.6	7.7	65
fluorenone	0.447	0.131	0.062	25.5	54.5	19	43
DMABN	0.486	0.173	0.103	17.6	29.5	34	35
(DMABN)$_2$	0.514	0.236	0.166	11.9	16.9		69
DMANB	0.286	0.163	0.093	31.7	56.6		47
(DMANB)$_2$	0.490	0.279	0.209	10.7	14.4		82

(a) values determined from the average heights of the singlet (Paddon-Row 12-bond) and triplet transients.
(b) obtained from reference 37.

The values of Θ_{corr} for DMABN, DMANB and fluorenone are found to be reasonably close to the rotational relaxation times calculated for a spherical geometry, Θ_R. The value of Θ for Michler's ketone, however, is seen to be much shorter than Θ_R, even though the value is calculated assuming a spherical geometry which tends to give a lower limit. We conclude that an additional, intramolecular dipole relaxation process is occurring in the triplet state of Michler's ketone. This process probably involves the interchange between two energetically equivalent, mirror-image dipolar states or resonance structures as was previously suggested by Fessenden et al.[37] The flip-flop time of 7.6 ps determined is in good agreement with a value of 7.7 ps, determined by Fessenden.

In Figure 8.5 are shown the TRMC transients for a DAD molecule with two-fold, D_2, symmetry consisting of a central naphthalene acceptor and anilino donors (An[2]N[2]An). Also
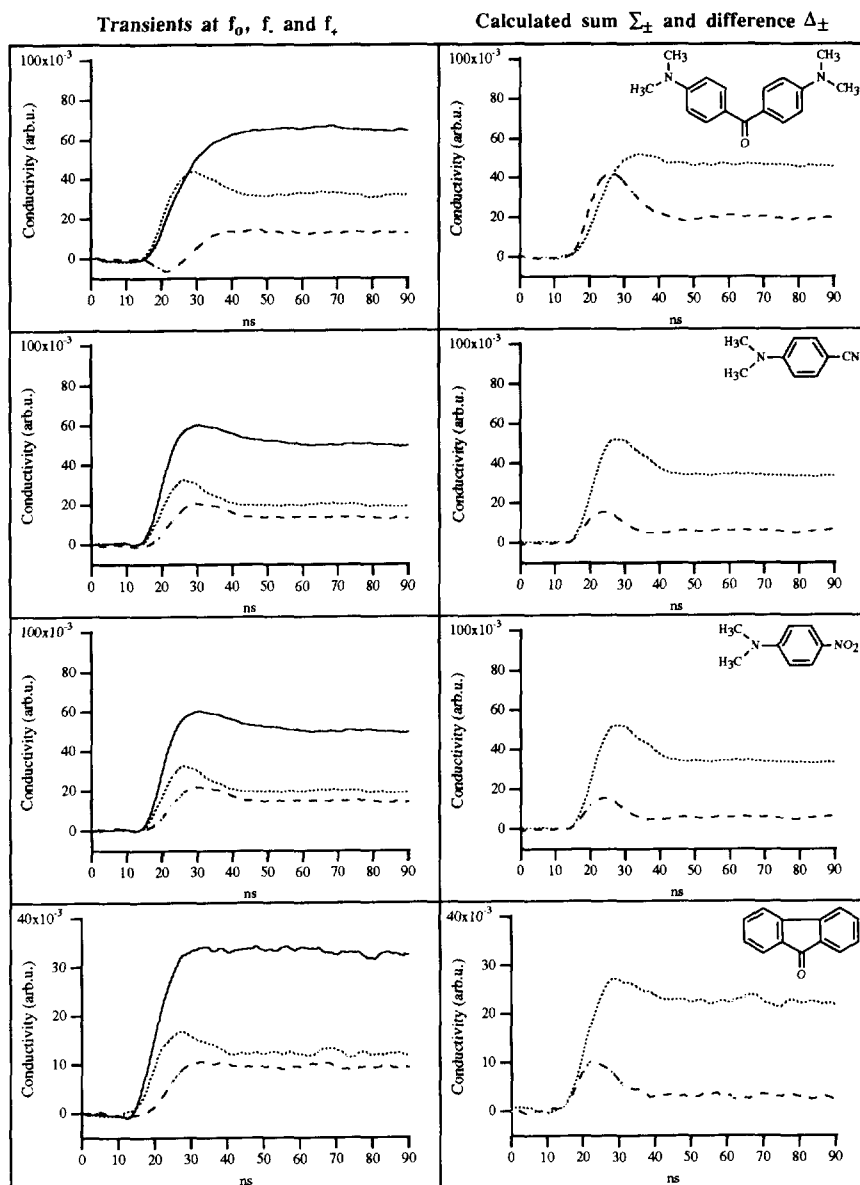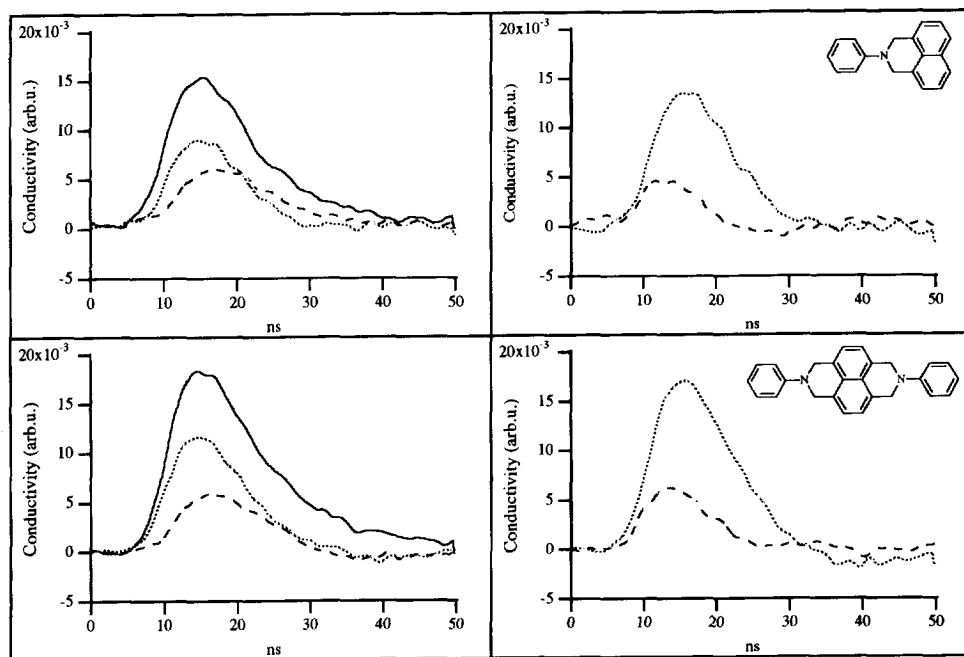
Figure 8.5: *On the left hand side are shown the TRMC transient observed on flash-photolysis of the compounds shown in benzene, monitored at the cavity resonance frequency, f_0, (full line), and at the upper, f_+ (dashed), and lower, f_- (dotted), half-power frequencies. On the right hand side are shown the sum, Σ_+ (dotted), and difference, Δ_+ (dashed), combinations of the transients monitored at the half-power frequencies for the traces on the left. Σ_+ is proportional to ε'' and Δ_+ is a function of ε'.*

shown are transients for the model DA compound, An[2]N. A large $\Delta\varepsilon''$ change is indicated for both compounds, showing the excited states to be highly dipolar. The transients follow closely the risetime-convoluted laserpulse and are associated with the S_1 states of these compounds with lifetimes of 1.6 ns (DAD) and 1.5 ns (DA), as determined by time-resolved fluorescence measurements. Perhaps surprisingly, not only does the symmetrical compound display a large dipolar TRMC transient, but in addition this is even larger than that observed for the DA compound, despite the much larger size and hence longer rotational relaxation time of the former molecule. The values of $\mu_S{}^2/\Theta$ based on the above lifetimes are given in Table 8.2.

Using disk and cylinder approximations for the geometry of the An[2]N model compound, excited state dipole moments of 15.0 and 16.4 D are calculated, respectively, in good agreement with an estimate of 15.1 D made on the basis of solvatochromic shift measurements.[43] This corresponds closely to complete charge separation between the anilino nitrogen and naphthalene moieties. When the same calculations are made for An[2]N[2]An much larger μ_S values of 21.7

220

to 28.4 D are estimated. This unlikely result is attributed to the occurrence of an intramolecular flip-flop dipole inversion process in addition to rotational diffusion. The value of Θ_I required to yield a value of μ_S for An[2]N[2]An equal to that for An[2]N is approximately 100 ps.

The overal timescale for dipole relaxation for An[2]N[2]An is much longer than $1/\Theta$ which explains why the f_+ and f_- transients are similar in magnitude for both compounds in Figure 8.5. The solvatochromic shifts for the DA and DAD compounds are found[43] to be almost identical, which would support the existence of a non-symmetrical $An^+[2]N^-[2]An$ state with a dipole relaxation time much longer than the several picoseconds characteristic of solvent relaxation. Clearly the S_1 state of the An[2]N[2]An molecule must undergo a large geometrical distortion in which the symmetry is completely broken. A barrier on the order of 0.15 eV towards flip-flop inversion would appear to exist.

Table 8.2: *Lifetime of the CS state, τ_S; conductivity parameter (μ_S^2/Θ); rotational relaxation time Θ_{disk}, calculated using a disk geometry; rotational relaxation time Θ_{cyl}, calculated using a cylindrical geometry; dipole moment μ_{disk}, calculated using Θ_{disk} and dipole moment μ_{cyl}, calculated using Θ_{cyl}. The quantum yield Φ for the formation of the charge separated state is assumed unity. Calculated flip-flop dipole relaxation times, Θ_I (cyl) and Θ_I (disk), based on the dipole moments calculated for An[2]N.*

Compound	τ_S[a]	μ_S^2 / Θ	Θ_{disk}	Θ_{cyl}	μ_{disk}	μ_{cyl}	Θ_I (cyl)[b]	Θ_I (disk)[b]
	ns	D^2/ps	ps	ps	D	D	ps	ps
An[2]N[2]An	1.6	2.34	201	345	21.7	28.0	111	94
An[2]N	1.5	1.92	117	140	15.0	16.4		

(a) from fluorescence measurements.

(b) Θ_I is the intramolecular dipole inversion process.

8.2.2 Acceptor-donor-donor-acceptor molecules (ADDA)

In Figure 8.6 are shown the TRMC transients of $(DMABN)_2$ and $(DMANB)_2$. Their asymmetrical DA counterparts DMABN and DMANB are shown in Figure 8.4. All four compounds form long-lived triplet states on photoexcitation. Values of Δ_+/Σ_+, derived from the average height of the triplet transients, are listed in Table 8.1. Also listed are the values of the corrected dipole relaxation time, Θ_{corr}, calculated using equation (9), with a limiting value of 0.07 subtracted from Δ_+/Σ_+. For comparison also the values of the uncorrected dipole relaxation time, Θ_{uncorr}, calculated using Δ_+/Σ_+, are presented in Table 8.1.

As already mentioned in the previous section the values of Θ_R, calculated for DMABN and DMANB, are seen to be reasonably close to the measured values of Θ_{corr}. They are also similar

Transients at f_0, f_- and f_+

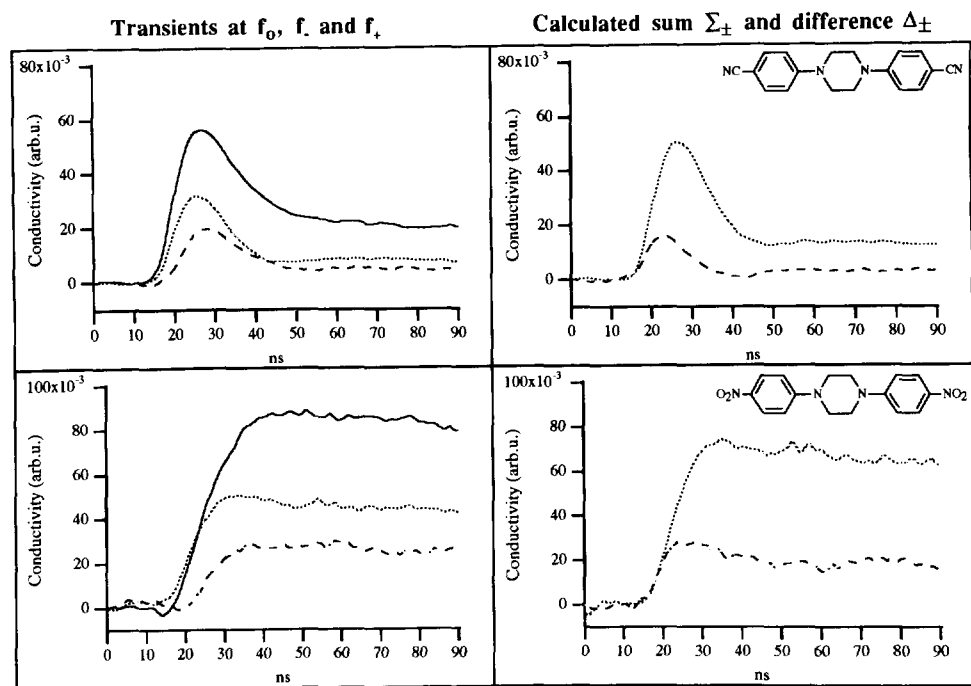### Calculated sum $\Sigma_\pm$ and difference $\Delta_\pm$

Figure 8.6: *On the left hand side are shown the TRMC transient observed on flash-photolysis of the compounds shown in benzene, monitored at the cavity resonance frequency, f_0, (full line), and at the upper, f_+ (dashed), and lower, f_- (dotted), half-power frequencies. On the right hand side are shown the sum, $\Sigma_\pm$ (dotted), and difference, $\Delta_\pm$ (dashed), combinations of the transients monitored at the half-power frequencies for the traces on the left. $\Sigma_\pm$ is proportional to ε'' and $\Delta_\pm$ is a function of ε'.*

to values measured for the rotational relaxation times of the ground state molecules. The values of Θ_R calculated for $(DMABN)_2$ and $(DMANB)_2$ are seen to be much longer than the measured dipole relaxation times, even though the values were calculated assuming a spherical geometry, which tends to give a lower limit to Θ_R. We conclude that, also in this case, an additional, intramolecular dipole relaxation process is occurring in the triplet states of the symmetrical molecules. This process, which involves the interchange between two energetically equivalent, mirror-image dipolar states or resonance structures, is illustrated in Figure 8.7 for $(DMABN)_2$. In view of the value of Θ_R estimated, it is clear that dipole relaxation in the T_1 state of $(DMABN)_2$ and $(DMANB)_2$ must be controlled almost exclusively by interchange between the weakly coupled resonance structures with $\Theta_I \approx 15$ ps, rather than by molecular tumbling.

For DMABN and $(DMABN)_2$ dipolar singlet state contributions to the loss transient can be

separated from the overal TRMC signal. This allows the dipole moments of the S_1 states to be estimated. As for the D_2 symmetry DAD compound in the previous section, the dipole moment of the S_1 state of $(DMABN)_2$ was found to be much larger, at 24.3 D, than the 13.0 D for DMABN based on the rotational relaxation times. At the time this apparent anomaly was not understood. However if we take into account dipole relaxation by flip-flop interconversion with a time constant of 17 ps, as found for the triplet state, rather than the 202 ps rotational relaxation time initially used, the net dipole moment of the S_1 state of $(DMABN)_2$ decreases to 10.0 D. This value is a net dipole moment since the dipole moment of the excited DMABN moiety is opposed by the dipole moment of the non-excited or effectively ground state companion which would be expected to be approximately 7 D, as illustrated in Figure 8.7. The dipole moment of the excited, emissive moiety will therefore be close to 17 D, which would explain the somewhat greater solvatochromic shift found for the dimer.[21]

The suggestion by Launay et al.,[21] that $(DMABN)_2$ could be used as a molecular switching device would therefore appear to be well founded. Extended Hückel calculations[46] have shown that the weak orbital overlap between the two DMABN moieties can give rise to symmetry-broken, dipolar excited states.
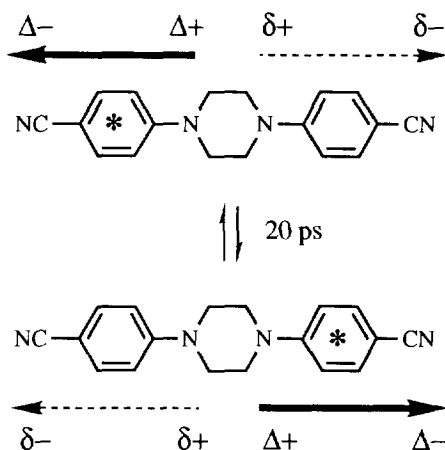

Figure 8.7: A schematic representation of the switching between dipolar resonance structures of $(DMABN)_2$. The net dipole moment of 10.0 D estimated for the S_1 state is equal to the difference between that of the locally excited, "on" moiety, ≈ 17 D, and that of the "off" moiety, which is taken to be close to the 6.6 D of a ground state DMABN molecule.

8.3 DONOR-ACCEPTOR COMPOUNDS WITH THREE-FOLD SYMMETRY[3]

The structures of the molecules studied in this section are shown in Figure 8.8. They will be referred to in the text from top to bottom in the figure as DEABP, p-ETP and m-ETP. Their preparation and characterization have been reported previously.[45]

A transient change in dielectric loss on flash-photolysis was observed for all three compounds, as shown in Figure 8.8 for cyclohexane solutions. The transients are characterized by an initial decay during the first few tens of nanoseconds after the flash, followed by a much slower decay which extends into the microsecond region. We attribute the dielectric loss transients observed to the formation of a short-lived dipolar S_1 state which undergoes intersystem crossing to yield a relatively long-lived dipolar triplet state (T_1).

From time-resolved fluorescence measurements, the lifetimes of the S_1 states of DEABP, p-ETP and m-ETP have been determined to be 8.0, 11.5 and 6.9 ns, respectively, in cyclohexane. The calculated fits to the data in Figure 8.8 were made using these S_1 state lifetimes and a lifetime of several microseconds for T_1. The good agreement between the experimental TRMC transients and the calculated curves during the early decay period, provides strong evidence in support of the assignment of the initial loss component to the dipolar nature of the S_1 state. Equally good agreement was found using the fluorescence lifetimes to fit the TRMC transients for n-hexane, t-decalin and benzene solutions. From the fits to the absolute magnitude of the transients the parameter μ_S^2/Θ was determined and the values are listed in Table 8.3.

The present results substantiate the conclusion that the fluorescent, S_1 states of p-ETP and m-ETP are dipolar as previously reported based on the solvatochromic shifts of the emission bands.[22] The present results further demonstrate that symmetry-breaking in S_1 and T_1 occurs even in a nonpolar, saturated hydrocarbon environment. A specific solvent-solute interaction would appear therefore to be unnecessary for this phenomenon to occur. A local geometrical distortion of the molecule must however accompany temporary localization of the dipole in a particular orientation. This could possibly involve a twist of a diethylamino moiety similar to that suggested to play an important role in the excited states of simple donor-acceptor compounds containing the dialkylanilino moiety (see Chapter 3).[44]

The dielectric loss transient for the S_1 state of m-ETP can be seen in Figure 8.8 to be considerably larger than for the para-compound. This is shown quantitatively by the μ_S^2/Θ values in Table 8.3. If we assume the dipole relaxation time, Θ, for the two molecules to be similar then the ratio $\mu_S(meta)/\mu_S(para)$ is determined to be 1.6±0.2. This is in agreement with the ratio of 1.7 derived from the dipole moments of 16.4 and 9.5 D, estimated for m-ETP and p-ETP, respectively, from the solvatochromic shift data[22] in low polarity solvents.

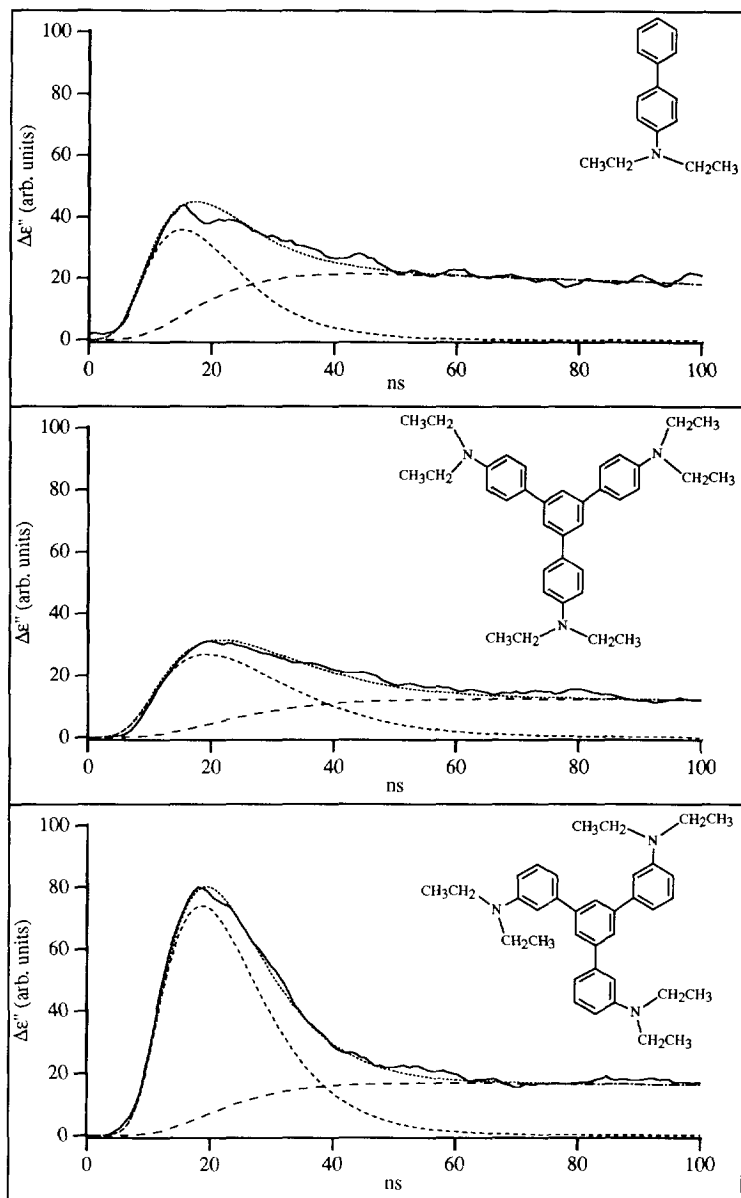**Figure 8.8:** *Transient changes in the dielectric loss, $\Delta\varepsilon''$, on flash-photolysis of cyclohexane solutions of the compounds shown (full line). The short and long dashed traces are the computed contributions of the S_1 and T_1 states, respectively, with the former based on the measured fluorescence lifetime. The dotted line is the sum of the computed S_1 and T_1 traces.*

Table 8.3: *Fluorescence lifetime, τ_S; conductivity parameter (μ_S^2/Θ); rotational relaxation time Θ_{disk}, calculated using a disk geometry; calculated dipole moment μ_S using Θ_{disk} and $\Theta^{-1} = \Theta_I^{-1} + \Theta_R^{-1}$.*

Solute	Solvent	τ_S (ns)	μ_S^2/Θ (D^2/ps)	Θ_{disk} (ps)	μ_S (D)	μ_S [a] (D)
DEAB	cyclohexane	8	0.40	141[b]	6.8	-
p-ETP	n-hexane	10.3	0.45	134	7.8	6.7
	cyclohexane	11.5	0.28	440	11.2	7.7
	t-decalin	11.7	0.18	918	12.8	7.1
	benzene	9.7	0.42	334	11.9	8.8
m-ETP	n-hexane	6.8	1.06	134	11.9	10.2
	cyclohexane	6.9	0.95	440	20.5	14.2
	t-decalin	6.8	0.58	918	23.0	12.7
	benzene	6.2	0.79	334	16.2	12.0

(a) based on $1/\Theta = 1/\Theta_R + 1/\Theta_I$ with $\Theta_I = 400$ ps, $\Theta_R = \Theta_{disk}$
(b) calculated assuming a cylinder geometry

Absolute dipole moments have been derived from the μ_S^2/Θ values using the rotational relaxation[46] times for a disk-shaped molecule, given in Table 8.3 as Θ_{disk}. These absolute μ_S values are seen to be somewhat larger than those derived from the fluorescence measurements except for the lowest viscosity liquid, n-hexane. In addition they display a tendency to increase with increasing solvent viscosity in the order n-hexane ($\eta = 0.31$ cP), benzene ($\eta = 0.65$ cP), cyclohexane ($\eta = 1.02$ cP), t-decalin ($\eta = 2.17$ cP). The most probable cause of this is that dipole relaxation occurs by interchange between the three energetically equivalent dipolar resonance structures illustrated in Figure 8.9, in addition to rotational relaxation of the whole molecule via spinning and tumbling. This will result in an overall relaxation, Θ, given by equation (2), with Θ_I viscosity independent.

Using a value of $\Theta_I \approx 400$ ps, together with the calculated values of Θ_{disk}, was found to result in dipole moment values for the different solvents which had a minimum scatter about a common mean. These values are given in the last column of Table 8.3. The mean values found are 12.3 and 7.6 D for m-ETP and p-ETP respectively.

These mean values of μ_S are lower than those derived from the solvatochromic shift data. This could be due to an overestimate of the effective molecular radius in calculating μ_S from the emission results. In view of the localized nature of the dipolar state a smaller effective radius than that used, which was based on the total molecular volume, might have been more

appropriate. This would have resulted in smaller dipole moment estimates.

The TRMC values require an upward correction if the parameter of interest is the dipole moment of the localized exciton state which is presumably the dipole moment relevant to the solvent dependence of the emission. This can be seen from Figure 8.9, since the localized excited state dipole is seen to be opposed by the dipole moments of the other two, "dormant" diethylanilino groups. The individual dipole moments of these dormant groups would be expected to be similar to the 1.8 D of ground state N,N-diethylaniline. An amount of $2 \times 1.8\cos(60°) = 1.8$ D should therefore be added to the net dipole moment for S_1, in order to arrive at the dipole moment associated with the localized excitation, μ_S. This gives $\mu_S = 14.1$ and 9.4 D for m-ETP and p-ETP respectively.

An intramolecular dipole relaxation time of 400 ps corresponds to a mean residence time at a given site of 600 ps for a system with three-fold symmetry.[47] Because dipole relaxation is very much slower than the reciprocal radian frequency of the microwaves used, $1/\omega \approx 15$ ps, one
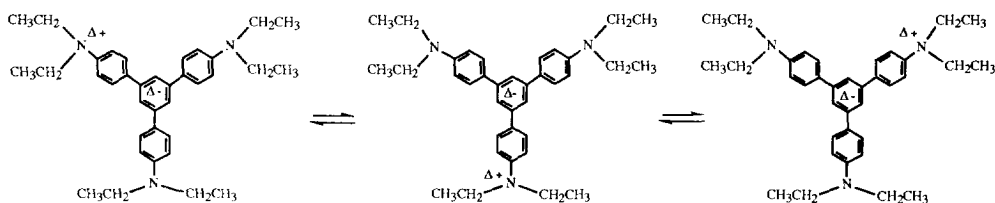

Figure 8.9: Three energetically equivalent dipolar excited states of p-ETP. The positive charge centre, Δ+, remains localized for approximately 600 ps, while the negative charge centre, Δ-, appears to be highly delocalized resulting in a large S_1 polarizability.

would expect to find a negligible change in the molecular polarizability (and hence ε') from this source according to the relationship (1). If $\Delta\varepsilon'$ is small compared with $\Delta\varepsilon''$, the TRMC transients monitored at the half-power frequencies of the microwave cavity should be similar in temporal form and approximately half the size of the transient monitored at the cavity resonance frequency.[1] This is by no means the case for p-ETP as shown by the results in Figure 8.10A.

The combination transients for p-ETP are shown in Figure 8.10B. Σ_+ is similar to the $\Delta\varepsilon''$ transient found at resonance as it should be. The Δ_+ transient, however, is seen to be even larger than Σ_+, indicating a large change in polarizability on excitation. A considerably smaller Δ_+ transient is found for m-ETP and even smaller for the model compound, DEABP. The relatively large change in polarizability found for the ETP compounds would appear therefore to be related to their molecular symmetry.

As mentioned above the high polarizability of S_1 cannot be attributed to rapid dipole
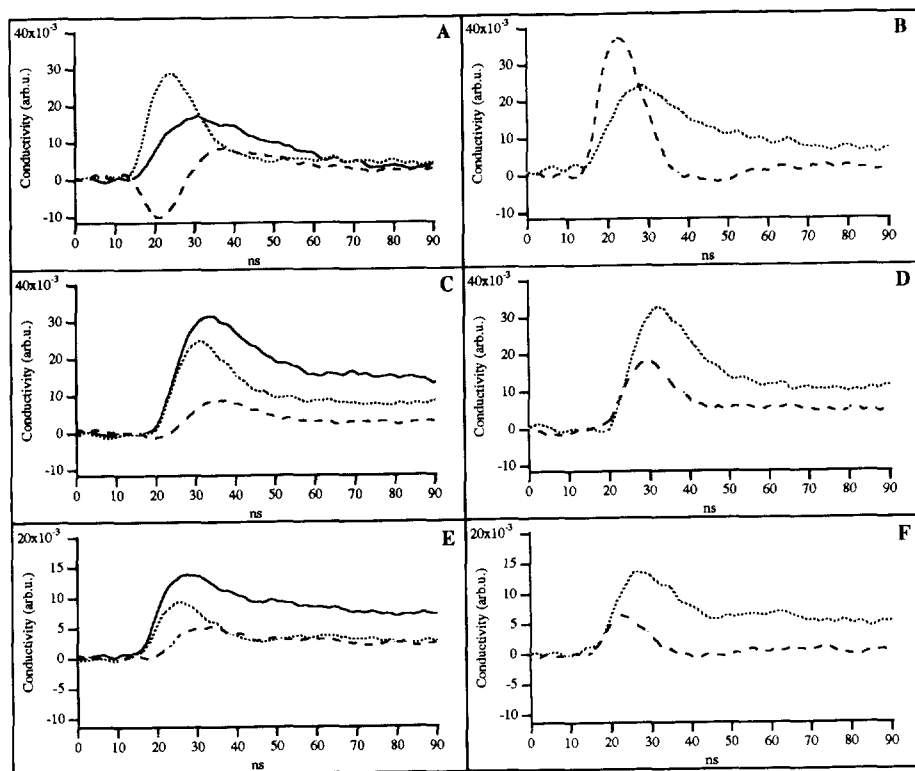
Figure 8.10: A,C,E) On the left hand side are shown the TRMC transients observed on flash-photolysis of solutions of p-ETP, m-ETP and DEABP, respectively, in benzene, monitored at the cavity resonance frequency, f_0, (full line), and at the upper, f_+ (dashed), and lower, f_- (dotted), half-power frequencies. B,D,F) On the right hand side are shown the sum, $\Sigma_\pm$ (dotted), and difference, $\Delta_\pm$ (dashed), combinations of the transients monitored at the half-power frequencies for the traces on the left. $\Sigma_\pm$ is proportional to ε'' and $\Delta_\pm$ is a function of ε'.

relaxation since $\Theta_I \gg 1/\omega$. It would appear therefore that while the positive charge is localized close to a particular diethylamino group for several hundred picoseconds, the corresponding electron is highly delocalized over the triphenylbenzene unit. That the S_1 states of p-ETP and m-ETP should have high electronic polarizabilities has been suggested previously on the basis of preliminary, Hückel molecular orbital calculations.[22] If the large change in polarizability found for p-ETP and m-ETP proves to be a general property of symmetrical assemblies of donor-acceptor chromophoric, units then such molecules could represent a new class of compounds for generating not only 2nd order but also 3rd order nonlinear optical effects.[23,48]

8.4 BIARYLS

8.4.1 Introduction

Molecules consisting of two identical aromatic moieties joined by a single carbon-carbon bond are of considerable photophysical interest because of their often unusual and unexpected optical absorption and emission behaviour. The characteristics of such biaryl assemblies are extremely sensitive to the electronic coupling between the aromatic moieties and hence to the electron densities at the bridging carbon atoms, the dihedral angle between the aromatic planes, and the relative energy levels of locally excited and intramolecular charge separated states. As a result of excitonic interactions and the possibility of charge separation, the emissive properties and decay kinetics can differ dramatically from those of the S_1 state of the parent monomer and are often very sensitive to changes in molecular structure and the environment.[4-20,49-61]

The ring systems of biaryls can be either orthogonal or close to coplanar with respect to one another. In the case of an orthogonal orientation, leading to a minimal interaction between the two units, the optical absorption or fluorescence spectrum will look like a slightly perturbed version of an isolated chromophore. In the other limit, the coplanar orientation, the electronic excitation will not be localized on either of the two halves and consequently the optical spectrum could differ considerably from that of the isolated chromophore.

For 1,1'-binaphthyl the absorption spectrum in solution as well as in the solid state resembles very much that of naphthalene, as first noted by Friedel et al.[49] Also the absorption spectrum and the quite well resolved fluorescence spectrum in a rigid 2-methyltetrahydrofuran glass at 77 K, as reported by Hochstrasser,[50] appeared to be almost identical to those of naphthalene. From these similarities it was concluded that the molecule in its ground state is strongly twisted about the single bond connecting the two naphthalene moieties (see Figure 8.11).[51-55] This is supported by an X-ray study[61] of the crystal which yields a dihedral angle, $\theta = 68°$. This implies that the ground state conformation is mainly determined by intramolecular hydrogen-hydrogen repulsion. In a fluid solution, however, the fluorescence spectrum consists of a broad structureless band.[50] The maximum of this emission is shifted considerably to the red by about 400 cm^{-1} in acetonitrile, as compared to the fluorescence spectrum in the solid. The red shift of the fluorescence spectrum and the decrease of the fluorescence lifetime by one order of magnitude have been interpreted[49-56] as a change in molecular geometry of 1,1'-binaphthyl, involving a decrease in the dihedral angle in solution as compared to the solid state, to a more favourable structure with larger interaction between the aromatic π-systems.

For 2,2'-binaphthyl the absorption spectrum is less naphthalenic and shifted to the red, in agreement with less steric hindrance towards a planar conformation. The fluorescence of 2,2'-

binaphthyl is however less perturbed than for the 1,1' analogue, indicating considerably less interaction in the excited state. For 1,2'-binaphthyl an intermediate situation exists and the absorption and emission spectra of this molecule fall in between those of the other two.[49]
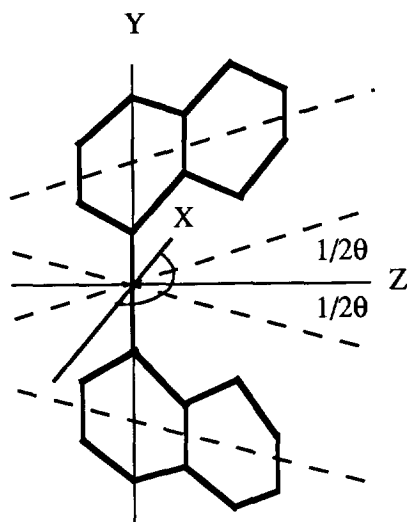

Figure 8.11: Coordinate system for 1,1'-binaphthyl.

For bianthryl, S_1 is essentially an excitonic doublet of two excited anthracene rings. The splitting is so small, however, that the two substates of the doublet behave as one state at ambient temperature in solution.[7-19] Of particular interest is the occurrence of dual emission for bianthryl.[4,5] As a result of a large research effort by many groups,[4-20] little doubt now remains that the dual emission results from an equilibrium between an initially formed, locally excited "LE" state and a "CS" state with complete charge separation between the two aromatic moieties. At a twist angle of 90°, electron transfer between the π-orbitals of the anthracenes is theoretically forbidden, because the two sets of ring orbitals are orthogonal. In the gas phase, the ground state torsion of bianthryl has a minimum at the perpendicular conformation, while the LE state has a double minimum located at ±12°-23° to either side of 90°.[64-66] The CS state of bianthryl is not observed in isolated bianthryl, because its energy seems to be above that of the LE state under these conditions.[20] However, bianthryl complexation with only one polar molecule in a supersonic jet is enough to lead to strongly lengthened fluorescence lifetimes, indicative of admixture of a forbidden CS component,[65] and complexes with more than one polar solvent molecule lead to the clear appearance of red-shifted fluorescence.[62,65,66] The

equilibrium is displaced increasingly towards the CS state with increasing ionic solvating power of the solvent. The accompanying decrease in energy of the CS state is evidenced by a bathochromic shift of the long-wavelength emission band. From this solvatochromic effect, a dipole moment of approximately 20 D has been estimated,[11] in agreement with complete centre-to-centre charge separation.

Evidence for a significant dipolar character of the S_1 state of bianthryl has been found even in nonpolar solvents. This evidence was provided by time-resolved studies of the increase in the microwave dielectric loss, ϵ'', of bianthryl solutions on flash-photolysis[12] and by the influence of an electric field on the fluorescence.[19]

On monitoring changes in the real component of the permittivity, ϵ', Fessenden et al.[15] found evidence that a large change in polarizability also accompanies excitation of bianthryl. This has been confirmed by the electrochromic measurements of Baumann et al.[19] and by more recent TRMC measurements.[1] This effect was attributed by Fessenden et al.[15] to flip-flop inversion of the A^+A^- dipole in a time of 9.2 ps, i.e. close to the reciprocal radian frequency of the microwaves used.

In the next sections we have attempted to see whether the photon-induced permittivity changes observed for bianthryl are more general by carrying out time-resolved microwave conductivity studies on solutions of naphthalene, anthracene and pyrene and their homosymmetric biaryl derivatives, of which the molecular structures are shown in Figure 8.12.

8.4.2 TRMC measurements at resonance

In Figure 8.12 are shown the TRMC transients observed at the resonance frequency, f_0, on flash-photolysis of benzene solutions of naphthalene, anthracene and pyrene monomers. For these compounds, no change in ΔP_R can be detected, indicating their S_1 states to be nonpolar as expected. In contrast, all of the biaryl compounds studied, display transient changes in ΔP_R which are outside the experimental noise limits, as is also shown in Figure 8.12. A dipolar character of the relaxed S_1 states of these molecules is therefore indicated. The transient for bianthryl, which is by far the largest, is without doubt attributable to a large contribution from a charge separated state as found by previous workers.[4-20]

Interestingly, the magnitudes of the loss transients for the biaryls are qualitatively in accordance with expectations based on the calculated driving force for complete charge separation from the locally excited state,[11] $\Delta E_{CS} = E(LE) - E(CS)$, which is given in Table 8.4. This correlation could, however, be simply happenstance since the lifetimes of the S_1 states, which also govern the heights of the signals, are in fact quite different as shown by the values in Table 8.4, which were determined from nanosecond-timescale fluorescence decays.
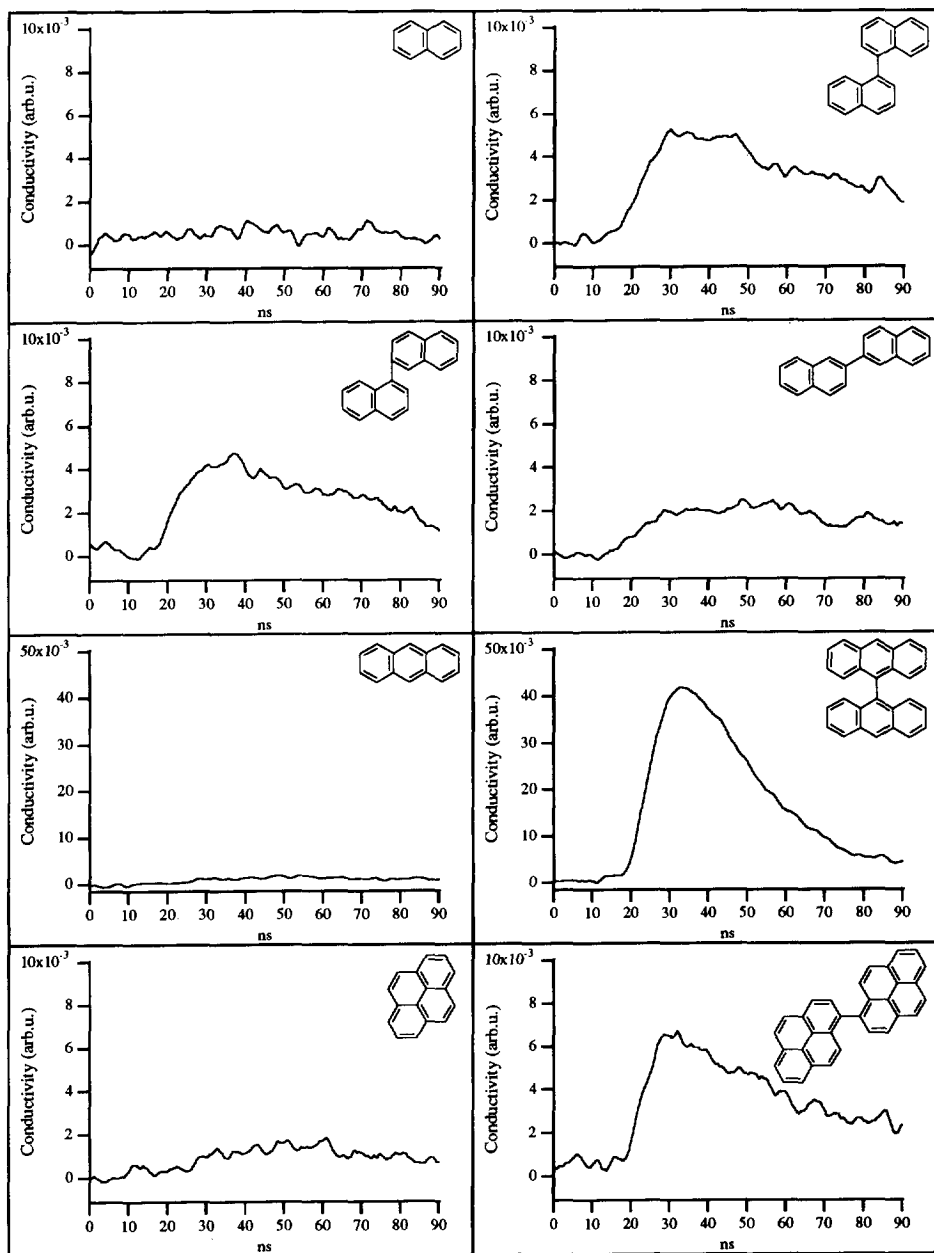
Figure 8.12: *TRMC transients observed on flash-photolysis of solutions of the compounds shown in benzene, monitored at the cavity resonance frequency,* f_0.

The TRMC transients have been fitted using the fluorescence lifetimes for τ_S, as described previously in Chapter 2. The transient for bianthryl could be fitted quite well with a single dipolar transient of lifetime equal to that found from the fluorescence measurements i.e. 12 ns. For the other solutes, however, an overall fit to the data could only be obtained by including an additional dipolar species with a lifetime of a few hundred nanoseconds. This longer-lived component could possibly be due to the formation of a dipolar triplet state. However at present we have no supporting evidence for this assignment.

In order to estimate the absolute magnitude of the effective dipole moments of the S_1 states, we need to know the dipole relaxation time, Θ. As discussed more fully in the next section, the abnormally large polarizability of S_1 of bianthryl is almost certainly not a result of rapid dipole relaxation via flip-flop inversion, as initially suggested by Fessenden et al.[15] We therefore take dipole relaxation to be controlled mainly by rotational tumbling of the molecules. Two rotational relaxation times have been calculated; one for a spherical geometry of the molecules, Θ_{sphere}, and one for a cylinder-shaped geometry, Θ_{cyl}, of diameter 0.55 nm. Considering the actual shapes of the molecules, these values of Θ should represent lower and upper limits which will give lower and upper limits, respectively, to μ_S.

The values of Θ used are listed in Table 8.4 together with the estimates of μ_S. As can be seen, μ_S decreases in the order expected based on the ΔE_{CS} values, as was apparent from the raw TRMC transients. This is also the same order found for the magnitude of solvent perturbations of the emission spectra of these molecules.[11] Comparison of the solvent dependence of the fluorescence of 1,1'-binaphthyl and bianthryl in 3-methylpentane and acetonitrile reveals a small but distinct shift of ≈ 400 cm^{-1} for the first compound and a much larger shift of 3000 cm^{-1} for the latter.[54] The spectrum of bianthryl is also broadened, indicative of the formation of a highly dipolar state. The solvent perturbation of the emission for 2,2'-binaphthyl is extremely small,[11] in agreement with the dipole moment estimate of only approximately 2 D.

In the case of 9,9'-bianthryl it has been shown that initial excitation to a locally excited, A*A, state is followed on a subnanosecond timescale at room temperature by intramolecular electron transfer resulting in the formation of the A^+A^- giant dipole CS state. LE and CS have been suggested to be in equilibrium according to:[14,18]

LE <---> CS   (10)

In benzene at room temperature the fractional population of CS, F(CS) = [CS]/([CS] + [LE]), has been estimated to be 0.64.[14]

Table 8.4: *Fluorescence lifetime, τ_S; spherical rotational relaxation time, Θ_{sphere}; cylindrical rotational relaxation time, Θ_{cyl}; calculated experimental dipole moments μ_{sphere} and μ_{cyl}, using a spherical and a cylindrical geometry for the molecular shape, respectively; theoretical calculated dipole moment of the "pure" CS state, μ_{max}; fraction of CS state present at equilibrium, using a cylindrical geometry, $F(CS)_{cyl}$; fraction of CS state present at equilibrium using a spherical geometry, $F(CS)_{sphere}$ and calculated energy difference ΔE_{CS} of the lowest CS and LE states of various biaryls.*

Solute	τ_S	Θ_{cyl}	Θ_{sphere}	μ_{cyl}[a]	μ_{sphere}[a]	μ_{max}[b]	$F(CS)_{cyl}$	$F(CS)_{sphere}$	ΔE_{CS} (solv)[c]
	(ns)	(ps)	(ps)	(D)	(D)	(D)			(eV)
9,9'-bianthryl	12.0	327	89	18.5	9.8	20.7	0.799	0.220	-0.3
1,1'-bipyrenyl	1.9	444	101	13.2	6.3	33.1	0.159	0.040	0.0
1,1'-binaphthyl	2.8	152	64	6.5	4.1	22.2	0.078	0.030	0.5
1,2'-binaphthyl	3.8	152	64	4.5	3.0	25.7	0.031	0.014	-
2,2'-binaphthyl	15.7	152	64	2.4	1.6	31.0	0.006	0.003	0.8

(a) determined assuming F(CS) = 1.
(b) $\mu_{max} = 4.48 \times r_{Ar\text{-}Ar}$ ($r_{Ar\text{-}Ar}$ = center-to-center distance in Å).[11]
(c) ΔE_{CS} (solv) = E(CS) - E(LE) = IP - EA - E(LE) + C.[11]

The effective dipole moment of the molecule as measured in the present experiments for such an equilibrium situation is given by:[67]

$$\mu_S{}^2 = \mu_{LE}{}^2 [1 - F(CS)] + \mu_{CS}{}^2 F(CS) \tag{11}$$

where μ_S is the measured overall dipole moment and μ_{LE} and μ_{CS} are the dipole moments of the locally excited and charge separated states respectively. In the present case it is reasonable to take $\mu_{LE}=0$, which leads to expression (12) for F(CS):

$$F(CS) = [\mu_S/\mu_{CS}]^2 \tag{12}$$

Taking for μ_{CS}, the values given by Rettig,[11] which are based on complete, centre-to-centre charge separation, together with the present μ_S estimates, we have derived the values of F(CS) listed in Table 8.4. The value of F(CS) = 0.64 found for bianthryl in benzene by Barbara et al.[14] is seen to lie within the, admittedly very large, range of 0.5±0.3, estimated on the basis of the present results. If we apply equation (12) in reverse, using F(CS) = 0.64 and μ_S to derive

estimates of μ_{CS}, lower and upper limits of 12.1 and 23.1 D are found.

The application of equation (12) to the other biaryl derivatives assumes that the same type of equilibrium two-state model proposed for bianthryl is operative. While this may not necessarily be the case (see next section), the parameter F(CS) will still give a measure of the charge transfer character of S_1 for a particular compound. This is seen to decrease markedly from the value of *ca* 0.5 for bianthryl to only *ca* 0.005 for 2,2'-binaphthyl.

8.4.3 TRMC measurements at half-resonance

In Figure 8.13 are shown the sum, $\Sigma_\pm$, and the difference, $\Delta_\pm$, of the TRMC transients found at the half-power resonance frequencies f_+ and f_-. $\Sigma_\pm$ is proportional to $\Delta\varepsilon''$ and is accordingly very similar to the transients found at resonance shown in Figure 8.12. The faster response time for the half-resonance data is responsible for slight qualitative differences in the shape of the transients.

$\Delta_\pm$ is directly proportional to $\Delta\varepsilon'$ if the species responsible is long-lived compared with the time window of the observations. The proportionality factor under these conditions has been derived.[1] However, because changes in ε' are non-dissipative, i.e. the additional power stored in the cavity when ε' increases is released when ε' decreases, the behaviour of $\Delta_\pm$, for species which are formed and decay within the time-window of the observations, is complex and oscillatory. This type of behaviour can be seen in Figure 8.13. We have not, as yet, developed a convolution fitting procedure for this type of transient. Because of this the information that can be derived at present is only qualitative.

Beginning with the monomer solutions: While the $\Delta_\pm$ transients, for naphthalene and pyrene are within the noise limits of the measurement, that for anthracene, while still small, is clearly measureable as shown in Figure 8.13. This can be explained by the much smaller electronic polarizability of the S_1 state of naphthalene, which is L_b in character, compared with the L_a S_1 state of anthracene. The absolute values of the change in average electronic polarizability, $\Delta\alpha_e$, accompanying the S_0 to S_1 transitions have been measured by electrooptical absorption measurements and found to be 2 and 18×10^{-40} Cm^2/V, respectively.[68,69] Interestingly, the polarizability change associated with the vertical S_0 to S_1 Franck-Condon transition in bianthryl has also been measured and is found to be 19×10^{-40} Cm^2/V, i.e. very close to that for anthracene.[70] This is in agreement with the fact that excitation involves a local transition in one of the anthryl moieties. Therefore, in the absence of subsequent relaxation, the $\Delta_\pm$ TRMC transient for bianthryl would be expected to be similar in magnitude to that for anthracene.

As can be seen in Figure 8.13, readily measureable $\Delta_\pm$ transients are in fact observed for all of the biaryl compounds with that for bianthryl being approximately a factor of 10 larger than
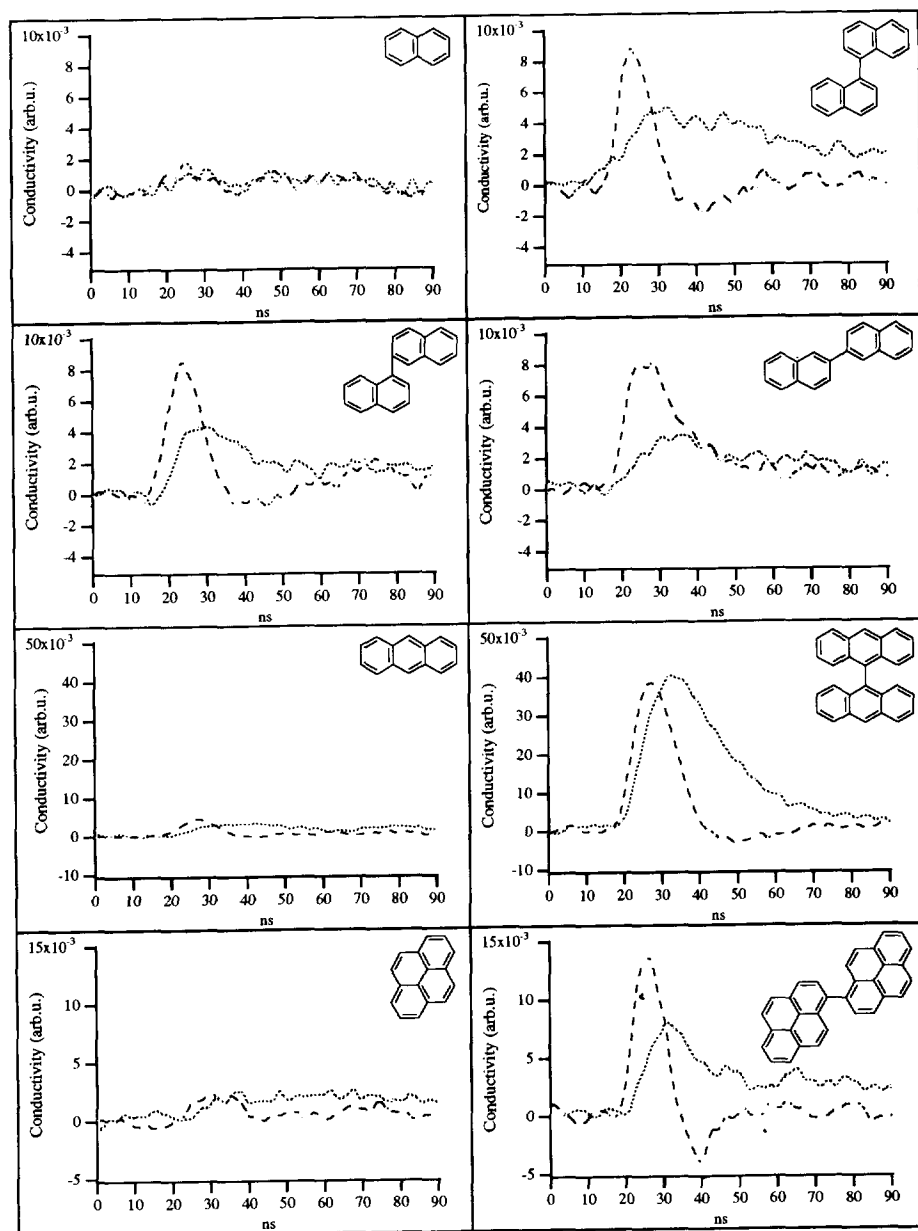
Figure 8.13: *The sum,* $\Sigma_{\pm}$ *(dotted line), and difference,* $\Delta_{\pm}$ *(dashed line), of the transient changes in the mirowave power reflected by the cavity at the half-resonance frequencies on flash-photolysis (7 ns, 308 nm) of solutions of the compounds shown in benzene.* $\Sigma_{\pm}$ *is proportionel to the change in dielectric loss of the solution,* $\Delta\varepsilon''$. $\Delta_{\pm}$ *is a function of the change in dielectric constant,* $\Delta\varepsilon'$.

the monomer. Abnormally large polarizabilities of the relaxed S_1 states of the biaryl compounds are therefore indicated. This must be related in some way to the equilibrium between the LE and CS states.

A large polarizability of the relaxed S_1 state of bianthryl was first observed by Fessenden et al.[15] as an abnormally large microwave phase shift on flash-photolysis of a benzene solution. This was attributed to rapid dipole relaxation via flip-flop switching between "degenerate" A^+A^- and A^-A^+ structures. From relationship (1) the dipole relaxation time was estimated to be 9.2 ps. The possibility that the change in ε' observed was due to a change in the electronic polarizability of the molecule, $\Delta\alpha_e$, was not considered. For a combined change in α_e and the dipole relaxation component, α_D, we have:

$$\Delta\varepsilon' = [\varepsilon(\infty) + 2]^2 N_*\{\Delta\alpha_e + \Delta\alpha_D\}/9\varepsilon_0 \tag{13}$$

$$\text{with } \Delta\alpha_D = \mu_S^2/[1 + (\omega\Theta_*)^2]3k_BT \tag{14}$$

The total polarizability change, $\Delta\alpha_S = \Delta\alpha_e + \Delta\alpha_D$, which was attributed only to dipole relaxation by Fessenden et al.[15] can be determined by substituting in equation (14) their values of $\Theta = 9.2$ ps, $\mu_S = 3.9$ D and f = 9.15 GHz. The value found is $\Delta\alpha_S = 110\times10^{-40}$ Cm^2/V. This is to be compared with the value of $\Delta\alpha_S$ for the Franck-Condon transition of only 19×10^{-40} Cm^2/V and the total ground state polarizability of bianthryl of 62×10^{-40} Cm^2/V, from which α_S for the relaxed S_1 state is determined to be 172×10^{-40} Cm^2/V. This very large value corresponds to a molecular polarization, $\Delta\alpha/3\varepsilon_0$, of 650 Å^3, which is close to the volume of a complete bianthryl molecule. The order of magnitude larger $A_\pm$ transient found for bianthryl compared with anthracene in the present work is in agreement with the large $\Delta\alpha_S$ value found by Fessenden et al.[15]

An exceptionally large polarizability of the relaxed S_1 state of bianthryl has also been reported by Baumann et al.[19] from electrooptical fluorescence measurements; $\alpha_S = 1.14\times10^{-10}$ a^3 Cm^2/V with "a" the effective molecular radius. For a molecular density of 1.0 g/cm^3 the molecular volume is 588 Å^3, which results in $\alpha_S = 160\times10^{-40}$ Cm^2/V. Since these experiments were carried out at optical frequencies, any dipole relaxation terms should be absent leaving only the electronic polarizability.

On comparing the Baumann[19] value with that determined by Fessenden et al., one is forced to conclude that the major contribution to $\Delta\alpha_S$ in the microwave experiment must be due to the large value of $\Delta\alpha_e$, with little room left over for a contribution to the polarizability from dipole relaxation. The rapid flip-flop dipole relaxation mechanism, proposed by Fessenden et al., is

therefore no longer required to explain the microwave data. On the basis of the dipole moments and rotational relaxation times, given in the previous section, see Table 8.4, we estimate the contribution to $\Delta\alpha_S$ from dipolar rotational relaxation to lie between 8 and 32×10^{-40} Cm^2/V, depending on whether a cylindrical or spherical geometry is chosen for the calculation of the rotational relaxation time.

Since the dipolar character of the other biaryls is less than that for bianthryl we conclude that the large $\Delta_{\pm}$ transients for these compounds are also mainly a result of a large electronic polarizability of their relaxed S_1 states rather than rapid dipole relaxation. We are unable to identify the underlying cause of this effect. One possibility is a large polarizability associated with the radical ion centres in the CS state. In this connection, we have observed large polarizability changes in rigid donor-spacer-acceptor assemblies of dimethylaniline as donor and anthracene and pyrene as acceptor,[72] which might be due to a large polarizability of radical anions of the aromatic hydrocarbon moieties.
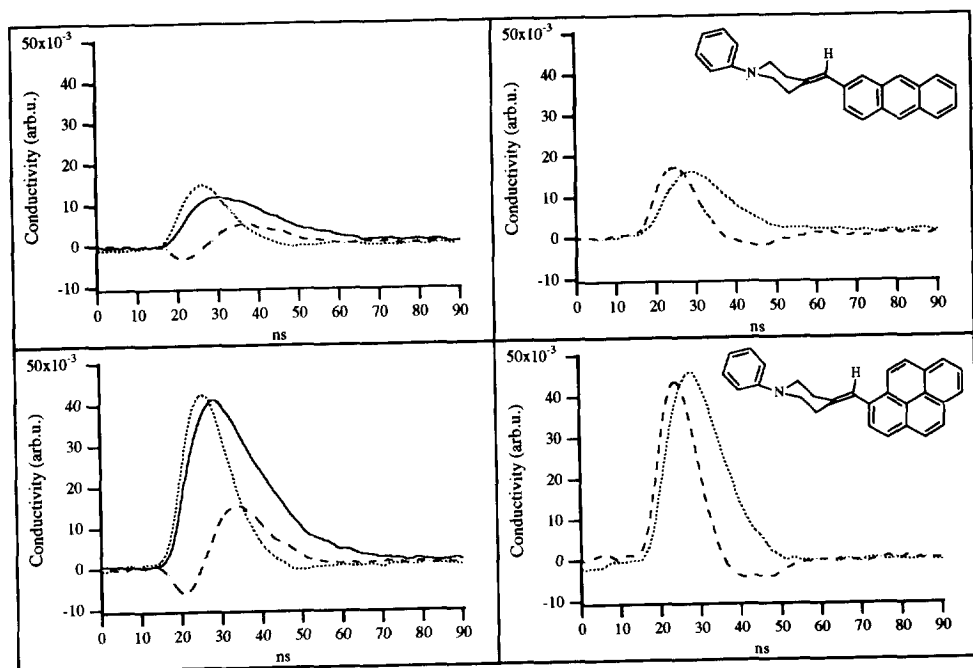

Figure 8.14: On the left hand side are shown the TRMC transients observed on flash-photolysis of the compounds, with their structures shown, in benzene, monitored at the cavity resonance frequency, f_0, (full line), and at the upper, f_+ (dashed), and lower, f_- (dotted), half-power frequencies. On the right hand side are shown the sum, $\Sigma_{\pm}$ (dotted), and difference, $\Delta_{\pm}$ (dashed), combinations of the transients monitored at the half-power frequencies for the traces on the left. $\Sigma_{\pm}$ is proportional to ε'' and $\Delta_{\pm}$ is a function of ε'.

The TRMC transients taken at f_0, f_-, and f_+, together with $\Sigma_{\pm}$ and $\Delta_{\pm}$ transients for these σ-bond DA compounds are shown in Figure 8.14, where a very large $\Delta_{\pm}$ contribution is apparent. However for these compounds there exists an equilibrium between the LE and a CS states. The potential energy surface of the S_1 state could therefore be relatively flat due to combined excitonic and LE-CS interactions, resulting in a high degree of electron delocalization over the molecule. We hope to resolve this question by extending this research to other aromatic assemblies and by obtaining quantitative data on the polarizability changes from the $\Delta_{\pm}$ transients.

8.4.4 Mixing of LE and CS states

The above results were discussed in terms of an equilibrium two-state model, ignoring mixing between the zero-order electronic configurations of LE and CS. Without mixing we assumed in a zero order approach that the dipole moments obtained from the TRMC measurements were from the equilibrium mixture of LE and CS. However in studying the solvent dependence of the fluorescence lifetime of the CS state of bianthryl, Barbara et al.[14,18] concluded that there was a substantial degree of LE/CS mixing ($\approx$ 1 kcal/mol). The mixed states are referred to as LE' and CS'. For 1,1'-binaphthyl the bathochromic shift of the fluorescence in going from the solid state to the liquid state has been explained by mixing of charge-transfer character into the zero-order LE state.[11] The LE and CS states can only mix for $\theta \neq 90°$. The degree of charge-transfer character depends on the angle between the naphthyl moieties and also on the position of substitution in the ring. Positions with strong local electron density favour the formation of a CS state.

This leads to the conclusion that for the binaphthyls the TRMC signal results from an LE state with a small amount of charge-transfer character, LE'. The equilibrium is on the side of the LE' state because the CS' state is higher in energy. For bianthryl on the other hand the CS' state is lower in energy than the LE' state and thus the equilibrium is on the side of the CS' state. Whether or not this picture is completely valid is not sure. If the coupling between LE and CS is strong, this may actually make the LE'-CS' interconversion a gradual rather than abrupt transition and result in a "flat" potential energy surface. This strong mixing may also result in considerable delocalization of charge over the molecule, resulting in a large polarizability, as observed. Under these conditions separation into individual LE' and CS' may be impossible. This is depicted in Figure 8.15 for bianthryl and for binaphthyl.
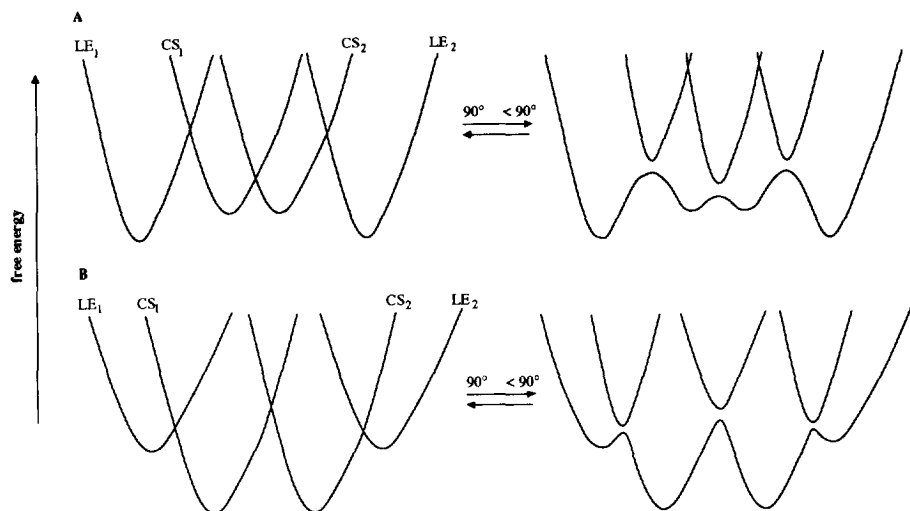
Figure 8.15: *Potential energy curves for the two degenerate LE$_1$ and LE$_2$ states, together with the two degenerate CS$_1$ and CS$_2$ states before mixing (left hand side) and after mixing (right hand side). Situation A is applicable to the binaphthyls for which the CS states are higher in energy than the LE states and situation B is applicable to bianthryl, for which the CS states are lower in energy than the LE states. With smaller energy difference between LE and CS, the energy surface will become more flat and thus the electron will be more delocalized.*

8.4.5 Conclusions

The homosymmetric biaryls 9,9'-bianthryl, 1,1'-bipyrenyl, 1,1'-, 1,2'- and 2,2'-binaphthyl all display a dipolar character of their relaxed S$_1$ state in benzene solution in complete contrast to the corresponding monomeric compounds. Upper and lower limits to the effective dipole moments have been calculated based on a spherical or cylindrical molecular geometry respectively. These decrease from 18.5 to 9.8 D for bianthryl to 2.4 to 1.6 D for 2,2'-binaphthyl. This is the same order in which the calculated driving force for charge separation from the locally excited state decreases. On the basis of an equilibrium between a nonpolar LE state and a completely charge separated CS state, the fractional CS content is determined to decrease from *ca* 0.5 for bianthryl to *ca* 0.005 for 2,2'-binaphthyl.

An increase in polarizability which occurs in the S$_1$ state of anthracene could just be observed while no evidence could be found for a polarizability change for naphthalene or pyrene. This is in agreement with the L$_a$ character of S$_1$ for anthracene and the L$_b$ nature of S$_1$ states of the last two compounds and with the much larger $\Delta\alpha$ value determined for anthracene than for naphthalene in electrochromic measurements.[69]

240

All of the biaryl compounds showed evidence of a very large change in polarizability on photoexcitation; close to an order of magnitude larger than that found for anthracene for which $\Delta\alpha = 18 \times 10^{-40}$ Cm^2/V. The underlying reason for this is not yet clear. Rather than a mechanism involving flip-flop dipole inversion, as originally proposed by Fessenden et al., we believe that the ultrahigh polarizabilities are probably electronic in nature. This could be due to very large polarizabilities associated with the local radical ion sites in the CS state or to an extensive, "flat" potential energy surface resulting from the mixing of states. Further experiments are underway which we hope will shed more light on this problem.

8.5 ACKNOWLEDGEMENT

8.6 REFERENCES

1   J.M. Warman, W. Schuddeboom, S.A. Jonker, M.P. de Haas, M.N. Paddon-Row, K.A. Zachariasse
     and J.P. Launay, *Chem. Phys. Lett.* **1993**, *210*, 397-403.
2   W. Schuddeboom, J.M. Warman, F.C. de Schryver and M. van de Auweraer,
     Chem. Phys. Lett. **1994**, *222*, 586-591.
3   W. Schuddeboom, J.M. Warman and K.A. Zachariasse, to be published in *Chem. Phys. Lett.*
4   F. Schneider and E. Lippert, *Ber. Bunsenges. Physik. Chem.* **1968**, *72*, 1155-1160.
5   F. Schneider and E. Lippert, *Ibid* **1968**, *74*, 24.
6   F. Schneider and E. Lippert, *Ber. Bunsenges. Phys. Chem.* **1970**, *74*, 624.
7   H. Beens and A. Weller, *Chem. Phys. Lett.* **1969**, *3*, 666.
8   E.M. Kosower and K. Tanizawa, *Chem. Phys. Lett.* **1972**, *16*, 419.
9   N. Nakashima, M. Murakawa and N. Mataga, *Bull. Chem. Soc. Japan*, **1976**, *49(4)*, 854.
10   W. Rettig and M. Zander, *Ber. Bunsenges. Phys. Chem.* **1983**, *87*, 1143.
11   M. Zander and W. Rettig, *Chem. Phys. Lett.* **1984**, *110*, 602-610.
12   R.J. Visser, P.C.M. Weisenborn, P.J.M. van Kan, B.H. Huizer, C.A.G.O. Varma, J.M. Warman and
     M.P. de Haas, *J. Chem. Soc., Farad. Trans. 2*, **1985**, *81*, 689.
13   M.A. Kahlow, T.J. Kang and P.F. Barabara, *J. Phys. Chem.* **1987**, *91*, 6452.
14   T.J. Kang, M.A. Kahlow, D. Giser, S. Swallen, V. Nagarajan, W. Jarzeba and P.F. Barabara,
     J. Phys. Chem. **1988**, *92*, 6800.
15   D.B. Toublanc, R.W. Fessenden and A. Hitachi, *J. Phys. Chem.* **1989**, *93*, 2893.
16   N. Mataga, H. Yao, T. Okada and W. Rettig, *J. Phys. Chem.* **1989**, *93*, 3383.
17   P.F. Barabara and W. Jarzeba, *Advan. Photochem.* **1990**, *15*, 1.
18   T.J. Kang, W. Jarzeba, P.F. Barabara and T. Fonseca, *Chem. Phys.* **1990**, *149*, 81.
19   W. Baumann, E. Spohr, H. Bischof and W. Liptay, *J. Luminesc.* **1987**, *37*, 227-233.

20 W. Rettig and W. Baumann in *Progress in Photochemistry and Photophysics*, J.F. Rabek, Ed.; CRC press: Boca Raton, London, 1990, Chapter 3, 79.

21 J-P. Launay, M. Sowinska, L. Leydier, A. Gourdon, E. Amouyal, M-L Boillot, F. Heisel and J.A. Miehé, *Chem. Phys. Lett.* 1989, *160*, 89.

22 G. Verbeek, S. Depaemelaere, M. Van der Auweraer, F.C. De Schryver, A. Vaes, D. Terrell and S. De Meutter, *Chem. Phys.* 1993, *176*, 195.

23 I. Ledoux, J. Zyss, J.S. Siegel, J. Brienne and J-M. Lehn, *Chem. Phys. Lett.* 1990, *172*, 440.

24 M. Joffre, D. Yaron, R.J. Silbey and J. Zyss, *J. Chem. Phys.* 1992, *97*, 5607.

25 J-L. Brédas, F. Meyers, B.M. Pierce and J. Zyss, *J. Am. Chem. Soc.* 1992, *114*, 4928.

26 J. Zyss, *J. Chem. Phys.* 1993, *98*, 6583.

27 J. Zyss, C. Dhenaut, T. Chauvan and I. Ledoux, *Chem. Phys. Lett.* 1993, *206*, 409.

28 V. Bonacic-Koutecky, P. Bruckmann, P. Hiberty, J. Koutecky, C. Leforestier and L. Salem, *Angew. Chem., Int. Ed. Engl.* 1975, *14*, 575-576.

29 L. Salem and P. Bruckmann, *Nature* 1975, *258*, 526-528.

30 L. Salem, *Science* 1979, *191*, 822-830.

31 G.D. Scholes, K.P. Ghiggino, A.M. Oliver and M.N. Paddon-Row, *J. Am. Chem. Soc.* 1993, *115*, 4345.

32 D.S. McClure, *Electronic Spectra of Molecules and Ions in Crystals;* Academic Press: New York, 1959.

33 J. Jortner, S.A. Rice and R. Silbey in *Modern Quantum Chemistry;* O. Sinanoglu, Ed.; Academic Press: New York, 1965; Vol. 3; 139.

34 T. Förster in *Modern Quantum Chemistry;* O. Sinanoglu, Ed.; Academic Press: New York, 1965; Vol. 3; 93.

35 T. Förster, *Discuss. Faraday Soc.* 1959, *27*, 7.

36 W.T. Simpson and D.L. Peterson, *J. Chem. Phys.* 1957, *26*, 588.

37 R.W. Fessenden and A. Hitachi, *J. Phys. Chem.* 1987, *91*, 3456.

38 G. Williams, *Trans. Farad. Soc.* 1968, *64*, 1219.

39 J.M. Warman, M.P. de Haas, M.N. Paddon-Row, E. Cotsaris, N.S. Hush, H. Oevering and J.W. Verhoeven, *Nature* 1986, *320*, 615.

40 M.N. Paddon-Row, A.M. Oliver, J.M. Warman, K.J. Smit, M.P. de Haas, H. Oevering and J.W. Verhoeven, *J. Phys. Chem.* 1988, *92*, 6958.

41 J.M. Warman, K.J. Smit, M.P. de Haas, S.A. Jonker, M.N. Paddon-Row, A.M. Oliver, J. Kroon, H. Oevering and J.W Verhoeven, *J. Phys. Chem.* 1991, *95*, 1979.

42 J.M. Warman, M.P. de Haas, H. Oevering, J.W. Verhoeven, M.N. Paddon-Row, A.M. Oliver and N.S. Hush, *Chem. Phys. Lett.* 1986, *128*, 95.

43 S.I. van Dijk, P. Groen, P.G. Wiering and J.W. Verhoeven, to be published.

44 A. Gourdon, J.-P. Launay, M. Bujoli-Doeuff, F. Heisel, J.A. Miehé, E. Amouyal and M.-L. Boillot, *J. Photochem. Photobiol. A*, in press.

45 M. Van der Auweraer, F.C. De Schryver, G. Verbeek, C. Geelen, D. Terrell and S. de Meutter, *Eur. Pat. EP349034* 1993.

46 T. Tao, *Biopolymers* 1969, *8*, 609.

47 J.D. Hoffman and H.G. Pfeiffer, *J. Chem. Phys.* 1954, *22*, 132.

48 V. Bollaert, F.C. De Schryver, P. Tackx, A. Persoons, J.J.H. Nusselder and J. Put, *Advanced Materials* 1993, *5*, 268.

49 R.A. Friedel, M. Orchin and L. Reggel, *J. Am. Chem. Soc.* 1948, *70*, 199.

50 R.M. Hochstrasser, *Can. J. Chem.* 1961, *39*, 459.

51 M.F.M. Post, J. Langelaar and J.D.W. van Voorst, *Chem. Phys. Lett.* 1975, *32*, 59-62.

52 M.F.M. Post, J.K. Eweg, J. Langelaar, J.D.W. van Voorst and G. ter Maten, *Chem. Phys.* 1976, *14*, 165-176.

53   M.F.M. Post, J. Langelaar and J.D.W. van Voorst, *Chem. Phys. Lett.* **1977**, *46*, 331-333.

54   R.W. Bigelow and R.W. Anderson, *Chem. Phys. Lett.* **1978**, *58*, 114.

55   K. Gustav, J. Sühnel and U.P. Wild, *Chem. Phys.* **1978**, *31*, 59-65.

56   H.T. Jonkman and D.A. Wiersma, *J. Chem. Phys.* **1984**, *81*, 1573-1582.

57   D.P. Millar and K.B. Eisenthal, *J. Chem. Phys.* **1985**, *83*, 5076.

58   H.J. Kim and J.T. Hynes, *J. Phys. Chem.* **1990**, *94*, 2736-2740.

59   W. Rettig, W. Majenz, R. Lapouyade and M. Vogel, *J. Photochem. Photobiol. A: Chem.* **1992**, *65*, 95-110.

60   M. Fadouach, B. Benali, A. Kadiri, C. Cazeau-Dubroca and G. Nouchi, *Spectrochim. Acta.* **1992**, *48A*, 1491.

61   K.A. Kerr and J.M. Robertson, *J. Chem. Soc. B.* **1969**, 1146.

62   K. Yamasaki, K. Arita, O. Kajimoto and K. Hara, *Chem. Phys. Lett.* **1986**, *23*, 277.

63   L.R. Khundar and A.H. Zewail, *J. Chem. Phys.* **1986**, *84*, 1302.

64   A. Subaric-Leitis, Ch. Monte, A. Roggan, W. Rettig, P. Zimmermann and J. Heinze, *J. Chem. Phys.* **1990**, *93*, 4543.

65   K. Honma, K. Arita, K. Yamasaki and O. Kajimoto, *J. Chem. Phys.* **1991**, *94*, 3496.

66   O. Kajimoto, K. Yamasaki, K. Arita and K. Hara, *Chem. Phys. Lett.* **1986**, *125*, 184.

67   W. Schuddeboom, S.A. Jonker, J.M. Warman, U. Leinhos, W. Kühnle and K.A. Zachariasse, *J. Phys. Chem.* **1992**, *96*, 10809.

68   R. Mathies and A.C. Albrecht, *J. Chem. Phys.* **1974**, *60*, 2500-2508.

69   W. Liptay, G. Waltz, W. Baumann, H.J. Schlosser, H. Deckers and N. Detzer, *Z. Naturforsch.* **1971**, *26a*, 2020-2038.

70   W. Liptay in *Excited States Vol I:* Academic Press: New York, **1974**, 129-255.

71   R.M. Hermant, *PhD Thesis*, University of Amsterdam, **1990**.

SUMMARY

In this thesis the photophysical properties of various donor-acceptor (DA) and symmetrical organic compounds were investigated using the Time-Resolved Microwave Conductivity (TRMC) technique in combination with steady-state and time-resolved fluorescence techniques. Four types of molecules are studied: π-conjugated donor-acceptor molecules, σ-bond separated bichromophoric and trichromphoric DA molecules, and both symmetrical molecules containing multiple donor and acceptor sites as well as homosymmetrical molecules. On flash-photolysis of the molecules charge separated states are formed whose properties depend on aspects such as the nature of the donor and acceptor group, the length and the nature of the bridging unit, geometrical aspects such as flexibility and rotation, orbital symmetry and the dielectric properties of the bulk medium. With the TRMC technique the changes in dielectric loss, ε'', on formation of the dipolar transients can be detected with nanosecond time-resolution, by measuring the decrease in power of X-band microwaves at the resonance frequency of a cavity. If measurements are made at the half-power resonance frequencies of the cavity, additional information can be gained on the change in dielectric constant, ε', or molecular polarizability.

In chapter 1 a general introduction has been given about the various types of molecules studied and the events which possibly can occur on flash-photolysis of solutions of these molecules.

Chapter 2 deals with the theoretical background of the TRMC technique and the apparatus used. The complete data analysis is described in order to extract the dipole moments of the transients from the experimental transients. The TRMC measurements are restricted to nonpolar alkanes and the pseudo-polar solvents benzene and dioxane, the properties of which are also described in this chapter. A detailed discussion of the rotational relaxation time has also been given.

In chapter 3 the effects of alkyl substitution and solvent on charge separation for a series of π-conjugated dialkylaminobenzonitriles are studied. There are two excited states present in these compounds, a locally excited state, LE, and a charge separated state, CS, which are in equilibrium. This equilibrium shifts to the CS state with increasing solvent polarity and with increasing alkyl-chain length.

In chapter 4 the influence of the variation of the acceptor strength, the rigidity of the bridge and the solvent polarity on charge separation in some flexible and semi-rigid σ-bond bichromophoric DA compounds are investigated. Charge-transfer in these compounds can occur either by Through Bond Interaction through the σ-bonds or by initial folding for the flexible bridged compounds bringing donor and acceptor close together. For the semi-rigid compounds in alkane solvents electron-transfer for strong DA pairs is followed by electrostatically driven folding ("harpooning"), resulting in the formation of a folded excited state.

Chapter 5 deals with trichromophoric σ-bond D_2D_1A compounds which can be divided into two types, with the only difference being a 1.2 Å shift of the amino nitrogen of D_1. The first series has four sigma bonds between A and D_1 and three between D_2 and D_1, so the general structure is denoted $D_2[3]D_1[4]A$. The second series has three sigma bonds between A and D_1 and four between D_2 and D_1, so the general structure is denoted $D_2[4]D_1[3]A$. The aim of these molecules is to ensure that the charge separation steps, if they occur, will take place sequentially and unidirectionally. The conclusion drawn from these results is that for the $D_2[3]D_1[4]A$ type of compounds there is electronic coupling between D_2 and D_1 via the piperazine ring and the two donors function as a combined donor rather than as separate decoupled sites. The $D_2[4]D_1[3]A$ compound, with D_2 a p-methoxyanilino group, does show two-step electron transfer even in the alkanes and therefore acts as a real trichromophoric compound.

Chapter 6 deals with the second harmonic generation properties of corona poled polymethylmethacrylate thin polymerfilms containing both σ-bond as well as π-bond DA compounds of the same length. From the comparison of σ- and π-bridged DA systems it appears that for relatively short bridges comparable β values can be achieved. This is mainly because in the D-σ-A systems a much larger difference in dipole moment of the ground and excited state, $\Delta\mu_{ct}$, compensates for the considerably lower oscillator strength of the CT transition. While a two-level model rather accurately predicts β values for D-π-A systems, expansion to include the effect of mixing between the CT excited state and locally excited D or A states appears necessary for D-σ-A systems.

In chapter 7 photoexcitation of the symmetrical molecules tetraphenylethylene (TPE) and p-methoxytetraphenylethylene dissolved in alkanes is shown to result in changes in both the real, ε', and the imaginary, ε'', components of the complex permitivitty of the solutions. The change in ε'' provides evidence for the dipolar, or "zwitterionic", nature of the twisted ^{1}p* "phantom state" formed from S_1 by rotation around the central carbon-carbon bond. A minimum dipole moment of *ca* 7.5 D for the individual resonance states is found. Dipole relaxation occurs by intramolecular flip-flop exchange between the zwitterionic structures on a timescale close to $1/\omega$, i.e. *ca* 15 ps. The fluorescence of TPE in alkane solvents has two decay components, one with a decay time less than 200 ps and a second with a decay time of 1.9 ns. The former ($\lambda_{max} \approx$ 490 nm) is assigned to emission from the partially relaxed S_1 state prior to twisting. The latter ($\lambda_{max} \approx$ 540 nm) is assigned to emission from a small, *ca* 1%, concentration of the relaxed S_1 state in equilibrium with the ^{1}p* state in the alkanes.

In chapter 8 charge separation in 2- and 3-fold symmetrical DA compounds as well as in a series of homosymmetric biaryls, with no specific donor and/or acceptor sites, has been studied. In completely symmetrical molecules charge separation is not to be expected and will only take

place upon symmetry lowering. In 2- and 3-fold symmetrical DA molecules large dipolar transients are observed as well as large changes in molecular polarizability. For the 2-fold symmetrical DA molecules dipole relaxation times on the order of 20 ps are determined. It is concluded that flip-flop interchange between two energetically equivalent, mirror-image dipolar states or resonance structures is the major dipole relaxation pathway. In a 3-fold symmetrical DA molecule evidence is found also for a large change in both dipole moment and polarizability. It is concluded that a state is formed in which the positive charge remains localized for approximately 600 ps on the donor and the negative charge is delocalized on the central aromatic moiety.

The homosymmetric biaryls all display a dipolar character of their relaxed S_1 state in benzene solution in complete contrast to the corresponding monomeric compounds. On the basis of an equilibrium between a nonpolar LE state and a completely charge separated CS state, a fractional CS content is determined which decreases following the same order in which the calculated driving force for charge separation from the locally excited state decreases. All of the biaryl compounds show evidence of a very large change in polarizability on photoexcitation. Rather than a mechanism involving flip-flop dipole inversion it is believed that the ultrahigh polarizabilities are probably electronic in nature.

Samenvatting

In dit proefschrift zijn een aantal donor-acceptor (DA) en symmetrische organische moleculen onderzocht m.b.v. de Time-Resolved Microwave Conductivity (TRMC) techniek in combinatie met steady-state en tijdsopgeloste fluorescentie technieken. Er zijn vier typen moleculen bestudeerd: π-geconjugeerde donor-acceptor moleculen, σ-gebrugde bichromofore en trichromofore DA moleculen, symmetrische moleculen met meerdere donor en acceptor groepen en homosymmetrische moleculen. D.m.v. laser-excitatie van de moleculen worden ladingsgescheiden toestanden gevormd. De eigenschappen hiervan hangen af van het donor-en/of acceptor type, de lengte en de aard van de tussenliggende brug, van geometrische aspecten als flexibiliteit en rotatie, van de symmetry van de orbitalen en van de dielectrische eigenschappen van het omliggende bulk medium. Veranderingen in dielectrisch verlies, ε'', tengevolge van de formatie van een dipolaire ladingsgescheiden toestand kunnen met de TRMC techniek worden waargenomen, met een nanoseconde tijdsresolutie, door het verlies in het vermogen van X-band microgolven op de resonantie frequentie van de TRMC cel te meten. Wanneer dezelfde metingen worden uitgevoerd op de half-vermogen resonantie frequenties van de cel, kan er extra informatie worden verkregen over veranderingen in de dielectrische constante, ε', ofwel de moleculaire polariseerbaarheid.

In hoofdstuk 1 wordt een overzicht gegeven van de onderzochte moleculen en de fysische gebeurtenissen die mogelijk kunnen optreden na excitatie van de moleculen in oplossing.

Hoofdstuk 2 behandelt de theoretische achtergrond van de TRMC techniek. Er wordt beschreven hoe het uiteindelijke dipoolmoment uit de experimentele data verkregen kan worden. De TRMC metingen kunnen alleen worden uitgevoerd in apolaire alkanen en in de semi-polaire oplosmiddelen benzeen en dioxaan. Tevens worden de rotationele relaxatietijden van de moleculen gedetailleerd beschreven.

In hoofdstuk 3 worden de effecten van alkyl substitutie en het oplosmiddel op de ladingsscheiding in een serie π-geconjugeerde dialkylaminobenzonitrilen bestudeerd. Er blijken twee verschillende aangeslagen toestanden te worden gevormd, die met elkaar in evenwicht zijn: een lokaal aangeslagen toestand, LE, en een ladingsgescheiden toestand, CS. Met hoger wordende polariteit van het oplosmiddel en met langer wordende alkyl staart schuift het evenwicht naar de kant van de CS toestand.

In hoofdstuk 4 wordt de invloed van de sterkte van de acceptor, de invloed van de flexibiliteit van de brug en de invloed van de polariteit van het oplosmiddel op de mate van ladingsscheiding in enkele flexibele en semi-rigide, σ-gebonden bichromofore DA verbindingen beschreven. Ladingsscheiding kan in de flexibele verbindingen optreden door Through Bond Interactie door de σ-bindingen of rechtstreeks, doordat na opvouwen van de verbinding donor en acceptor ruimtelijk dichtbij elkaar kunnen komen. In de semi-rigide verbindingen met een

sterk DA paar wordt electron overdracht gevolgd door electrostatisch geïnduceerd opvouwen ("harpooning"), hetgeen resulteert in de formatie van een gevouwen aangeslagen toestand.

In hoofdstuk 5 worden twee typen σ-gebrugde trichromofore D_2D_1A verbindingen behandeld die van elkaar verschillen door een 1.2 Å shift van een aminostikstofatoom in D_1. In de eerste serie ($D_2[3]D_1[4]A$) zitten er drie sigma bindingen tussen D_2 en D_1 en vier tussen D_1 en A. In de tweede serie ($D_2[4]D_1[3]A$) zitten er vier sigma bindingen tussen D_2 en D_1 en drie tussen D_1 en A. Deze moleculen zijn ontworpen om de ladingsscheiding stapsgewijs in één richting te laten plaatsvinden. Uit de resultaten blijkt dat D_2 en D_1 in $D_2[3]D_1[4]A$, via de piperazine ring, electronisch gekoppeld zijn. Hierdoor functioneren de twee donors als één gecombineerde donor in plaats van als twee gescheiden donors. De $D_2[4]D_1[3]A$ verbinding, waar D_2 een p-methoxyaniline groep is, geeft electron-overdracht in twee stappen en is dus een echte trichromofore verbinding.

In hoofdstuk 6 worden de Second Harmonic Generation eigenschappen beschreven van corona uitgerichte polymethylmethacrylate dunne polymeerfilms, waarin σ-gebrugde of π-gebrugde DA verbindingen van dezelfde lengte zijn opgelost. Door de σ- en π-gebrugde DA systemen te vergelijken blijkt dat voor relatief korte bruglengten vergelijkbare β waarden worden bereikt. Dit komt voornamelijk doordat in de D-σ-A verbindingen het verschil in dipoolmoment tussen de grond en de aangeslagen toestand, $\Delta\mu_{ct}$, erg groot is. Dit compenseert voor de aanzienlijk lagere oscillator sterkte van de CT overgang. Waar het twee-niveau model de β waarde voor de D-π-A systemen nauwkeurig voorspelt, is het voor de D-σ-A systemen nodig om de menging tussen de CT aangeslagen toestand en de lokaal in D of A aangeslagen toestanden in de berekening mee te nemen.

In hoofdstuk 7 wordt aangetoond dat photo-excitatie van de symmetrische moleculen tetraphenylethyleen (TPE) and p-methoxytetraphenylethyleen opgelost in alkanen resulteert in veranderingen in zowel het reële deel, ε', alsmede in het imaginaire deel, ε", van de complexe permitiviteit van de oplossingen. De verandering in ε" is het bewijs voor het dipolaire of "zwitterionische" karakter van de getwiste $^1p*$ "phantom" toestand, welke uit de S_1 toestand wordt gevormd door rotatie rond de centrale koolstof-koolstof binding. Gevonden is een minimum dipoolmoment van *ca* 7.5 D, voor de afzonderlijke resonantie structuren. Dipool relaxatie geschiedt vermoedelijk via intramoleculaire flip-flop uitwisseling tussen de zwitterionische structuren op een tijdschaal dicht bij 1/ω, i.e. *ca* 15 ps. De fluorescentie van TPE in alifatische oplosmiddelen bestaat uit twee decay componenten, één met een decay tijd van minder dan 200 ps en een tweede met een decay tijd van 1.9 ns. De korte component ($\lambda_{max}\approx490$ nm) wordt toegeschreven aan fluorescentie vanuit een gedeeltelijk gerelaxeerde S_1 toestand voor rotatie rond de centrale koolstof-koolstof binding. De tweede component

($\lambda_{max} \approx 540$ nm) wordt toegeschreven aan emissie vanuit een lage (*ca* 1%) concentratie van een gerelaxeerde S_1 toestand in evenwicht met de ^{1}p* toestand in de alkanen.

In hoofdstuk 8 wordt het optreden van ladingsscheiding in twee- en drievoudig symmetrische DA verbindingen, alsmede in een serie homosymmetrische biarylen beschreven. Door de hoge symmetrie in deze moleculen valt ladingsscheiding (in eerste instantie) niet te verwachten en kan mogelijk alleen optreden wanneer de symmetrie wordt verlaagd.

In enkele twee- en drievoudig symmetrische DA moleculen worden dipolaire toestanden waargenomen evenals grote veranderingen in de moleculaire polariseerbaarheid. Voor de twee-voudig symmetrische DA moleculen worden dipool relaxatietijden in de orde van 20 ps waargenomen. De conclusie is dat flip-flop uitwisseling tussen twee energetisch gelijke spiegelbeeld dipolaire toestanden of resonantie structuren het belangrijkste dipool relaxatie pad is. In een drievoudig symmetrisch DA molecuul wordt een grote verandering in zowel het dipoolmoment, alsmede in de polariseerbaarheid waargenomen. Hieruit wordt geconcludeerd dat er een toestand wordt gevormd, waarbij de positieve lading gedurende 600 ps gelokaliseerd blijft op de donor en de negatieve lading gedelokaliseerd is over het centrale aromatische gedeelte.

De gerelaxeerde S_1 toestand van enkele homosymmetrische biarylen heeft, in tegenstelling tot de overeenkomstige monomeer verbindingen, een dipolair karakter in een benzeen oplossing. Op basis van een evenwicht tussen een niet polaire LE toestand en een compleet ladingsgescheiden CS toestand is er een fractionele CS concentratie bepaald, die afneemt in dezelfde volgorde waarmee de berekende drijvende kracht voor ladingsscheiding uit de lokaal aangeslagen toestand afneemt. Wanneer de biaryl verbindingen geëxciteerd worden vertonen ze allen een grote verandering in polariseerbaarheid. Deze hoge polariseerbaarheden zijn vrijwel zeker electronische van aard en niet het gevolg van flip-flop dipool uitwisseling.

250

CURRICULUM VITAE

De schrijver van dit proefschrift werd op 1 oktober 1965 geboren te Zaandijk. De middelbare schoolopleiding werd van 1978 tot 1984 gevolgd aan de openbare scholengemeenschap Rooswijk te Zaandijk. Het diploma Atheneum-β werd op 7 juni 1984 behaald. Vervolgens werd van 1984 tot 1988 scheikunde gestudeerd aan de Universiteit van Amsterdam met als specialisatie fysisch-organische chemie. Op 16 november 1988 werd het doctoraal examen behaald. Van december 1988 tot december 1990 werd binnen de vakgroep Organische scheikunde in de werkgroep van Prof. Dr. J.W. Verhoeven aan de Universiteit van Amsterdam een AIO-2 opleiding gevolgd. Het betrof onderzoek naar nieuwe organische materialen met niet lineaire optische eigenschappen. Gedurende de periode van het onderzoek is samengewerkt met DSM en Philips. Op 22 maart 1991 werd het AIO-2 examen behaald. Op 1 april 1991 werd begonnen aan een driejarig promotieonderzoek onder leiding van Dr. J.M. Warman binnen het Interuniversitair Reactor Instituut aan de Technische Universiteit Delft. Het onderzoek dat in deze periode is uitgevoerd wordt in dit proefschrift beschreven.